Numerical analysis of the interaction between rockbolts and rock mass for coal mine drifts in Vietnam

Von der Fakultät für Geowissenschaften, Geotechnik und Bergbau
der Technischen Universität Bergakademie Freiberg
genehmigte

DISSERTATION

zur Erlangung des akademischen Grades

Doktor-Ingenieur

Dr.-Ing.

vorgelegt

von Dipl.-Ing. Cong Le Van
geboren am 11.03.1965 in Thanh Hoa

Gutachter: Professor Dr.-Ing. habil. Heinz Konietzky, Freiberg
Professor Dr.-Ing. Per Nicolai Martens, Aachen
Professor Dr.-Ing. Matthias Reich, Freiberg

Tag der Verleihung: 19.12.2008

Acknowledgement

The thesis has been finished within 4 years of intense work at the Chair of Rock Mechanics at the Geotechnical Institute of the Technical University Bergakademie Freiberg in Germany.

I address my great thanks to Professor Konietzky for his supervision and help in performing the numerical simulations and software developments. His helpful advices and teaching is greatly appreciated. Furthermore, his kindness, support, valuable guidance are gratefully acknowledged. I am also greatly thankful to all the colleagues at the Chair for Rock Mechanics at the Geotechnical Institute, especially to Dr. Hausdorf for his scientific support and to Mrs. Griebsch for her help in final formatting of the thesis and administrative support.

I thank Professor Martens and his co-workers for support and education during my stay at the RWTH Aachen.

I am deeply grateful to the Vietnamese government for the scholarship and provided assistance in the connection between Vietnam and Germany. Vietnamese government always creates conditions for us to implement our tasks. Again, I thank the Board of the 322 Project very much for their help in providing support during the time I stayed in Freiberg. I also express my gratitude to Vietnamese embassy in Berlin for their interest in my work.

I also thank all Vietnamese colleagues and friends in Freiberg because of their friendship and kind assistance.

I would like to thank DAAD for assistance and the additional financial contribution. They gave me so many opportunities to learn more about Germany and they gave me the chance to participate at German language course in both Hanoi and Köln.

Also, i am very thankful to the Institute of Mining Science and Technology (IMSAT), Vietnam National Coal, Mineral Industries Group (VINACOMIN) in Hanoi for providing documents, for giving me the permission to study abroad, for their technical and scientific support as well as for the financial contribution to my study.

I would like to thank my parents for their continuous support and education all the time and their hard working to bring us up.

Finally, I thank my wife and my son for their kind support. I owe my wife Ha Ly a debt of gratitude for her patience, understanding and taking care of my family for the four years I stayed in Germany and I thank my son Thanh Do for encouraging to finish my thesis in Germany.

Abstract

Since decades rockbolts are widely used as a support measure in mining and civil engineering. The presented literature review under special consideration of the situation in underground Vietnamese coal mines has revealed both, successful applications but also still a lack of understanding the interaction between rockbolts and rock mass and consequently reserves in optimization and improvement of safety.

A procedure for anchor design based on numerical simulations is proposed for Vietnamese coal mines, which includes the following steps:

- Determination of rockmechanical parameters
- Transformation of rockmechanical parameters into rock mass parameters by using rockmass classification schemes
- Set-up of numerical model including the real geological situation
- Simulation of excavation without anchorage and investigation of model response (determination of stability/instability, deformations, safety factors etc.)
- Incorporation of anchors into the modelling and investigation of model response, especially in respect to the reinforcement effect
- Parameter studies and optimization by choosing different bolting schemes
- Development of an proposal for optimized drift anchorage

Exemplary, the proposed procedure was applied to 5 different coal mines in Vietnam including different anchors schemes and different geological layering. A detailed evaluation of the model response in form of the displacements, stresses, deformations, plastifications and anchor forces was performed. In addition to this standard evaluation a modified c-Φ-reduction method (common in use in soil mechanics to characterise slope stability), which includes the reduction of the tensile strength, was applied to characterise the safety achieved by bolting by a safety factor. Also, a so-called ‘reinforcement’-factor based on the c-Φ-reduction method was introduced, which allows to characterize the improvement of reinforcement in a quantitative manner for different rockbolting schemes. Individual reinforcement factors were determined for the 5 different mines and different rockbolt pattern. Also, a general trend how length and distance

between bolts improve the reinforcement effect was obtained by a curve-fitting procedure on the basis of all performed simulations.

Software routines for non-linear anchor behaviour were developed and tested for FLAC and FLAC^{3D}, which allow to incorporate strain hardening, unloading and reloading and consequently cyclic loading in future simulations.

The developed methodology and software routines are a sound basis for future anchor optimization and safety improvement in Vietnamese coal mines. The work documents, that numerical simulations give deep physical insight into the interaction between rockbolts and rockmass and allow a physical based quantitative rockbolt design.

Table of contents

Acknowledgement 2

Abstract 3

Table of contents 5

1 Introduction 8

2 Literature review 9

2.1 Introduction 9

2.1.1 General 9

2.1.2 Rockbolt types 11

2.2 Existing rockbolt theories 15

2.2.1 Design principles 15

2.2.2 Selection of rockbolt systems 17

2.2.3 Bolting theories 18

2.3 Guidelines for the selection of the rockbolt system 21

2.3.1 Empirical design recommendations according to the US Corps of Engineers 22

2.3.2 Empirical assessments based on rock mass characterization 23

2.3.3 Design chart for rockbolt reinforcement by Panek 24

2.3.4 Design chart for rock bolt reinforcement based on the Q system 25

2.3.5 Recommendation based on the Rock Mass Rating System RMR 26

2.4 Rockbolt design 28

2.4.1 Design based on the suspension principle 28

2.4.2 Design based on beam-building principle 30

2.5 Interaction between the rockbolt and the rock mass 37

3 Simulation of nonlinear behaviour for cable and rockbolt elements 39

3.1 Overview of FLAC 39

3.2 Introduction to cable and rockbolt element 40

3.2.1 Numerical implementation of the cable element 41

3.2.2 Numerical implementation of the rockbolt element 43

3.3 Set-up numerical models with nonlinear character in 2D and 3D 44

3.3.1 Nonlinear characteristics 44

3.3.2 Input data for the cable model 45

3.3.3 Input data for the rockbolt model 45

3.4 Response of the numerical model with nonlinear behaviour 47

3.4.1 Response of numerical nonlinear cable element 47
3.4.2 Response of numerical nonlinear rockbolt element 52
3.5 Nonlinear cable and rockbolt elements in 3D simulations 54
3.5.1 Overview of FLAC^{3D} 54
3.5.2 3D numerical cable element 55
3.5.3 3D numerical rockbolt element 57
3.6 Conclusions 60
4 Numerical anchor modelling for Vietnamese coal mines 60
4.1 Introduction to the numerical constitutive rock mass model 60
4.2 Geological and technical conditions at Vietnamese mine sites 61
4.2.1 Geological and technical description of mine sites 61
4.2.2 Rock properties 67
4.2.3 Technical conditions 69
4.2.4 Rock mass properties 70
4.3 Set-up of numerical models 79
4.3.1 General solution procedure 79
4.3.2 Model types 81
4.4 Model analysis 85
4.4.1 Cao Thang mine 86
4.4.2 Mao Khe mine 102
4.4.3 Duong Huy mine 109
4.4.4 Mong Duong mine 118
4.4.5 Khe Cham mine 127
4.5 Determination of safety factors using the c-Φ reduction method 136
4.5.1 Theoretical basis of the method 136
4.5.2 General procedure 136
4.5.3 Safety factors for considered mines 137
5 Interaction between rock mass and rockbolt - reinforcement factors 143
5.1 Analytical model to describe the bolting effect 143
5.2 Reinforcement factors 146
5.3Relation between reinforcement factors (K_r) and parameters of bolting pattern 148
6 Conclusions and recommendations 151
6.1 Conclusions 151

6.2 Recommendations 153

References: 154

List of Figures 163

List of Tables 174

List of Abbreviations 177

1 Introduction

Rockbolts are an effective and widely used support measure and an element of reinforcement in civil engineering and mining. Bolting theories are progressing and their applications become more and more common in the world. Furthermore, rockbolts can be applied under very different geological and technical conditions. Rockbolts are cost-effective because of their simple composition and their relatively low labour and energy consumption. But the interaction mechanisms of the rockbolts with the rock mass and combination with other kind of support are still not fully understood. Therefore, a more detailed investigation of this interaction can lead to an increase in safety and more economic design. This work will contribute to that topic by using the numerical modelling approach under special consideration of the application of anchors to stabilize drifts in underground coal mines in Vietnam. Full cement grouted rockbolts, split set anchors and resin grouted anchors have been tested and are used in underground coal mines in Vietnam. So far the rockbolt design and dimensioning in Vietnamese coal mines is performed by empirical and simple analytical approaches. Besides all the advantages of these methods, a deeper physical understanding of the interaction between anchors and rockmass, an optimization and quantitative characterization of the effect of anchorage was still missing.

Therefore, within this work a methodology was developed and exemplary applied for 5 different mines, which allows to predict the effect of anchorage by applying different schemes in a quantitative manner. The methodology starts with determination of rock-mechanical parameters by standard laboratory testing and their transition into rock mass parameters. The second step is the set-up of a numerical model, which corresponds to the geological, geomechanical and technical conditions. Different quantitative parameters, obtained by the numerical simulation, are proposed to deduce quantitative parameters to estimate the effect of anchorage. Besides standard values, a safety factor determined by the so-called c-Φ-reduction method and a reinforcement factor K_r to estimate the reinforcement effect were introduced. Based on the investigation of 5 different mine situations, a generalized relation and design chart was deduced, which allows to assess the general effect of different rockbolt pattern on the reinforcement effect. Finally, a new constitutive law for rockbolts was developed, which allows to include cyclic loading and non-linearities in a very realistic manner.

2 Literature review

2.1 Introduction

2.1.1 General

According to statistics, bolting is now one of the most dominant support methods in both mining and civil engineering [Agioutantis, Z.; Stiakakis, C.; Stiakakis, N.; 2001].
It can be applied under very different geological conditions. Moreover, rockbolting is not only cost-effective, but can also be applied under quite different technological conditions. It can be combined with other support measures such as shotcrete, steel props or concrete lining to create a more competent structure. Rockbolts can be installed simply and quickly and in fully mechanized manner.

The roles of rockbolting within the ground control management is illustrated by Figure 2.1 [Lautsch, 2001].

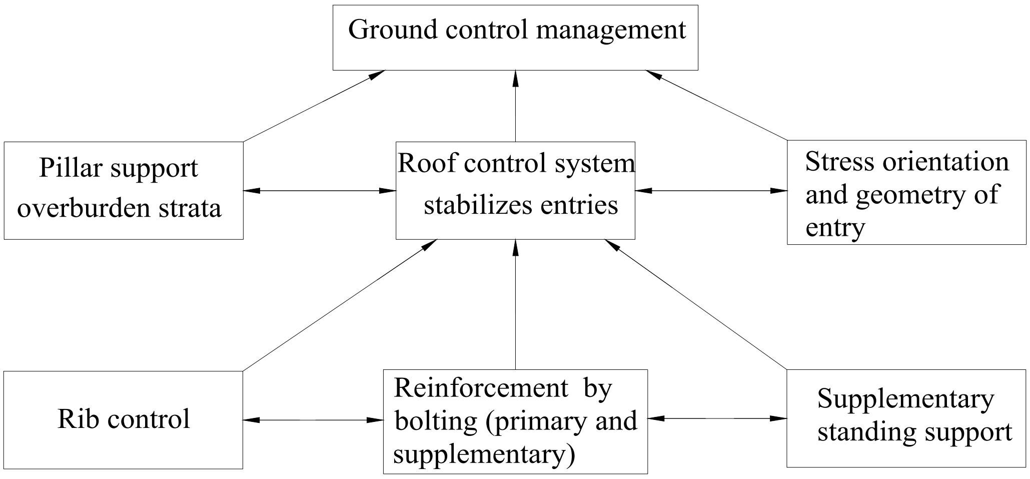
Ground control management
Pillar support overburden strata
Roof control system stabilizes entries
Stress orientation and geometry of entry
Rib control
Reinforcement by bolting (primary and supplementary)
Supplementary standing support

Figure 2.1 Element of ground control management (Lautsch, 2001).

When an opening is excavated the rock mass tends to move into it. The movement and potential failure or collapse of the rock mass around the opening is a function of stress field, rock properties, geological structure, excavation method, stand-up time, geometry and size of the opening.
The normal way to keep the stability of openings is the installation of support. The active ones, and rockbolts belong to this category, are reinforcements of the rock mass.

Rockbolts have a long history of about one hundred years and became a key technology for supporting underground and civil engineering constructions. Kovari [2004] has given a detailed overview about the history of bolting, which is outlined shortly below. In 1913, the bolting method was invented in Germany and protected by a patent. Timber and other support measures were partly replaced by rockbolts. In 1934, the next important publication introducing expansion bolt anchors combined with shotcrete was issued. 9 years later, the next detailed publication was issued by Weigel from the United States. In the period from 1943 to 1950 the use of rockbolts was of great importance for coal mines both in North America and Europe. Rockbolts have replaced steel support to a great extend. At that time a comprehensive work about the theory of rockbolting was published by E. Thomas. A lot of publications, text books and technical standards about rockbolts also appeared at that time. Rockbolts have contributed to reduce accidents and the costs in mining and tunnelling. In 1952, the Swedish engineers Flygare and Lundqvist have applied for a patent on rockbolts. In their papers, the advantages of the rockbolts and shotcrete and their combination were demonstrated. At that time, mechanical point anchored bolts were mainly used in USA. The annual consumption was up to 25 million. Beginning in 1956, synthetic epoxy resins were utilized. From here the application of rockbolts was widespread worldwide for supporting tunnels as well as underground mines. In 1960 bolts were applied to support roofs in 546 U.S. coal mines [Seth & Woodruff, 1996]. App. 3.1 million bolts were used in these mines. In 1959, the first resin capsule system was introduced in Germany. In the following year the installation of steel rockbolts was mechanised. In 1963, Rabcewicz wrote about NATM (New Austrian Tunnelling Method) – a new method for tunnelling in which the rockbolts and shotcrete are the important components of the support system. The mechanical expanding shell bolt appeared in the seventies for underground mining.

A lot of research work on analytical and numerical models to describe the reinforcement effect by rockbolts has been recently performed in the world. In the following, some of the most important publications are summarized.

A new analytical model was developed by Pellet and Egger [1996]. A displacement function along a joint was established in which the mechanical properties of the material, rock strength and joint angle are related to the bolts. An analytical model was created by Samit and Anand [1997] using beam-column theory in order to analyze the reinforcement by the rockbolts. Rock beam is assumed to be isotropic and linearly elastic. The solution is a coupled set of governing equations which need to be solved by numerical methods. The result shows that the critical buckling load of the rock beam is drastically influenced by the rock modulus. Another analytical model was set up to describe the loading process of the bolt and the enhancing of the reinforcement effect by Stillborg [1999]. The investigation of the influence of a number of rock mass layers to the stability of the opening and the minimum solid beam thickness of the bolted area can be determined according to Junlu [1999] using FLAC simulations. In this case the author uses cable elements.

Research on the stability of rock cavern roofs was carried out by Ziping [2001]. The author used numerical codes UDEC and DIANA to simulate rockbolts and cable bolts. The results confirm the efficiency of rockbolts in forming roof arches, in reducing roof displacements and in improving the reinforcement of the rock mass.

In another study, the interaction between rock mass and support measures was investigated by using the convergence – confinement method by Oreste [2003]. The stiffness of several support types was determined in order to set up corresponding support response curves. For rockbolts, the author has made the suggestion of an increase in cohesion (see chapter 2.5) and application of an increased global stiffness to the bolted area.

A further analytical model was set up by Yujing [2004] based on an improved shear-lag-model to investigate the interaction between rockbolts and the medium. The result of the analysis allows a quantitative evaluation of the support performance.

Research based on the theory of the ground reaction curve was performed by Fahimifar and Soroush [2004]. The results are algebraic complex differential equations so that it needs the incorporation of numerical methods to get solutions for the interaction between the rock mass and grouted rockbolts.

An analytical model for point anchored rockbolts was created by Bobet [2005] under elastic plane strain conditions for a circular cross section. An accurate solution for the relation between displacements and the load was obtained.

Numerical models were set up under specific mine conditions using the codes Phase2 and FLAC^{3D} to investigate the effects of rockbolting by Bagheri [2008] and Sasaoky et al. [2008] using Mohr-Coulomb theory. The simulations showed that the displacements at the roof can be controlled by rockbolts alone or by rockbolts in combination with shotcrete.

2.1.2 Rockbolt types

Nowadays, various types of rockbolts are used as exemplary illustrated by Figure 2.2. Rockbolts can be categorized by applying different criteria like the mode of interaction between rockbolt and rock mass or material the rockbolt consists of. Based on the mode of interaction, rockbolts can be classified into three main groups:

- Mechanically anchored rockbolts,
- Grouted rockbolts and cable bolts,
- Friction rockbolts.

Below a more detailed description is given for common rockbolt types used in coal mining worldwide.

a. Description of mechanically anchored rockbolts

The mechanically anchored rockbolts can be divided into three subtypes depending on the anchor property:

1. Rockbolt with slot and wedge at the end,
2. Rockbolt with conventional expansion shell,
3. Rockbolt with bail expansion shell.

The typical one in this group is the expansion shell anchor. The anchorage between rockbolt and ground is carried out by the expansion shell to create a frictional force. When it is installed, the shell expands due to the tapered form of the plug and the shell is split into 4 or 2 parts so that this action creates the interaction between bolt and the wall of borehole when the bolt is pulled at the threaded end of bolt by tightening the nut. The length of the borehole should be at least 100 mm longer than the bolt, otherwise the bail is dislodged by being forced against the end of the hole. The expansion shell is anchored against the wall of the borehole by friction and interlock. The capacity of this kind of rockbolts can be up to 18 tons.

Mechanically anchored rockbolts have some advantages. They work immediately after installation due to the activation of friction. Moreover, the cost is rather low and it is simple to manufacture. Besides that, it has also a few disadvantages (see chapter 2.2.2). Using this kind of rockbolts the difficulties are the potential loosening due to blast vibrations or chips of rock around the shell. Therefore, they are mainly used for temporary reinforcement or in combination with later grouting or corrosion protection. For correct installation, skilled manpower and close supervision are required. The diameter of the boreholes must be controlled.

b. Description of grouted rockbolts and cable bolts

They are widely used because of the simple constitution and low costs. The grouted rockbolts include cement grouted and resin grouted rockbolts. The bond between the anchor and the borehole wall is performed by chemical resin or the cement grout mixture. The bond is provided along a part or full length of the anchor and the borehole wall (Fig. 2.2).

b.1 Cement grouted rockbolts

This kind of bolt has the advantage that it is a durable and competent structure, easy to install with high corrosion protection. These anchors have a capacity of up to 10 tons. The disadvantage is that it doesn’t work immediately after the installation because it takes some time (typically hours to days) to cure before gaining its full capacity. Also, if water is present some types of grout cannot harden.

b.2 Resin grouted rockbolts, [The Minova, 2006]

Chemical resin is utilized to create the linkage between anchor and rock mass instead of a cement grout mixture. The greatest advantage of this type of bolt is that it can work immediately after installation. It takes just a few seconds to a few minutes until the anchor reaches its full functionality. Furthermore, additional pretension is easily to apply. Disadvantages are, that resin based systems are more expensive than cement grouted ones, that resin has a limited lifetime and that resin is a hazardous chemical product (environmental problems).

b.3 Grouted cable bolts

The composition of this kind is similar to the cement or resin grouted rockbolts, but the steel rebar is replaced by a steel cable. In some cases, bolts are needed with extreme length which can be even greater than the span of the opening so that only a flexible material (cable) can be applied. The capacity can be up to 50 tons. Besides these advantages one have to take into account, that they do not work immediately after installation due to the water curing. Also, installation under water is difficult.

c. Friction rockbolts

The linkage between bolt (steel tube) and borehole wall is a frictional force. There are two popular types of friction bolts, the split set and the Swellex anchors.

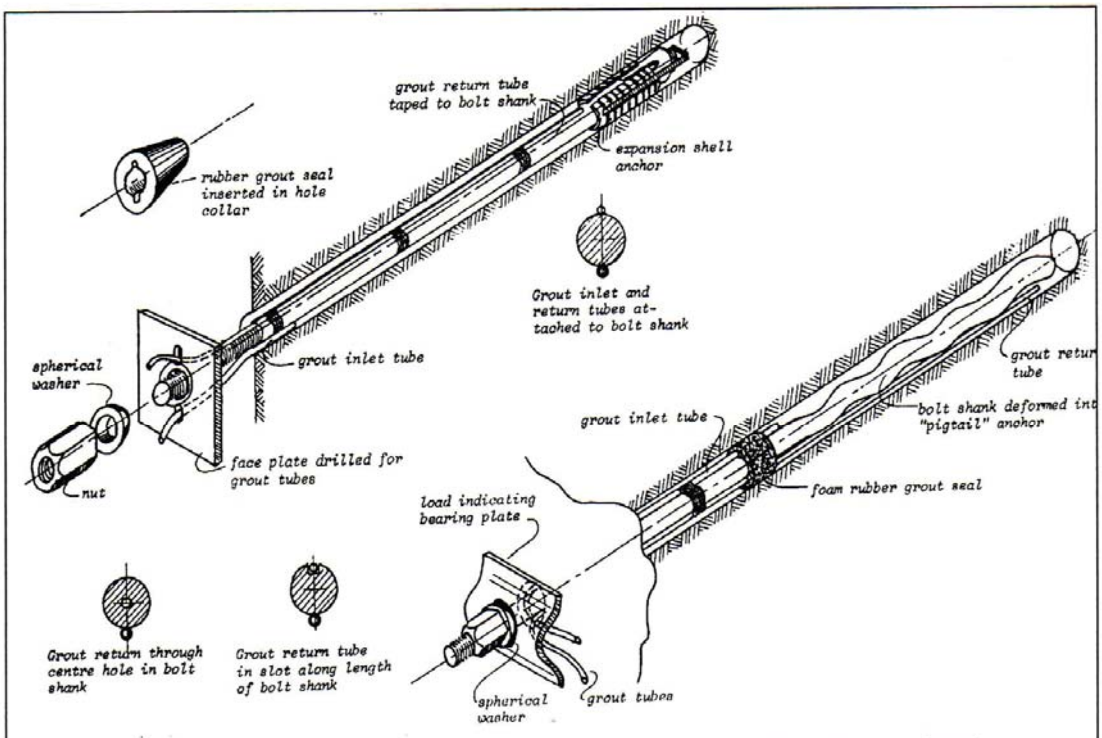
grout return tube
taped to bolt shank
expansion shell
anchor
rubber grout seal
inserted in hole
collar
Grout inlet and
return tubes at-
tached to bolt shank
spherical
washer
grout inlet tube
face plate drilled for
grout tubes
nut
Grout return through
centre hole in bolt
shank
Grout return tube
in slot along length
of bolt shank
grout retur
tube
bolt shank deformed int
"pigtail" anchor
grout inlet tube
foam rubber grout seal
load indicating
bearing plate
spherical
washer
grout tubes

a) mechanically anchored tensioned, grouted b) grouted anchored, tensioned

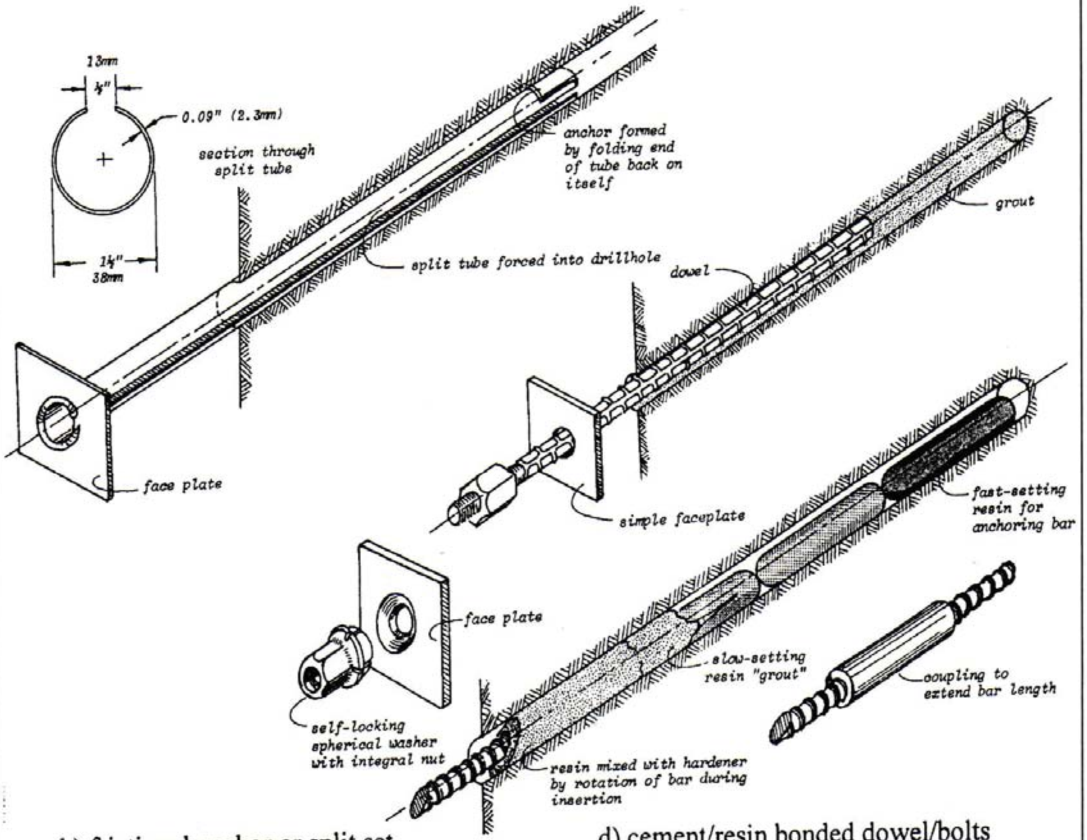
13mm
½"
0.09" (2.3mm)
section through
split tube
1½"
38mm
anchor formed
by folding end
of tube back on
itself
split tube forced into drillhole
face plate
grout
dowel
simple faceplate
fast-setting
resin for
anchoring bar
face plate
slow-setting
resin "grout"
coupling to
extend bar length
self-locking
spherical washer
with integral nut
resin mixed with hardener
by rotation of bar during
insertion

b) frictional anchor or split set d) cement/resin bonded dowel/bolts

Figure 2.2 Rockbolt types (adopted from Hoek & Brown, 1980).

c.1 Split set anchors

The split set anchors consist of a steel tube with a “C” shaped cross section. Its diameter is greater than that of the borehole. Therefore, during installation into the borehole by hammering, a radial spring force is generated by compression of the “C” shaped tube. Installation creates a frictional force along the total length of the tube. The capacity may be up to 16 tons. Friction rockbolts are simple to install and the system works immediately after installation. The main disadvantages are relatively high costs and the fact, that these rockbolts are unprotected against corrosion. The diameter of the borehole must be controlled to prevent a loss of frictional force.

c.2 Swellex anchors

Swellex anchors are made of a high strength but ductile metal. The cross section is a closed folded tube. The diameter of the folded tube is 25 to 28 mm and the expanded diameter is 33 to 39 mm. The installation of Swellex is very simple and quick. No mechanical pushing force is required, but it is activated by injection of high pressure water (about 30 MPa) which inflates the folded tube into a circular tube so that the circular tube comes into high frictional contact to the borehole wall. The capacity of this rockbolt type may be up to 22 tons. Swellex anchors are simply and quickly to install. The system works immediately after installation and can be applied under quite different geological conditions. The disadvantages are the high costs and the demand for a special equipment pump system for generation of high water pressure to inflate the anchors.

2.2 Existing rockbolt theories

2.2.1 Design principles

Rockbolt systems are designed essentially based on considering the stress field around the opening and analysing the structure of the rock mass. The stress field should be considered by magnitude and direction as well as its influence on the rock mass. The change of stresses in the rock mass depends on a number of factors such as excavation geometry, rock mass condition and inherent rock stress situation. Whereas close to the surface rock mass conditions are most important, with ongoing depth the ratio between the induced stresses and the strength of the rock mass become more and more important for the stability of excavation. There are some methods available to estimate the stability of openings through that relationship when the opening is unsupported [Vo, 1998].

During the design of a rockbolt system a lot of factors have to be considered. The most important factor is rock mass characteristic including geological and hydrological conditions. Special attention should be paid also to the stress state, the groundwater conditions, possible failure modes, scale of the project and the adjacent excavations.

The design of rockbolt systems can be performed by:

- Analytical solutions,
- Empirical assessments,
- Numerical modelling.

Several design procedures have been developed for rockbolts. Generally, these procedures relate the characteristics of the rock mass, the stress conditions and the opening geometry to each other and allow to develop a proposal for support requirements.

Two design methods can be distinguished:

1. Empirical methods

This technique relies on previous experience. A list of empirical rules in relation to support and rock mass parameters was deduced and can be applied if similar mine conditions exist. The experience obtained by numerous field studies are used to develop design charts which allow to obtain design parameters for different ground conditions.

2. Analytical and numerical methods

These methods rely on rock mechanics and strength theory to solve support problems. These approaches generally require the determination of quantitative parameters which characterize the rock (strength and deformation), the support characteristics and the stress conditions. A simple but often used approach was developed by Hoek and Brown [1980]. By analyzing the structure of the rock mass surrounding the opening, blocks or wedges can be determined by stereographic projection techniques. Then the rock bolt scheme can be determined for a specific case. This method was further developed and now corresponding software (e.g. the code UNWEDGE) is replacing the calculations by hand.

2.2.2 Selection of rockbolt systems

For the selection of an appropriate rockbolt system in mining and especially in underground coal mining, the following general guidelines are given:

1. Mechanically anchored rockbolts should not be applied under following conditions:
    - soft rock that may affect the gripping force of the anchor,
    - in areas with seismic or blast loading due to the potential loss of tension,
    - for longterm bolting in fluid and/or aggressive environment because of the lag of protection of bolts,
    - in rock mass with large deformations,
    - in areas, where rock bursts or spalling may occur,
    - in areas where tension of rockbolts cannot be checked,
    - in areas where moments due to shear forces exist,
    - in areas, where the bond between the steel rod and the rock mass is too hard to establish.

2. Grouted rockbolts or cable bolts should not be used under the following conditions:
    - when quality of the grouting agent cannot be checked,
    - when continuous flow of groundwater into the borehole is observed,
    - when the system is immediately loaded after installation of the anchors,
    - when open joints or voids exist unless the grouting can be checked,
    - in case of extensive deformations if untensioned rockbolts are used,
    - in case of rockburst or spalling problems if pre-tensioned rockbolt are used.

3. Friction rockbolts should not be applied under the following conditions:
    - for long time bolting unless there is a way to protect the surface of bolts,
    - when moments due to shear forces occur.

4. Split set rockbolts should not be used under the following conditions:
    - in soft or fractured rock due to the potential loss of tension in the bolts,
    - in a cramped area,
    - where control of borehole diameters is difficult to achieve.

5. Swellex standard rockbolts should not be used where extensive deformations occur.

2.2.3 Bolting theories

The bolting effects can be explained by one or combinations of the following basic mechanisms: suspension, beam building, keying, improved properties of the rock mass and arching effect. These theories are explained in more detail below.

a. Suspension theory

When an underground opening is excavated, displacements of the surrounding rock mass occur. The magnitude and direction of these movements depend on many elements including strength of the rock mass, rock pressure and layering or fracturing. Also, size and shape (cross section) have an influence. Rockbolts can be able to suspend loosened rock layers to form a stable, solid rock as illustrated by Figure 2.3 [Jeremic, 1987].

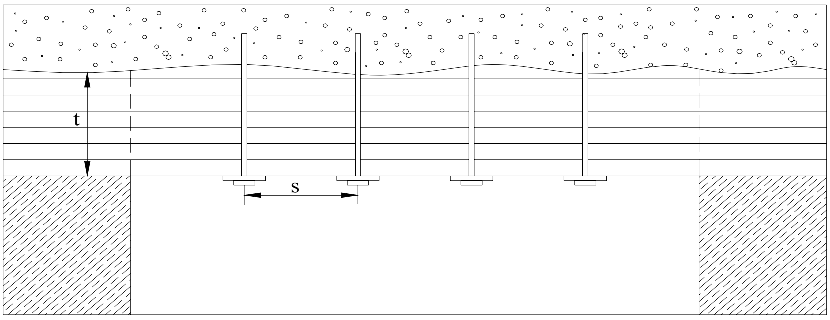

Figure 2.3 Suspension effect of rockbolts.

b. Beam theory

An other theory for designing rockbolt systems is the beam building. In this case, rockbolt stitches a number of thin, weak layers to a thicker, stronger layer, which has the effect to create a composite beam. Bolts go through these layers and make them working together well and force all the layers to move together with the same displacement (Fig. 2.4).

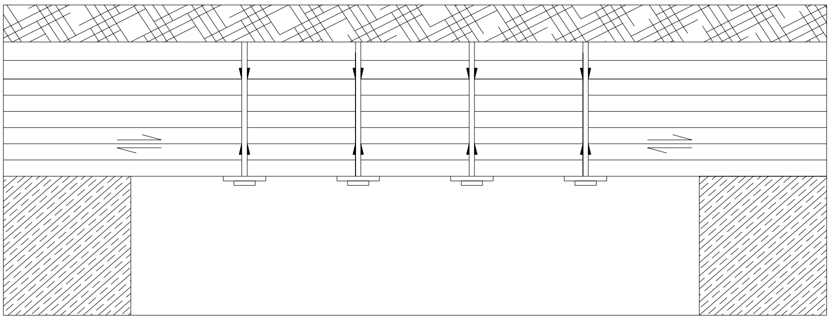

Figure 2.4 Beam building effect of rockbolts.

c. Theory of keying, Hobst [1983]

The third theory of bolting design is keying. The keying effect is based on the resisting force between the interface of the joints, blocks or discontinuities. This theory can be applied for roof strata which are either highly fractured and blocky or contain one or several sets of joints with different orientations. Rockbolts provide significant frictional forces along fractures, cracks or discontinuities. Sliding and/or separation along the interface is thus prevented or reduced to acceptable limits, as shown in Figure 2.5.

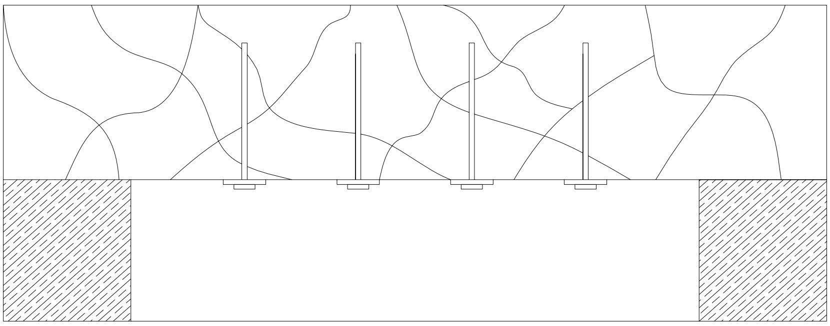

Figure 2.5 Keying effect of roof bolts.

d. Theory of improving the properties of the rock mass

Rockbolts are connected to the rock mass by cement grout, resin or mechanical linkage so that this area can be considered as a new composite material. The steel bar of the rockbolt has a high tensile strength, high Young's modulus and creates interlocking, so it improves deformation modulus and also ductility of the rock mass. For instance, when rockbolts are applied the coefficient K_s (see chapter 2.4.1.) increases and the rock mass strength rises correlatively.

d.1 Improving the deformation modulus of the rock mass

The increase of the Young's modulus and shear modulus by bolting is presented by Aydan [1989] according to the following formula:

$$\begin{aligned} \Delta E_x &= \left(E_b - E_m\right) \cdot n \\ \Delta G_y &= (G_b - G_m) \cdot n \qquad (2.1) \\ \Delta G_z &= (G_b - G_m) \cdot n \end{aligned}$$

where E_m,E_b elastic modulus of the rock mass and steel bar, respectively

G_m,G_b shear modulus of the rock mass and steel bar, respectively

and $n = A_b/A_t$

with A_b cross section of the steel bar

A_t cross section of the representative volume.

d.2 Improving the strength of the rock mass

Improvement of the strength of the rock mass can be incorporated by increasing the cohesive strength of the rock mass according to Fig. 2.6 [Zhao & Zhu, 2003]. The Mohr - Coulomb criterion is used to express the effect of the rockbolting as follows:

$$\sigma_1 = N_\phi \sigma_3 + 2c^* \sqrt{N_\phi} \tag{2.2}$$

where $$c^* = c + \Delta c = \frac{1}{2} \Delta\sigma_3 \sqrt{N_\phi} \tag{2.3}$$

$$N_\Phi = \frac{1+\sin\phi}{1-\sin\phi} \tag{2.4}$$

$$\Delta\sigma_3 = \frac{A_b \sigma_b \sin\phi}{s^2} \tag{2.5}$$

with s: spacing of the rockbolt, A_b: cross section of the rockbolt and

$$\sigma_b = E_b \varepsilon_b \text{ stress in the bolt.} \tag{2.6}$$

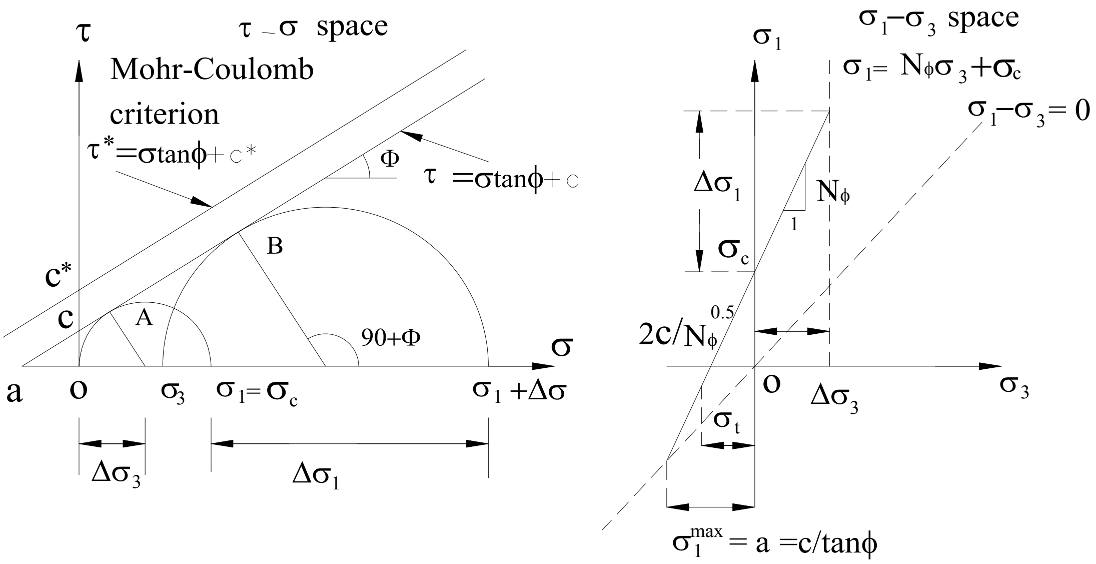
τ
τ – σ space
Mohr-Coulomb
criterion
τ*=σtanϕ+ c*
Φ
τ =σtanϕ+ c
B
c*
c
A
90+Φ
σ
a
o
σ3
σ1= σc
σ1 +Δσ
Δσ3
Δσ1
σ1
σ1–σ3 space
σ1= Nϕσ3+σc
σ1–σ3= 0
Δσ1
Nϕ
1
σc
0.5
2c/Nϕ
o
Δσ3
σ3
σt
σ1max = a =c/tanϕ

Figure 2.6 Strength increase of the rock mass by increasing confining stress.

e. Theory of arching

A natural arch is formed when an opening is excavated. The height of the natural loosening arch depends on the properties of the rock mass, the shape and size of the cross section of the opening as well as the excavation method. Rockbolts can be used to maintain the stability of the natural arch. Bolting can help to form an artificial arch according to Figure 2.7 [Stillborg, 1986]. Both, tensioned and untensioned grouted rockbolts can be used to create an artificial arch. The shear resistance is mobilized in the rock to improve the stability of the opening.

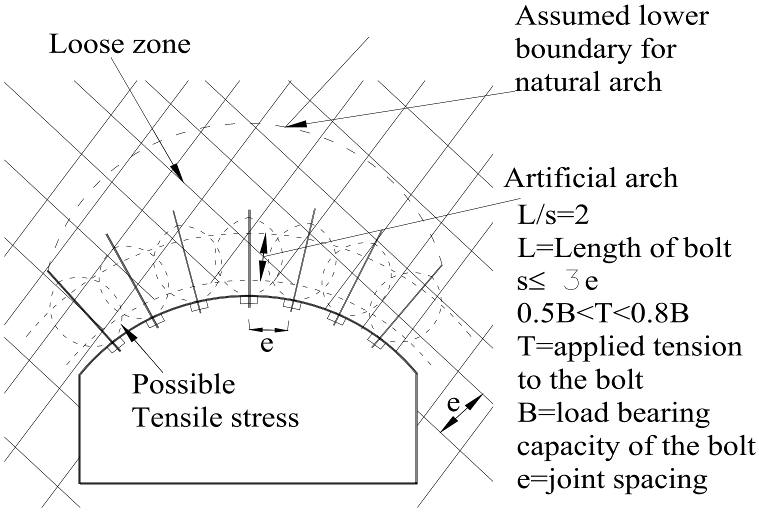
Loose zone
Assumed lower boundary for natural arch
Artificial arch
L/s=2
L=Length of bolt
s≤ 3e
0.5B<T<0.8B
T=applied tension to the bolt
B=load bearing capacity of the bolt
e=joint spacing
e
e
Possible Tensile stress

Figure 2.7 Traditional artificial arch forming [Lang, 1959].

2.3 Guidelines for the selection of the rockbolt system

In principal, three different approaches can be distinguished:

- Analytical approaches,
- Empirical assessments,
- Numerical simulations.

The empirical assessments are based on the rock mass classification, case histories and the experience of the engineers. The following three empirical assessment systems are widely and successfully used for rockbolt design.

1. Empirical design recommendations according to the US Corps of Engineers.
2. Empirical assessments based on the rock mass classification by Bieniawski.
3. Empirical assessments based on the Q-system by Barton et al.

2.3.1 Empirical design recommendations according to the US Corps of Engineers

These rules, formulated by the US Corps of Engineers, are the summary of an analysis of many important rock reinforcement case histories. Table 2.1 summarizes these findings [Stillborg, 1986].

Table 2.1 Typical design recommendations for rockbolts according to the US Corps of Engineers [Stillborg, 1986].

Parameter	Empirical rules
1. Minimum length and maximum spacing	
- Minimum length	Greatest of:
	(a) 2 x bolt spacing (b) 3 x thickness of critical and potentially unstable rock blocks (c) For element above the spring line: - Spans < 6 m : 0.5 span - Spans between 18 and 30 m: 0.25 x span - Spans between 6 and 18 m: interpolate between 3 and 4.5 m (d) For element below the spring line: - Height <18 m: as (c) above - Height >18 m: 0.2 x height
- Maximum spacing	Least of: (a) 0.5 x bolt length (b) 1.5x width of critical and potentially unstable rock blocks (c) 2.0 m
- Minimum spacing	0.9 to 1.2 m
2. Minimum average confining pressure	
- Minimum average confining pressure at yield point of elements	Greatest of: (a) Above spring line: Either pressure = vertical rock load of 0.2 x opening width or 40kN/m^2 (b)Below spring line: Either pressure = vertical rock load of 0.1 x opening height or 40kN/m^2 (c) At intersection: 2x confining pressure determined above

2.3.2 Empirical assessments based on rock mass characterization

Guidelines for excavation and support systems in rock tunnels were published by Hudson [2000] according to a general rock mass characterization given in Table 2.2.

Table 2.2 Types of bolting according to Peng and Tang Hudson [2000].

Types of rock bolt	Types of anchor	Suitable strata type	Comments
Point-anchored bolt (tensioned)	- Slot and wedge	- Hard rock	Used in the early stages
	- Expansion shell + Standard anchor + Bail anchor	+ Medium-strength rock + Soft rock	Most commonly used in USA
	- Explosive set	- Lower-strength rock	Limited use
	- Resin grout + Pure point anchor + Combination system	- All strata especially for weak rock	Recently increased usage + Resin length less than 24 inch + Resin length greater than 24 inch
	- Combination anchor (expansion shell and no mix resin)	- Most strata	Good anchorage with ‘no mix resin’
Full-length grouted bolt (nontensioned)	- Cement + Perforated + Injection + Berg jet + Cartridge	- Most strata	Disadvantages: (1) shrinkage of cement (2) longer setting time
	- Resin + Injection + Cartridge	- All strata	Recently increased use especially for weak strata
Special bolt + Yieldable bolt	Expansion shell	Medium-strength rock	It is an expansion-shell bolt with yielding device
+ Pumpable bolt	Resin anchor	Weak strata	Complex in installation
+ Helical bolt	Expansion shell	Most strata	In experimental stage
+ Split set	Full-length fraction	weak strata	Cheap but needs special installation equipment
+ Roof truss	Expansion shell	Adverse roof	Recommended for use at intersection and/or heavy pressure area
+ Cable sling	Cement anchor and full-length friction	Weak strata	Substitute for timber, steel or truss support

+ Lateral force system	Full-length 2-piece steel	Soft strata	Applying full-length lateral force (compression to the strata)
+ Swellex bolt	Full-length holding	Water-bearing strata	Using high-pressure water to swell the steel tube thus holding the rock

2.3.3 Design chart for rockbolt reinforcement by Panek

This is a special nomogram applicable for horizontally bedded roofs in weak rock with pretensioned bolts. The design procedure includes 6 steps (Figure 2.8):

1. Selection of the length of the bolts based on the thickness of layer in the roof.
2. Determination of the pretension of the bolts.
3./4. Determination of the density of the bolt (bolt number in a row and distance between rows).
5./6. Checking of the span of the opening in order to determine the reinforcement factor.

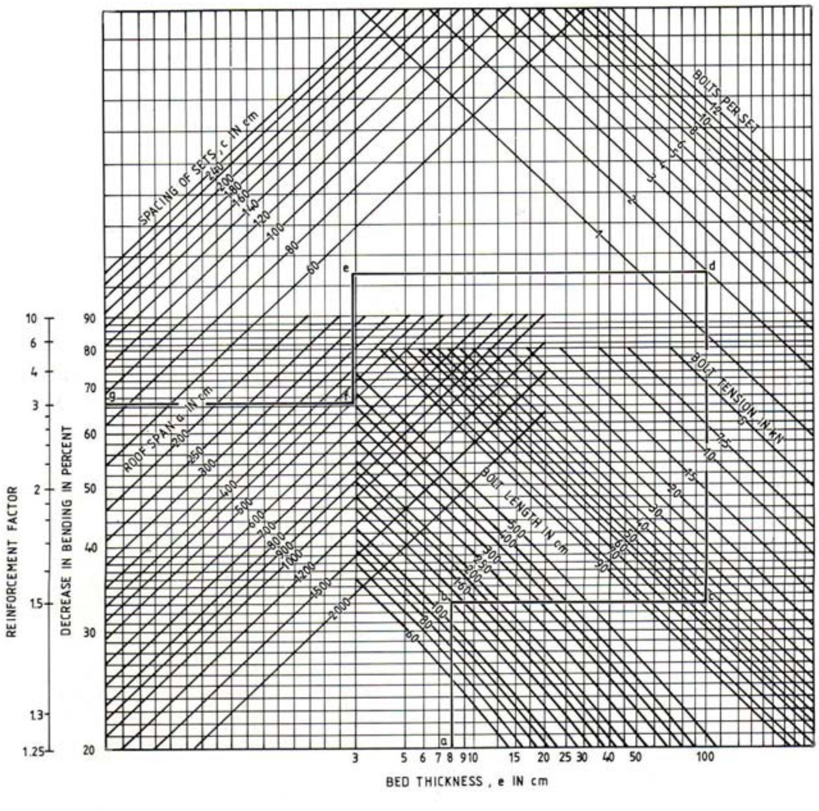

Design chart for rockbolt reinforcement of horizontally-bedded weak rock. After PANEK (1964).

Figure 2.8 Nomogram for rockbolt reinforcement of horizontally bedded rock. [Hudson, 1993]

2.3.4 Design chart for rock bolt reinforcement based on the Q system

This recommendation is based on the ratio between span or height of the opening and coefficient ESR and Q designation [Barton & Lien, 1974 and 1980]. The rock mass is categorised by Barton into 9 qualities from extreme good to exceptionally poor based on the quality of the rock mass Q (Fig. 2.9). The quality of the rock mass Q is assessed by rock quality designation (RQD), joint set number (Jn), joint roughness number (Jr), joint alteration number (Ja), joint water reduction number (Jw) and stress reduction factor (SRF). The value of Q-rating can be calculated by the formula:

$$Q = \frac{RQD}{J_n} \cdot \frac{J_r}{J_a} \cdot \frac{J_w}{SRF} \qquad (2.7)$$

The value of ESR depends on the scale of the opening [Barton et al., 1974]. Values of ESR range from 0.8 to 5. Reinforcement is categorised into the following types [Grimstad & Barton, 1993]:

1. Unsupported area,
2. Spot bolting,
3. Systematic bolting,
4. Systematic bolting with 40÷100 mm unreinforced shotcrete,
5. Fibre-reinforced shotcrete, 50÷ 90 mm, and bolting,
6. Fibre-reinforced shotcrete, 90÷ 120 mm, and bolting,
7. Fibre-reinforced shotcrete, 120÷ 150 mm, and bolting,
8. Fibre-reinforced shotcrete, > 150 mm, with reinforced ribs of shotcrete and bolting,
9. Cast concrete lining.

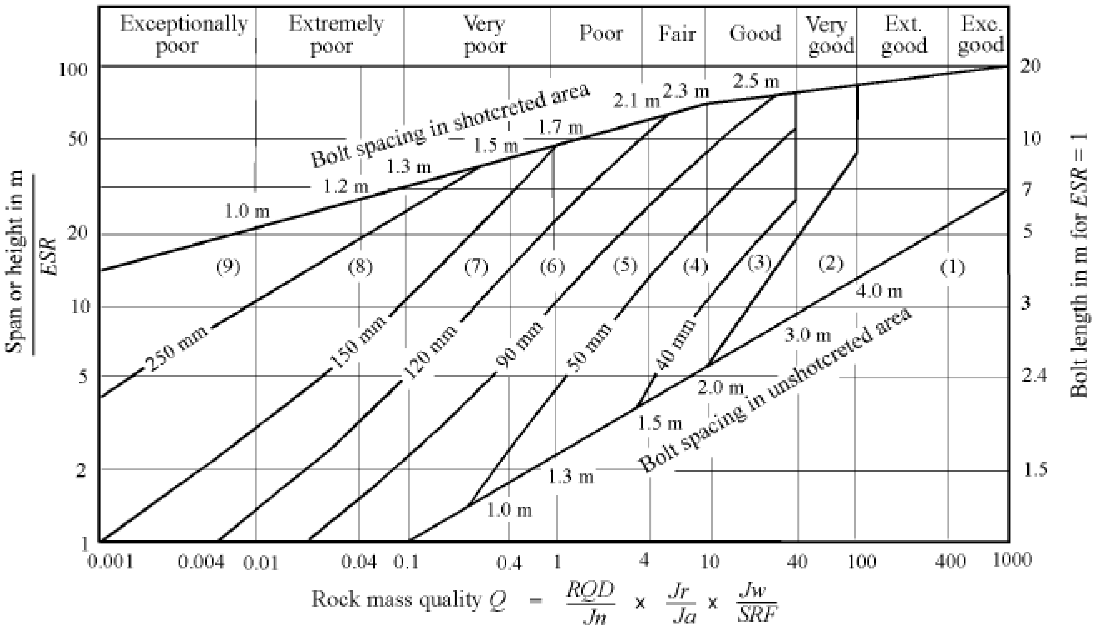

Figure 2.9 Nomogram for rockbolt design based on Q designation.

2.3.5 Recommendation based on the Rock Mass Rating System RMR

This recommendation is based on the Rock Mass Rating System (RMR). The rock mass is classified into 5 groups by its rating. The maximum point of 100 is then divided into 5 equal parts, each one has a maximum of 20, 40, 60, 80 and 100 points, respectively (Tab. 2.3). The assessment of RMR is based on parameters of the rock mass such as strength of the intact rock, rock quality designation (RQD), spacing of discontinuities, the condition of discontinuities, ground water and stress field [Bieniawski, 1989].

Table 2.3 Guidelines for excavation and support systems in rock tunnels [Bieniawsky, 1979].

Rock mass class	Excavation	Support		
		Rock bolts (20 mm in diameter, fully bonded)	Shotcrete	Steel sets
Very good rock I RMR: 81÷100	Full face 3 m advance	Generally no support required except for occasional spot bolting		
Good rock II RMR: 61÷ 80	Full face 3 m advance 1.0÷1.5 m advance Complete support 20 m from face	Local bolts in crown 3 m long, spaced 2.5 m with occasional wire mesh	50 mm crown where required	None
Fair rock III RMR: 41÷ 60	Top heading and bench, 1.5÷ 3 m advance in top heading. Commence support after each blast. Complete support 10 m from face	Systematic bolts 4 m long, spaced 1.5÷2 m in crown and wall with wire mesh in crown	50÷100 mm in crown and 30 mm in sides	None
Poor rock IV RMR: 21÷ 40	Top heading and bench, 1.0÷ 1.5 m advance in top heading. Install support concurrently with excavation 10 m from face	Systematic bolts 4÷5 m long, spaced 1.0÷1.5 m in crown and wall with wire mesh	100÷150 mm in crown and 100 mm in sides	Light to medium ribs spaced 1.5 m where required
Very poor rock V RMR: <20	Multiple drifts, 0.5÷ 1.5 m advance in top heading. Install support concurrently with excavation. Shotcrete as soon as possiple after blasting	Systematic bolts 5÷6 m long, spaced 1.0÷1.5 m in crown and wall with wire mesh. Bolt invert	150÷200 mm in crown and 150 mm in sides and 50 mm on face	Medium to heavy ribs spaced 0.75 m with steel lagging and fore-poling if required. Close invert

(Shape: horseshoe; width: 10 m; vertical stress: below 25 MPa; construction: Drilling and blasting).

2.4 Rockbolt design

2.4.1 Design based on the suspension principle

In Vietnam and other countries a method based on the suspension method and recommended by the VNIMI – Institute (Vo, 1998) is applied. The procedure is outlined below and contains several steps.

a. Safety factor of the rock mass

$$n_r = \frac{\sigma_t K_s \xi}{K_2 \lambda_1 \gamma H} \quad (2.8)$$

$$n_s = \frac{\sigma_c K_s \xi}{K_1 \lambda_1 \gamma H} \quad (2.9)$$

where: n_r safety factor of the roof rock mass

σ_t tensile strength of the intact rock

ξ coefficient adjustment for a long term

K_s coefficient adjustment for structural weakness discontinuities

K_2 coefficient which accounts for the stress concentration in the roof

λ_1 lateral pressure coefficient

γ density of the rock mass

H depth of the opening

σ_c compressive strength of the intact rock

K_1 coefficient which accounts for the stress concentration in the sidewalls

n_s safety factor of the sidewall rock mass

Coefficients K_s, ξ can be selected by the distance between the discontinuities (see Tab. 2.4, coefficient ξ for brittle rock $\xi = 1{,}0 \div 0{,}7$; for the ductile rock $\xi = 0{,}5 \div 0{,}7$).

Table 2.4 Value of the structural coefficient (K_s).

Average distance between the discontinuities (m)	Value of K_s
> 1.5	0.9
1.5 ÷ 1.0	0.8
1.0 ÷0.5	0.6
0.5 ÷ 0.1	0.4
< 0.1	0.2

b. Determination of parameters of the rockbolts

The density of the rockbolts is calculated by the formula:

$$S = \frac{q_r n_r}{P_{rb}} \qquad (2.10)$$

where S rockbolt density (pieces /m^2)

q_r roof pressure

n_r coefficient of safety $n_r > 1$

P_{rb} capacity of the rockbolts, for the fully grouted rockbolt it is the lowest value of P_{rb} based on the three following cases:

- The yield of the steel bar is determined by:

$$P_{rb1} = F_c R_k \qquad (2.11)$$

where F_c cross section of the steel bar

R_k tensile yield strength

- The bonding of steel bar and concrete is calculated by formula:

$$P_{rb2} = \pi d_s c_1 l_z \qquad (2.12)$$

where d_s diameter of steel bar

c_1 cohesion between steel bar and cement grout (determined by experiment)

l_z length of steel bar in the grout

- Bonding of cement grout with the borehole wall is determined by formula:

$$P_{rb3} = \pi d_b c_2 l_z \qquad (2.13)$$

where d_b diameter of the borehole

c_2 cohesion between borehole wall and cement grout (determined by experiment)

The distance between bolts is calculated by the formula

$$d = \sqrt{\frac{1}{s}} \qquad (2.14)$$

Table 2.5 Value of the coefficients n_s, n_r.

Value of n_r, n_s	Recommendation
$n_r \geq 4$ $n_s \geq 4$	Roof and sidewall of the opening are very stable, solid, no support required, spotted shotcrete at jointed and weathered places
$n_r < 1$ $n_s < 1$	Roof and sidewall are weak so that support is required
$1 < n_r < 4$ $1 < n_s < 4$	Roof and sidewall of the opening are stable, solid, but combination between rockbolt and shotcrete is required

2.4.2 Design based on beam-building principle

This principle is based on the shape of the cross section and the structure of the rock mass. It was introduced in a broad spectrum by several authors. Some design procedures are presented here exemplary.

a. Design considerations based on simple geometrical considerations [e.g. Konietzky, 2005]

a.1 The opening has rectangular shape and rock mass is homogeneous

Length of the bolts determine the height of the considered beam. Each anchor has a load capacity N with n pieces distributed along span 2b of the cross section so that they create a prestress in the beam (Fig. 2.10).

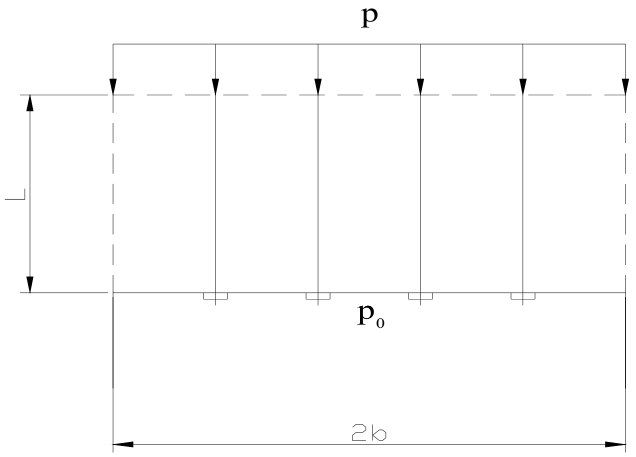

Figure 2.10 Sketch for calculating the length of the bolts.

This vertically directed prestress p^0 is calculated by the formula:

$$p^0 = \frac{nN}{2b} \tag{2.15}$$

The prestress p^0 will be mobilized through Poisson's ratio k, which creates a tension along the length of the bolt by friction. To prevent shearing, the following condition must be satisfied:

$$\text{nNL} = \frac{2pb^2}{\lambda f} \tag{2.16}$$

where:
- b half of the opening span
- λ lateral pressure coefficient
- f Protodjakonov coefficient ($f = \tan\phi$)
- p vertical pressure
- L length of the bolts

a.2 The opening has rectangular shape and the rock mass consist of layers

Rockbolts sustain preliminary stress p^0 so that shearing will not occur along the bedding planes. Shear stress distribution in the intact bolted beam along the length L is given below (h is the height of the beam, range of y: $h/2 \le y \le +h/2$, see Fig. 2.11)

$$\tau(x, y) = 1.5\frac{Q(x)}{L}\left[1 - 4\left(\frac{y}{L}\right)^2\right] \tag{2.17}$$

Therefore, $$\tau_{\max}(x) = \tau(y{=}0) = 1.5\frac{Q(x)}{L} \tag{2.18}$$

where $Q(x) = px$

Failure along the bedding planes will occur, if one or both of the following conditions are satisfied:

- The cohesionless layers sustain a normal stress $p^0 = \dfrac{nN}{2b}$ (2.19)
- The layers sustain a horizontal shear force:

$$F_s = bp^0 \tan\phi' = b\,\frac{nN}{2b}f' = \frac{nN}{2}f' \tag{2.20}$$

where ϕ' frictional angle; f' frictional coefficient between layers.

This shear force F_s must be equal to the driving shear force F_Q:

$$F_Q = \frac{3}{4}\frac{pb^2}{L} \tag{2.21}$$

For $F_s = F_Q$ we get $\dfrac{nN}{2}f' = \dfrac{3}{4}\dfrac{pb^2}{L}$ or $nNL = \dfrac{3}{2}\dfrac{pb^2}{f'}$ (2.22)

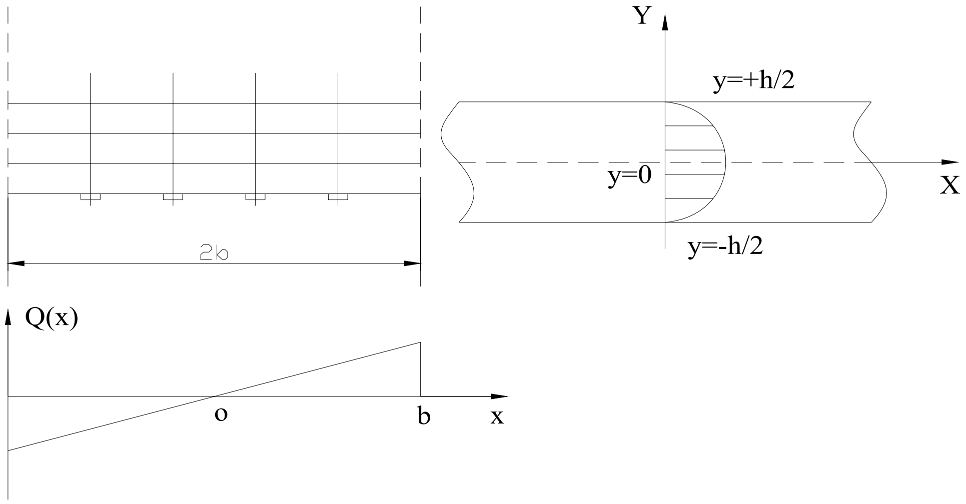

Figure 2.11 Sketch for creating the beam in a laminated flat roof.

a.3 The opening has rectangular shape and anchors create a beam

It is assumed that a bolted beam sustains a moment distribution. The moment will not cause a failure of the bolted beam. It forms a compressive arch. That binding arch induces a side-shear force F_T as a horizontal force according to Figure 2.12:

$$F_T = \frac{p_0 b^2}{2 f_0} \tag{2.23}$$

where f_0 is the rise of the arch.

The incorporated force F_T has a triangular distribution. A tensile stress does not exist. The side-shear force F_T is also defined by the compressive strength of the rock:

$$F_T = \frac{\sigma_c}{2} h \tag{2.24}$$

The triangular load distribution causes another arch line and the height of the new arch is

$$f_0 = L - \frac{2}{3} h = L(1 - \frac{2}{3}\alpha) \tag{2.25}$$

where $\alpha = \dfrac{arch\ slab\ h}{thickness\ of\ the\ bolted\ area\ L}$ (h=αL)

From equations (2.23) and (2.24) we obtain

$$f_0 = \frac{pb^2}{\sigma_c \alpha L} \tag{2.26}$$

From equations (2.25) and (2.26) we obtain

$$\alpha = \frac{3}{4}\left(1 \pm \sqrt{1 - \frac{8}{3}\frac{pb^2}{\sigma_c L^2}}\right) \tag{2.27}$$

α takes only a real value, so that the length of the bolt can be expressed as follows:

$$L \le \frac{4}{3}\frac{pb}{f\sigma_c} + \frac{1}{2}fb \tag{2.28}$$

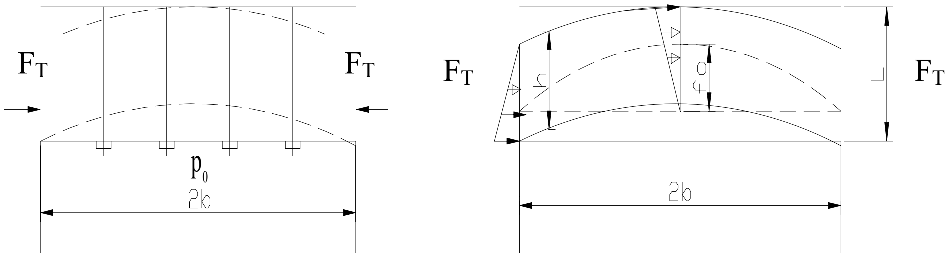

Figure 2.12 Sketch for creating a beam in a homogeneous flat roof

a.4 The opening has arched shape and the anchors create a beam

The anchors create a stable composite arch. The effective thickness of the "bond link age" d is equal to the length of anchor minus the distance between the bolts a (Fig. 2.13).

$$d = L - a \tag{2.29}$$

Within the area d, the anchor force A is equal to the induced radial pressure $\sigma_r = A/a^2$ (Distance of the bolt in square grid).

Stress without rockbolt is characterized by radial stress $\sigma_r = \sigma_3 = 0$ and tangential stress $\sigma_\varphi = \sigma_1$. The stress with rockbolt is characterized by a radial stress $0 + \Delta\sigma_3 = \Delta\sigma_3$, where the radial stress $\Delta\sigma_3 = A/a^2$ is calculated by the anchor force. The tangential stress is given by $\sigma_\varphi + \Delta\sigma_1$. $\Delta\sigma_1$ is the increment of tangential stress and calculated by radial stress $\Delta\sigma_3$ and the increase of the rock mass load capacity given by $\Delta\sigma_1=\alpha_1\Delta\sigma_3$ with $\alpha_1 = \tan^2(\frac{\pi}{4}+\frac{\varphi}{2})$. For intact rock, φ is frictional angle of the rock mass. For broken rock, φ is frictional angle of the fracture area (joint friction angle). The axial force of the bolt N is created according to the following formulas:

$$\Delta\sigma_1 = \alpha_1\sigma_r \tag{2.30}$$

$$N = a_1\,\sigma_r\,(L\text{-}a) = \frac{a_1 A}{a^2}(L\text{-}a) \tag{2.31}$$

The pressure of the composite arch p_a and radius r_a are given by:

$$r_a = r_0 + L - a / 2 \qquad (2.32)$$

$$p_a = \frac{N}{r_a} = \frac{a_1 A}{a^2} \; \frac{L-a}{r_0 + L - a/2} \qquad (2.33)$$

p_a is proportional to a_1 and inverse proportional to a^2.

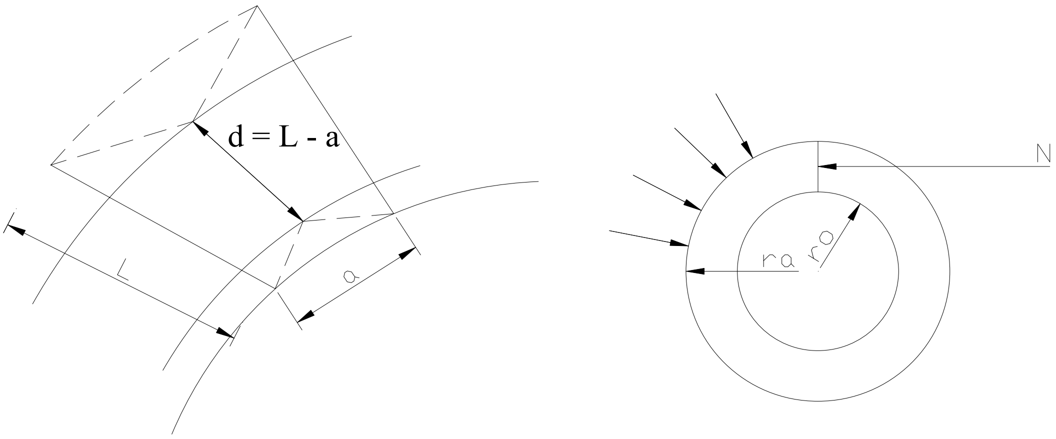

Figure 2.13 Sketch for creating a beam in the arched roof.

b. Rockbolt design introduced by Junker

Junker et al. [2006] propose a design method based on the fissure body suspension. The analytical solution considers a rectangular cross section. It is assumed, that the bolting creates a beam – structure in the roof and that the triangular load from the key block in the roof is transmitted by the beam to the sidewalls.

The following equations are used for the calculation of the rockbolt pattern:

$$\sigma_{max} = M_{max} 6/(bd) \qquad (2.34)$$

where

$$d = (M_{max} 6/(\sigma_z f_g d))^{1/2} \qquad (2.35)$$

$$q_0 = 2(K_F s f_{dyn} + F_{EHB})/B \qquad (2.36)$$

$$M(x) = F_A x - q_0 x^3/(3B) + \sum_{i=1}^{n} FS(i)(x - x(FS(i))) \qquad (2.37)$$

$$d = L_A - a \qquad (2.38)$$

K_F	body weight of the key block
s	safety factor
f_{dyn}	coefficient for dynamic loading part
FA, FB	reaction forces in the stope A, B
FS(i)	force of the i-th prop
x (FS(i))	distance between the i-th prop and the stope

q_0	peak value of the triangle-shaped line load due to the body weight of the key block
x	chosen axes in cross-section direction, defined as x from stope A
B	cross section width
M_{max}	maximum bending moment
M(x)	bending moment at location x
σ_{max}	maximum tensile stress in the beam due to bending
d	beam height
b	beam width
a	distance between rockbolts
fg	rock mass structural factor
L_A	anchor length

c. The opening has arched shape and rock mass is homogeneous

The beam’s capacity can be determined according to Nguyen [1998]:

$$F_Q = 0.5th\sigma_c \tag{2.39}$$

where t width of the beam

h height of the beam

σ_c compressive strength of the rock

Pressure applied to the beam is determined by the equation

$$F_T = \frac{ql_0^2}{8f_0} \tag{2.40}$$

where $l_0 = L + 2h_1\sin\alpha + 2h\sin\alpha$; l_0 is span of the beam and L is span of the opening; $h_1 = a_1/f$; a_1 is distance between the bolts and f is stiffness of the rock mass according to Protodjakonov classification.

The distance f_0 is calculated by:

$$f_0 = f_1 + h_1(1-\cos\alpha) + 0.5h(1-\cos\alpha) \tag{2.41}$$

where: f_1 rise of the arch

α is angle of the arch

$$f_2 = f_1 + h_1(1-\cos\alpha) \tag{2.42}$$

$q = q_1 + \gamma h$ pressure applied to the beam and

$q_1 = L_1\gamma n/2f$; n=2÷3 is coefficient of safety.

l_z length of bolt (in solid rock $l_z = 0.3$)

with $L_1 = L + 2h + 2h_1$

Fig. 2.14 explains the meaning of the quantities. To stabilize the beam, the beam's capacity F_Q must be equal to pressure F_T:

$$\left[2\sigma_c(1-\cos\alpha) - q\sin^2\alpha\right]h^2 + \left(4\sigma_c f_2 - 2ql_1\sin\alpha\right)h - ql_1^2 = 0 \qquad (2.43)$$

By solving this equation we obtain the thickness of the beam (h). The length of the bolt is calculated by:

$$l_a = h + h_l + 1.5l_z \qquad (2.44)$$

The distance between bolts can be calculated by:

$$d = (0.5 \div 0.7)l_a \qquad (2.45)$$

The load applied to one rockbolt is

$$q_a = \gamma d^2(h + h_1) \qquad (2.46)$$

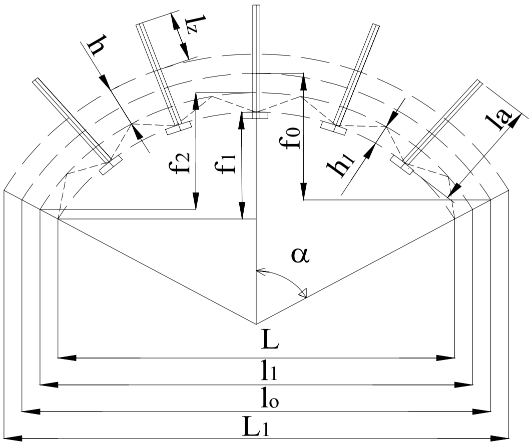

Figure 2.14 Sketch for beam creation in bolted arch shaped roof.

d. The opening has rectangular shape and the rock mass is homogeneous

The pressure applied to the beam is:

$$F_T = \frac{qL^2}{4l_1} \qquad (2.47)$$

The height of the beam is determined so that strength of the rock is greater than the induced stress:

$$l_1 = \sqrt{\frac{qL^2}{\sigma_c}} \qquad (2.48)$$

The length of the rockbolt is calculated by the formula:

$$l_a = l_l + h_l + 1.5l_z \qquad (2.49)$$

The distance between rockbolts can be calculated by the formula:

$$d = \sqrt{\frac{6m^2 l_a \left(0{,}5 f_\pi \gamma l_a + k\tau_p\right)}{n\gamma\left(L - L_1\right) L tg\delta}} \qquad (2.50)$$

where m ≤ 2÷3; size of rock block.

$f_\pi = 0.3 \div 0.6$; coefficient which accounts for jointed level of the rock mass,

k = 1/20 ÷1/30; empirical coefficient,

τ_p shear strength of the rock mass,

$\delta = 60 \div 80°$; angle of the rock at the abutment,

n safety factor, with $L_1 = \eta\sqrt{0.04\sigma_n t_i / n\gamma \cos\alpha}$,

$\eta = 0.5 \div 0.8$ is a coefficient which takes into account rheology,

t_i distance of the discontinuities,

α angle between the discontinuities.

2.5 Interaction between the rockbolt and the rock mass

Before, during and after the excavation and installation of the support the stress and strain development depends on the rock mass, the opening geometry, the support system and time delay of support installation. The interaction between the support and the rock mass can be described by the ground reaction curve [Deere et al., 1970]. The relationship between radial deformation and radial load depends on the ground properties and mechanical support parameters, the required support curve and the delay of the support installation (Fig. 2.15). Segment OA represents the radial displacement before the support is installed. Line AA' displays the load in case the support is incompressible. But obviously, the support is deformed and equilibrium is reached at point C. At that time the radial displacement is represented by segment OB and the support deformation is equal to AB. The corresponding support load is represented by BC. Line AeE represents ground arch falling. Line AF means the support is too flexible and line GH means that the support is installed too late.

In addition, the assessment of the reinforcement by rockbolts can be performed by analytical calculations, ordinary in-situ tests or numerical analysis [Oreste, 2003].

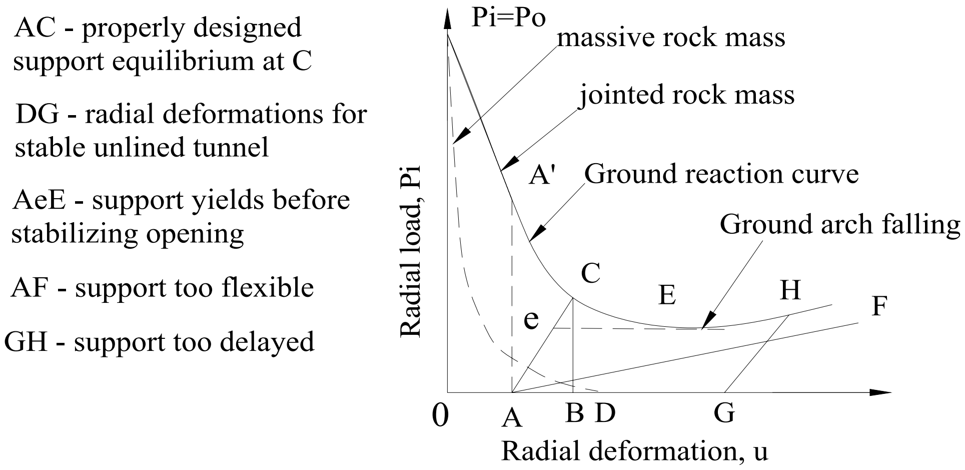
AC - properly designed support equilibrium at C
DG - radial deformations for stable unlined tunnel
AeE - support yields before stabilizing opening
AF - support too flexible
GH - support too delayed
Pi=Po
massive rock mass
jointed rock mass
A'
Ground reaction curve
Ground arch falling
C
E
H
F
e
Radial load, Pi
0
A
B
D
G
Radial deformation, u

Figure 2.15 Concept of ground reaction curve.

Experimental results were obtained by performing tests on models with and without rockbolts (Table 2.6). The results reveal a significant increase in Young's modulus and strength when rockbolts are applied to the models [Sakurai & Kawashima, 1992].
The interaction is also documented by Figure 2.16. This diagram shows the relation between stress and strain in both hard rock and soft rock with and without bolts.

Table 2.6 Value of the rock strength after and before application of rockbolts.

Parameters	Without RB(a)	With RB(b)	Ratio (b/a)
Young's Modulus (MPa)	82	383	4.67
Compressive strength (kPa)	280	980	3.5
Young's Modulus (MPa)	72	137	1.9
Compressive strength (kPa)	280	450	1.6
Young's Modulus (MPa)	78	118	1.51
Compressive strength (kPa)	280	340	1.21

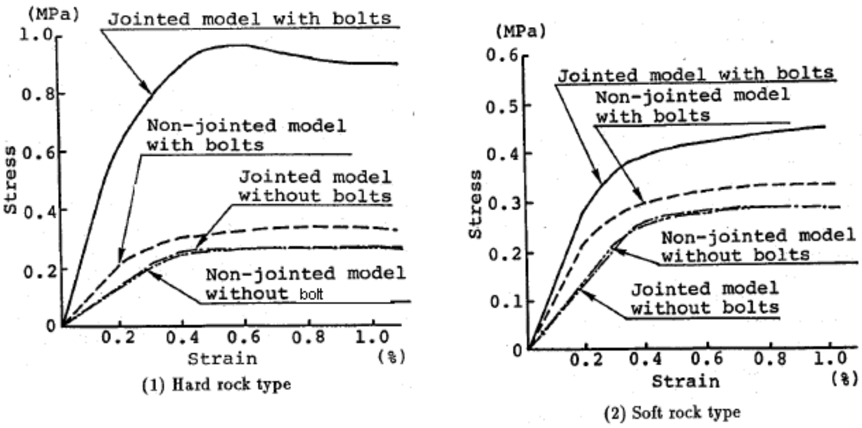

(1) Hard rock type

(2) Soft rock type

Figure 2.16 Experimental stress-strain relation obtained from models with and without bolts [Sakurai & Kawashima, 1992].

The effect of rockbolts can also be explained by an increase in cohesion and internal friction angle of the surrounding rock mass. Obviously, calculating the magnitude of such an increase is difficult. The rock support interaction in tunnels was also studied by the convergence- confinement method. Some authors (Grasso et al., 1989 and 1991; Indraratna & Kaiser, 1987; Oreste, 2003) suggest a formula for calculating the increased cohesion:

$$C^* = C + \frac{1+\sin\varphi}{2\cos\varphi}\Delta\sigma_3 \tag{2.51}$$

where: φ friction angle of the rock mass

C natural cohesion of the rock mass

$$\Delta\sigma_3 = \frac{T_{med}}{S_t S_l} \tag{2.52}$$

$\Delta\sigma_3$ confinement produced by the action of the grouted bolts

T_{med} mean force along each bolt

S_t and S_l transversal and longitudinal spacing, respectively.

3 Simulation of nonlinear behaviour for cable and rockbolt elements

3.1 Overview of FLAC

FLAC [ITASCA 2005] is the abbreviation of "Fast Lagrangian Analysis of Continua" and is developed and maintained by ITASCA. The FLAC software is based on the explicit finite difference method. FLAC can simulate the behaviour of materials such as soils, rocks and structural buildings. Besides that, it can solve a wide range of complex problems in geotechnics, civil engineering and mining. In addition, the imbedded internal programme language, called FISH, and the C^{++}-DLL-Technique allows to implement user-defined constitutive models, so that it is a perfect tool for design, studies and research in rock mechanics, soil mechanics or similar fields.

FLAC can simulate large objects including the following subjects and phenomena:

- Interfaces
- State of plane strain, plane stress or axi-symmetry
- Ground water flow
- Structural elements
- Dynamic analysis
- Creep analysis
- Thermal phenomena
- Thermal-hydro-mechanical coupling

3.2 Introduction to cable and rockbolt element

There are many structural elements introduced in FLAC such as beam, cable, pile, liner, rockbolt, strip and support members. The purpose of structural elements is to stabilize a rock or soil mass. Each structural element has its own characteristic features. The numerical structural elements are simulated based on their real properties either as elastic or elasto-plastic elements.

The structural elements can generally bear static or dynamic load or fail in case of overload. In reality, besides pure loading also unloading and reloading in plastic period occurs (e.g. during blasting, earthquake loading or complex static loading paths).

In FLAC, so far there is no built-in function written in order to describe cyclic elasto-plastic behaviour of structural elements. Therefore, FISH-functions were developed, implemented and tested to improve the cable and rockbolt elements, so that they can simulate cyclic elasto-plastic behaviour including hardening. The simulations are carried out in models with cable and rockbolt element which have one or several segments.

3.2.1 Numerical implementation of the cable element

The cable element is a one-dimensional axial element that can sustain tension and compression forces, but it doesn't have the capacity to bear bending moments. Cable elements can model a wide variety of support measures which mainly have tensile capacity including rockbolts. Moreover, it can be used for modelling the shear resistance along their length as it is provided by the shear resistance between the grout and the cable bar, and between the grout and rock mass. In respect to anchors the cable element can be considered as a steel bar with high slenderness, so it has the capacity to sustain uniaxial tension and compression.

a. Axial behaviour

The axial stiffness is described by cross section A and Young's modulus E of the cable. The increment of the axial force is determined by the formula:

$$\Delta F^t = -\frac{EA}{L}\Delta u^t \tag{3.1}$$

where L contributing cable length

A cross-sectional area of the cable element

E Young's modulus of the cable element

The components of the element are displayed in Figure 3.1, where

$\Delta u^t = \left(u_1^b - u_1^a\right)\cdot t_1 + \left(u_2^b - u_2^a\right)\cdot t_2$ is the increment of axial displacement.

The force and displacement components of the numerical cable element include:

- Displacement at nodal point is computed along the cable axis,
- Out-of-balance force at each nodal point, shear force along the grout annulus got from axial force,
- Axial displacement obtained from out-of-balance force and mass cumulated at each nodal point.

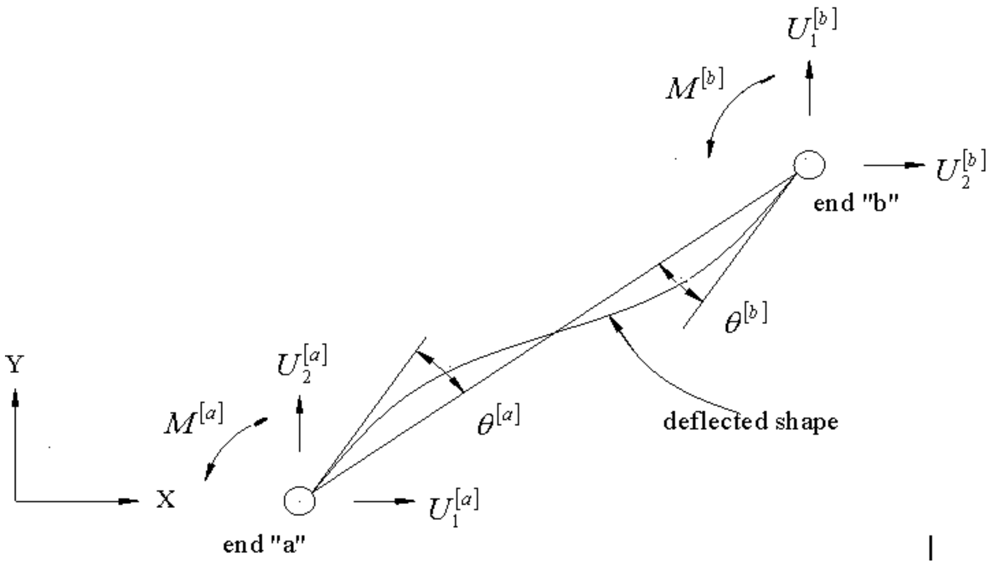
$U_1^{[b]}$
$M^{[b]}$
$U_2^{[b]}$
end "b"
$\theta^{[b]}$
Y
$U_2^{[a]}$
$M^{[a]}$
$\theta^{[a]}$
deflected shape
X
$U_1^{[a]}$
end "a"

Figure 3.1 Components of a numerical cable element (t_1, t_2 direction cosines of the element referred to tangential direction)[ITASCA 2005].

b. Shear behaviour of grout annulus

A spring-slider system, simulated at the nodal points, is presented for shear behaviour of the grout annulus. K_{bond} is the grout shear stiffness of the numerical interface between the grout/rock mass and grout/cable element.

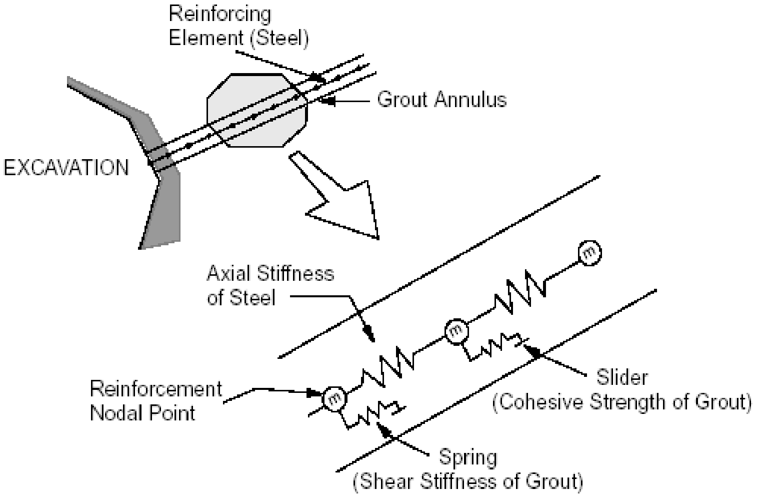
Reinforcing Element (Steel)
Grout Annulus
EXCAVATION
Axial Stiffness of Steel
Reinforcement Nodal Point
Slider (Cohesive Strength of Grout)
Spring (Shear Stiffness of Grout)

Figure 3.2 Outline of numerical cable element [ITASCA 2005].

The grout shear stiffness is determined by shear force and relative displacement between components of cable following formula 3.2:

$$\frac{F_s}{L} = K_{bond}(u_c - u_m) \tag{3.2}$$

where F_s shear force which is developed along the interface between cable and grid

u_c axial displacement of the cable

u_m axial displacement of the rock mass

The cohesive strength of the grout is controlled by parameter S_{bond}. The stress-dependent frictional resistance of the grout is parameter $S_{friction}$. The input properties for the cable element can be determined by the following relations [ITASCA 2005]:

- Grout shear stiffness K_{bond}:

$$K_{bond} \approx \frac{2\pi G}{10\ln(1+2t/D)} \tag{3.3}$$

- Cohesive bond strength S_{bond}:

$$S_{bond} = \pi(D+2t)\tau_{peak} \tag{3.4}$$

where G grout shear modulus

t thickness of grout annulus

D diameter of the cable

$$\tau_{peak} = \tau_1 Q_B \tag{3.5}$$

where τ_1 is equal to half the uniaxial compressive strength of either rock or grout which has a smaller value. Q_B describes the quality of the bond between grout and rock.

3.2.2 Numerical implementation of the rockbolt element

The rockbolt element is derived from the pile element which combines the cable and beam element. It can transfer normal forces, shear forces and bending moments to the grid. Furthermore, rockbolt has capacity of tensile fracture, strain-softening behaviour and the effect of changes in confining stress. The rockbolt element can simulate nonlinear effects, grout or resin bonding. The properties of the rockbolts are similar to those of cables, but have also some additional features [ITASCA 2005]:

- Rockbolt elements interact with the grid through shear and normal coupling springs.
- Coupling springs are nonlinear linkages that transfer forces and displacements between the rockbolt elements and the grid at its nodes.
- Shear coupling springs describe the shear behaviour of the grout.
- Behaviour of the normal coupling springs include the capability of the model to simulate load reversal and the formation of a gap between the rockbolt and the grid.

- Normal coupling springs simulate the effect of a squeezing medium around the rockbolt; a force-displacement law for the normal springs can also be defined externally by a FISH function.
- Shear response of the rock mass/grout interface can be estimated by the following parameters:
  - Frictional resistance of the shear coupling springs,
  - Stiffness of the shear coupling springs,
  - Cohesive strength of the shear coupling springs.
- The normal behaviour of the rockbolt/grid interface can be estimated by a linear spring with a limiting normal force.
- Cohesive (and tensile) strength exist for the normal coupling springs.
- Stiffness and frictional resistance exist for the normal coupling springs.

3.3 Set-up numerical models with nonlinear character in 2D and 3D

3.3.1 Nonlinear characteristics

The cable element is not designed to bear bending moments, but this element is able to model a wide variety of support measures which mainly have tensile capacity, including rockbolts. Cable elements can be used for modelling the shearing resistance along their length, as provided by the shear resistance between the grout and the cable, or the grout and the host medium. Axial displacement is obtained by integration of the law of motion using the computed out-of-balance axial force and a mass lumped at each nodal point based on accelerations.

To incorporate non-linearity to the cable elements, the Young's modulus was adjusted. This was realized by using a reduction factor A (Table 3.1, which gives an example)
In the elastic period, the relationship between stress and strain obeys the Hooke's law:

$$\varepsilon = \sigma / E \qquad (3.6)$$

Table 3.1 Properties of the non-linear elasto-plastic cable element [Hausdorf 2006].

Value of ε			Δσ (Mpa)	Δε	E (GPa)	Factor A=225 GPa/ E
0.000	≤ ε ≤	0.002	450	0.002	225	1
0.002	≤ ε ≤	0.007	0	0.005	0.0	(∞)
0.007	≤ ε ≤	0.030	80	0.023	3.5	64
0.030	≤ ε ≤	0.070	116	0.040	2.9	78
0.070	≤ ε ≤	0.090	42	0.020	2.1	107
0.090	≤ ε ≤	0.100	12	0.010	1.2	188

According to Table 3.1 the Young's modulus is adjusted by the factor A so that the non-linear behaviour given by Figure 3.4 is obtained. The approach developed by Hausdorf [2006] only contains the loading phase and is not able to simulate unloading, reloading and cyclic loading.

3.3.2 Input data for the cable model

The input data are shown in Table 3.3. To create a nonlinear behaviour of the cable, a Fish function was written based on data from Table 3.1.

3.3.3 Input data for the rockbolt model

Because of the different composition of the numerical cable and the numerical rockbolt model, different properties have to be specified. Table 3.2 shows the properties for the rockbolt model.

The rockbolt element has shear stiffness (Cs_sstiff), normal stiffness (Cs_nstiff) and cohesive as well as tensile strength (in both shear and normal direction), but the cable element has only shear stiffness (K_{bond}) and cohesive strength (S_{bond}, only in shear direction).

Table 3.2 Input data for rockbolt element used for numerical model.

Properties	Symbol	Unit	Value
Rock mass:			
Bulk modulus	K	Pa	1e9
Shear modulus	G	Pa	1e9
Density	Dens	kg/m^3	1000
Rockbolt and grout:			
Elastic modulus of the rockbolt steel	E	GPa	125e9
Cross sectional area of the rockbolt bar	Area	m^2	2e-4
Moment of inertia of the rockbolt bar	I	m^4	3.22e-9
Exposed perimeter of the rockbolt		m^2	5e-2
Maximum tensile force	Yield	N	7.8e4
Interaction between the rockbolt and the rock mass:			
Stiffness of the normal coupling spring	Cs_nstiff	N/m/m	1e9
Cohesive strength of the normal coupling spring	Cs_ncoh	N/m	1e20
Friction resistance of the normal coupling spring	Cs_nfric	degree	45°
Stiffness of the shear coupling spring	Cs_sstiff	N/m/m	0.5e9
Cohesive strength of the shear coupling spring	Cs_scoh	N/m	1e20
Friction resistance of the shear coupling spring	Cs_sfric	degree	45°

Table 3.3 Input data for simulation of cable element.

Properties	Symbol	Unit	Value
Rock mass:			
Bulk modulus	K	Pa	1e9
Shear modulus	G	Pa	1e9
Density	Dens	kg/m^3	1000
Cable and grout:			
Pretension	Tension	N	11000
Yield strength	Yield	N	7.8e4
Young’s modulus	E	Pa	125e9
Cross section	Area	m^2	2e-4
Gout shear stiffness	K_{bond}	N/m/m	1e8
Shear strength of the grout	S_{bond}	N/m	1e9

3.4 Response of the numerical model with nonlinear behaviour

3.4.1 Response of numerical nonlinear cable element

To investigate the model under cyclic loading and multi-segment elements it was necessary to extend the approach developed by Hausdorf [2006]. At first the case of pure loading is documented, followed by the unloading and reloading case.

a. Cable element under pure tensile loading

The model has a square cross section of 2 x 1 m and a length of 10 m. The lower end is fixed in both x and y direction. At the upper end a vertical constant velocity is applied (Figure 3.3). The cable is located at the centre of the cross section. For the test, the Mohr-Coulomb model is used with structural cable element.

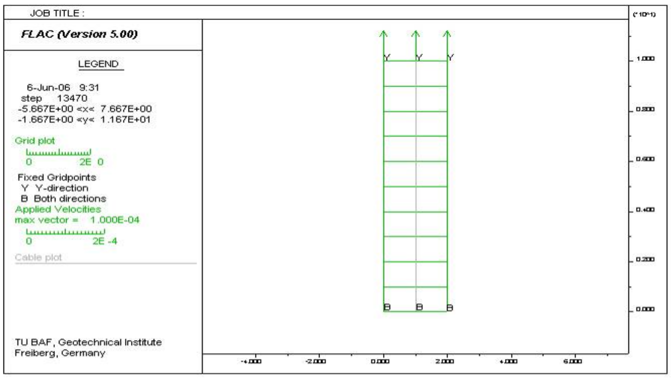
JOB TITLE :
FLAC (Version 5.00)
LEGEND
6-Jun-06 9:31
step 13470
-5.667E+00 <x< 7.667E+00
-1.667E+00 <y< 1.167E+01
Grid plot
0 2E 0
Fixed Gridpoints
Y Y-direction
B Both directions
Applied Velocities
max vector = 1.000E-04
0 2E -4
Cable plot
TU BAF, Geotechnical Institute
Freiberg, Germany
(*10^1)
1.000
0.800
0.600
0.400
0.200
0.000
-4.000
-2.000
0.000
2.000
4.000
6.000
Y
B

Figure 3.3 Numerical model for testing cable and rockbolt structural elements.

The relationship between stress (σ) and strain (ε) is in conformance with Table 3.1. The relationship between the axial forces versus axial strain during the pure loading test has several stages - see Figure 3.4:

- Elastic stage - segment 0-1, the maximum strain in this period is 0.2% with a force up to 50 kN.
- Perfect plastic stage - segment 1-2, the maximum strain in this period is 0.5% up to 0.7% with a force up to 50 kN.
- Plastic hardening stage (nonlinear) - segment 2-3, the maximum strain in this period is 10% with a force value up to 78 kN.

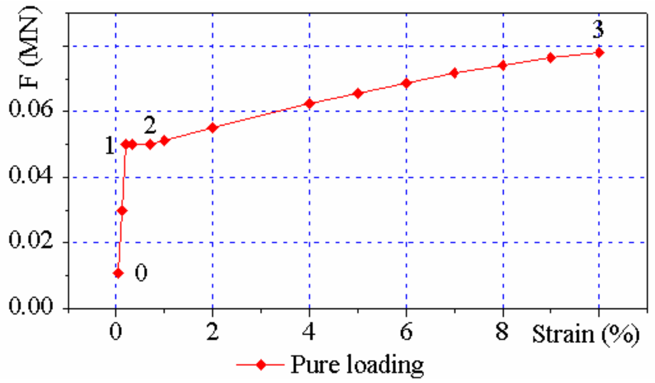

Figure 3.4 Development of axial force F (MN) versus axial strain (%) of the cable element in the pure loading process [Hausdorf 2006].

b. Cable element under cyclic loading

The structural element can have one or several segments so both of them have to be investigated. The reproduction of the cyclic behaviour was achieved by a substantial extension of the FISH-function developed by Hausdorf [2006]. First results were already presented in 2006 by Hausdorf, Le & Konietzky [2006].

b.1 Cable element with one segment

The aim of the test performed is to simulate the elasto-plastic hardening behaviour of anchor materials in a realistic manner. Loads are not only monotonously increasing but include also cyclic unloading and reloading. The anchors are simulated here as “cable” elements which have one segment. The model has the same properties as in the case of pure loading. The test is carried out by applied vertical displacement velocity at first in tensile direction (loading), then in compressive direction (unloading) for several computational steps. The load cycle is repeated several times to simulate loading, unloading and reloading.

The curve shown in Figure 3.6, a zigzag line, is obtained when unloading and reloading processes occur and represents the strain versus calculation steps.

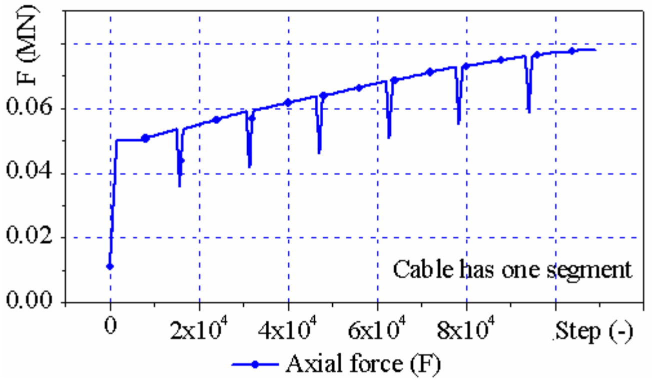

Figure 3.5 Development of the axial force F (MN) versus calculation steps of the non-linear one segment cable element in the unloading and reloading process.

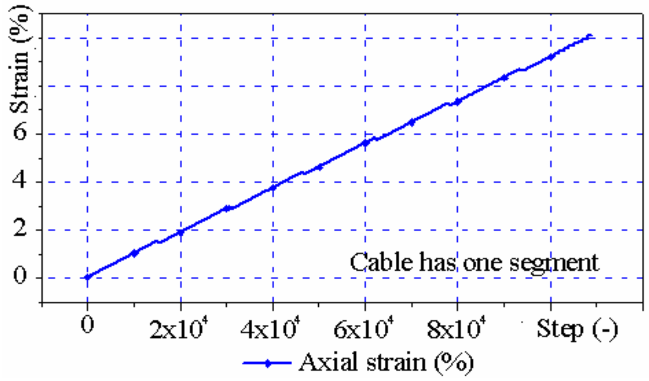

Figure 3.6 Development of the axial strain (%) versus calculation steps of the nonlinear one segment cable element in the unloading and reloading process.

Figure 3.7 illustrates the behaviour of the cable element during loading with several unloading and re-loading phases.

Observing the numerical curve in Figure 3.7, it can be seen that the perfect plastic deformation stage comes after the elastic one if the load exceeds the elastic limit. An unloading - reloading cycle is running in a segment which parallels the elastic line (E unloading = E reloading = E loading-elastic), and ends at the standard characteristic curve. There is a residual strain when unloading occurs in the elasto-plastic period (Figure 3.7).

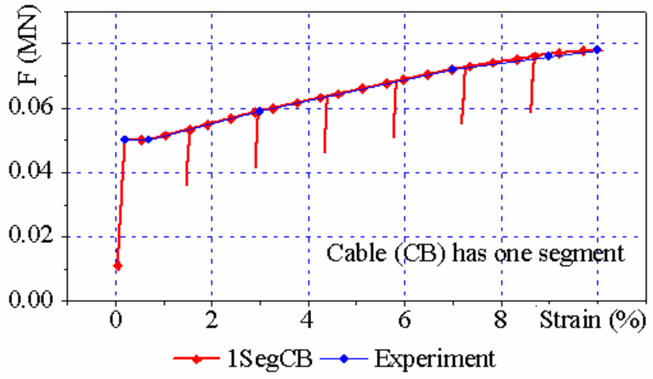

Figure 3.7 Development of axial force F (MN) versus axial strain (%) of the nonlinear one segment cable element (CB) in the unloading and reloading process.

In the case of total unloading ($F_{axial} = 0$) which is not simulated here, one can determine the irreversible plastic strain at ε-axis. This value, of course, depends on the value of the maximum force which was reached before unloading.

When comparing the curve in un-re-loading stage with the experimental one in pure loading stage (Figure 3.4), it can be seen that they are quite coincident except for the section of unloading and reloading, where no experimental data were available.

b.2 Cable element with five segments

In this case, the cable element is divided into five segments. The most common reason to specify the number of the segment > 1 is to improve the accuracy of the results, especially if the cable elements interact with the host medium. Results from running the routine are shown in Figures 3.8, 3.9 and 3.10. The response of cable segments (1/5 of the whole length of the cable) is investigated. Five curves are displayed in the same coordinate system and coincidence can be observed.

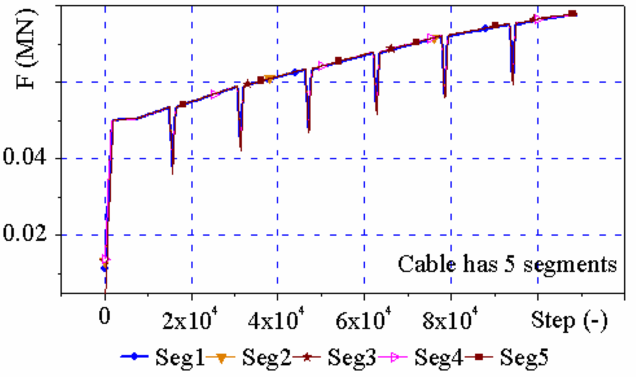

Figure 3.8 Development of axial force F (MN) versus calculation steps of the nonlinear five segment cable element (Seg) in the unloading and reloading process.

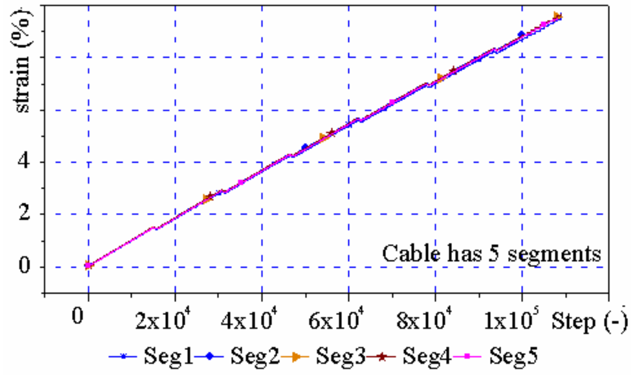

Figure 3.9 Development of the strain (%) versus calculation steps of the nonlinear cable element for five segments (Seg) in the unloading and reloading process.

The graphs given in Figures 3.8, 3.9 and 3.10 show a nearly perfect accordance between the results of each cable segment and both the numerical single segment and the experimental results.

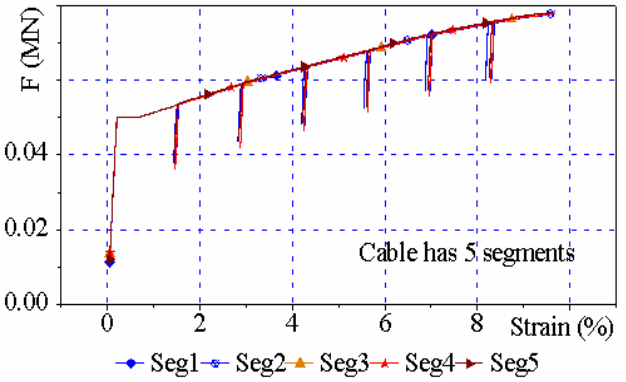

Figure 3.10 Development of the axial force F (MN) versus axial strain (%) of the nonlinear five segment cable element (Seg) in the unloading and reloading process.

3.4.2 Response of numerical nonlinear rockbolt element

The numerical model of the rockbolt is analog to that of the cable. A non-linear rockbolt element was created by a Fish-function which allows modelling of softening - hardening material behaviour under unloading and re-loading. The input data are obtained from Tables 3.1 and 3.2.

a. Rockbolt element with one segment

The stress – strain behaviour of the rockbolt element in loading, unloading and reloading tests is very similar to that of the cable element (Figures 3.11 and 3.12) because same initial and boundary conditions are applied and the same constitutive law for the anchor was used.

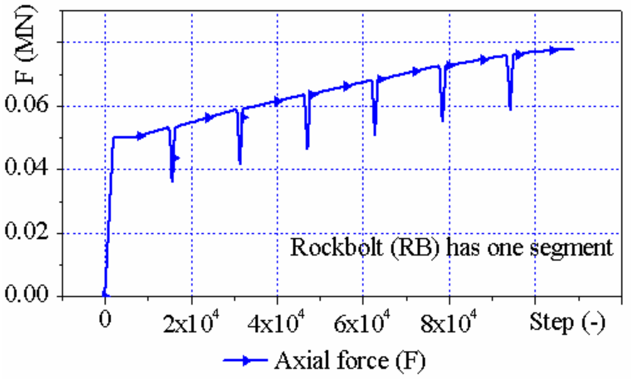

Figure 3.11 Development of the axial force F (MN) versus calculation steps of the nonlinear one segment rockbolt element during unloading and reloading.

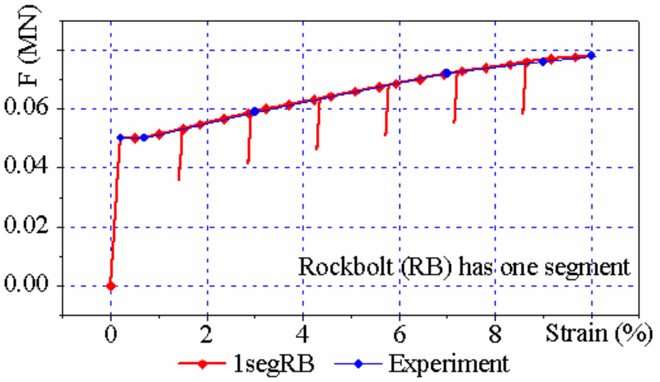

Figure 3.12 Development of the axial force F (MN) versus axial strain (%) of the nonlinear one-segment rockbolt element (1segRB) during unloading and reloading.

b. Rockbolt element with five segments

Figures 3.13, 3.14 and 3.15 demonstrate the nearly identical behaviour of several segments during loading, unloading and re-loading.

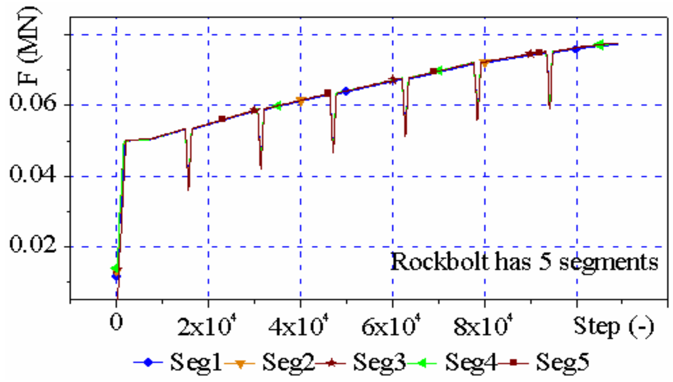

Figure 3.13 Development of the axial force F (MN) versus calculation steps of nonlinear five segment rockbolt element (Seg) during unloading and reloading.

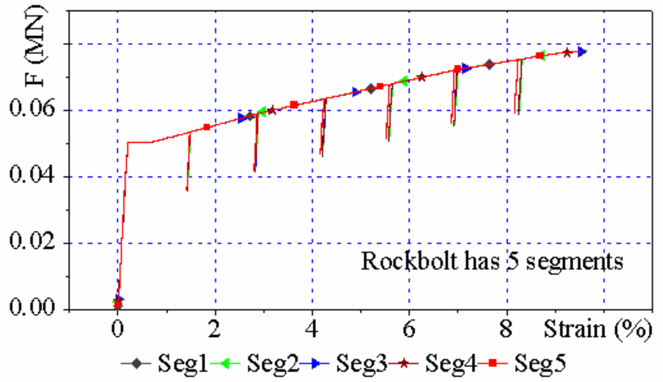

Figure 3.14 Development of the axial force F (MN) versus axial strain (%) of nonlinear five segment rockbolt element (Seg) during unloading and reloading.

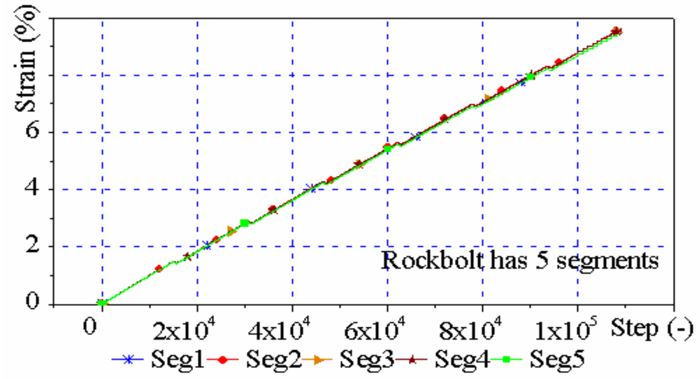

Figure 3.15 Axial strain (%) versus step number of nonlinear five segment rock bolt element (Seg) during unloading and reloading.

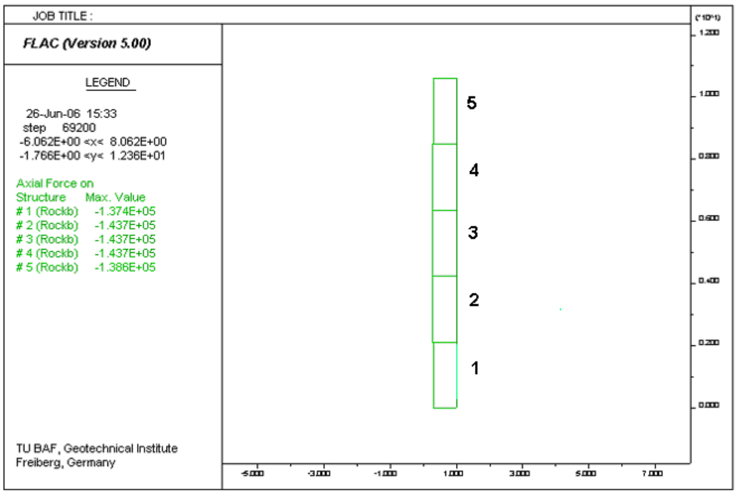
JOB TITLE :

FLAC (Version 5.00)

LEGEND

26-Jun-06 15:33
step 69200
-6.062E+00 <x< 8.062E+00
-1.766E+00 <y< 1.236E+01

Axial Force on
Structure Max. Value
1 (Rockb) -1.374E+05
2 (Rockb) -1.437E+05
3 (Rockb) -1.437E+05
4 (Rockb) -1.437E+05
5 (Rockb) -1.386E+05

TU BAF, Geotechnical Institute
Freiberg, Germany

Figure 3.16 Distribution of axial force [N] in nonlinear five-segment rockbolt element.

Figure 3.16 shows the anchor forces inside the five segments at a certain point in time during the simulations.

3.5 Nonlinear cable and rockbolt elements in 3D simulations

3.5.1 Overview of FLAC ^{3D}

FLAC ^{3D} [ITASCA 2006] is created basically from FLAC. The code is also based on the explicit finite difference method. The distinct difference between FLAC and FLAC^{3D} is the extension to the third dimension.

3.5.2 3D numerical cable element

Cable structural element is simulated similar as in FLAC, but the 3D interaction between the cable element and the surrounding rock mass is considered.

a. Introduction to the 3D cable element

As in FLAC, the cable element has one or several segments. It has the same features in both 2D and 3D. Each cable element has two nodes (Figure 3.17). It is a straight- line segment of uniform cross-section and material properties with one axially oriented translational degree-of-freedom per node. The mode of yield of the cable occurs in tension or compression but not in bending. Cables are bonded to the grid with shear directed frictional interaction.

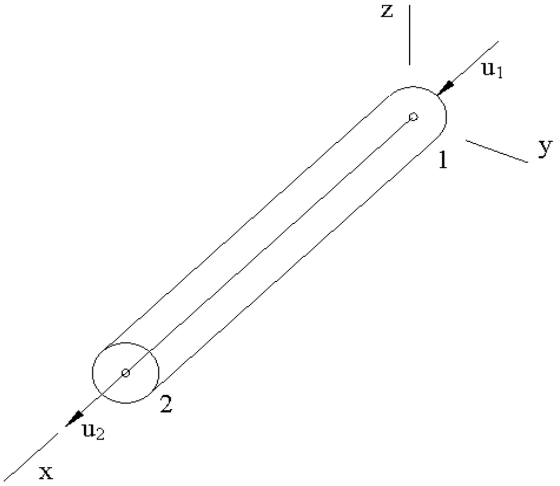

Figure 3.17 Cable SELs coordinate system and 2 active degrees-of-freedom of the cable element (SELs-structural elements).

Cable may be anchored at a specific point in the grid, or with grout so that force develops along its length in response to the relative motion between the cable and the grid. Cable has capacity to work in point-loaded or pretension mode.

b. Input data of the 3D cable element test

The properties of the rock, the cable element and the grout, which are used for the test simulations, are summarized in Table 3.4.

Table 3.4 Properties of the numerical nonlinear 3D cable element.

Properties	Symbol	Unit	Value
Rock mass:			
Bulk modulus	Bu	Pa	1e9
Shear modulus	Sh	Pa	1e9
Density	Dens	kg/m^3	1000
Cable and grout:			
Pretension	Pretension	N	11000
Yield strength	Ytens	N	7.8e4
Young’s modulus	Emod	Pa	125e9
Cross section	Xcarea	m^2	2e-4
Grout friction angle	Gr_fric	Degree	60
Shear strength or cohesion	Gr_coh	N/m	1e10
Grout stiffness	Gr_k	N/m/m	1e8
Grout exposed perimeter	Gr_per	m	0.05

The test model consists of 40 elements (2 x 2 in horizontal x, y direction and 10 in vertical z direction according to Figure 3.21). The cable is located at the centre of the cross section, from point (1, 1, 0) to point (1, 1, 10) and has one segment. The bottom of the model is fixed and at the upper end a vertical displacement velocity is applied (z direction). By applying varying velocities in the z - direction loading, reloading and unloading are simulated. The numerical tests were performed with same boundary and initial conditions and same constitutive laws as already described in chapter 3.4.

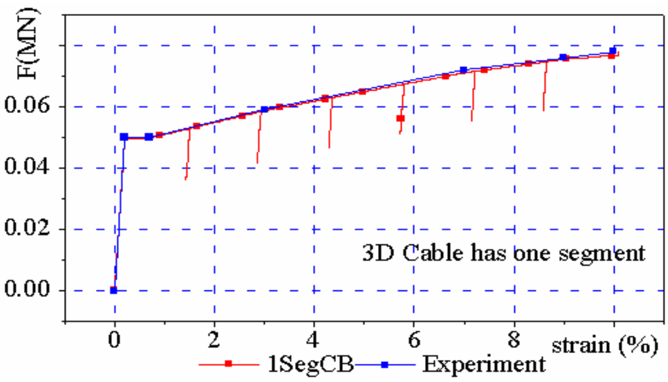

Figure 3.18 Development of axial force F (MN) versus axial strain (%) of the nonlinear one segment cable element (CB) in the unloading and reloading process.

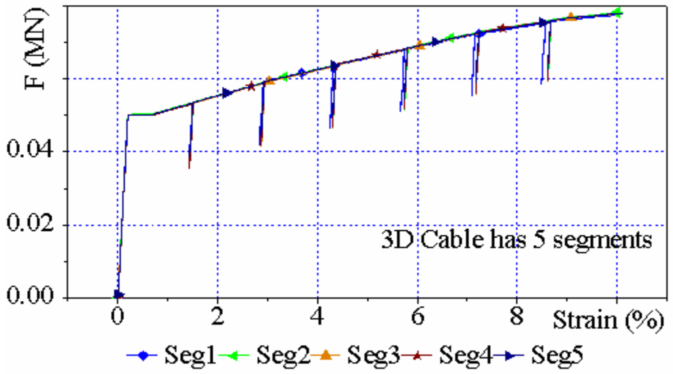

Figure 3.19 Development of axial force F (MN) versus axial strain (%) of the nonlinear five segment cable element (CBSeg) in the unloading and reloading process.

Due to the 3-dimensional nature of the problem and the different programming style a new FISH-function was developed to reproduce non-linear behaviour for cable and rockbolt element in FLAC^{3D}. Results of 3D cable simulations are illustrated in Figure 3.18 for the case of a cable with one segment and Figure 3.19 for that with five segments.

3.5.3 3D numerical rockbolt element

The rockbolt element has some similarities with the cable, beam and pile element. A special material model was developed to simulate the behaviour of rockbolts based on the pile element. A pile element has the following characteristic features:

- The pile element has two nodes.
- It is a straight finite element.
- It has six degrees-of-freedom per node.
- It has the structural behaviour of a beam: frictional interaction between the pile and the grid are normal-directed and shear-directed.
- It has skin-friction and end-bearing.
- It can be loaded at point or with distributed loads.
- It has the ability to account for changes in confining stress around the reinforcement, strain softening behaviour of material and tensile rupture.

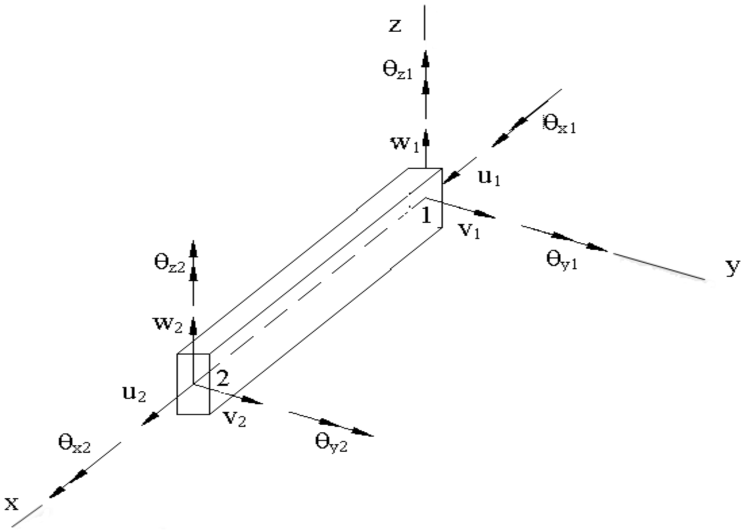

Figure 3.20 Pile-SEL coordinate system and 12 active degrees-of-freedom of the beam finite element used by each pile-SEL in FLAC^{3D}.

To perform this test, the input data according to table 3.5 were selected. Figure 3.21 shows the model set-up.

Table 3.5 Properties of the nonlinear 3D rockbolt model.

Properties	Unit	Value
Rock mass:		
Bulk modulus	Pa	1e9
Shear modulus	Pa	1e9
Density	kg/m^3	1000
Rockbolt and grout:		
Tensile yield-force limit	N	7.8e4
Compressive yield-force limit	N	1e20
Poisson’s ratio	-	0.3
Young’s modulus	Pa	125e9
Second moment with respect to pileSEL y-axis, Iy	m^4	2e-8
Second moment with respect to pileSEL z-axis, Iz	m^4	2e-8
Polar moment of inertia, J	m^4	4e-8
Cross section	m^2	2e-4
Normal coupling spring friction angle	Degree	60
Shear coupling spring friction angle	Degree	60
Normal behaviour of the rock bolt/medium interface		
Cohesive strength of the normal coupling spring	N/m	1e20
Cohesive strength of the shear coupling spring	N/m	1e20
Coupling spring normal stiffness	N/m/m	1e9
Cohesive strength of the shear coupling spring	N/m/m	0.5e9
Tensile failure strain (non-dimensional)	-	1
Ydirection	-	1,0,0
Exposed perimeter	m	0.08

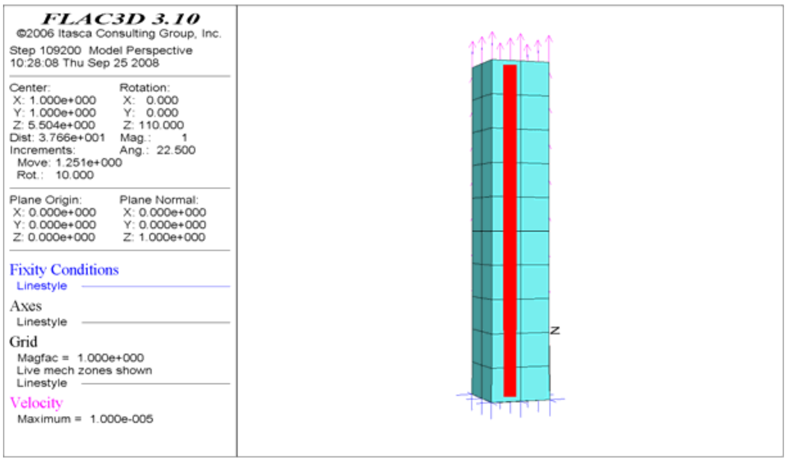

```
FLAC3D 3.10
©2006 Itasca Consulting Group, Inc.
Step 109200  Model Perspective
10:28:08 Thu Sep 25 2008

Center:              Rotation:
 X: 1.000e+000        X:   0.000
 Y: 1.000e+000        Y:   0.000
 Z: 5.504e+000        Z: 110.000
Dist: 3.766e+001     Mag.:       1
Increments:          Ang.:  22.500
  Move: 1.251e+000
  Rot.:   10.000

Plane Origin:        Plane Normal:
 X: 0.000e+000        X: 0.000e+000
 Y: 0.000e+000        Y: 0.000e+000
 Z: 0.000e+000        Z: 1.000e+000

Fixity Conditions
  Linestyle
Axes
  Linestyle
Grid
  Magfac =  1.000e+000
  Live mech zones shown
  Linestyle
Velocity
  Maximum =  1.000e-005
```

Figure 3.21 Model with one segment structural element in FLAC^{3D}.

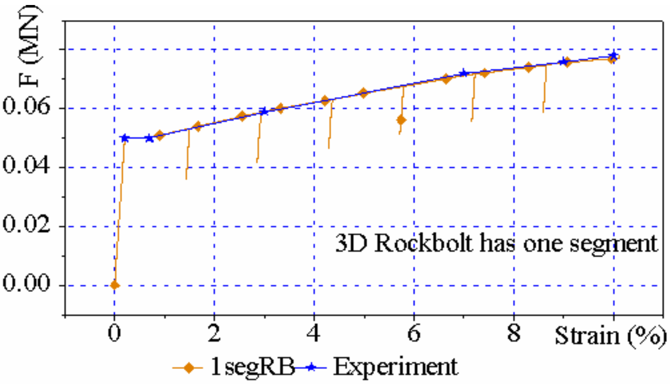

Figure 3.22 Development of axial force F (MN) versus axial strain (%) of the nonlinear one segment rockbolt element during loading, unloading and reloading.

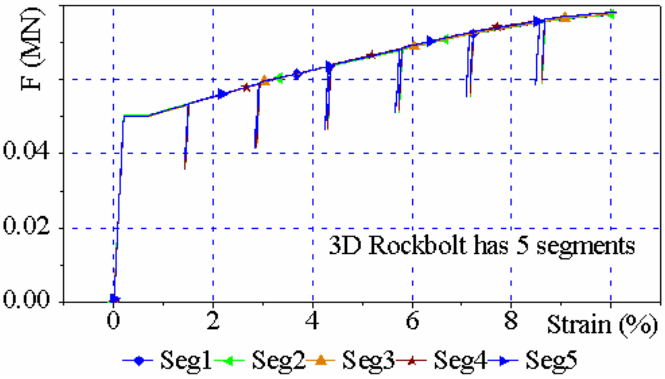

Figure 3.23 Development of axial force F (MN) versus axial strain (%) of the nonlinear five segment rockbolt element (Seg) during loading, unloading and reloading.

The test is carried out in the same way as for the cable element. Results from tests with the nonlinear 3D rockbolt element are presented in Figure 3.22 for rockbolt which has one segment and Figure 3.23 for rockbolt which has five segments.

3.6 Conclusions

Based on the evaluation of the numerical tests the following conclusions can be drawn:

- The new developed constitutive laws for the non-linear cable and rockbolt element were successfully tested and revealed nearly perfect agreement with the theoretical stress – strain relation.

- The significant extension in relation to the non-linearity already developed by Hausdorf [2006] is the incorporation of unloading and reloading, the programming for rockbolt elements and the transfer into 3D by the development of the FISH – functions for FLAC ^{3D}.

- In addition, the user routines allow the simulation of cables and rockbolts with one or several segments. The use of several segments allows to obtain a better resolution in considering the interaction between anchor and rock mass.

4 Numerical anchor modelling for Vietnamese coal mines

4.1 Introduction to the numerical constitutive rock mass model

There are a lot of different constitutive models in FLAC which can be used for rock mass simulations such as Elastic, Drucker-Prager, Mohr-Coulomb, Hoek-Brown “Cam-Clay”etc. depending on the characteristics of the material being modelled and the intended application of the model analysis. The Mohr-Coulomb model is commonly used in rock and soil mechanics. For this reason it is chosen here.

The elastic part of the Mohr-Coulomb model includes the Hooke’s law. The increment of principal stress has the following form:

$$\Delta\sigma_1 = \alpha_1 \Delta e_1^e + \alpha_2(\Delta e_2^e + \Delta e_3^e)$$

$$\Delta\sigma_2 = \alpha_1 \Delta e_2^e + \alpha_2(\Delta e_1^e + \Delta e_3^e) \qquad (4.1)$$

$$\Delta\sigma_3 = \alpha_1 \Delta e_3^e + \alpha_2(\Delta e_1^e + \Delta e_2^e)$$

where $\alpha_1 = K + 4G/3$ and $\alpha_2 = K - 2G/3$

e_i with $i = 1,3$ are corresponding principal strain increments.

The Mohr-Coulomb yield function is given by:

$$f_s = \sigma_1 - \sigma_3 N_\varphi + 2C\sqrt{N_\varphi} \quad (4.2)$$

where: C cohesion, φ friction angle of the rock mass,

$$N_\varphi = \frac{1 + \sin\varphi}{1 - \sin\varphi},$$

σ_1, σ_3 principal stresses.

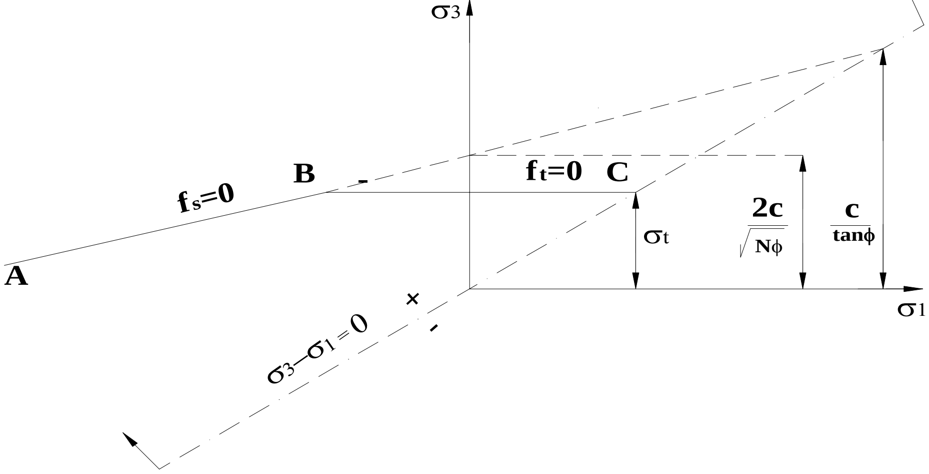

Figure 4.1 Mohr - Coulomb failure criterion expressed in the σ_1-σ_3 space.

The failure envelope f_s is defined by the line AB (see Figure 4.1), the line BC represents the tensile failure line f_t:

$$f_t = \sigma_t - \sigma_3 \quad (4.3)$$

Yield in shear occurs if $f_s = 0$ and tensile failure occurs if $f_t = 0$.

4.2 Geological and technical conditions at Vietnamese mine sites

4.2.1 Geological and technical description of mine sites

Vietnamese coal mines are mainly located in the Quang Ninh province, which is a mountainous region in the northeast of Vietnam. Coal seams spread on a great area from Dong Trieu to Mong Cai (Fig. 4.2). There are a lot of coal mines in operation in Quang Ninh both underground and at the surface (open pits).

Rockbolts have been widely applied in almost all Vietnam coal mines in the main roadways. Following empirical rules and analytical calculations, the designer or specialist decide to use rockbolts or not. The stability of the roadways is monitored after supported by measuring displacements and convergencies and by observed deformations. Local roof collapse and extreme deformations are often observed due to the complicated geotechnical conditions.

Within this work five underground coal mines were investigated in respect to the stabilities and anchorage of roadways. These five mines were chosen because most of the necessary input data were available.

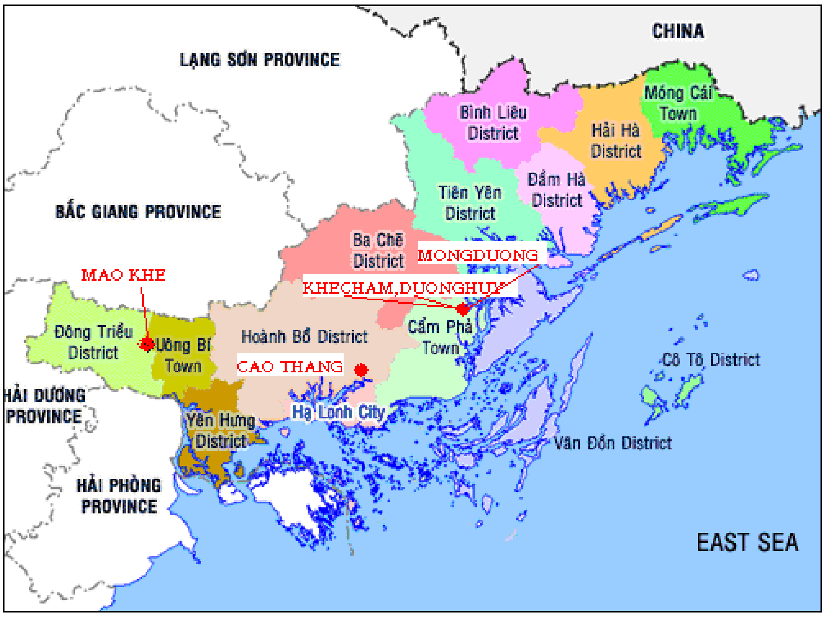
LẠNG SƠN PROVINCE
CHINA
Móng Cái Town
Bình Liêu District
Hải Hà District
Đầm Hà District
Tiên Yên District
BẮC GIANG PROVINCE
Ba Chẽ District
MONGDUONG
KHECHAM,DUONGHUY
MAO KHE
Đông Triều District
Uông Bí Town
Hoành Bồ District
Cẩm Phả Town
CAO THANG
Cô Tô District
HẢI DƯƠNG PROVINCE
Yên Hưng District
Hạ Long City
Vân Đồn District
HẢI PHÒNG PROVINCE
EAST SEA

Figure 4.2 Locations of selected Vietnamese underground coal mines.

a. Cao Thang mine conditions

Roadway segments which are selected for application of rockbolting are driven in conglomerate and sandstone at a depth of 180 m below the surface. Rock mass surrounding the opening is stratified as given in Figure 4.3:

- Conglomerate: This is a common rock in this area, it is intercalated with the other rock layers and has a grey-white or ash colour, its structure has a block form. This rock is mainly composed of quartz.
- Sandstone: is also a common rock in the Quang Ninh area, bedding 12 up to 35 cm thick, in white-grey, ash-grey colour, jointed block structure. Rock mass layers are distributed in a thickness of 60 meters up to 70 meters.

- Siltstone is widespread in Quang Ninh area, bedding 8 up to 22 centimetres in thickness. It is a semi-hard rock.
- Claystone has a black, grey colour. It is a soft, easily breakable and detachable rock. The thickness of the thin layers is 5 up to 12 cm.

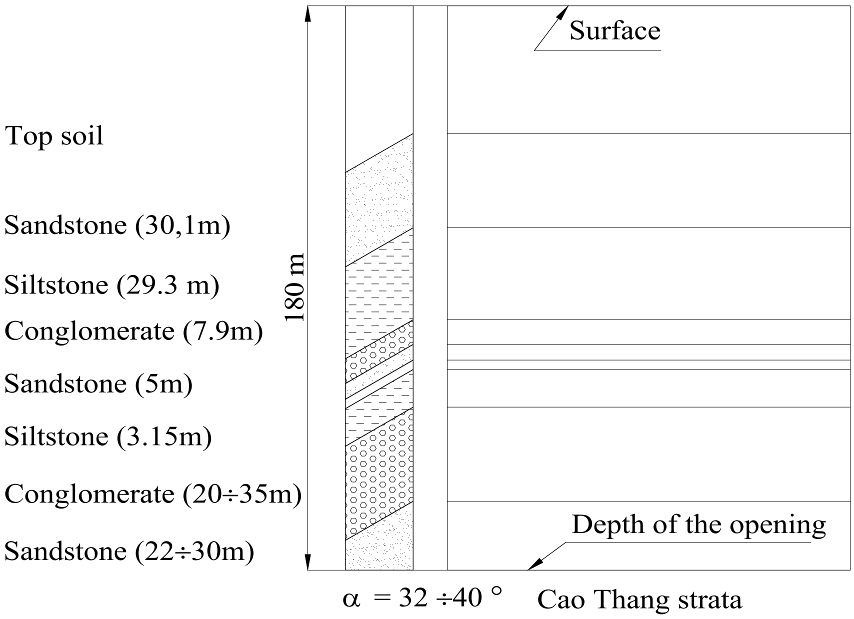
Surface
Top soil
Sandstone (30,1m)
Siltstone (29.3 m)
Conglomerate (7.9m)
Sandstone (5m)
Siltstone (3.15m)
Conglomerate (20÷35m)
Sandstone (22÷30m)
180 m
Depth of the opening
α = 32 ÷40 °
Cao Thang strata

Figure 4.3 Cao Thang mine stratified log.

Figure 4.4 shows the numerical model with drift location indicating the geological layering according to the profile shown in Fig. 4.3.

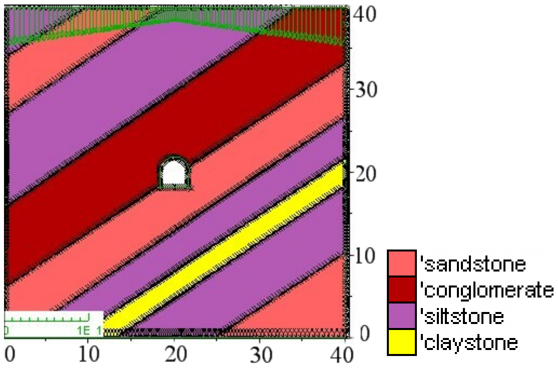
40
30
20
10
0
0
10
20
30
40
'sandstone
'conglomerate
'siltstone
'claystone

Figure 4.4 Cao Thang model with dimensions in meter.

b. Mao Khe mine conditions

Roadway segments which are selected for application of rockbolts are driven in sandstone at a depth of 100 m below the surface. Rock mass surrounding the opening is stratified as shown in Figure 4.5.

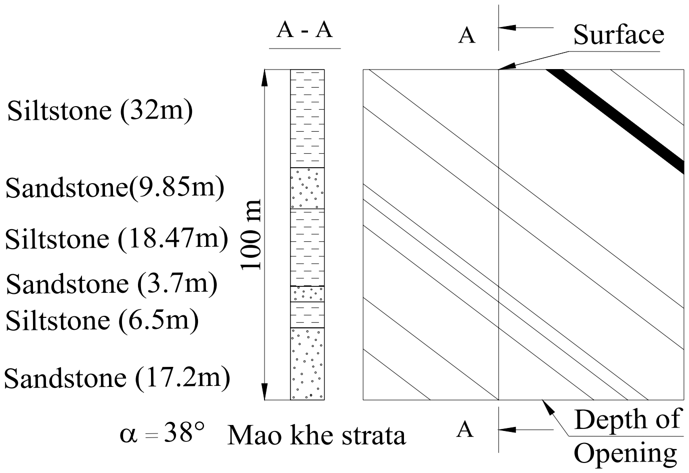
A - A
A
Surface
Siltstone (32m)
Sandstone(9.85m)
Siltstone (18.47m)
Sandstone (3.7m)
Siltstone (6.5m)
Sandstone (17.2m)
100 m
α = 38°
Mao khe strata
A
Depth of
Opening

Figure 4.5 Mao Khe mine stratified log.

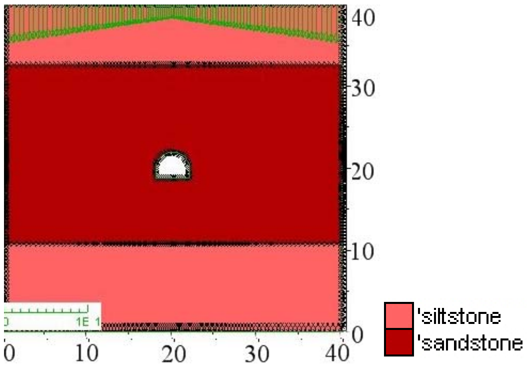
40
30
20
10
0
0
10
20
30
40
'siltstone
'sandstone

Figure 4.6 Mao Khe model with dimensions in meter.

Figure 4.6 shows the numerical model with drift indicating the geological layering according to the profile given in Figure 4.5.

c. Duong Huy mine conditions

Roadway segments which are selected for application of rockbolts are driven in sandstone and conglomerate at a depth of 230 m below the surface. Rock mass surrounding the opening is stratified as given in Figure 4.7.

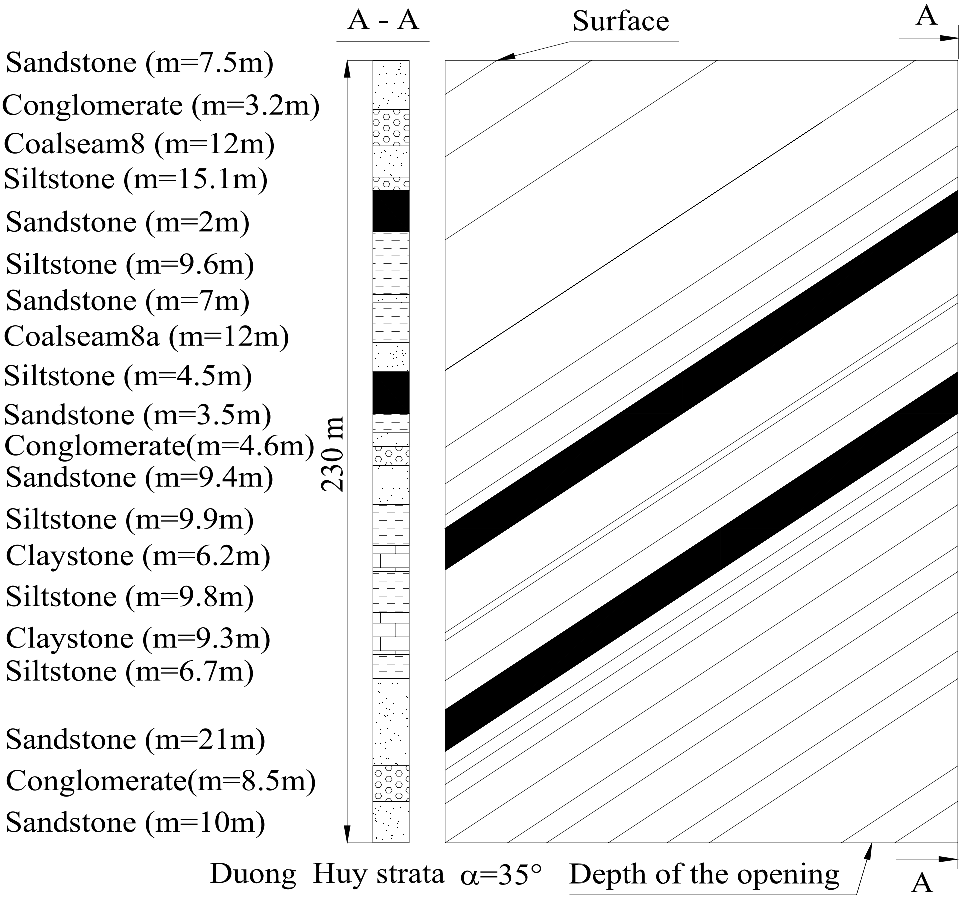
A - A
Surface
A
Sandstone (m=7.5m)
Conglomerate (m=3.2m)
Coalseam8 (m=12m)
Siltstone (m=15.1m)
Sandstone (m=2m)
Siltstone (m=9.6m)
Sandstone (m=7m)
Coalseam8a (m=12m)
Siltstone (m=4.5m)
Sandstone (m=3.5m)
Conglomerate(m=4.6m)
Sandstone (m=9.4m)
Siltstone (m=9.9m)
Claystone (m=6.2m)
Siltstone (m=9.8m)
Claystone (m=9.3m)
Siltstone (m=6.7m)
Sandstone (m=21m)
Conglomerate(m=8.5m)
Sandstone (m=10m)
230 m
Duong Huy strata
α=35°
Depth of the opening
A

Figure 4.7 Duong Huy mine stratified log.

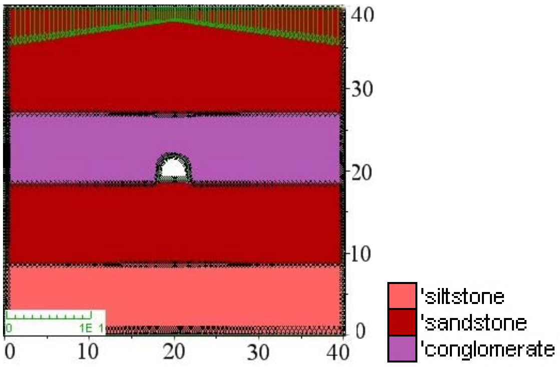
40
30
20
10
0
0
10
20
30
40
'siltstone
'sandstone
'conglomerate

Figure 4.8 Duong Huy model with dimensions in meter.

Figure 4.8 shows the corresponding numerical model including layering and drift location.

d. Mong Duong mine conditions

Roadway segments which are selected for application of rockbolts are driven in sandstone at a depth of 150 m below the surface. Rock mass surrounding the opening is stratified as given in Figure 4.9.

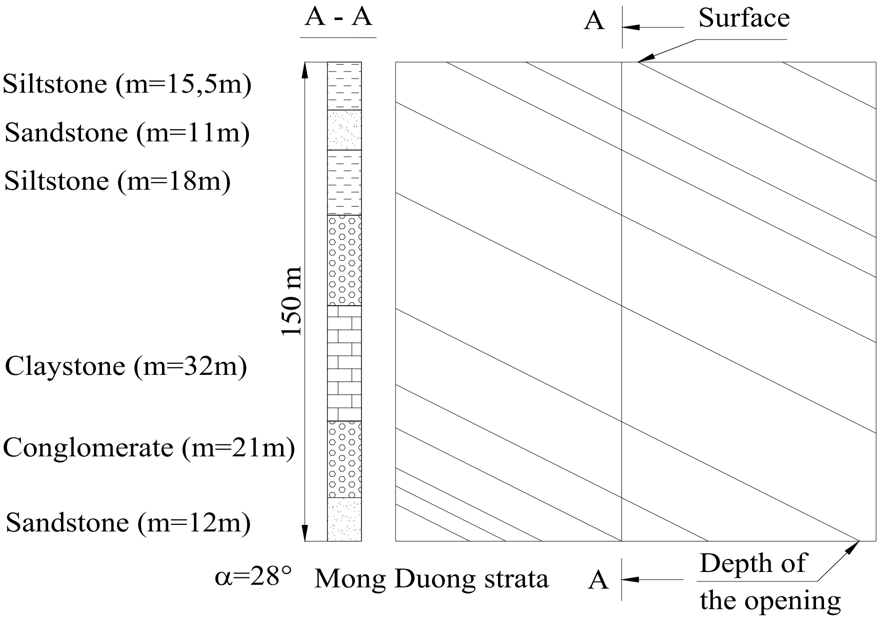
A - A
A
Surface
Siltstone (m=15,5m)
Sandstone (m=11m)
Siltstone (m=18m)
150 m
Claystone (m=32m)
Conglomerate (m=21m)
Sandstone (m=12m)
α=28°
Mong Duong strata
A
Depth of
the opening

Figure 4.9 Mong Duong stratified log.

Figure 4.10 shows the corresponding numerical model with geological layering and drift location.

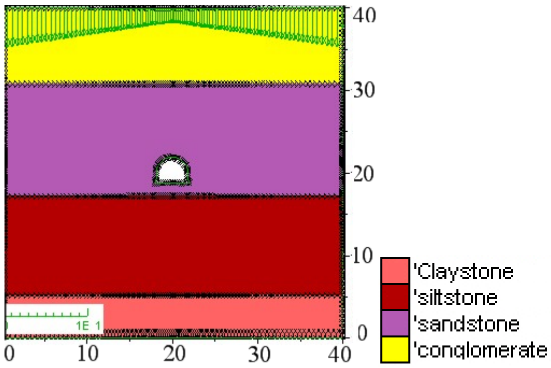
40
30
20
10
0
0
10
20
30
40
1E 1
'Claystone
'siltstone
'sandstone
'conglomerate

Figure 4.10 Mong Duong model with dimension in meter.

e. Khe Cham mine conditions

Roadway segments which are selected for application of rockbolts are driven in sandstone and conglomerate at a depth of 150 m below the surface. Rock mass surrounding the opening is stratified as shown in Figure 4.11.

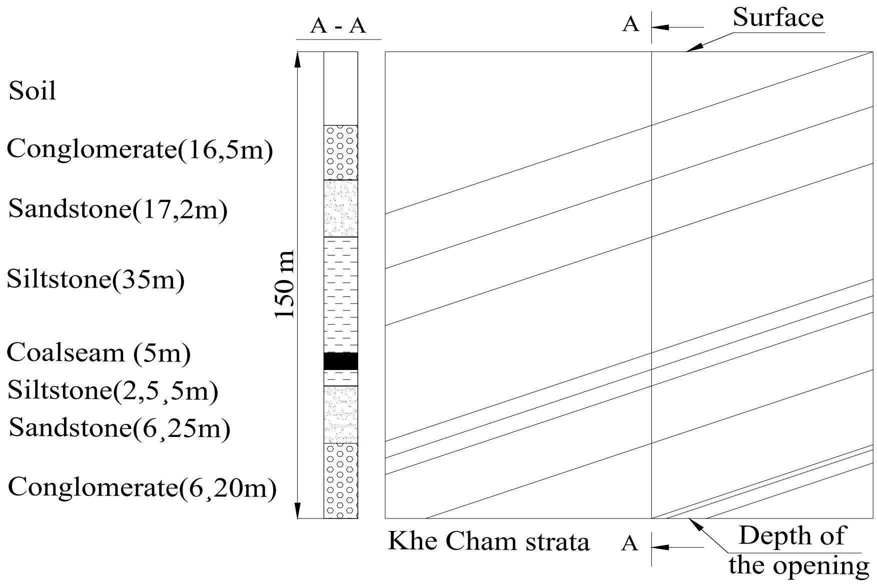
A - A
A
Surface
Soil
Conglomerate(16,5m)
Sandstone(17,2m)
Siltstone(35m)
150 m
Coalseam (5m)
Siltstone(2,5¸5m)
Sandstone(6¸25m)
Conglomerate(6¸20m)
Khe Cham strata
A
Depth of
the opening

Figure 4.11 Khe Cham mine stratified log.

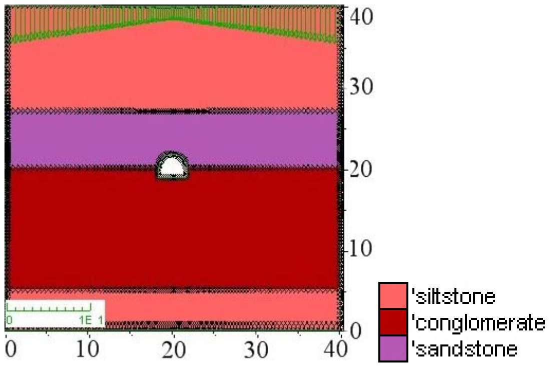
40
30
20
10
0
0
10
20
30
40
'siltstone
'conglomerate
'sandstone

Figure 4.12 Khe Cham model with dimension in meter.

Figure 4.12 shows the corresponding numerical model with geological layering and drift location.

4.2.2 Rock properties

The properties of the rocks were obtained by the Institute of Mining Science and Technology – Hanoi, Vietnam [IMSAT – 1990, 1998, 2000, 2002a, 2002b]. Samples were taken from the field and tested in the laboratory. In some cases the so-called “Schmidt Hammer” was used to determine them and furthermore engineering geological data were collected at the excavation face such as joint spacing, length of the joints etc. at each cycle of excavation. The data for the five roadways, which were collected from the reports are summarized in the Tables 4.1 to 4.5.

Table 4.1 Physical properties of the intact rock surrounding Cao Thang mine roadway.

Type of Rock mass	Properties of the rock								
	σ_c (MPa)	σ_t (MPa)	ρ (g/cm^3)	C (MPa)	φ (deg.)	E (GPa)	ν (-)	K (GPa)	G (GPa)
Conglomerate	65.00	5.60	2.51	19.72	28.00	8.58	0.27	6.22	3.38
Sandstone	74.20	8.70	2.60	23.18	26.00	5.10	0.19	2.74	2.14
Siltstone	47.40	3.20	2.62	14.80	30.00	3.76	0.22	2.23	1.54
Claystone	21.70	2.20	2.60	7.88	27.00	3.35	0.25	2.23	1.34

Table 4.2 Physical properties of intact rock surrounding Mao Khe mine roadway.

Type of rock mass	Properties of the rock								
	σ_c (MPa)	σ_t (MPa)	ρ (g/cm^3)	C (MPa)	φ (deg.)	E (GPa)	ν (-)	K (GPa)	G (GPa)
Siltstone	58.60	6.10	2.55	5.90	33.00	18.80	0.22	7.00	4.20
Sandstone	99.60	8.70	2.55	28.40	36.00	10.50	0.20	11.20	7.76

Table 4.3 Physical properties of the intact rock surrounding Duong Huy mine roadway.

Type of rock mass	σ_c (MPa)	σ_t (MPa)	ρ (g/cm^3)	C (MPa)	φ (deg.)	E (GPa)	ν (-)	K (GPa)	G (Gpa)
Sandstone	84.60	4.63	2.63	20.00	31.00	30.60	0.26	21.6	12.10
Conglomerate	75.00	6.50	2.51	22.60	32.00	8.59	0.18	6.23	3.38
Siltstone	34.70	3.85	2.60	16.90	32.00	0.94	0.21	0.54	0.39
Claystone	31.00	5.00	2.22	2.90	29.00	2.69	0.27	1.96	1.06

Table 4.4 Physical properties of intact rock surrounding Mong Duong mine roadway.

Type of Rock mass	σ_c (MPa)	σ_t (MPa)	ρ (g/cm^3)	C (MPa)	φ (deg.)	E (GPa)	ν (-)	K (GPa)	G (Gpa)
Conglomerate	60.00	4.50	2.63	42.60	32.00	11.00	0.13	5.04	4.84
Sandstone	89.40	8.80	2.62	22.80	33.00	27.30	0.17	14.10	1.16
Siltstone	41.50	4.80	2.62	5.50	35.00	11.60	0.22	8.11	4.13
Claystone	17.10	5.20	2.58	7.00	30.00	2.70	0.18	1.60	1.11

Table 4.5 Physical properties of the intact rock surrounding Khe Cham mine roadway.

Type of Rock mass	σ_c (MPa)	σ_t (MPa)	ρ (g/cm^3)	C (MPa)	φ (deg.)	E (GPa)	ν (-)	K (GPa)	G (Gpa)
Siltstone	58.87	41.40	2.64	19.53	29.00	7.93	0.25	5.29	3.17
Sandstone	86.85	11.22	2.63	34.36	30.00	9.88	0.22	7.56	3.85
Conglomerate	108.05	8.73	2.55	44.52	33.00	11.67	0.20	7.77	4.66
Claystone	17.43	2.24	2.53	9.00	25.00	1.08	-	-	-

4.2.3 Technical conditions

Standard rockbolt patterns vary slightly in the different mines. Details are given in the IMSAT-reports [IMSAT -1990, 1998, 2000, 2002a, 2002b]. Parameters given in Table 4.6 are typical and used a basic data set for the subsequent numerical simulations.

Table 4.6 Technical properties of used standard rockbolt pattern.

Parameters	Unit	Value	Symbol
Length of the bolts	m	1.5	L
Distance between bolts in a row	m	0.8	D
Distance between rows	m	0.8	D
Number of bolts in a row	piece	8.0	-
Diameters of borehole	mm	38.0	d_{lk}
Diameters of steel bar	mm	20.0	d_s
Type of rockbolt		Fully grouted cement	-

Table 4.7 Technical conditions of roadways.

Technical conditions	Name of the mines				
	Cao Thang	Mao Khe	Duong Huy	Mong Duong	Khe Cham
Cross section area (m^2)	14.2	11.0	10.4	11.0	9.4
Height of cross section (m)	4.0	3.2	3.3	3.2	3.0
Span (m)	4.0	4.0	3.8	4.0	3.6
Depth (m) below surface	180	100	230	150	150

Table 4.7 gives the geometrical dimensions of the roadways in the different mines. Exemplary, Figure 4.13 illustrates the geometry of the roadway for the Mong Duong mine including the anchor scheme according to Table 4.6.

4.2.4 Rock mass properties

Rock mass properties required for simulations can be divided into two classes: elastic deformation properties such as Young's modulus (E), Poisson's ratio, bulk modulus (K), shear modulus (G) and strength properties such as compressive strength, tensile strength, cohesion, friction angle. Determination of appropriate rock mass properties is the most difficult task because of the random joints, holes, weakness plane, water and other characteristics of the rock mass in the nature (inhomogeneity and damage). Intact rock properties were determined from laboratory or simple field tests. Their values (Table 4.1 to 4.6) were converted into rock mass properties by using rock mass classification schemes.

The applied procedure is based on the empirical Hoek-Brown criterion – which has been widely used in rock mechanics analysis for estimating rock mass strength from geological data and description of the rock mass.

Equation of Hoek-Brown failure criterion is as follows [Hoek et al., 2002]:

$$\sigma_1 = \sigma_3 + \sqrt{m\sigma_c\sigma_3 + s\sigma_c^2} \tag{4.4}$$

where: σ_1 major principal stress, σ_3 minor principal stress,

σ_c uniaxial compressive strength of the intact rock,

σ_t uniaxial tensile strength,

m, s constants of rock type.

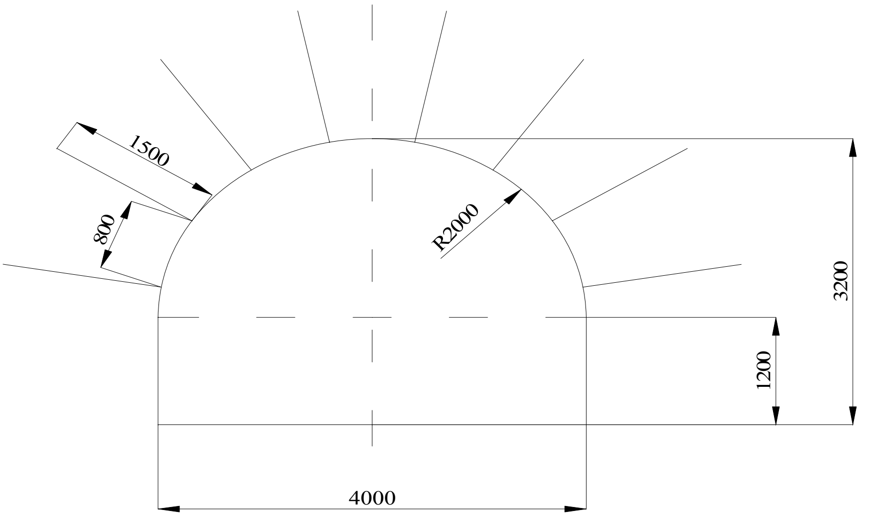

Figure 4.13 Cross section of Mong Duong roadway with area of 11.08 m^2.

Relationship between tensile and compressive strength is given by formula:

$$\sigma_t = -\frac{1}{2}\sigma_c\,(m - \sqrt{m^2 + 4s}\,) \tag{4.5}$$

The program Rocklab [Rockscience 2008] was used to deduce the parameters. It allows to draw the Hoek-Brown failure envelope, and to calculate equivalent Mohr-Coulomb parameters. In order to determine generalized Hoek-Brown strength parameters of a rock mass like the material constants m_b, s and a, the following steps were performed:

- Unconfined compressive strengths of intact rock σ_{ci} were obtained from Table 4.1.
- Intact rock constant m_i was selected according to the rock type (Table 4.18).
- Geological strength index GSI was selected. GSI was introduced by Hoek to estimate reduction of rock mass strength. It can be estimated directly by using parameter RMR or by Table 4.21 [Hoek & Brown, 1997].
- Disturbance factor D is selected. Guidelines for estimating the disturbance factor D are given in Table 4.19.

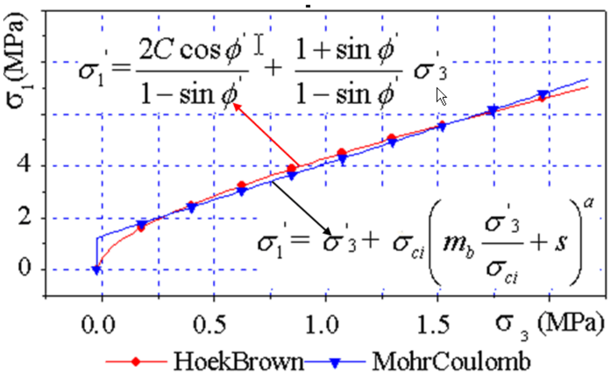

Figure 4.14 Hoek-Brown envelope and equivalent Mohr – Coulomb envelope.

The equation of the Mohr-Coulomb criterion is:

$$\sigma_1 = \frac{2c\cos\phi}{1-\sin\phi} + \frac{1+\sin\phi}{1-\sin\phi}\sigma_3 \tag{4.6}$$

Equivalent friction angle and cohesion have to be determined for a certain stress range by following formulas:

$$\phi = \sin^{-1}\left[\frac{6am_b\left(s + m_b\sigma_{3n}\right)^{(a-1)}}{2(1+a)(2+a) + 6am_b\left(s + m_b\sigma_{3n}\right)^{(a-1)}}\right] \tag{4.7}$$

$$C = \frac{\sigma_{ci}\left[(1+2a)s+(1+a)m_b\sigma_{3n}\right](s+m_b\sigma_{3n})^{(a-1)}}{(1+a)(2+a)\sqrt{\frac{1+(6am_b(s+m_b\sigma_{3n})^{(a-1)})}{(1+a)(2+a)}}} \qquad (4.8)$$

where: $\sigma_{3n} = \frac{\sigma'_{3\max}}{\sigma_{ci}}$

and $\sigma'_{3\max}$ is upper limit of confining stress which is determined for underground excavation by the formula:

$$\frac{\sigma'_{3\max}}{\sigma'_{cm}} = 0.47\left(\frac{\sigma'_{cm}}{\gamma H}\right)^{-0.94} \qquad (4.9)$$

where: σ'_{cm} rock mass strength.

Deformation modulus can be calculated by following formula [Hoek & Diederichs 2005]:

$$E_{rm} = 100000\frac{1-D/2}{1+e^{((75+25D-GSI)/11)}} \qquad (4.10)$$

and the modulus of intact rock can estimated from the compressive strength by:

$$E_i = MR\sigma_{ci} \qquad (4.11)$$

where the modulus ratio MR proposed by Deere is given in Table 4.10

The rock mass properties for the 5 mines under investigation obtained by the above mentioned calculation scheme are shown in the Tables 4.12 to 4.21. The corresponding Hoek-Brown failure envelopes and the deduced Mohr-Coulomb failure envelopes are given in Figures 4.15 to 4.19. Besides the procedure given by formulas 4.7 and 4.8 a more conservative approach can be used which fits exactly the uniaxial compressive strength, obtained by the Hoek-Brown failure criterion and the friction angles according to Tables 4.14 to 4.17, 4.20 and 4.21. These Mohr-Coulomb failure envelopes, called 'Procedure 2' in Figures 4.15 to 4.19, were used in all subsequent calculations and evaluations.

Table 4.8 Values of constant m_i for intact rock [Rockscience 2008].

Rock type	Class	Group	Texture			
			Coarse	Medium	Fine	Very fine
Sedimentary	Classic		Conglomerate 21±3	Sandstone 17±3	Siltstone 7±2	Claystone 4±2
			Bereccia 19±5		Greywacke 18±3	Shales 6±6
						Marls 7±2
	Non-Classic	Carbonates	Crystalline Limestone 12±3	Sparitic Limestones 10±3	Micritic Limestones 9±2	Dolomites 9±3
		Evaporites		Gypsum 8±2	Anhydrite 12±2	
		Organic				Chalk 7±2

Table 4.9 Guidelines for estimating the disturbance factor D (sedimentary rocks) [Rockscience 2008].

Description of rock mass	Suggested value of D
Excellent quality-controlled blasting or excavation by tunnel boring machine results in minimum disturbance to the confined rock mass surrounding a tunnel	D=0
Mechanical or hand excavation in poor quality rock mass (no blasting) results in minimum disturbance to the surrounding rock mass	D=0
Where squeezing problems result in significant floor heave, disturbance can be severe unless a temporary invert is placed	D=0.5
Very poor quality blasting in a hard rock tunnel results in severe local damage, extending 2 or 3 m, in the surrounding rock mass	D=0.8
Small scale blasting in civil engineering slopes results in modest rock mass damage, particularly if controlled blasting is used, however, stress relief results in some disturbance	D=0.7 Good blast D=1.0 Poor blast
Very large open pit mine slopes suffer significant disturbance due to heavy production blasting and also due to stress relief from overburden removal	D=1 Production blast
In some softer rocks excavation can be carried out by ripping and dozing and degree of damage to the slopes is less	D=0.7 Mechanical excavation
Very large open pit mine slopes suffer significant disturbance due to heavy production blasting and also due to stress relief from overburden removal.	D=1 Production blast
In some softer rocks excavation can be carried out by ripping and dozing and degree of damage to the slopes is less	D=0.7 Mechanical excavation

Table 4.10 Guidelines for the selection of the modulus ratio MR [Rockscience 2008].

Rock type	class	Group	Texture			
			Coarse	Medium	Fine	Very fine
Sedimentary	Classic		Conglomerate 300-400	Sandstone 200-350	Siltstone 350-400	Claystone 200-300
			Bereccia 230-350		Greywacke 350	Shales 150-250
						Marls 150-250
	Non-Classic	Carbonates	Crystalline Limestone 400-600	Sparitic Limestones 600-800	Micritic Limestones 800-1000	Dolomites 350-500
		Evaporites		Gypsum 350	Anhydrite 350	
		Organic				Chalk 1000

Table 4.11 Values of the geological strength index GSI based on geological descriptions [Rockscience 2008].

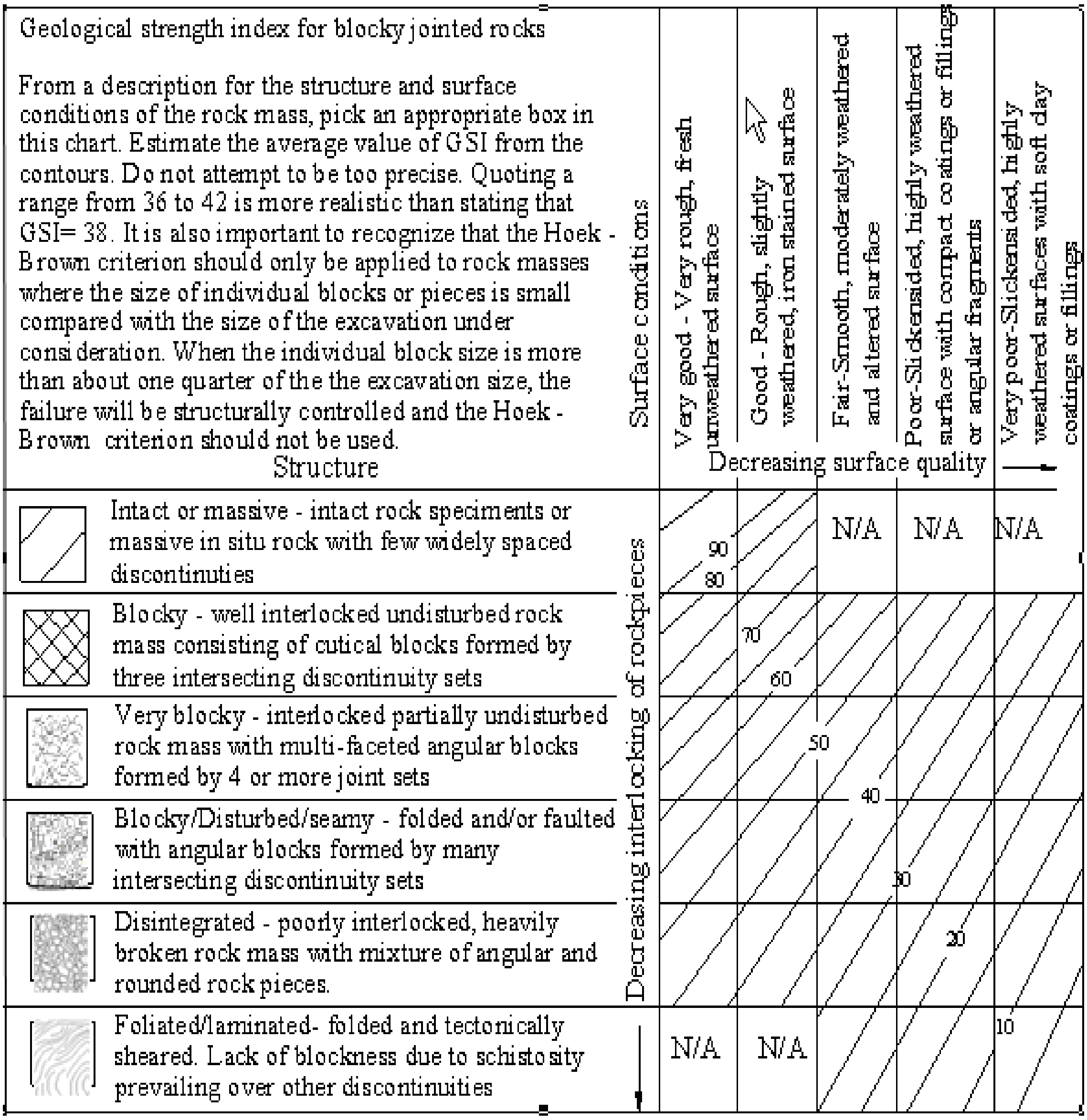

Geological strength index for blocky jointed rocks

From a description for the structure and surface conditions of the rock mass, pick an appropriate box in this chart. Estimate the average value of GSI from the contours. Do not attempt to be too precise. Quoting a range from 36 to 42 is more realistic than stating that GSI= 38. It is also important to recognize that the Hoek - Brown criterion should only be applied to rock masses where the size of individual blocks or pieces is small compared with the size of the excavation under consideration. When the individual block size is more than about one quarter of the the excavation size, the failure will be structurally controlled and the Hoek - Brown criterion should not be used.

Intact or massive - intact rock specimens or massive in situ rock with few widely spaced discontinuties

Blocky - well interlocked undisturbed rock mass consisting of cutical blocks formed by three intersecting discontinuity sets

Very blocky - interlocked partially undisturbed rock mass with multi-faceted angular blocks formed by 4 or more joint sets

Blocky/Disturbed/seamy - folded and/or faulted with angular blocks formed by many intersecting discontinuity sets

Disintegrated - poorly interlocked, heavily broken rock mass with mixture of angular and rounded rock pieces.

Foliated/laminated- folded and tectonically sheared. Lack of blockness due to schistosity prevailing over other discontinuities

Structure
Surface conditions
Very good - Very rough, fresh unweathered surface
Good - Rough, slightly weathered, iron stained surface
Fair-Smooth, moderately weathered and altered surface
Poor-Slickensided, highly weathered surface with compact coatings or fillings or angular fragments
Very poor-Slickensided, highly weathered surfaces with soft clay coatings or fillings
Decreasing surface quality
Decreasing interlocking of rockpieces
N/A
N/A
N/A
90
80
70
60
50
40
30
20
10
N/A
N/A

Table 4.12 Rock mass parameters for Cao Thang mine.

Rock type	Parameters		
	m_i	GSI	D
Conglomerate	18	44	1
Sandstone	11	41	1
Siltstone	7	46	1
Claystone	3	41	0

Table 4.13 Rock mass parameters for Mao Khe mine.

Rock type	Parameters		
	m_i	GSI	D
Sandstone	13	40	1
Siltstone	7	41	0.8

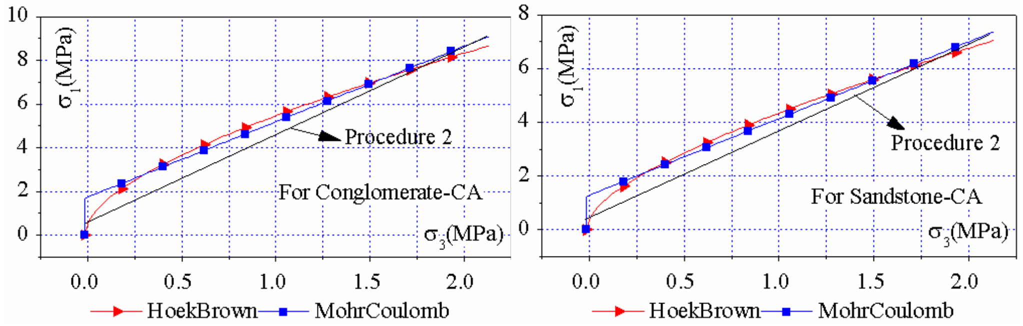

Figure 4.15 Equivalent Mohr envelope in principal stress space for conglomerate (left), sandstone (right); (Cao Thang mine).

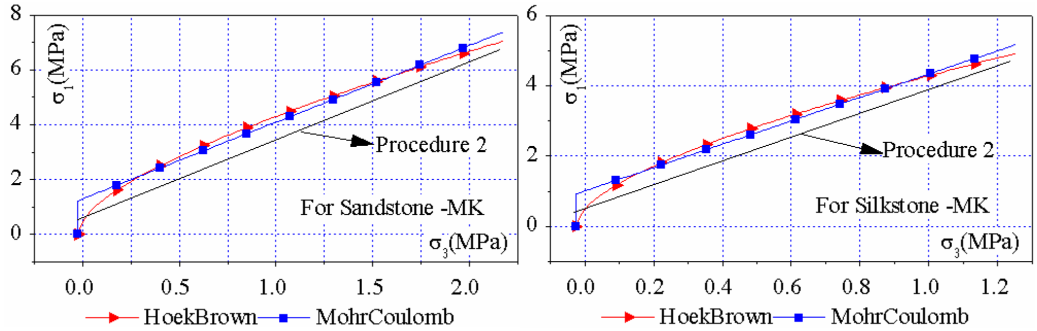

Figure 4.16 Equivalent Mohr envelope in principal stress space for sandstone (left), siltstone (right); (Mao Khe mine).

Table 4.14 Physical properties of the rock mass surrounding Cao Thang roadway.

Type of Rock mass	Properties of the rock mass								
	σ_c (MPa)	σ_t (MPa)	ρ (g/cm^3)	C (MPa)	φ (deg)	E (GPa)	ν	K (GPa)	G (GPa)
Conglomerate	0.56	0.017	2.51	0.170	28	1.095	0.27	0.794	0.431
Sandstone	0.49	0.024	2.60	0.152	26	0.665	0.19	0.358	0.279
Siltstone	0.49	0.039	2.62	0.142	30	0.696	0.22	0.414	0.285
Claystone	0.76	0.08	2.60	0.232	27	0.793	0.25	0.528	0.317

Table 4.15 Physical properties of the rock mass surrounding Mao Khe roadway.

Type of rock mass	Properties of the rock mass								
	σ_c (MPa)	σ_t (MPa)	ρ (g/cm^3)	C (MPa)	φ (deg)	E (GPa)	ν (-)	K (GPa)	G (GPa)
Sandstone	0.60	0.025	2.55	0.153	36	1.193	0.20	0.795	0.477
Siltstone	0.61	0.038	2.55	0.166	33	1.182	0.22	0.788	0.484

Table 4.16 Rock mass parameters for Duong Huy mine.

Rock type	Parameters		
	m_i	GSI	D
Conglomerate	18	44	1
Sandstone	17	42	1
Siltstone	7	60	0.8

Table 4.17 Physical properties of the rock mass surrounding Duong Huy roadway.

Type of Rock mass	Properties of the rock mass								
	σ_c (MPa)	σ_t (MPa)	ρ (g/cm^3)	C (MPa)	φ (deg)	E (GPa)	ν (-)	K (Gpa)	G (GPa)
Conglomerate	0.650	0.020	2.60	0.180	32	1.264	0.18	0.916	0.497
Sandstone	0.612	0.019	2.60	0.174	31	0.739	0.20	0.513	0.293
Siltstone	0.647	0.120	2.60	0.456	32	2.223	0.21	1.277	0.918

Table 4.18 Rock mass parameters for Mong Duong mine.

Rock type	Parameters		
	m_i	GSI	D
Conglomerate	20	44	1
Sandstone	15	40	1
Siltstone	8	45	0.8

Table 4.19 Rock mass parameters for Khe Cham mine.

Rock type	Parameters		
	m_i	GSI	D
Conglomerate	18	36	1
Sandstone	13	39	1
Siltstone	8	41	0.8

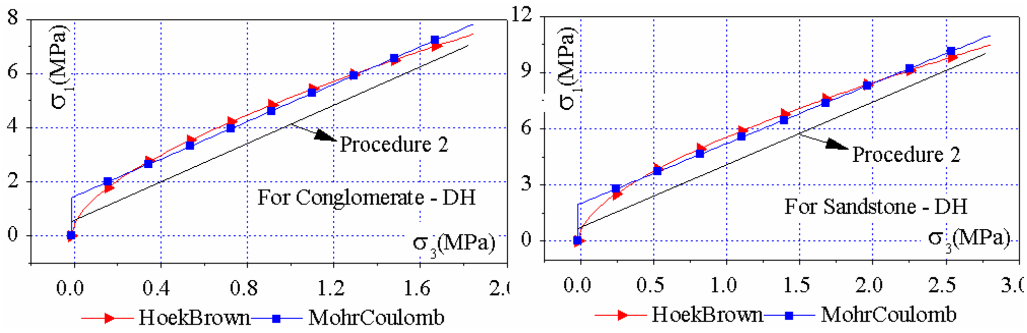

Figure 4.17 Equivalent Mohr envelope in principal stress space for conglomerate (left), sandstone (right); (Duong Huy mine).

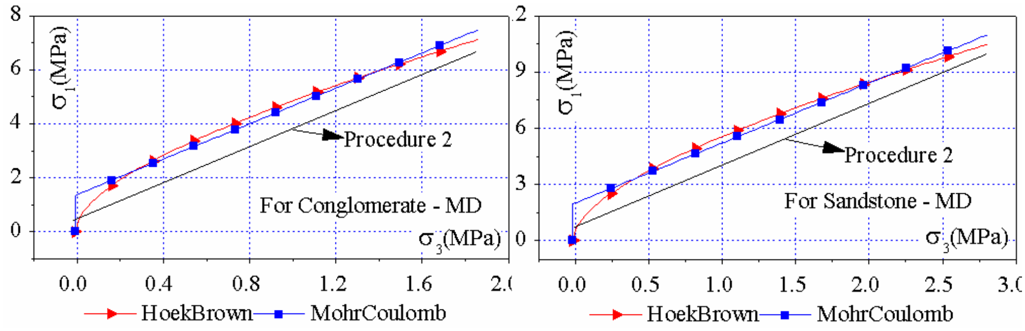

Figure 4.18 Equivalent Mohr envelope in principal stress space for conglomerate (left), sandstone (right); (Mong Duong mine).

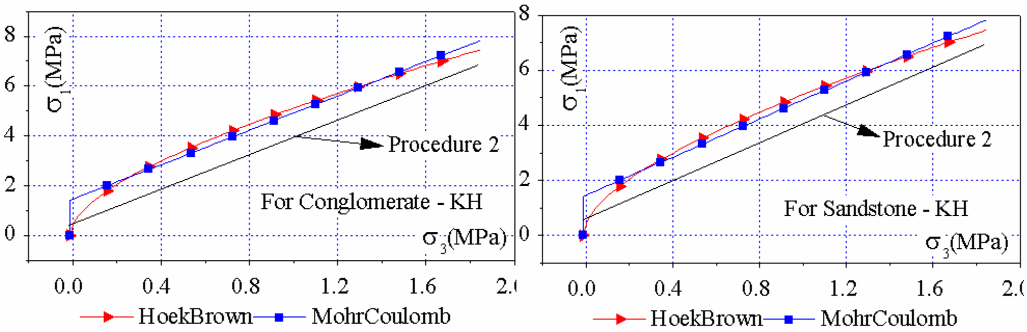

Figure 4.19 Equivalent Mohr envelope in principal stress space for conglomerate (left), sandstone (right); (Khe Cham mine).

Table 4.20 Physical properties of the rock mass surrounding Mong Duong roadway.

Type of rock mass	Properties of the rock mass								
	σ_c (MPa)	σ_t (MPa)	ρ (g/cm^3)	C (MPa)	φ (deg)	E (GPa)	ν (-)	K (Gpa)	G (GPa)
Conglomerate	0.360	0.01	2.63	0.100	32	0.886	0.20	0.406	0.39
Sandstone	0.535	0.02	2.62	0.145	33	0.977	0.17	0.678	0.38
Siltstone	0.601	0.03	2.62	0.173	35	1.049	0.22	0.625	0.43
Claystone	0.565	0.03	2.58	0.163	30	0.682	0.21	0.406	0.28

Table 4.21 Physical properties of the rock mass surrounding Khe Cham roadway.

Type of rockmass	σc (MPa)	σt (MPa)	ρ (g/cm^3)	C (MPa)	φ (deg.)	E (GPa)	ν (-)	K (GPa)	G (GPa)
Conglomerate	0.44	0.01	2.55	0.120	33	1.286	0.20	0.86	0.51
Sandstone	0.47	0.02	2.63	0.130	30	0.913	0.22	0.53	0.37
Siltstone	0.60	0.03	2.64	0.180	29	1.167	0.25	0.78	0.47

4.3 Set-up of numerical models

4.3.1 General solution procedure

To simulate and solve such a mechanical problem with FLAC a general solution procedure according to Figure 4.20 should be applied.

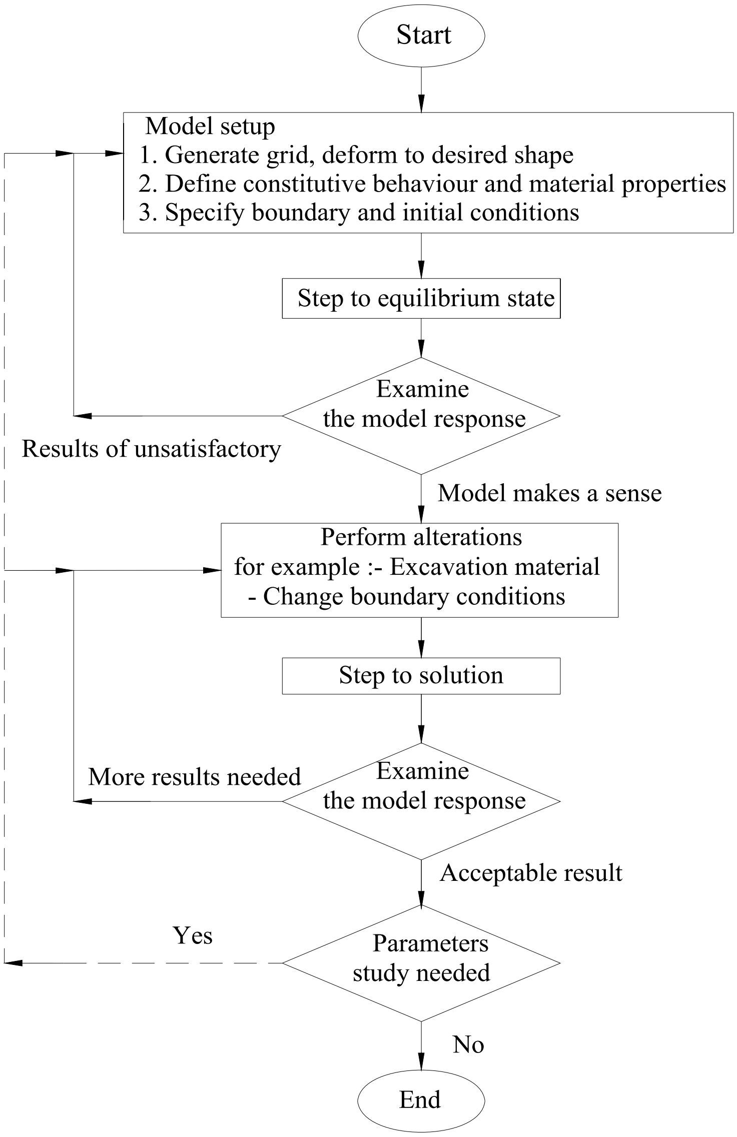
Start
Model setup
1. Generate grid, deform to desired shape
2. Define constitutive behaviour and material properties
3. Specify boundary and initial conditions
Step to equilibrium state
Examine the model response
Results of unsatisfactory
Model makes a sense
Perform alterations
for example :- Excavation material
- Change boundary conditions
Step to solution
More results needed
Examine the model response
Acceptable result
Yes
Parameters study needed
No
End

Figure 4.20 General solution procedure.

Exemplary, the procedure is explained in detail for the Cao Thang mine. The model is set up in form of a square 40 meters long each side. The opening is created in the centre of the model and located in both conglomerate and sandstone. The origin of the coordinate system is situated at the bottom left corner. A radial mesh with about 10000 elements (grid 100 x 100) is generated so that the element size increases away from the drift toward the boundary. This creates a finer grid at the boundary of the opening in order to increase accuracy of the results. Shape and size of the drift were chosen according to Table 4.7 and Fig. 4.13.

At the vertical boundaries and the model bottom the normal displacements are fitted. A vertical pressure is uniformly applied to the uppermost side (in a depth of 160 meters below surface) with a value of 4.16 MPa, which corresponds to the overburden weight. The two side pressures are in triangular distribution with maximum value of 2.5 MPa. The layers of the rock are inclined by 32 to 40 degrees (Fig. 4.4).
A primary stress field according to the overburden weight and the elastic law under assumption of vanishing lateral movement was initialized. So the initial vertical pressures inside the model obeys the law $p_v = \gamma H$. The two horizontal pressures in x (lateral) and z (out-of-plane component) direction were obtained by multiplying with horizontal earth pressure ratio λ $(\nu/(1-\nu))$. After setting all initial and boundary conditions the following steps were performed:

- Running the model in the elastic mode until equilibrium is reached.
- Application of elasto-plastic material properties for each layer and calculation until equilibrium. This is the simulation for the real primary in-situ state before engineering disturbs the medium by creation of an opening.
- Application of the so-called “soft core method” to simulate the 3D effect (values of elastic rock mass properties inside the future opening are decreased by multiplying with a coefficient of 0.4 and again calculation until equilibrium). This process creates displacements and stress redistributions similar to the stage (point in time) when bolting is performed.
- Creation of the opening and installation of anchors. A large strain mode option is used when the opening is excavated to update grid coordinates at each program step. Material properties listed in Table 4.1 are applied to the models. The structural elements are installed according to the scheme required.

- Application of the C – ϕ reduction method to determine the safety and reinforcement factors.

4.3.2 Model types

The models can be divided into two groups to investigate the interaction between the rockbolts and the rock mass according to Figure 4.21:

- In model type A no rockbolts are installed. That means the opening is unsupported after excavation. The response of models in form of displacements, stresses, deformations and velocities is monitored and recorded into files, figures and graphs.
- In model type B rockbolts are installed. Different rockbolt pattern are applied and investigated.

3 different type B can be distinguished:

- Type B1: rockbolts are installed only along the boundary of the roof (arch). See also Figure 4.13.
- Type B2: rockbolts are installed along the boundary of the roof (arch) and the sidewalls of the opening except for the floor.
- Type B3: rockbolts are installed along the whole boundary of the opening including the floor.

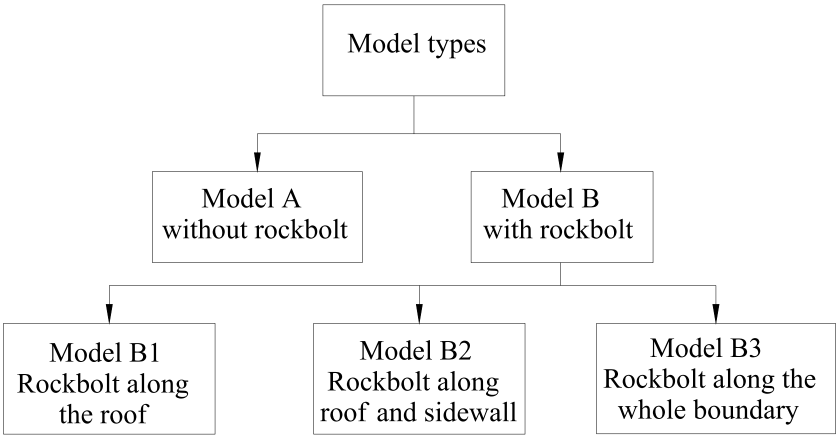
Model types
Model A
without rockbolt
Model B
with rockbolt
Model B1
Rockbolt along
the roof
Model B2
Rockbolt along
roof and sidewall
Model B3
Rockbolt along the
whole boundary

Figure 4.21 Types of models used for investigation.

Table 4.22 Rockbolt parameters used for model simulation.

Rockbolt parameters	Symbol	Unit	Value
Elastic modulus of rockbolt bar	E	GPa	200
Cross-sectional area of rockbolt bar	Area	m^2	3.14e-4
Moment of inertia of rockbolt bar	I	m^4	2e-8
Exposed perimeter of rockbolt bar	Per	m	6.28e-2
Maximum tensile force	Yield	kN	141
Cohesive strength of the normal coupling spring	Cs_ncoh	N/m	1e14
Stiffness of the normal coupling spring	Cs_nstiff	N/m/m	1e7
Friction resistance of the normal coupling spring	Cs_nfric	degree	30
Stiffness of the shear coupling spring	Cs_sstiff	N/m/m	1e7
Cohesive strength of the shear coupling spring	Cs_scoh	N/m	2.25e6
Friction resistance of the shear coupling spring	Cs_sfric	degree	30

Tables 4.23 to 2.27 give a detailed description of all applied rockbolt pattern. The short names for the applied rockbolt patterns are defined according to the following scheme:

- First two letters of the name denote the abbreviation of the mine name (e.g. caf48) where “ca” means Cao Thang Mine.
- Last number (e.g. 8) means distance between the bolts (here: 0.8 m).
- Number before the last one, if existing, indicates the length of the bolt (2, 3, 4 m), if not, default is 1.5 m for simplifying (‘1.5’ implicit in the name),
- Last letter in the middle, s or f, means rockbolts are installed either in the roof and sidewalls (s) or all around the boundary (f).
- The case “without rockbolt” is an exception. The first two letters of the name denote the name of the mine and number “0” indicates, that rockbolts, are not applied (e.g. ca0, mk0…).

In total 185 different numerical models were set-up, calculated and evaluated. If one includes the construction stages and the c-Φ-reduction method, much more than 1.000 model stages were calculated and investigated.

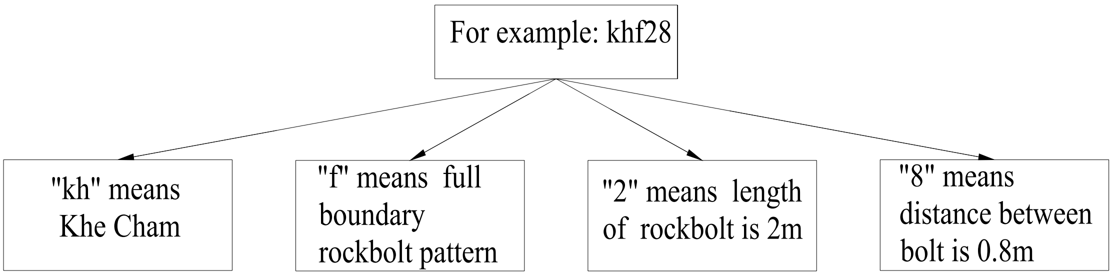
For example: khf28
"kh" means Khe Cham
"f" means full boundary rockbolt pattern
"2" means length of rockbolt is 2m
"8" means distance between bolt is 0.8m

Table 4.23 Types of rockbolt patterns for Cao Thang mine.

Rockbolt pattern	Parameters of the rockbolt (m)			
	Distance of 0.8			
Type B1	Bolt length 1.5	Bolt length 2.0	Bolt length 3.0	Bolt length 4.0
	ca8	ca28	ca38	ca48
Type B2	cas8	cas28	cas38	cas48
Type B3	caf8	caf28	caf38	caf48
Type B1	Distance of 0.6			
	ca6	ca26	ca36	ca46
Type B2	cas6	cas26	cas36	cas46
Type B3	caf6	caf26	caf36	caf46
Type B1	Distance of 0.4			
	ca4	ca24	ca34	ca44
Type B2	cas4	cas24	cas34	cas44
Type B3	caf4	caf24	caf34	caf44

Table 4.24 Types of rockbolt patterns for Mao Khe mine.

Rockbolt pattern	Parameters of the rockbolt (m)			
	Distance of 0.8			
Type B1	Bolt length 1.5	Bolt length 2.0	Bolt length 3.0	Bolt length 4.0
	mk8	mk28	mk38	mk48
Type B2	mks8	mks28	mks38	mks48
Type B3	mkf8	mkf28	mkf38	mkf48
Type B1	Distance of 0.6			
	mk6	mk26	mk36	mk46
Type B2	mks6	mks26	mks36	mks46

Type B3	mkf6	mkf26	mkf36	mkf46
Type B1	Distance of 0.4			
	mk4	mk24	mk34	mk44
Type B2	mks4	mks24	mks34	mks44
Type B3	mkf4	mkf24	mkf34	mkf44

Table 4.25 Types of rockbolt patterns for Duong Huy mine.

Rockbolt pattern	Parameters of the rockbolt (m)			
	Distance of 0.8			
Type B1	Bolt length 1.5	Bolt length 2.0	Bolt length 3.0	Bolt length 4.0
	dh8	dh28	dh38	dh48
Type B2	dhs8	dhs28	dhs38	dhs48
Type B3	dhf8	dhf28	dhf38	dhf48
Type B1	Distance of 0.6			
	dh6	dh26	dh36	dh46
Type B2	dhs6	dhs26	dhs36	dhs46
Type B3	dhf6	dhf26	dhf36	dhf46
Rockbolt pattern	Distance of 0.4			
Type B1	dh4	dh24	dh34	dh44
Type B2	dhs4	dhs24	dhs34	dhs44
Type B3	dhf4	dhf24	dhf34	dhf44

Table 4.26 Types of rockbolt patterns for Mong Duong mine.

Rockbolt pattern	Parameters of the rockbolt (m)			
	Distance of 0.8			
Type B1	Bolt length 1.5	Bolt length 2.0	Bolt length 3.0	Bolt length 4.0
	md8	md28	md38	md48
Type B2	mds8	mds28	mds38	mds48
Type B3	mdf8	mdf28	mdf38	mdf48
Type B1	Distance of 0.6			
	md6	md26	md36	md46
Type B2	mds6	mds26	mds36	mds46

Type B3	mdf6	mdf26	mdf36	mdf46
Type B1	Distance of 0.4			
	md4	md24	md34	md44
Type B2	mds4	mds24	mds34	mds44
Type B3	mdf4	mdf24	mdf34	mdf44

Table 4.27 Types of rockbolt patterns for Khe Cham mine.

Rockbolt pattern	Parameters of the rockbolt (m)			
	Distance of 0.8			
Type B1	Bolt length 1.5	Bolt length 2.0	Bolt length 3.0	Bolt length 4.0
	kh8	kh28	kh38	kh48
Type B2	khs8	khs28	khs38	khs48
Type B3	khf8	khf28	khf38	khf48
Type B1	Distance of 0.6			
	kh6	kh26	kh36	kh46
Type B2	khs6	khs26	khs36	khs46
Type B3	khf6	khf26	khf36	khf46
Type B1	Distance of 0.4			
	kh4	kh24	kh34	kh44
Type B2	khs4	khs24	khs34	khs44
Type B3	khf4	khf24	khf34	khf44

4.4 Model analysis

The influence of the rockbolts including the different rockbolt pattern is investigated by comparing the response of the models with and without rockbolts. The aim is to prove the reinforcement due to rockbolts, to quantify the increase of safety by defining a safety factor and applying the C-φ reduction method (see chapter 5).

In order to draw more general conclusions in respect to the interaction between rockbolts and rock mass, five different mines have been studied with different geological and technical conditions to confirm the effect of the rockbolts and to deduce more general laws of interaction between rockbolts and rock mass (see chapter 4.5).

Numerical simulations provide an enormous amount of information. The most important ones are presented in detail for the Cao Thang mine. For the other 4 mines only some selected results are shown.

Definition used in subsequent diagrams: a vertical line which starts from the top of the drift arch and is perpendicular to the horizontal surface is called **top line**.

4.4.1 Cao Thang mine

a. Models ca8 and ca0

The model ca8 belongs to type B1 where the length of the bolts is 1.5 m, and the distance between bolts is 0.8 m. Anchors are installed in the roof only.

a.1 Effect of changing stresses

Anchorage leads to an increase in tangential stresses near to the opening especially in the anchored roof area. The farfield is nearly unchanged. As Figure 4.22 indicates major principal stresses in the bolted area are increased by 1 to 2 MPa and provide additional confinement or arching.

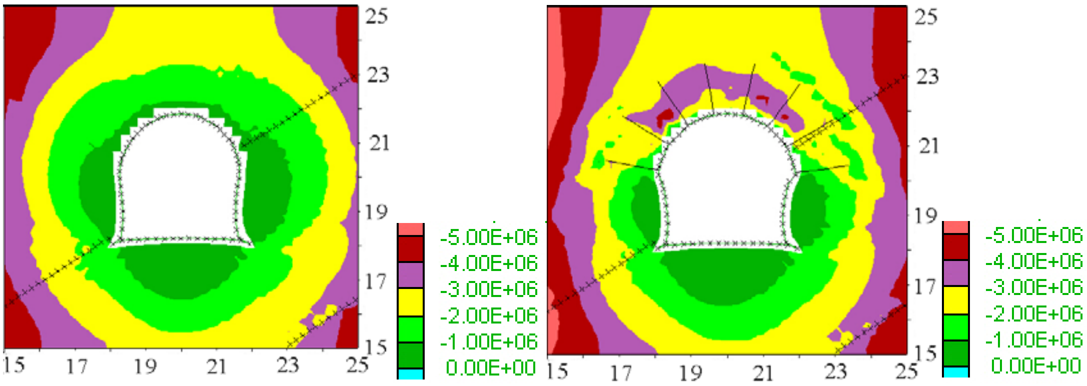

Figure 4.22 Contours of major principal stresses (Pa) without rockbolt ca0 (left) and with rockbolt ca8 (d = 0.8 m, right) with the length of the bolt l = 1.5 m; Dimension (m).

a.2 Effect of reducing displacements

The displacements and deformations in bolted area decrease compared to that in model without rockbolts. When the drift is unsupported, the maximum displacements are up to 16.5 cm at the top arch (Fig. 4.23 left). With anchorage the maximum displacements are restricted to about 10 cm (Fig. 4.23 right). The movement of rock mass takes the shape of the natural arch if displacements exceed critical values. The thickness of the area with high deformation gradients in Figure 4.23 (left) can be considered as a basis for the selection of a suitable length of the bolts. Displacement values between 9 to 11 cm observed between two adjacent bolts (Figure 4.23 (right)) gives us a suggestion of appropriate cross section of anchors.

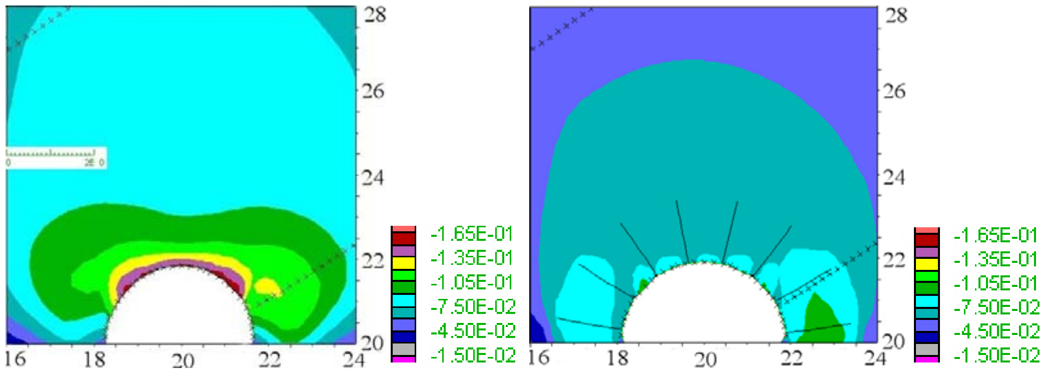

Figure 4.23 Contours of vertical displacement (m) without rockbolt ca0 (left) and with rockbolt ca8 (d = 0.8 m, right) with the length of the bolt l = 1.5 m; Dimension (m).

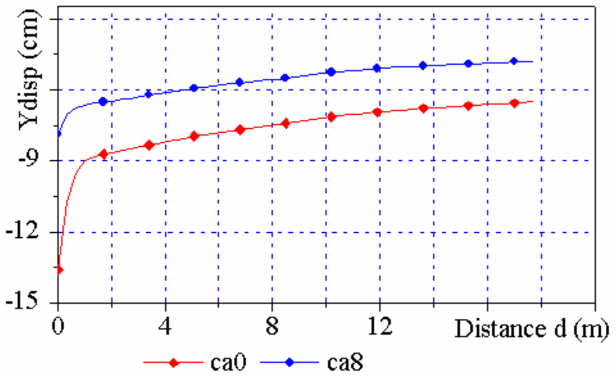

Figure 4.24 Vertical displacements ydisp (cm) along the top line d (m) without rockbolt ca0 and with rockbolt ca8 (d = 0.8 m, right) with the length of the bolt l = 1.5 m.

When rockbolts are installed in the roof, the displacements decrease considerably in the roof (Fig. 4.23 and 4.24) compared to that of the model without rockbolts, especially at the top of the arch. Figure 4.25 indicates that the deformation is limited around the arch boundary where bolts are installed. At the sidewall the movements have nearly the same amplitude in both models.

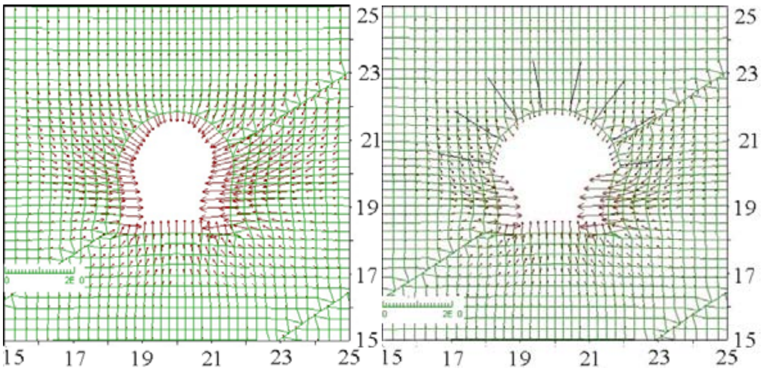

Max vector = 4.57e-1 Max vector = 4.544e-1

Figure 4.25 Displacement vectors (m) without rockbolts ca0 (left) and with rockbolts ca8 (d = 0.8 m, right) with the length of the bolts l = 1.5 m; Dimension (m).

a.3 Effect of reducing plasticity

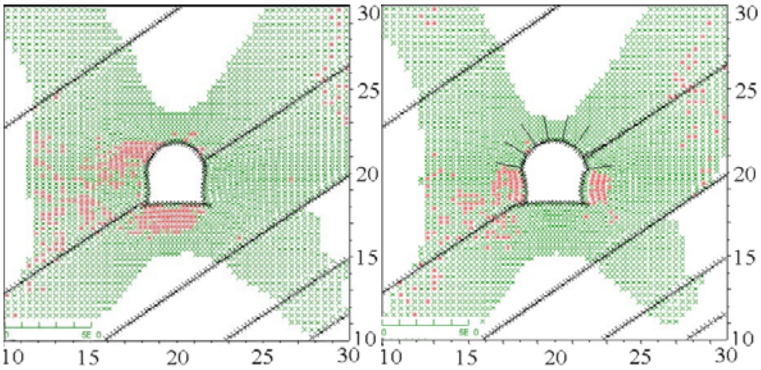

Figure 4.26 Plasticity area without rockbolt ca0 (left) and with rockbolt ca8 (d = 0.8 m, right) with the length of the bolt l = 1.5 m. The red elements show the yield in shear, the green ones represent the elastic state but plastic in past; Dimension (m).

As Figure 4.26 indicates active plasticity in the roof and the floor almost disappear if bolting is performed. Along both left and right sidewalls of the opening where rockbolts are not installed, the plasticity is only slightly changed.

a.4 Effect of increasing the safety factors

The safety factor increases in the bolted area and above. The values of safety factors in bolted areas increase up to 1.2 and higher in conglomerate layer. The white colour in Figure 4.27 indicates that the value of safety factor is more than 1.5.

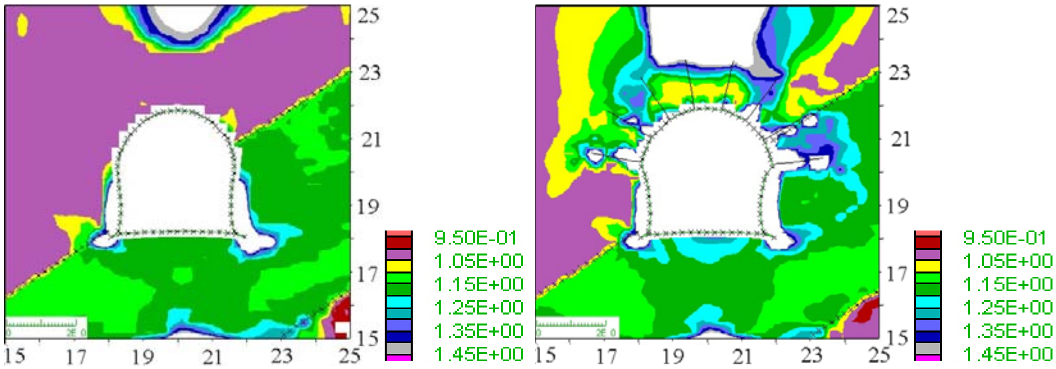

Figure 4.27 Safety factors without rockbolts ca0 (left) and with rockbolts ca8 (d = 0.8 m, right) with the length of the bolts l = 1.5 m; Dimension (m).

The safety factor is determined by the strength/stress ratio for each zone in the model using the Mohr – Coulomb failure criterion.

Safety factor (F) is defined by ratio:

$$F = \frac{r_b}{r_a} = \frac{\sigma_3 - \sigma_{1f}}{\sigma_3 - \sigma_1} \tag{4.13}$$

where: σ_1, σ_3 principal stresses

and

$$\sigma_{1f} = \left(\frac{1+\sin\phi}{1-\sin\phi}\right)\sigma_3 - 2C\sqrt{\frac{1+\sin\phi}{1-\sin\phi}} \tag{4.14}$$

where: ϕ friction angle,

r_a radius of the circle which represents the actual stress state,

r_b radius of the circle which represents the failure state (Fig. 4.28).

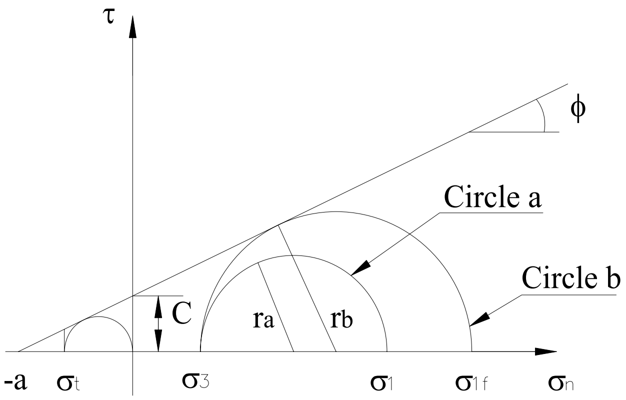

Figure 4.28 Determination of the safety factor by using Mohr-Coulomb criterion.

a.5 Effect of reducing the axial anchor force

The axial forces of the rockbolts are different for different rockbolt pattern. When the distance between bolts decreases, the axial force also reduces (Fig. 4.29). A reduction of the distance between anchors from 0.8 to 0.4 m lead to a reduction of about 40-50 % for the anchor forces.

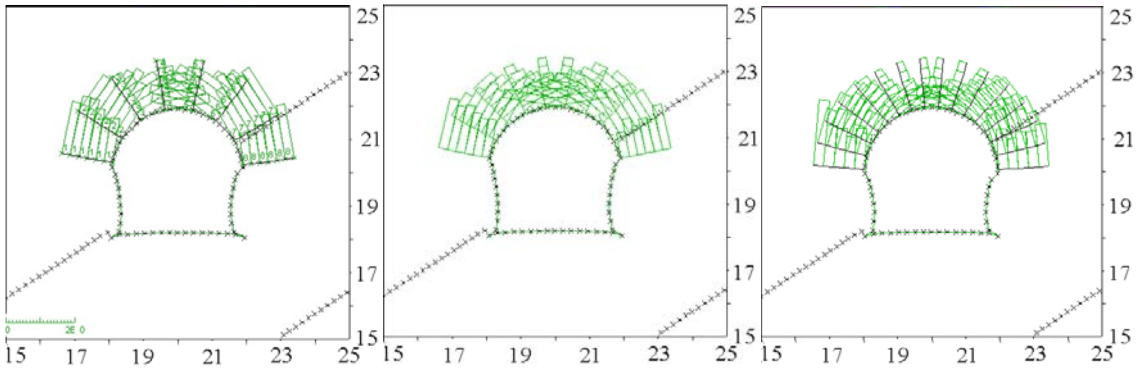

Max value: 0.91	Max value: 0.74	Max value: 0.58
Min value: 0.75	Min value: 0.50	Min value: 0.38

Figure 4.29 Axial anchor forces (MN) of the rockbolts for the models ca8 (d = 0.8 m), ca6 (d = 0.6 m); ca4 (d = 0.4 m) with the same length of bolts (l = 1.5 m) in all models; Dimension (m).

b. Models cas8 – cas28 – cas38 – cas48

These models belong to type B2 (anchors in the roof and sidewalls) in which the distance between rockbolts keeps the same value of 0.8 m but the length of the bolts change from 1.5 m to 2.0, 3.0 and 4.0 meters in the models cas8, cas28, cas38 and cas48, respectively.

b.1 Effect of reducing displacements and deformations

The displacements at the boundaries decrease when the length of the bolts increases from 1.5 m to 2.0, 3.0 and 4.0 m (Figure 4.30). Vertical displacements along the top line also reduce with increasing anchor length. The difference between 3.0 and 4.0 m anchor length is only marginal, so that from this point of view the optimum anchor length is about 3.0 m.

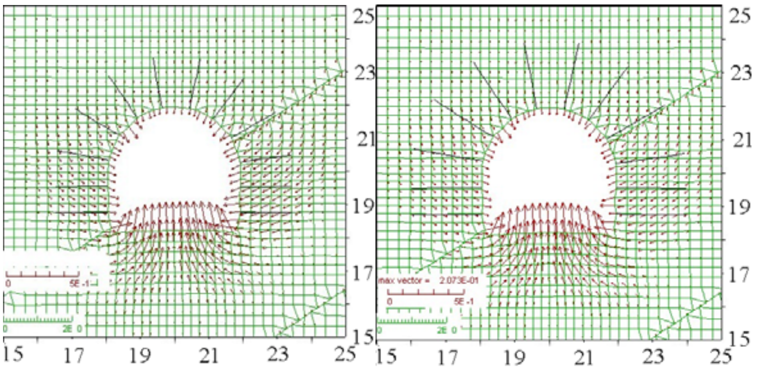
25
23
21
19
17
15
15
17
19
21
23
25
0
5E -1
2E 0
max vector = 2.073E-01

Max vector = 2.156E-01 Max vector = 2.073E-01

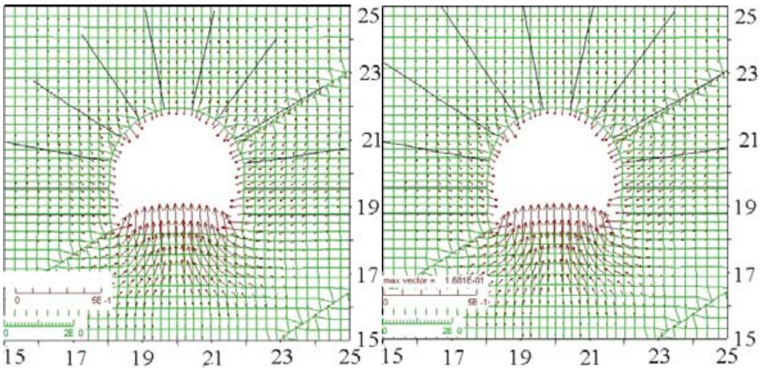
25
23
21
19
17
15
15
17
19
21
23
25
0
5E -1
2E 0
max vector = 1.681E-01

Max vector = 1.8386E-01 Max vector = 1.681E-01

Figure 4.30 Displacement vectors (m) for models cas8 (l = 1.5 m), cas28 (l = 2.0 m), cas38 (l = 3.0 m), cas48 (l = 4.0 m) with the same distance between bolts d = 0.8 m in all models. Dimension (m)

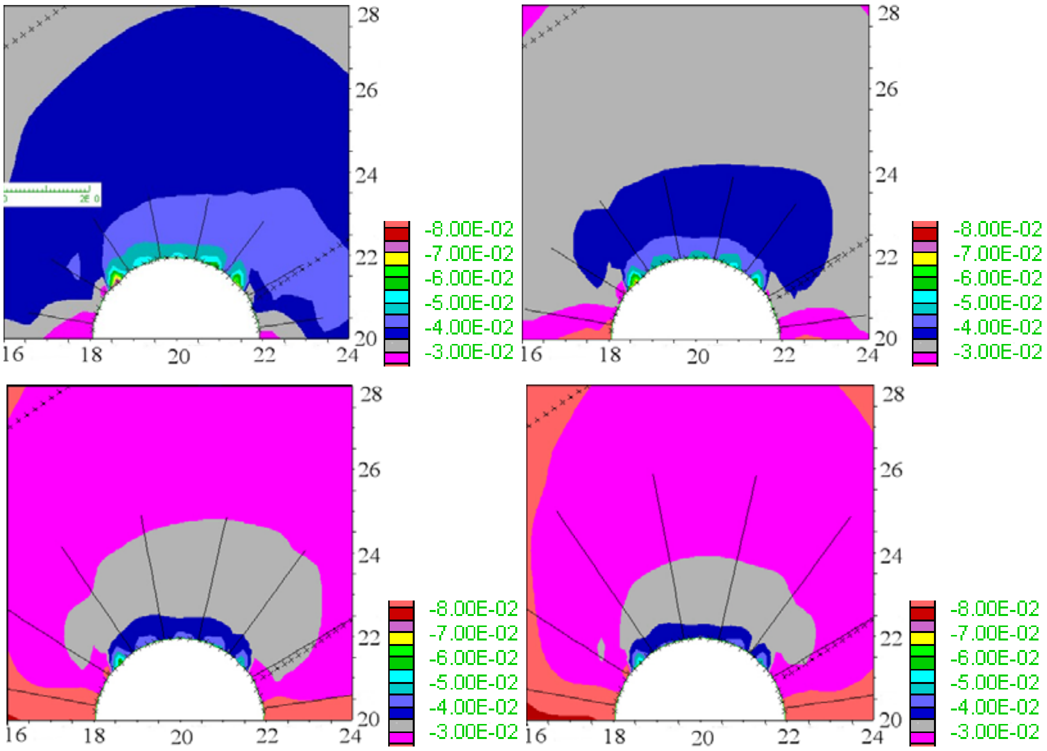

Figure 4.31 Contours of vertical displacements (m) for the models cas8 (l = 1.5 m), cas28 (l = 2.0 m), cas38 (l = 3.0 m) and cas48 (l = 4.0 m) with the same distance between bolts d = 0.8 m in all models; Dimension (m).

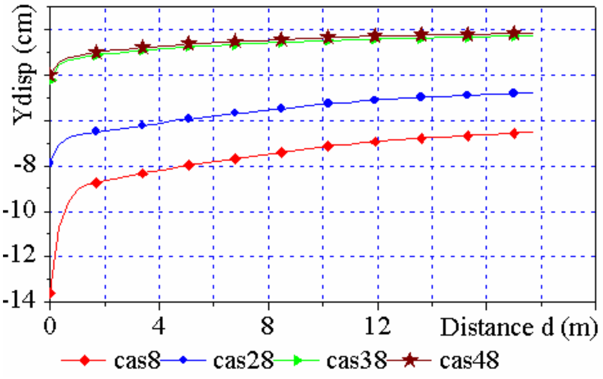

Figure 4.32 Vertical displacement Ydisp (cm) along the top line for the models cas8 (l = 1.5 m), cas28 (l = 2.0 m), cas38 (l = 3.0 m) and cas48 (l = 4.0 m) with the same distance between bolts d = 0.8 m in all models.

b.2 Effect of changing stresses

Increasing anchor length leads to a more uniform stress pattern and increased confinement, but the effect is not very pronounced.

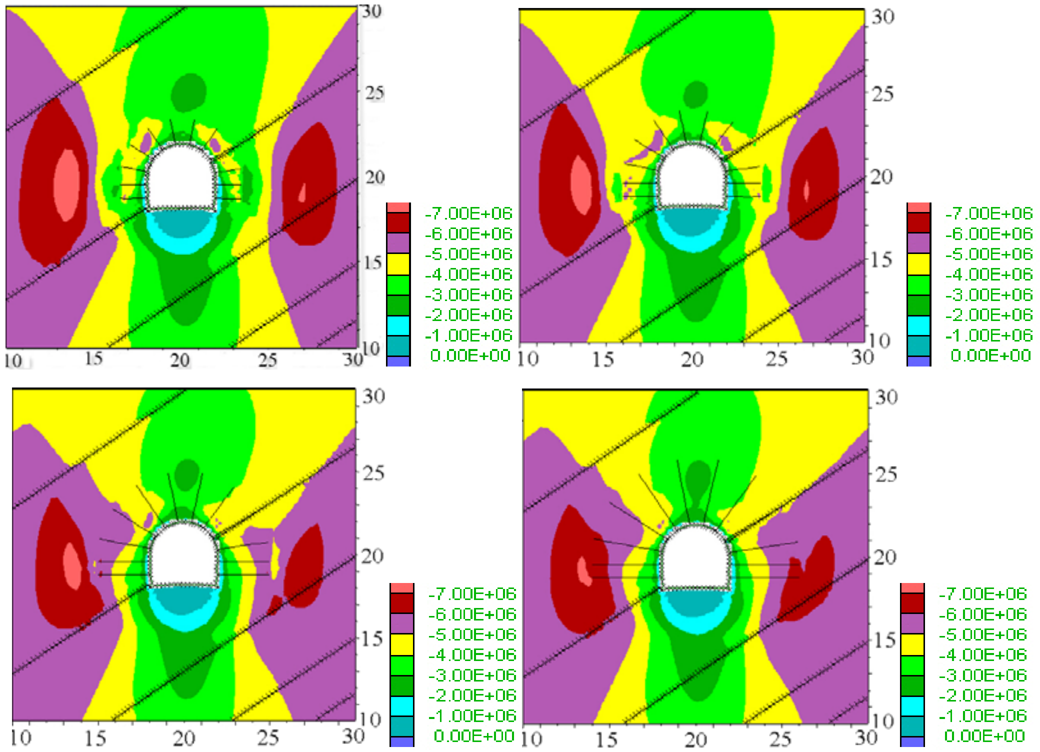

Figure 4.33 Contours of major principal stress (Pa) for the models cas8 (l = 1.5 m), cas28 (l = 2.0 m), cas38 (l = 3.0 m), cas48 (l = 4.0 m) with the same distance between bolts d = 0.8 m in all models; Dimension (m).

c. Models cas6 – cas4

These models belong to type B2 (anchors in the roof and the sidewalls) where the length of the bolts is l = 1.5 m, the distances d between bolts change from 0.6 to 0.4 m in models cas6 and cas4, respectively.

c.1 Effect of reducing the displacements and deformations

Displacement vectors decrease when the distance between bolts changes from 0.6 to 0.4 m, especially along the bolted boundary (Fig. 4.34). Vertical displacements along the top line are approximately 2 cm lower for the denser anchorage (Fig. 4.35).

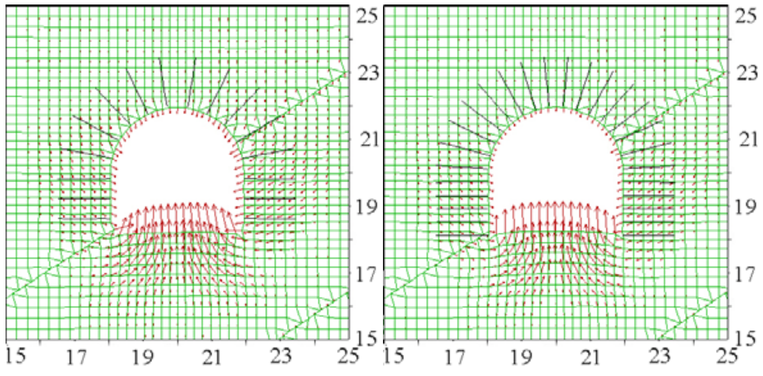

Max vector = 2.4e-1 Max vector = 2.065e-1

Figure 4.34 Displacement vectors (m) for the models cas6 (d = 0.6 m, left) and cas4 (d = 0.4 m, right) with the same length of bolt l = 1.5 m; Dimension (m).

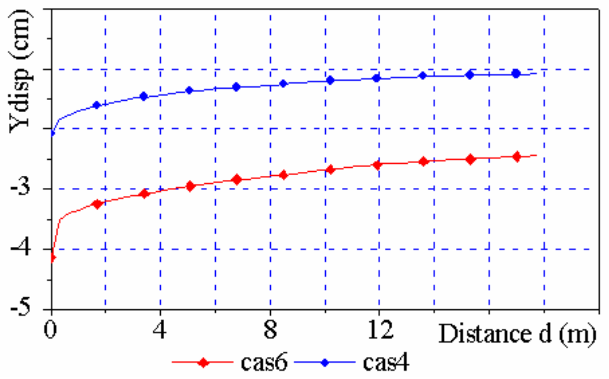

Figure 4.35 Vertical displacement Ydisp (cm) along the top line for the model cas6 (d = 0.6 m) and cas4 (d = 0.4 m) with the same length of bolt l = 1.5 m.

c.2 Effect of reducing plasticity

Active plasticity in the near-field of the opening decreases when the distance between bolts reduces (Figure 4.36).

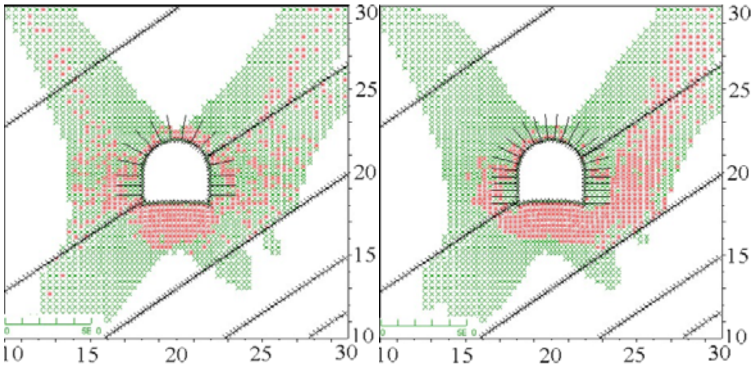

Figure 4.36 Plasticity that occurs in models cas6 (d = 0.6 m, left) and cas4 (d = 0.6 m, right) with the same length of bolt l = 1.5 m. The red elements show the yield in shear, the green ones represent the elastic state but plastic state in past; Dimension (m).

c.3 Effect of changing the major principal stresses

In model ca4 high tangential stresses in the near-field of the opening are spread over a larger area compared to model cas6. The increase of tangential stresses, which create additional confinement, are in the order of 1 MPa. Only in the unsupported floor the stress keeps almost unchanged (Fig. 4.37).

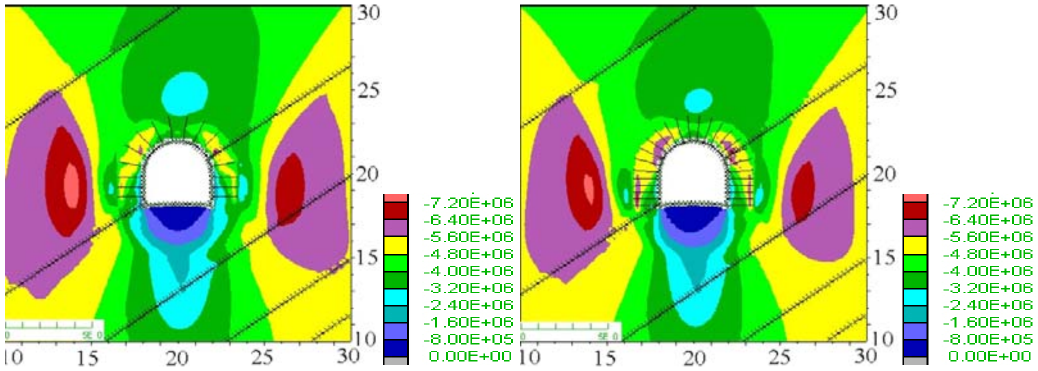

Figure 4.37 Contours of major principal stress (Pa) in models cas6 (d = 0.6 m, left), cas4 (d = 0.4 m, right) with the same length of bolt l = 1.5 m; Dimension (m).

c.4 Effect of reducing the axial anchor force

The axial force of the rockbolts reduce when the distance between them decreases (Fig. 4.38). A reduction of the distance between bolts from 0.6 to 0.4 m leads to a reduction of the anchor forces of app. 25÷40 %.

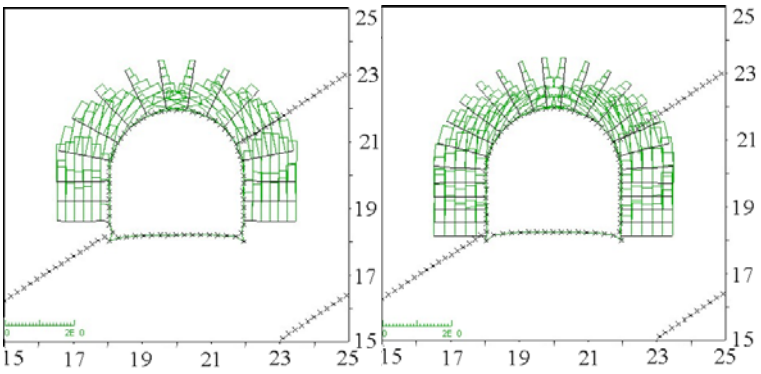

Maximum value 1.18 Maximum value 0.89

Minimum value 0.58 Minimum value 0.36

Figure 4.38 Axial forces (MN) of the rockbolts in models cas6 (d = 0.6 m, left), cas4 (d = 0.4 m, right) with the same length of bolt l = 1.5 m; Dimension (m).

d. Models caf8-caf6-caf4

These models belong to type B3 (anchorage along the complete boundary) where the length of the bolts is 1.5 m, the distance between rockbolts changes from 0.8 to 0.6 and 0.4 m.

d.1 Effect of reducing the displacements and deformations

When the distance between the bolts change from 0.8 to 0.6 and 0.4 m the vertical displacements along the top line beginning at the roof reduce from 4.2 cm to 3.0 cm, from 3.0 cm to 2.2 cm and finally from 2.4 cm to 1.6 cm in models caf8, caf6, caf4, respectively (in the same height from the boundary upwards). The denser the anchorage the lower the displacements (Fig. 4.39 and 4.40). The change in the displacements can be observed also along the top line (Fig. 4.41).

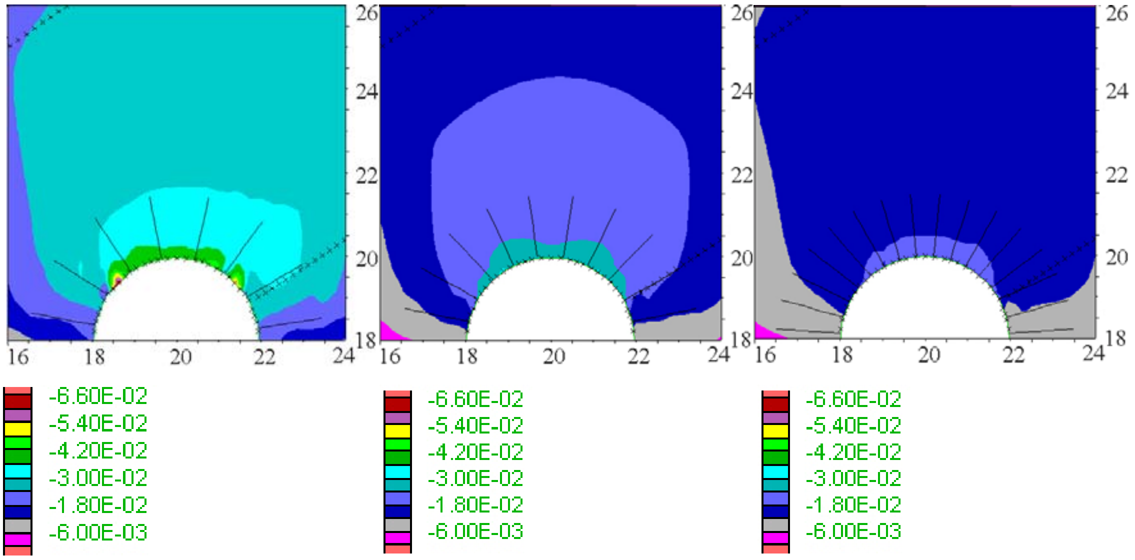

Figure 4.39 Contours of vertical displacements (m) for the models caf8 (d = 0.8 m), caf6 (d = 0.6 m), caf4 (d = 0.4 m) with the same length of bolt l = 1.5 m in all models; Dimension (m).

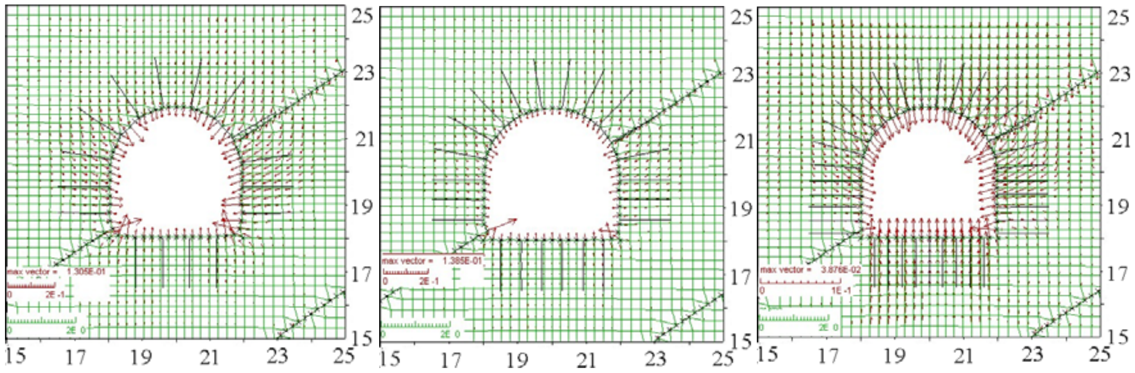

Max vector = 1.305e-1 Max vector = 1.385e-1 Max vector = 3.876e-2

Figure 4.40 Displacement vector (m) for the models caf8 (d = 0.8 m), caf6 (d = 0.6 m), caf4 (d = 0.4 m), with the same length of bolt l = 1.5 m in all models; Dimension (m).

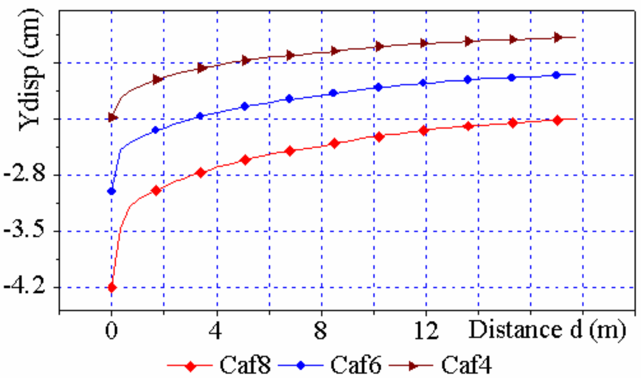

Figure 4.41 Vertical displacement Ydisp (cm) along the top line (m) for the models caf8 (d = 0.8 m), caf6 (d = 0.6 m) and caf4 (d = 0.4 m) with the same length of bolt (l = 1.5 m) in all models.

d.2 Effect of reducing plasticity

When the distance between the bolts changes from 0.8 m to 0.6 m and 0.4 m active plasticity is decreasing (Fig. 4.42).

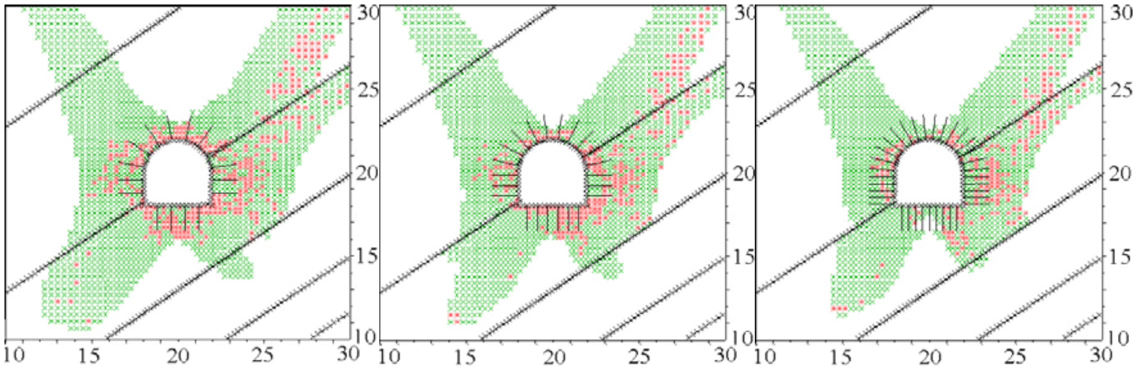

Figure 4.42 Plasticity for the models caf8 (d = 0.8 m), caf6 (d = 0.6 m), caf4 (d = 0.4 m) with the same length of bolt (l = 1.5 m) in all models. The red elements show the yield in shear, the green ones represent the elastic state but plastic state in past; Dimension (m).

d.3 Effect of changing stresses

If distance between rockbolts is reduced tangential stresses in the near-field of the opening increase. An increase of 1 to 2 MPa can be observed, if the distance between anchors is shorten from 0.8 to 0.4 m (Fig. 4.43). This leads to an additional confinement and arch building.

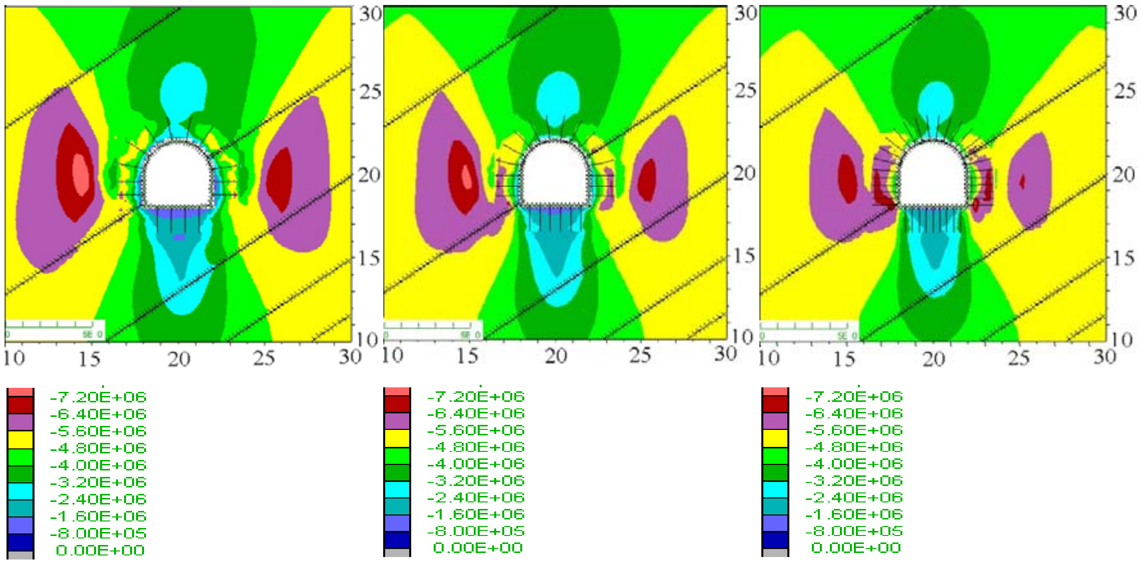
30
25
20
15
10
10
15
20
25
30
-7.20E+06
-6.40E+06
-5.60E+06
-4.80E+06
-4.00E+06
-3.20E+06
-2.40E+06
-1.60E+06
-8.00E+05
0.00E+00

Figure 4.43 Contour of major principal stress (Pa) for the models caf8 (d = 0.8 m), caf6 (d = 0.6 m), caf4 (d = 0.4 m) with the same length of bolts (l = 1.5 m) in all models; Dimension (m).

d.4 Effect of increasing the safety factors

In the nearfield of the opening, up to about 5 m from the surface into the rock mass, the safety factor is increased due to bolting. This significant increase is in the order of about 5 to 30 % as shown in Figure 4.44.

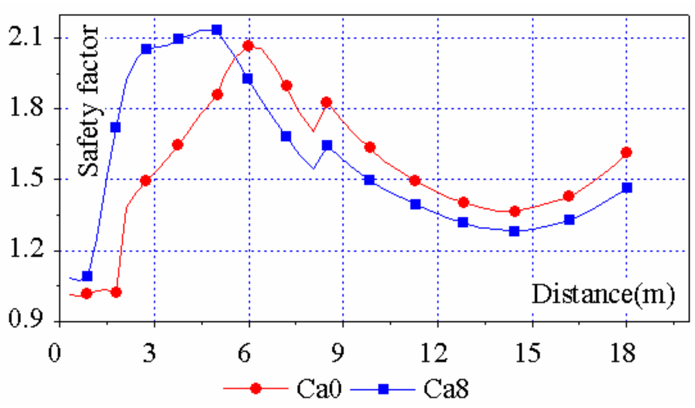

Figure 4.44 Safety factors along the top line for the models without rockbolt ca0 and with rockbolt ca8 (d = 0.8 m) with the length of bolts l = 1.5 m.

e. Comparison of displacements

e.1 Case 1

Group 1 includes the models ca8, ca28, ca38 and ca48 with following parameters of the rockbolts: distance between bolts d = 0.8 m, length of the bolts are 1.5 m, 2.0 m, 3.0 m and 4.0 m.

Group 2 consists of the models ca6, ca26, ca36 and ca46 with following parameters of the rockbolts: distance between bolts d = 0.6 m, length of the bolts are 1.5 m, 2.0 m, 3.0 m and 4.0 m.

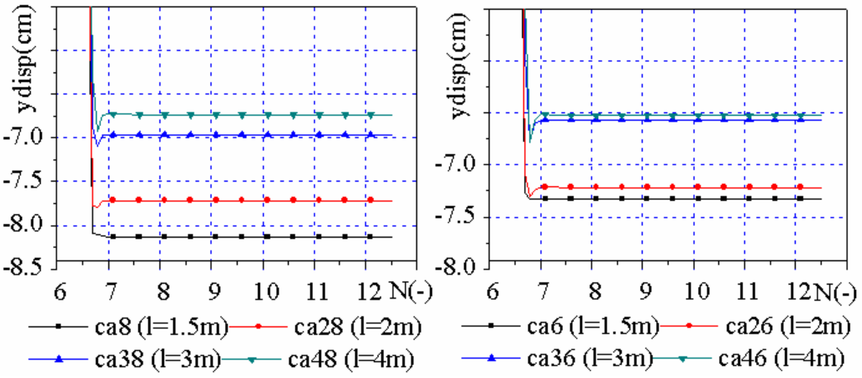

Figure 4.45 Vertical displacements ydisp versus calculation steps (Nx10^4) at the top of the roof for the models which belong to group 1 and group 2.

Group 1 and group 2 belong to model type B1. The graphs show that when the distance between bolts decreases from 0.8 m to 0.6 m, the displacements reduce (Fig. 4.45). Also, longer bolts reduce the displacements.

e.2 Case 2

Group 3 comprises the models cas6, cas26, cas36 and cas46 with the following parameter of the rockbolts: distance between bolts d = 0.8 m, length of the bolts are 1.5 m, 2.0 m, 3.0 m and 4.0 m.

Group 4 consists of the models cas4, cas24, cas34, cas44 with the following parameters of the rockbolts: distance between bolts d = 0.6 m, length of the bolts are 1.5 m, 2.0 m, 3.0 m and 4.0 m.

Group 3 and group 4 belong to model type B2. The graphs show that when the distance between bolts decreases from 0.6 m to 0.4 m, the displacements reduce (Fig. 4.46)

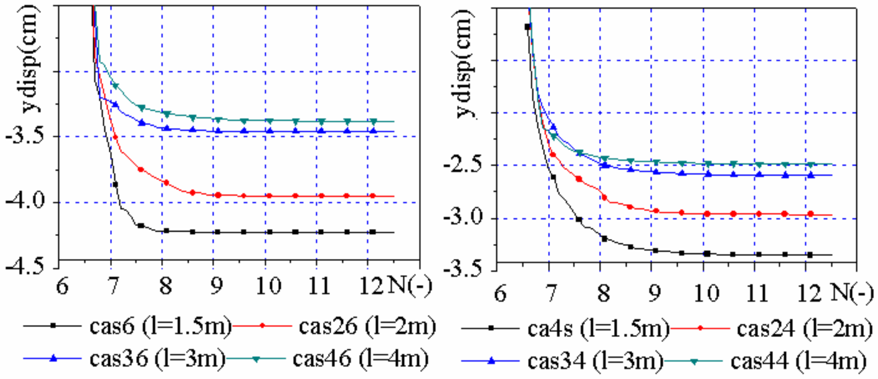

Figure 4.46 Vertical displacements ydisp versus calculation steps (Nx10^4) at the top of the roof in the models which belong to group 3 and group 4.

e.3 Case 3

Group 5 includes the models caf8, caf28, caf38 and caf48 with the following parameters of the rockbolts: distance between bolts d = 0.8 m, lengths of the bolts are 1.5 m, 2.0 m, 3.0 m and 4.0 m.

Group 6 consists of the models caf6, caf26, caf36 and caf46 with the following parameter of the rockbolts: distance between bolts d = 0.6 m, length of the bolts are 1.5 m, 2.0 m, 3.0 m, 4.0 m.

Group 5 and group 6 belong to model type B3. The graphs show that when the distance between bolts decreases from 0.8 m to 0.6 m, the displacement reduces remarkably (Fig. 4.47)

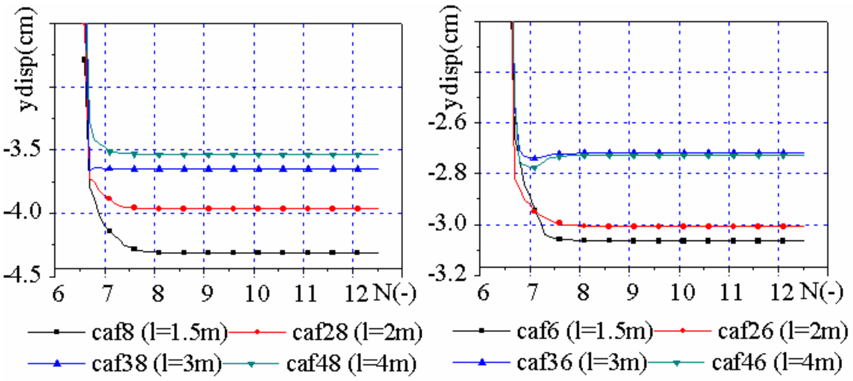

Figure 4.47 Vertical displacements ydisp (cm) versus calculation steps Nx10^4 at the top of the roof in the models which belong to group 5 and group 6.

The following conclusions can be drawn:

- Different rockbolt pattern lead to quite different displacements along the boundary of the opening.
- The displacements are direct proportional to the length of the bolts and inverse proportional to the distance between the bolts (Fig. 4.45, 4.46, 4.47)
- Bolting of the sidewall leads to a significant reduction of the displacements in the roof also und supplies higher overall stability.
- The extension of anchor length from 3 to 4 m does not give anymore significant improvements.

4.4.2 Mao Khe mine

A comparison between the unsupported (mk8) and the bolted model (mk0) reveal remarkable differences in the physical response. Model mk8 belongs to the type B1, where the anchor length is 1.5 m and the distance between anchors is 0.8 m.

The displacements and deformations clearly decrease in bolted area. The displacements reach 1.5 cm up to 2.0 cm without rockbolts but 2.0 cm up to 2.5 cm when bolting is applied (Fig. 4.48). The effect of displacement reduction can be clearly seen along the top line in Figure 4.49. Figure 4.50 indicates that the deformation reduction due to bolting is limited to area, where bolting is applied. The sidewall parts move with a similar amplitude in both models.

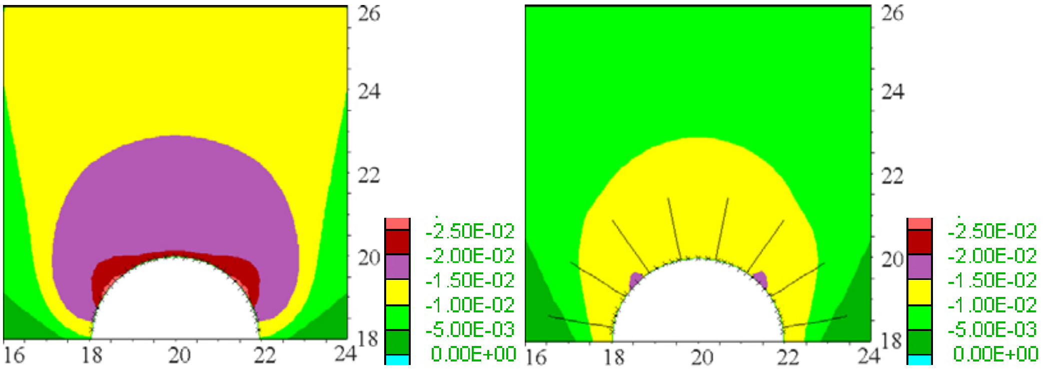

Figure 4.48 Contours of vertical displacement (m) without rockbolt mk0 and with rockbolts mk8 (d = 0.8 m) with the length of the bolt l = 1.5 m; Dimension (m).

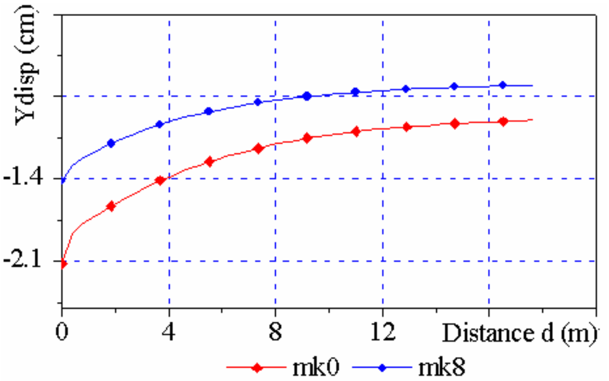

Figure 4.49 Vertical displacements Ydisp (cm) along the top line d (m) for the models without rockbolt mk0 and with rockbolt mk8 (d = 0.8 m) with the length of the bolt l = 1.5 m.

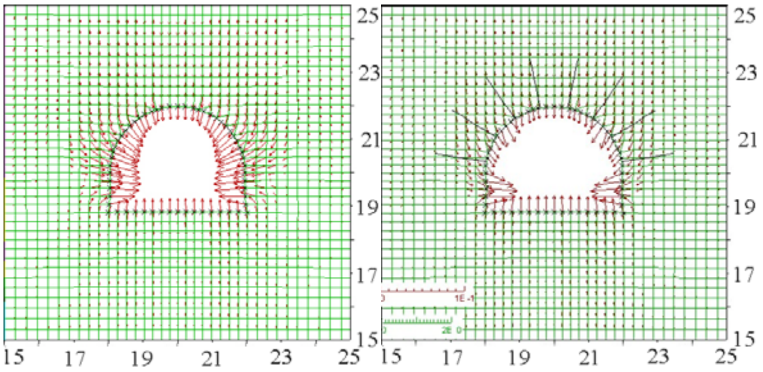
25
23
21
19
17
15
15
17
19
21
23
25

Max vector = 4.895e-2 Max vector = 3.743e-2

Figure 4.50 Displacement vector (m) for the models without rockbolt mk0 and with rockbolt mk8 (d = 0.8 m) with the length of the bolt l = 1.5 m; Dimension (m).

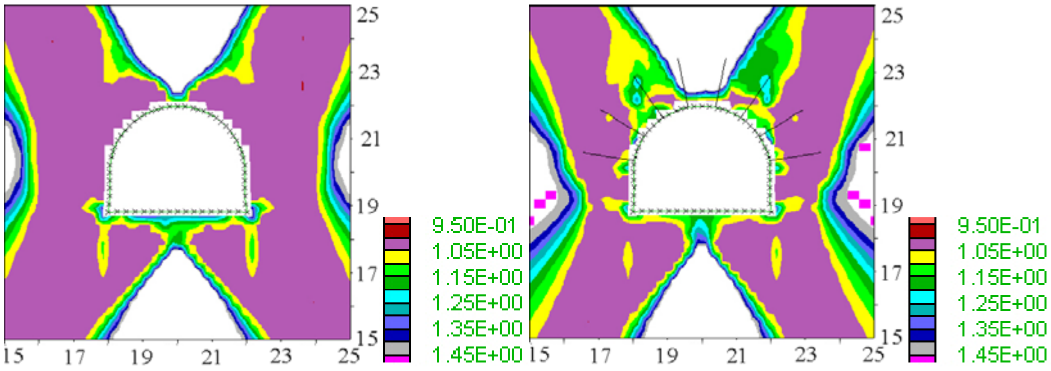
25
23
21
19
17
15
15
17
19
21
23
25
9.50E-01
1.05E+00
1.15E+00
1.25E+00
1.35E+00
1.45E+00

Figure 4.51 Safety factors for the models without rockbolt mk0 and with rockbolt mk8 (d = 0.8 m) with the length of the bolt l = 1.5 m; Dimensions (m).

The safety factor in the model without rockbolt is about 1.0. In the model with rockbolts the safety factors increase up to 1.2 and more. Especially the roof area shows safety factors greater than 1.2 if bolting is applied (Fig. 4.51).

Reduction of the distance between anchors would lead to significant reduction of forces in the anchors in all model types. The axial forces in the rockbolts are decreased by app. 30 to 40 % when the distance between them decreases from 0.8 m to 0.4 m (Fig. 4.52) and by app. 10 to 15% when the distance between them decreases from 0.8 m to 0.6 m (Fig. 4.53).

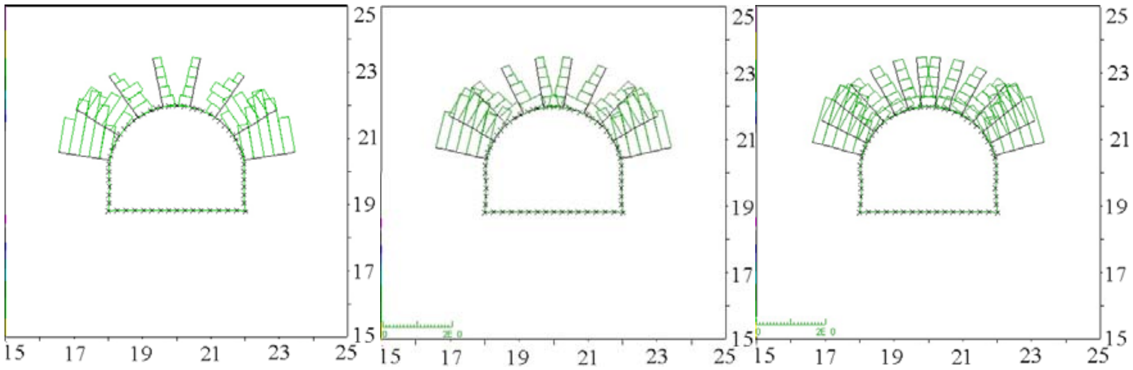
25
23
21
19
17
15
15
17
19
21
23
25
25
23
21
19
17
15
15
17
19
21
23
25
25
23
21
19
17
15
15
17
19
21
23
25

Max value: 0.622 Max value: 0.525 Max value: 0.43

Min value: 0.11 Min value: 0.115 Min value: 0.09

Figure 4.52 Axial force (MN) of the rockbolt for the models mk8 (d = 0.8 m), mk6 (d = 0.8 m), mk4 (d = 0.8 m) with the length of the bolt l = 1.5 m in all models; Dimension (m)

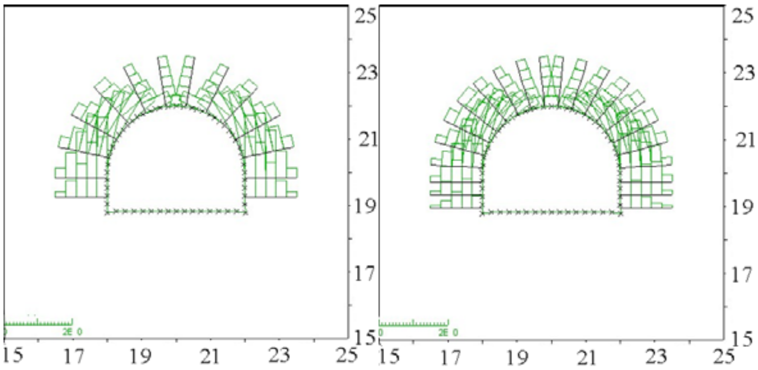

max value: 0.456 max value: 0.429

min value: 0.105 min value: 0.08

Figure 4.53 Axial force (MN) of the rockbolts for the models mks6 (d = 0.6 m), mks4 (d = 0.4 m) with the length of the bolts l = 1.5 m in all models; Dimension (m).

The positive effect of denser bolting can also be shown for the B3 type models here, rockbolts are installed along the full boundary of the opening. The distances between rockbolts change from 0.8 to 0.6 and 0.4 m, but the length of the bolt is always 1.5 m. When the distances between the rockbolts change from 0.8 to 0.6 and 0.4 meters the maximum vertical displacements decreases from 1.2 cm to 1.0 cm and 0.8 cm (Fig. 4.54).

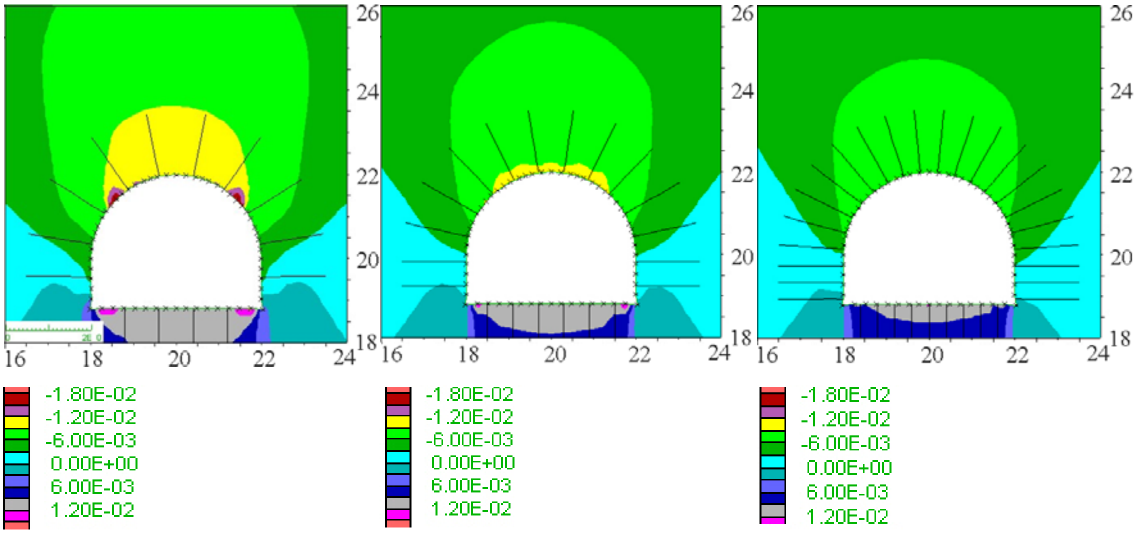

Figure 4.54 Contours of vertical displacement (MPa) for the models mkf8 (d = 0.8 m), mkf6 (d = 0.6 m), mkf4 (d = 0.4 m) with the length of the bolts l = 1.5 m in all models; Dimension (m).

This effect is also illustrated by the displacement vectors (Fig. 4.55) and the vertical displacements along the top line (Fig. 4.56).

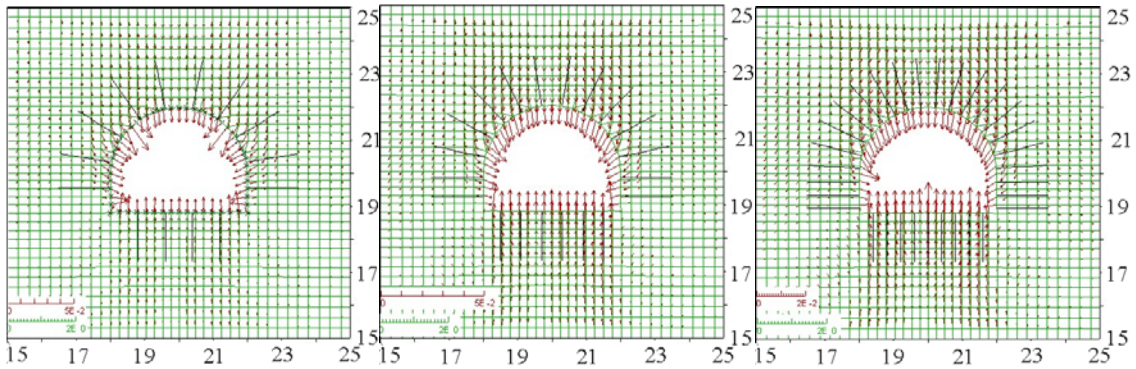

Max vector = 2.355e-2 Max vector = 1.51e-2 Max vector = 1.271e-2

Figure 4.55 Displacement vector (m) for the models mkf8 (d = 0.8 m), mkf6 (d = 0.6 m), mkf4 (d = 0.4 m) with the length of the bolts l = 1.5 m in all models, Dimension (m).

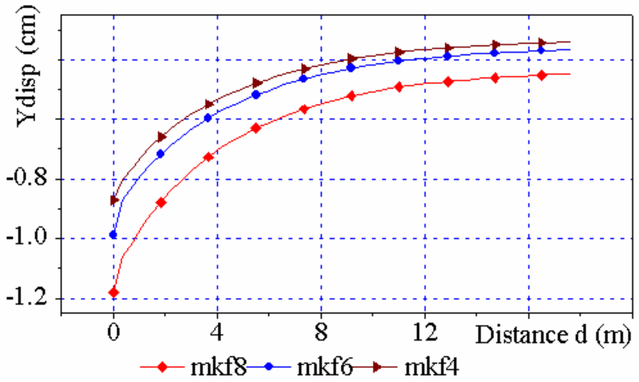

Figure 4.56 Vertical displacement Ydisp (cm) along the top line in model mkf8 (d = 0.8 m), mkf6 (d = 0.6 m) and mkf4 (d = 0.4 m) with the same length of bolts l = 1.5 m in all models.

There is no significant change in the safety factor along the top line even close to the boundary in the bolted area due to the fact, that already the unsupported opening shows a global safety factor of 1.75.

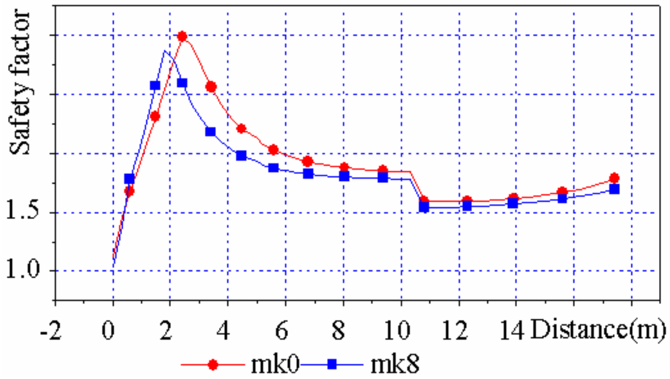

Figure 4.57 Safety factors along the top line for the models without rockbolts mk0 and with rockbolt mk8 (d = 0.8 m) with the length of bolts l = 1.5 m

Group 1 consists of the models mk8, mk28, mk38 and mk48 with the following parameters of the rockbolts: distance between bolts d = 0.8 m and length of the bolts are 1.5 m, 2.0 m, 3.0 m and 4.0 m. Group 2 includes the models mk6, mk26, mk36 and mk46 with the following parameters of the rockbolts: distance between bolts d = 0.6 m and the length of the bolts are 1.5 m, 2.0 m, 3.0 m and 4.0 m. Group 1 and group 2 belong to model type B1. The graphs show that the displacements decrease with the change of the rockbolt parameters, but there is only a slight change of just some millimetres. That means that already the models mk8 and mk6 have enough capacity to keep the displacements small (Fig. 4.58).

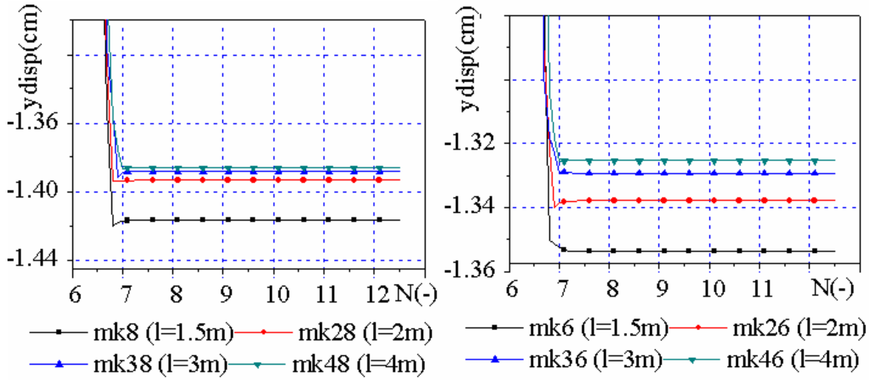

Figure 4.58 Vertical displacements ydisp versus calculation steps ($Nx10^4$) at the top of the roof in the models which belong to group 1 and group 2.

Group 3 comprises the models mks6, mks26, mks36 and mks46 with the following parameters of the rockbolts: distance between bolts d = 0.6 m and the length of the bolts are 1.5 m and 2.0 m, 3.0 m and 4.0 m. Group 4 consists of the models mks4, mks24, mks34 and mks44 with the following parameters of the rockbolts: distance between bolts d = 0.4 m and the length of the bolts are 1.5 m, 2.0 m, 3.0 m and 4.0 m. Group 3 and group 4 belong to model type B2, the graphs show that the displacements reduce when the parameters of the rockbolts change, but the displacement changes are very small and keep values of max. 2 mm. The models mks8 and mks6 have more capacity than mk8 and mk6 to keep the stability of the opening in this case (see Figure 4.59)

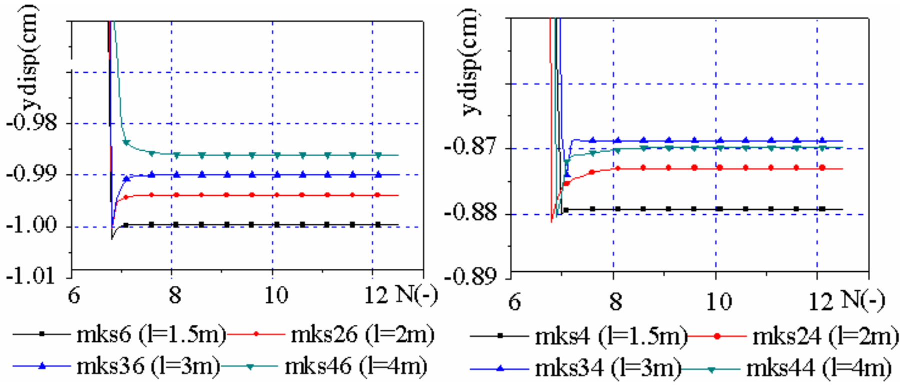

Figure 4.59 Vertical displacements ydisp versus calculation steps (Nx10^4) at the top of the roof in the models which belongs to group 3 and group 4.

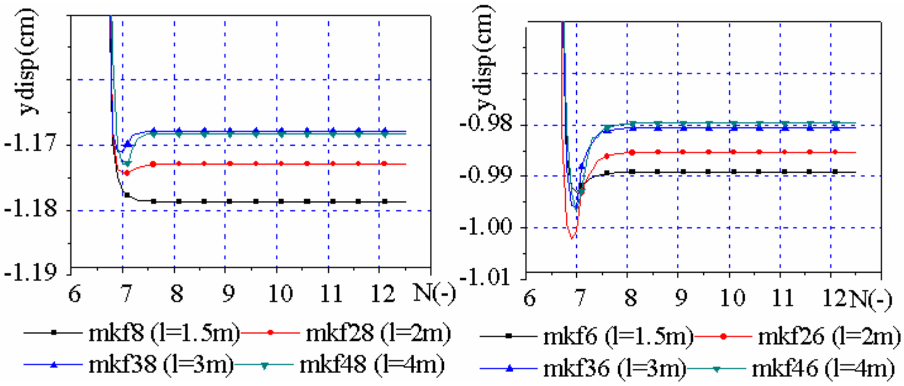

Figure 4.60 Vertical displacements ydisp versus calculation steps (Nx10^4) at the top of the roof in the models which belongs to group 5 and group 6.

Group 5 includes the models mkf8, mkf28, mkf38 and mkf48 with the following parameters of the rockbolts: distance between bolts d = 0.8 m and length of the bolts are 1.5 m, 2.0 m, 3.0 m and 4.0 m. Group 6 consists of the models mkf6, mkf26, mkf36 and mkf46 with the following parameters of the rockbolts: distance between bolts d= 0.6 m and length of the bolts are 1.5 m, 2.0 m, 3.0 m and 4.0 m. Group 5 and group 6 belong to model type B3. The graphs show that the displacements reduce when the parameters of the rockbolts change, but there is only a slight change of just 1 millimetre. That means models mkf8 and mkf6 have enough capacity to keep the stability (Fig. 4.60).

Remarks:

- Comparison of these rockbolt patterns shows that vertical displacement decreases when length of the bolt increases and the distance between bolts decreases (Fig. 4.58, 4.59 and 4.60).
- The length of the bolt changes from 1.5 m to 2.0, 3.0 and 4.0 m, but the displacements change very slightly (Figure 4.59 and 4.60) because the safety factor of the model without rockbolt is 1.75 so that the length of 1.5 m is great enough to avoid any significant displacements.
- In case of favourable geological conditions the rockbolt pattern of mk8 should be applied because longer bolts do not bring any additional benefit (see Fig. 4.58, 4.59 and 4.60). It might make sense to enlarge the distance between bolts to 1 or even 1.5 m.

4.4.3 Duong Huy mine

The standard anchor scheme (dh8) can reduce the displacements significantly compared to the unsupported case (dh0). Both models belong to type B1 where the length of the bolts is 1.5 m and the distance between rockbolts is 0.8 m. When the opening is unsupported, the maximum displacements reach 12 cm. Bolting reduces the maximum displacements to 9 cm (Fig. 4.61)

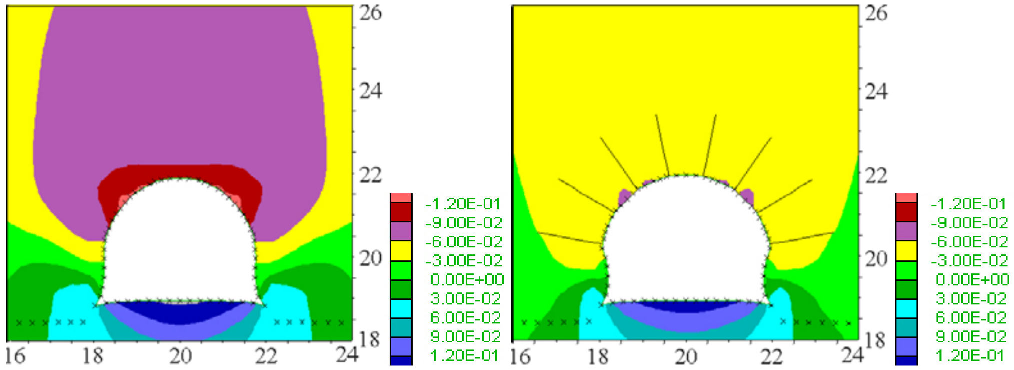

Figure 4.61 Contours of vertical displacement (m) for the models without rockbolts dh0 (left) and with rockbolts dh8 (d = 0.8 m, right) with the length of bolt l = 1.5 m; Dimension (m).

The effect of decrease in the displacements can clearly be seen also along the top line in Figure 4.62.

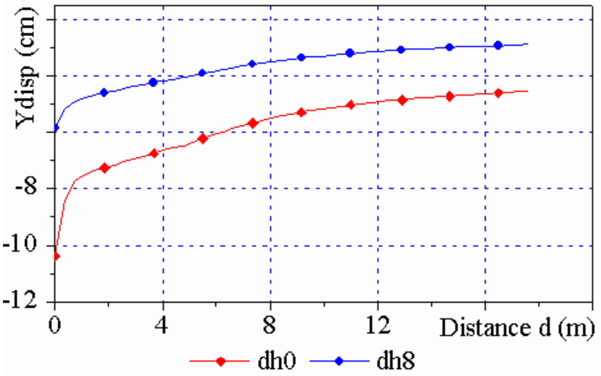

Figure 4.62 Vertical displacements Ydisp (cm) along the top line (m) for the models without rockbolts dh0 and with rockbolts dh8 (d = 0.8 m) with the length of bolt l = 1.5 m.

Figure 4.63 shows the deformation field, which indicates that the deformations are strongly limited in the area, where rockbolts are installed. At the sidewalls both models show a similar behaviour due to fact, that the sidewalls are unsupport in both cases.

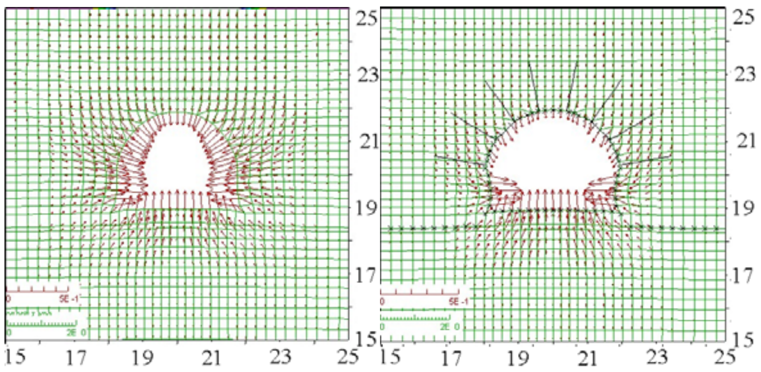

Max vector = 2.513e-1 Max vector = 2.01e-1

Figure 4.63 Displacement vector (m) for the models without rockbolt dh0 (left) and with rockbolts dh8 (d = 0.8 m, right) with the length of bolts l = 1.5 m; Dimension (m).

The effect of rockbolts in reducing the plasticity is documented by Fig. 4.64. Without rockbolting significant plastification is observed, whereas bolting avoids active plastifications in the roof and the sidewalls. Also, the area which is in general effected by elasto-plastic stress redistributions can be reduced by applying bolting.

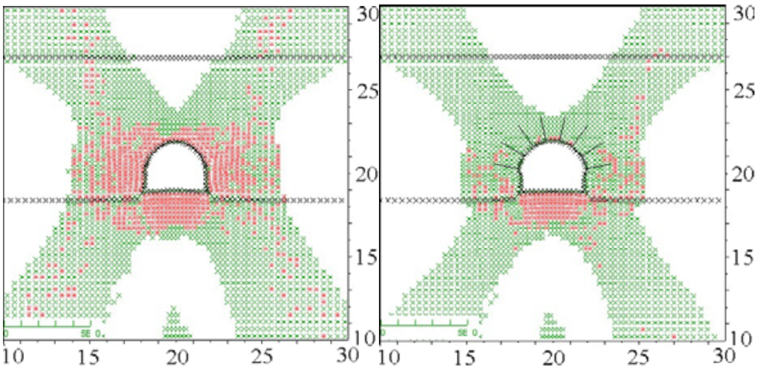

Figure 4.64 Plasticity for the models without rockbolts dh0 (left) and with rockbolts dh8 (d = 0.8 m, right) with the length of the bolt l = 1.5 m. The red elements show the yield in shear, the green ones represent the elastic state but plastic in past; Dimension (m).

As indicated by Figure 4.65 the bolting leads to a remarkable stress redistribution. Tangential stresses in the nearfield of the bolted arch are increased by several MPa.

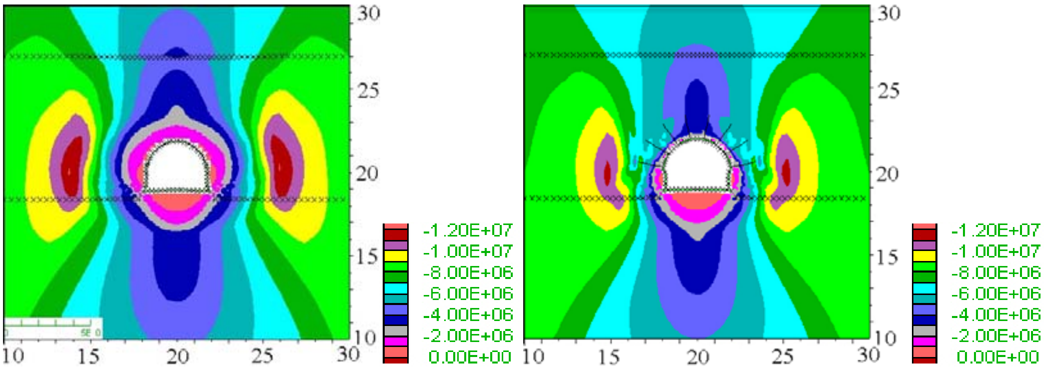

Figure 4.65 Contours of major principal stresses (Pa) for the model without rockbolts dh0 (left) and with rockbolts dh8 (d = 0.8 m, right) with the length of the bolt l = 1.5 m; Dimension (m).

Bolting leads to a significant increase in the safety factors in the roof and the sidewalls of the opening (Fig. 4.66). Compared to the model without rockbolts, where the safety factors are close to 1.0, the safety factors in the bolted model increase up to 1.2. White coloured areas correspond to safety factors > 1.5. Especially in the roof area, the safety is significantly improved.

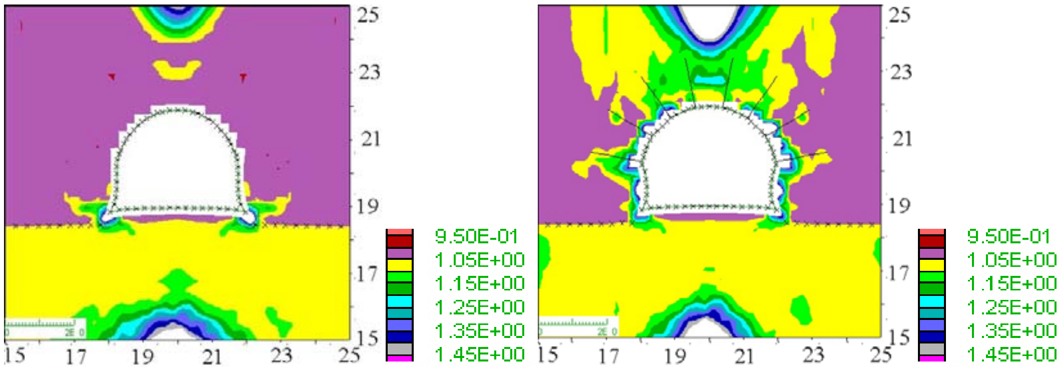

Figure 4.66 Safety factors for the models without rockbolt dh0 and with rockbolt dh8 (d = 0.8 m, right) with the length of the bolts l = 1.5 m; Dimension (m).

Figure 4.67 illustrates the effect of different bolting distances. When the distance between bolts decreases, then the axial force decreases, e.g. a reduction of the distance from 0.8 to 0.4 m would result in a reduction of contour displacements of about 30 %.

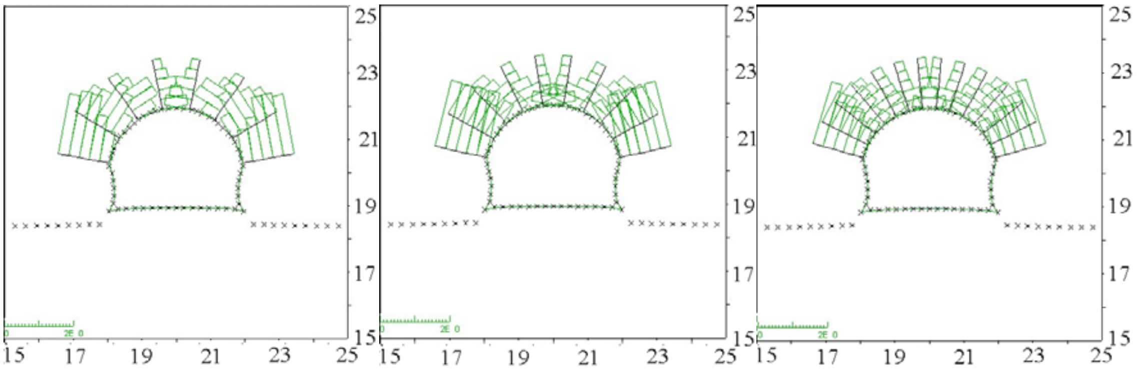

Max value 1.38 Max value 1.08 Max value 1.02

Min value 0.522 Min value 0.435 Min value 0.26

Figure 4.67 Axial force (MN) of the rockbolts for the models dh8 (d = 0.8 m), dh6 (d = 0.6 m), dh4 (d = 0.4 m) with the same length of the bolt l = 1.5 m in all models; Dimension (m).

The use of longer anchors at constant distance between anchors will also reduce displacements, but not that strong, which is documented by models, which belong to mode B2 (anchors in the roof and the sidewalls) with the lengths of the bolt varying from 1.5 m to 2.0, 3.0 to 4.0 m. The distance between the bolts has the same value of 0.8 m in all these models. As Fig. 4.68 and 4.69 show the reduction in displacements is marginal, even if the anchors would be 4.0 m long the reduction is just 10 % compared to the standard anchor scheme with 1.5 m long bolts.

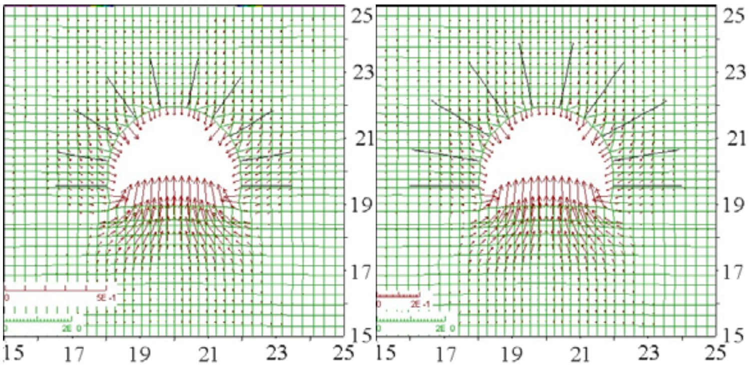

Max vector =1.529e-1 Max vector =1.446e-1

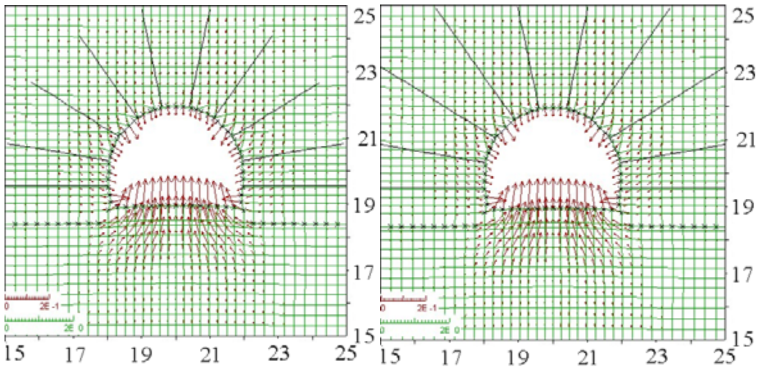

Max vector =1.403e-1 Max vector =1.397e-1

Figure 4.68 Displacement vector (m) for the models dhs8 (l = 1.5 m), dhs28 (l = 2.0 m), dhs38 (l = 3.0 m) and dhs48 (l = 4.0 m) with the same distance between bolts d = 0.8 m in all models; Dimension (m).

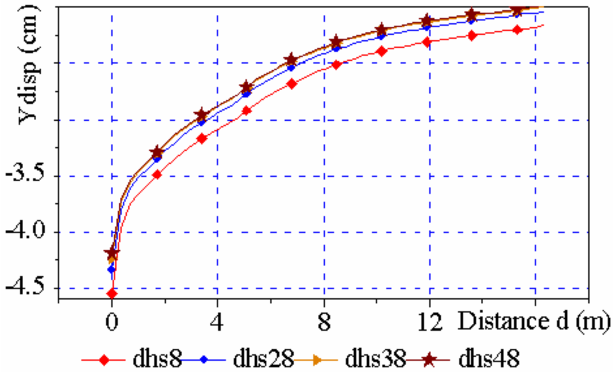

Figure 4.69 Vertical displacement Ydisp (cm) along the top line for the models dhs8 (l = 1.5m), dhs28 (l = 2.0 m), dhs38 (l = 3.0 m) and dhs48 (l = 4.0 m) with the same distance between bolts d = 0.8 m in all models.

The effect of bolting in relation to the displacements can slightly be increased if bolting is extended into the sidewalls. This is documented by models which belong to mode B2 where the length of the bolts is 1.5 m and the distances between bolts change from 0.6 to 0.4 m (Fig. 4.70 and 4.71).

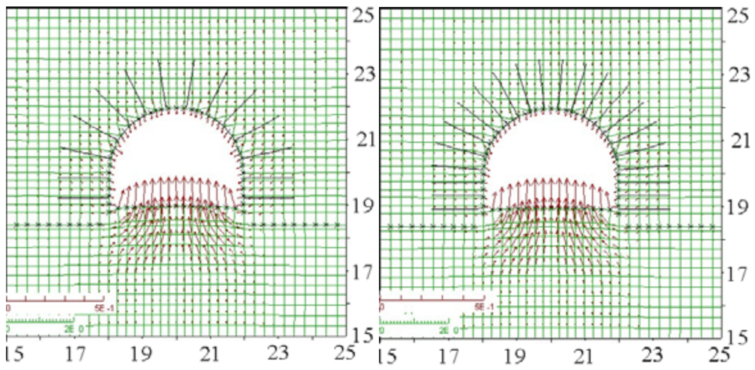
25
23
21
19
17
15
15
17
19
21
23
25
25
23
21
19
17
15
15
17
19
21
23
25

Max vector =1.587e-1 Max vector =1.494e-1

Figure 4.70 Displacement vector (m) for the models dhs6 (d = 0.6 m) and dhs4 (d = 0.4 m) with the same length of bolt l = 1.5 m; Dimension (m).

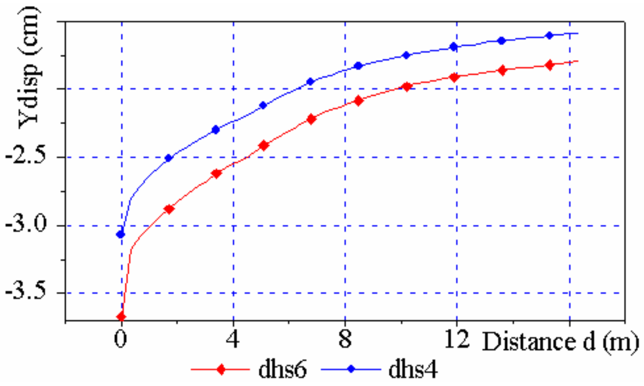

Figure 4.71 Vertical displacement Ydisp (cm) along the top line for the models dhs6 (d = 0.6 m) and dhs4 (d = 0.4 m) with the same length of bolt l = 1.5 m.

The anchor forces can be reduced by 15 to 30 % if the distance between the anchors is reduced form 0.6 m to 0.4 m as shown in Figure 4.72.

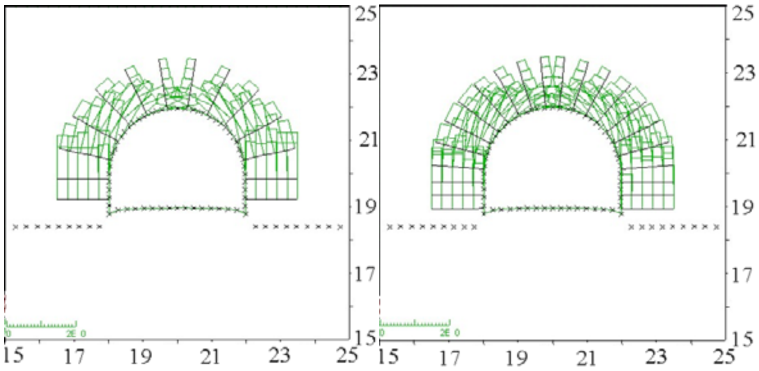

Maximum value: 1.051 Maximum value: 0.886

Minimum value: 0.468 Minimum value: 0.322

Figure 4.72 Axial force (MN) of the rockbolt for the models dhs6 (d = 0.6 m), dhs4 (d = 0.4 m) with the same length of bolt l = 1.5 m in all models; Dimension (m).

The effect of bolting in case they are installed along the full boundary of the opening (type B3) is illustrated by Figures 4.73 to 4.75. Within these models the distance between rockbolts change from 0.8 m to 0.6 m and 0.4 m, respectively, but the length of the bolts keeps unchanged (1.5 m). There is a decrease in the vertical displacements from 4.0 cm, 3.0 cm, 2.0 cm to finally 2.3 cm, 1.8 cm, 1.6 cm, respectively, observed in same height from the arch boundary up to the model surface).

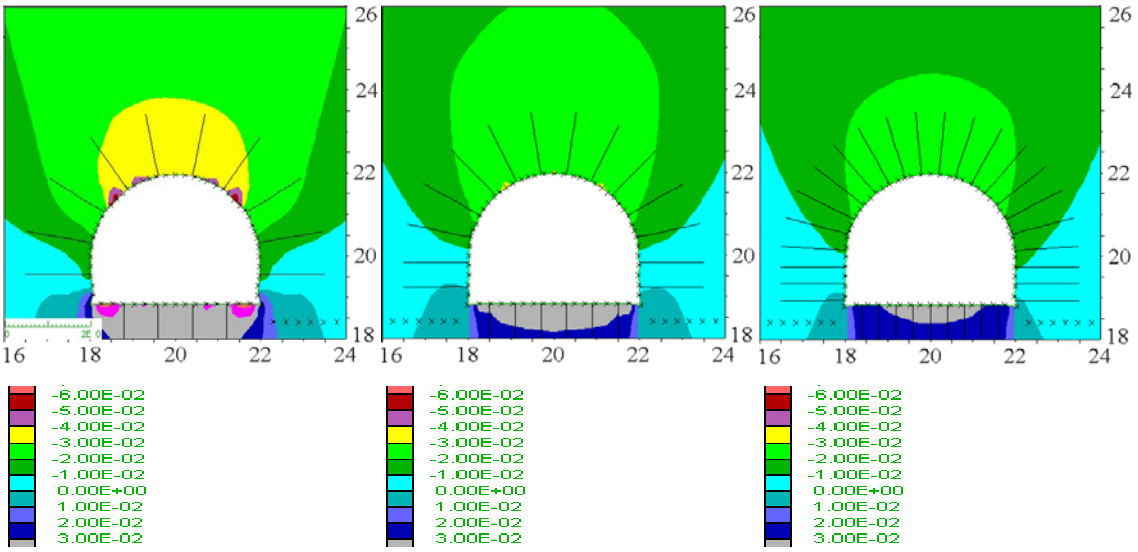

Figure 4.73 Contours of vertical displacement (m) for the models dhf8 (d = 0.8 m), dhf6 (d = 0.6 m), dhf4 (d = 0.4 m) with the same length of bolt l = 1.5 m in all models; Dimension (m).

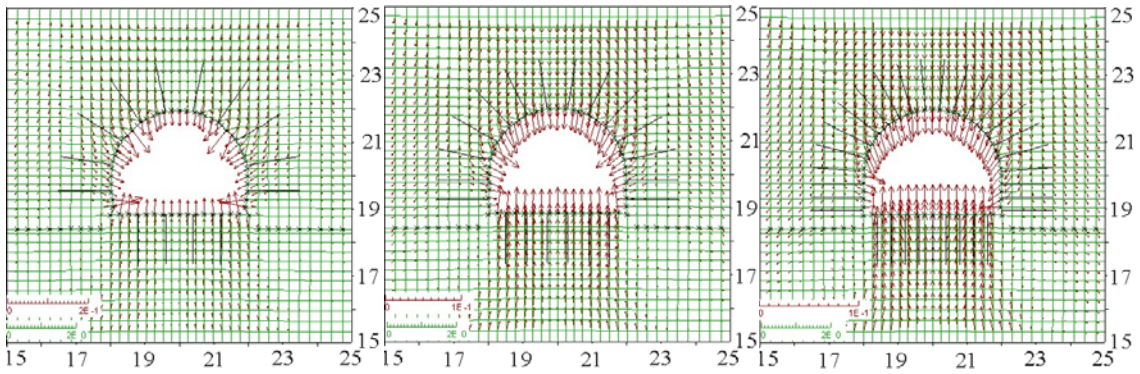

Max vector = 7.799e-2 Max vector = 4.139e-2 Max vector = 3.156e-2

Figure 4.74 Displacement vector (m) for the models dhf8 (d = 0.8 m), dhf6 (d = 0.6 m), dhf4 (d = 0.4 m) with the same length of bolt l = 1.5 m in all models; Dimension (m).

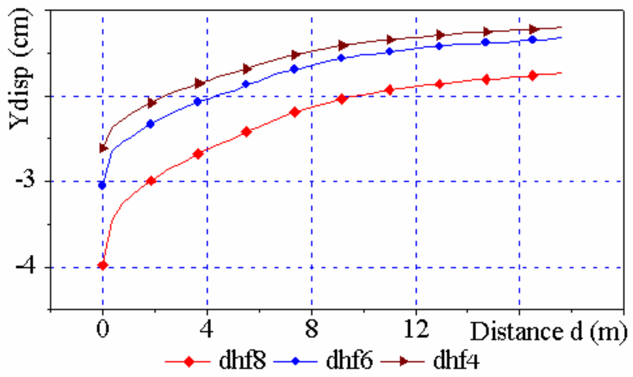

Figure 4.75 Vertical displacement Ydisp(cm) along the top line for the models dhf8 (d = 0.8 m), dhf6 (d = 0.6 m) and dhf4 (d = 0.4 m) with the same length of bolt l = 1.5 m in all models.

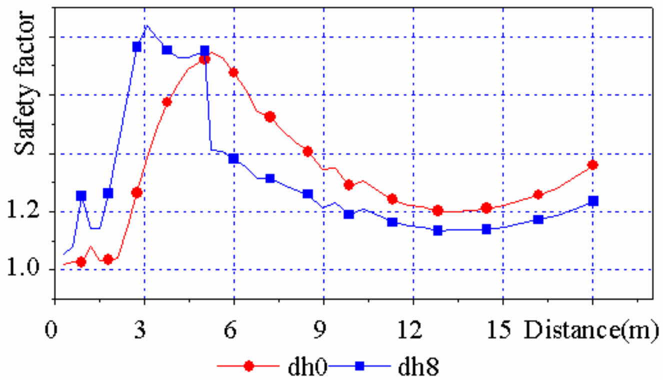

Figure 4.76 Safety factors along the top line for the models without rockbolt dh0 and with rockbolts dh8 (d = 0.8 m) with the length of the bolt l = 1.5 m.

As Figure 4.76 shows, bolting leads to an increase of safety factors up to a distance of 4 m from the surface of the opening. Within this area the increase is 20 % to 40 %.

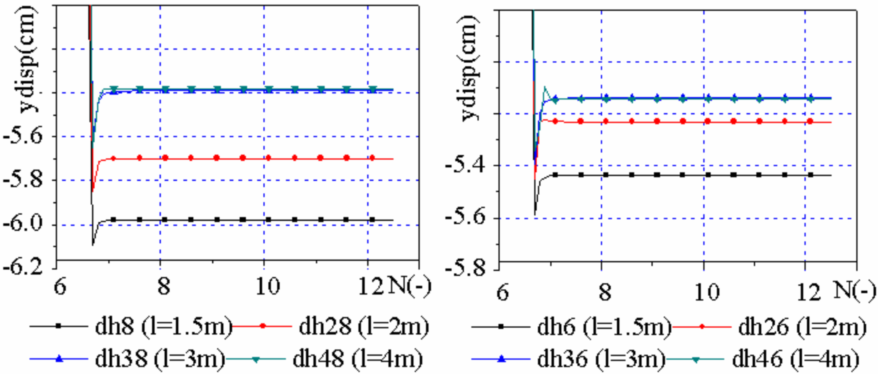

Figure 4.77 Vertical displacements Ydisp versus calculation steps ($Nx10^4$) at the top of the roof in the models which belong to group 1 and group 2.

Roof displacements were investigated in detail for several model groups for comparison. Group 1 includes models dh8, dh28, dh38, dh48 with distance between bolts d = 0.8 m and lengths of bolts are 1.5 m, 2.0 m, 3.0 m, 4.0 m. Group 2 consists of models dh6, dh26, dh36, dh46 with distance between bolts d = 0.6 m and lengths of the bolts are 1.5 m, 2.0 m, 3.0 m and 4.0 m. Group 1 and Group 2 belong to model type B1. The graphs indicate that the influence of the distance between anchors is bigger than the influence of the anchor length (see Figure 4.77).

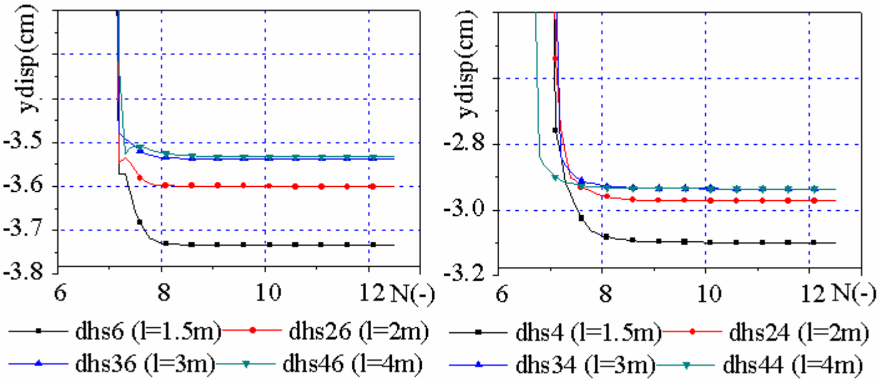

Figure 4.78 Vertical displacements Ydisp versus calculation steps ($N x10^4$) at the top of the roof in the models which belong to group 3 and group 4.

Group 3 comprises models dhs6, dhs26, dhs36 and dhs46 with distance between bolts d = 0.6 m and lengths of the bolts are 1.5 m, 2.0 m, 3.0 m and 4.0 m. Group 4 includes models dhs4, dhs24, dhs34 and dhs44 with distance between bolts d = 0.4 m and lengths of the bolts are 1.5 m, 2.0 m, 3.0 m and 4.0 m. Group 3 and Group 4 belong to model type B2. The graphs indicate that the changes in displacements are very small (see Fig. 4.78).

Group 5 consists of models dhf8, dhf28, dhf38 and dhf48 with distance between bolts d = 0.8 m and lengths of the bolts are 1.5 m, 2.0 m, 3.0 m and 4.0 m. Group 6 includes models dhf6, dhf26, dhf36 and dhf46 with distance between bolts d = 0.6 m and lengths of bolts are 1.5 m, 2.0 m, 3.0 m and 4.0 m. Group 5 and Group 6 belong to model type B3. The graphs again indicate that the changes in displacements are very small with no practical significants (see Fig. 4.79).

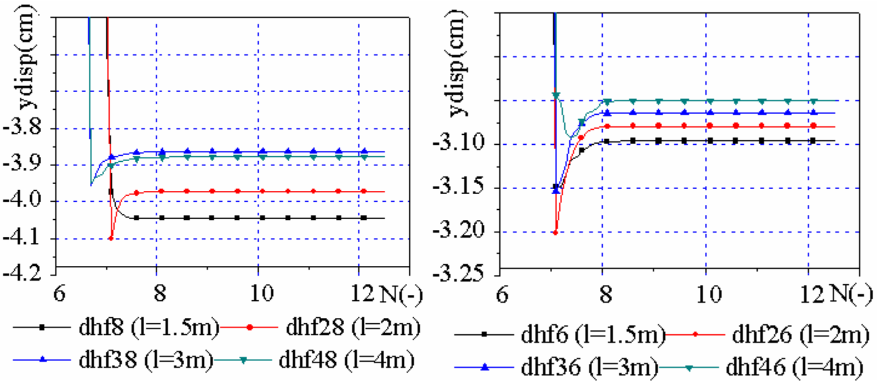

Figure 4.79 Vertical displacements Ydisp versus calculation steps (N x10^4) at the top of the roof in the models which belong to group 5 and group 6.

Remarks:

- Comparison of investigated rockbolt pattern shows that displacements decrease when the length of the bolts increases and the distance between bolts decreases (Fig. 4.77, 4.78 and 4.79).
- Standard bolting increases the safety factors significantly, but longer bolts or shorter distances between bolts would bring only minor improvements and only small reductions in displacements.

4.4.4 Mong Duong mine

The effect of bolting in relation to the displacement field is documented by the comparison between model md0 (without anchors) and model md8, which belongs to type B1 where the length of the bolts is 1.5 m and the distance between rockbolts is 0.8 m. When rockbolts are installed in the roof, the roof displacements decrease considerably (Fig. 4.80, 4.81). Whereas without bolts the maximum roof displacements at the boundary reach about 7 cm, they are restricted to about 4 cm if bolts are installed.

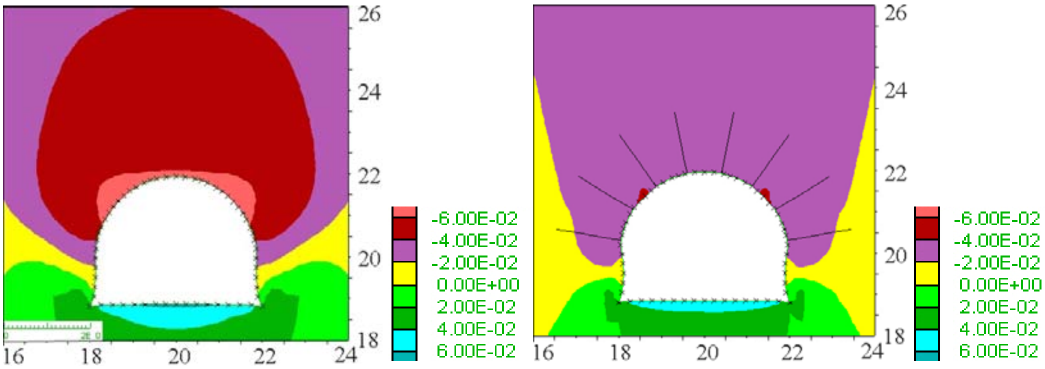

Figure 4.80 Contours of vertical displacement (m) for the models without rockbolt md0 (left) with rockbolts md8 (d = 0.8 m, right) with the length of the bolt l = 1.5 m; Dimension (m).

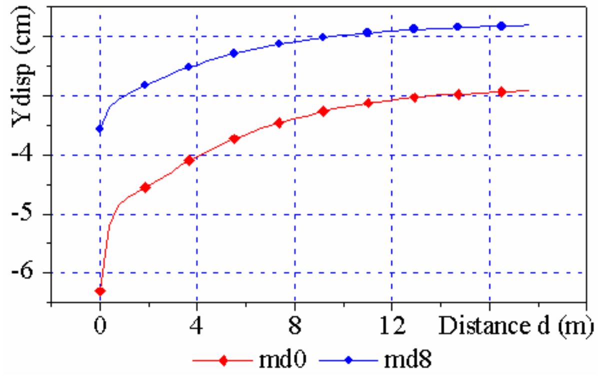

Figure 4.81 Vertical displacements Ydisp (cm) along the top line d (m) for the models without rockbolt md0 and with rockbolt md8 (d = 0.8 m) with the length of the bolt l = 1.5 m.

Figure 4.82 illustrates the deformation fields. At the unsupported sidewalls the observed displacements are very similar in both models. By bolting the maximum displacements can be reduced from 14 cm to 11 cm, which corresponds to a reduction of about 25 %.

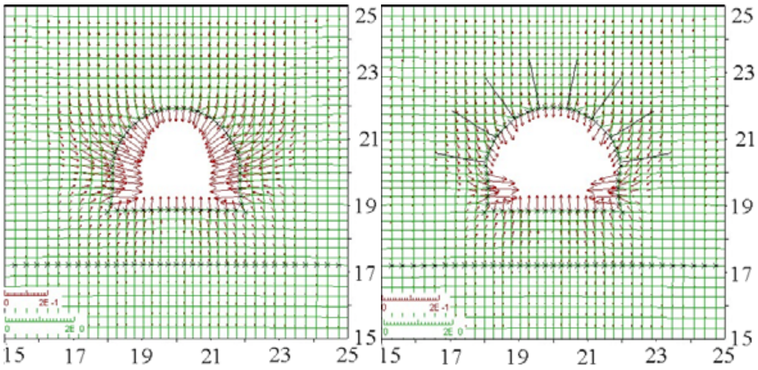

Max vector = 1.445e-1 Max vector = 1.104e-1

Figure 4.82 Displacement vectors (m) for the models without rockbolts md0 (left) and with rockbolts md8 (d = 0.8 m, right) with length of bolt l = 1.5 m; Dimension (m).

The bolting leads to a significant reduction of active plasticity around the opening and decreases the area effected by plasticty in general (Fig. 4.83 (right)).

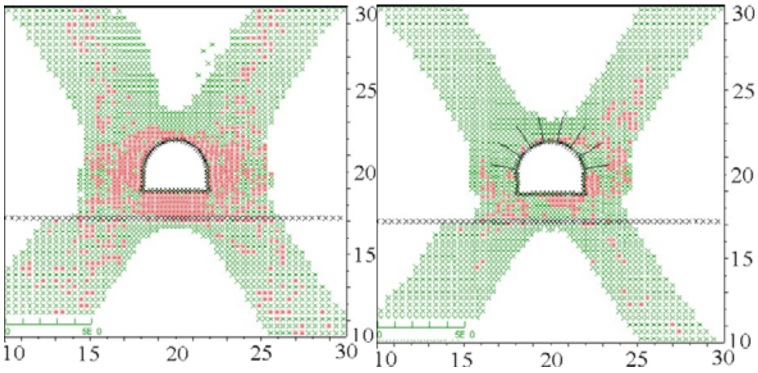

Figure 4.83 Plasticity for the models without rockbolts md0 (left) and with rockbolts md8 (d = 0.8 m, right) with length of bolt l = 1.5 m. The red elements show the yield in shear, the green ones represent the elastic state but plastic one in the past; Dimension (m).

Safety factors are strongly increased in the bolted area, especially in the roof. When the opening is unsupported, the safety factors are between 1.0 and 1.05 (Fig. 4.84 (left)). Bolting increases the safety factor in the roof area, so that values of 1.1 and more can be observed. The white area represents values greater than 1.5.

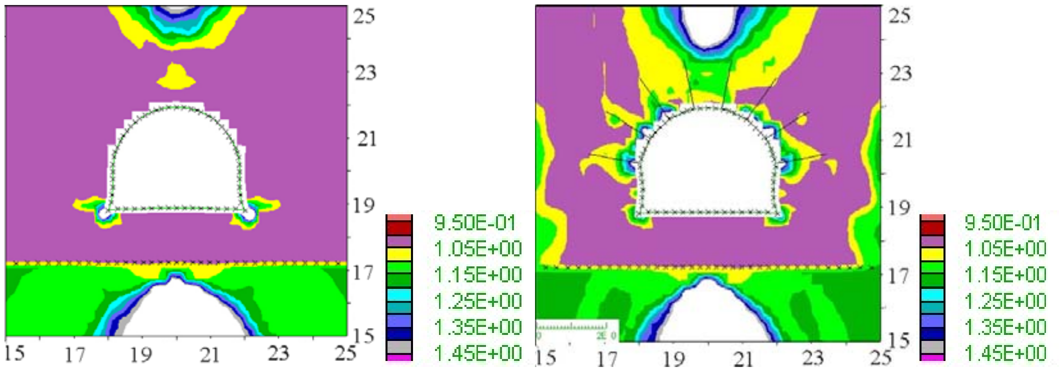

Figure 4.84 Safety factors for the models without rockbolt md0 and with rockbolt md8 (d = 0.8 m, right) with the length of the bolt l = 1.5 m; Dimension (m).

The distance between rockbolts will influence the axial forces in the bolts as Fig. 4.85 shows. The anchor forces are reduced by app. 20 % if the distance between anchors is reduced from 0.8 to 0.4 m.

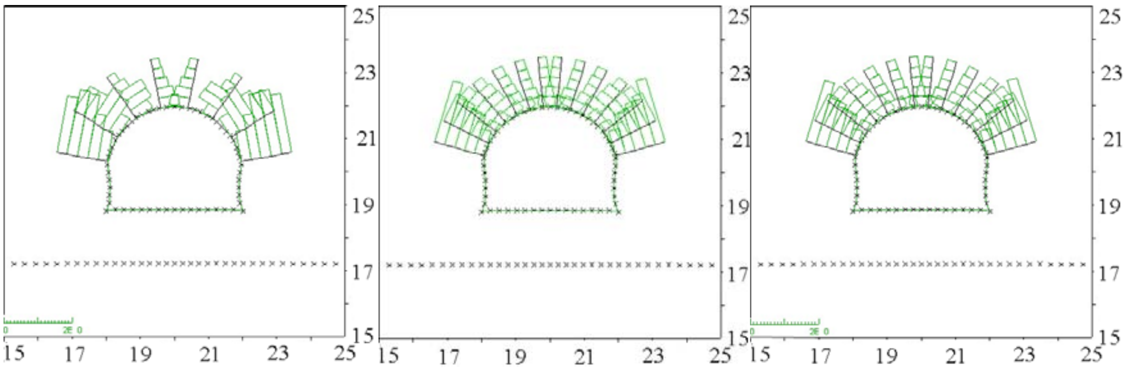

Max value: 1.048 Max value: 0.82 Max value: 0.81

Min value: 0.288 Min value: 0.30 Min value: 0.208

Figure 4.85 Axial force (MN) along the rockbolt for the models md8 (d = 0.8 m), md6 (d = 0.6 m), md4 (d = 0.4 m) with the same length of the bolt l = 1.5 m in all models; Dimension (m).

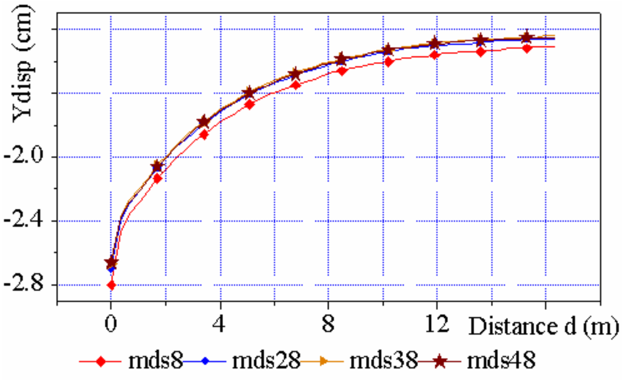

Figure 4.86 Vertical displacement Ydisp (cm) along the top line for the model mds8 (l = 1.5 m), mds28 (l = 2.0 m), mds38 (l = 3.0 m) and mds48 (l = 4.0 m) with the same bolt distance d = 0.8 m in all models.

When the distance between bolts keeps the same value (e.g. d=0.8 m) but the length of the bolt increases from 1.5 m to 2.0, 3.0, 4.0 m, the displacements decrease only slightly (Fig. 4.86), because when rockbolts are applied to models in mode B2, the models have already a safety factor of 1.4. That means, the system has enough capacity to avoid significant plastic deformations and any anchor scheme with longer anchors or reduced distance between anchors makes no sense.

In case bolting is applied in the roof and the sidewalls (model type B2 with length of the bolt of 1.5 m and distance between rockbolts are changed from 0.6 to 0.4 m) maximum displacements are reduced slightly by about 5 % (Fig. 4.87) and maximum vertical roof displacements are reduced by nearly 20 %, but on a low level of only about 2 cm (Fig. 4.88).

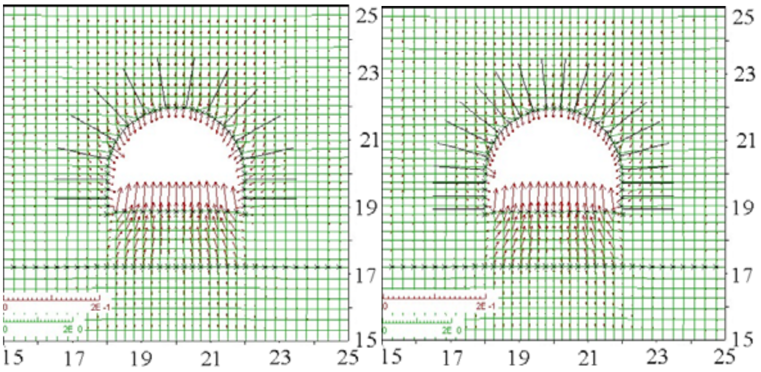

Max vector = 6.49e-2 Max vector = 6.116e-2

Figure 4.87 Displacement vector for the models mds6 (d = 0.6 m) and model mds4 (d = 0.4 m) with the same length of bolt l = 1.5 m in all models; Dimension (m).

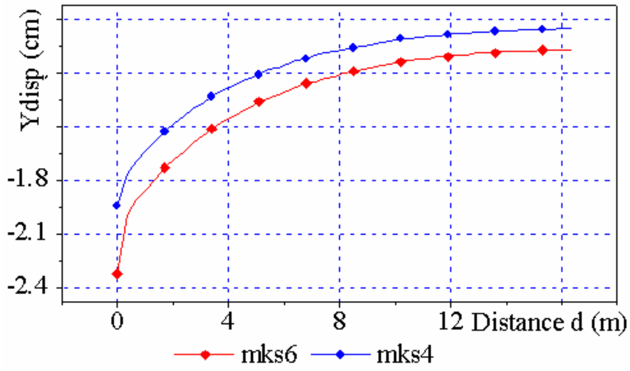

Figure 4.88 Vertical displacement Ydisp (cm) along the top line for the models mks6 (d = 0.6 m) and mks4 (d = 0.4 m) with the same length of bolt l = 1.5 m in all models.

When the distance between rockbolts reduces, the value of the axial forces also decrease (Fig. 4.89), e.g. a reduction of the distance between bolts from 0.6 m to 0.4 m reduces the anchor forces by app. 15 to 30 %.

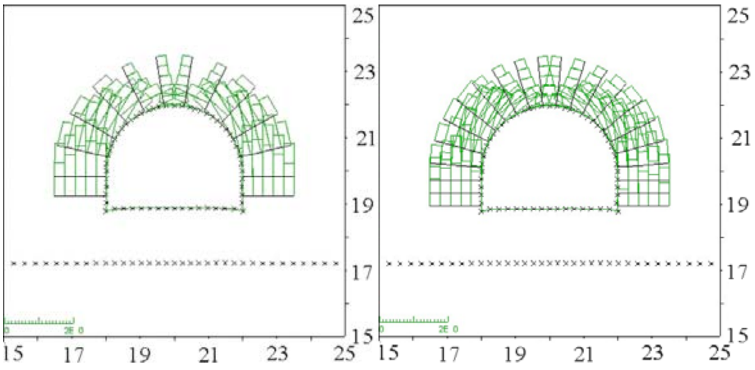

Maximum value: 0.7437 Maximum value: 0.631
Minimum value: 0.2718 Minimum value: 0.183

Figure 4.89 Axial force (MN) of the rockbolt for the models mds6 (d = 0.6 m), mds4 (d = 0.4 m) with the same length of bolt l = 1.5 m in all models; Dimension (m).

Next figures illustrate the bolting effect for models, which belong to mode B3 where length of bolts is 1.5 m and distance between bolts changes from 0.8 to 0.6 and 0.4 m.

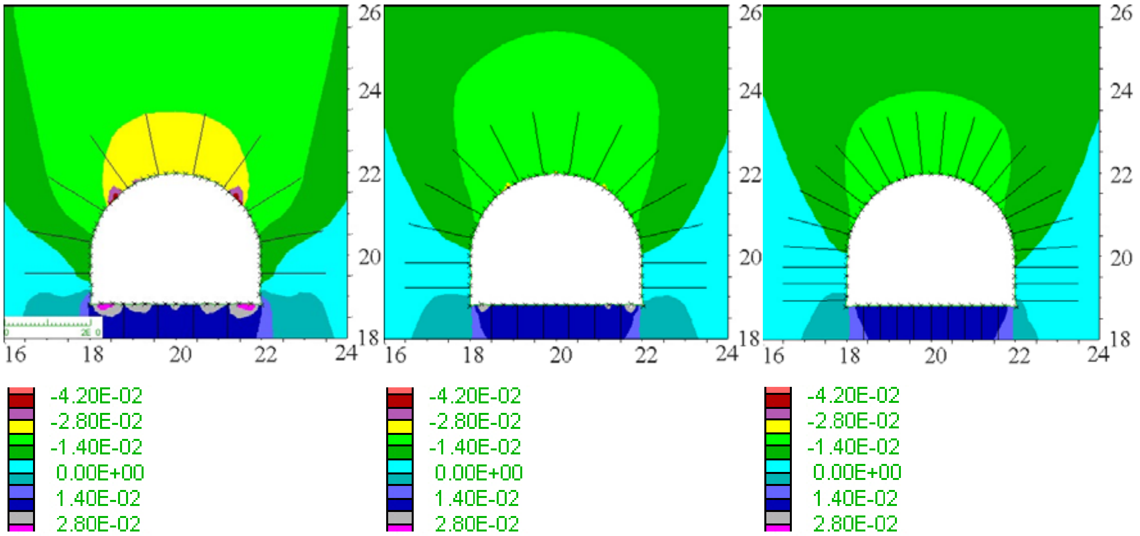

Figure 4.90 Contours of vertical displacement (m) for the models mdf8 (d = 0.8 m), mdf6 (d = 0.6 m), mdf4 (d = 0.4 m) with the same length of bolt l = 1.5 m in all models; Dimension (m).

When the distance between the bolts change from 0.8 m to 0.6 and 0.4 m but the length is equal to 1.5 m, the vertical displacements decrease from 4.0 cm, 3.0 cm and 2.0 cm to finally 2.0 cm, 1.8 cm and 1.6 cm in models mdf8, mdf6 and mdf4, respectively (from opening boundary up to the model surface).

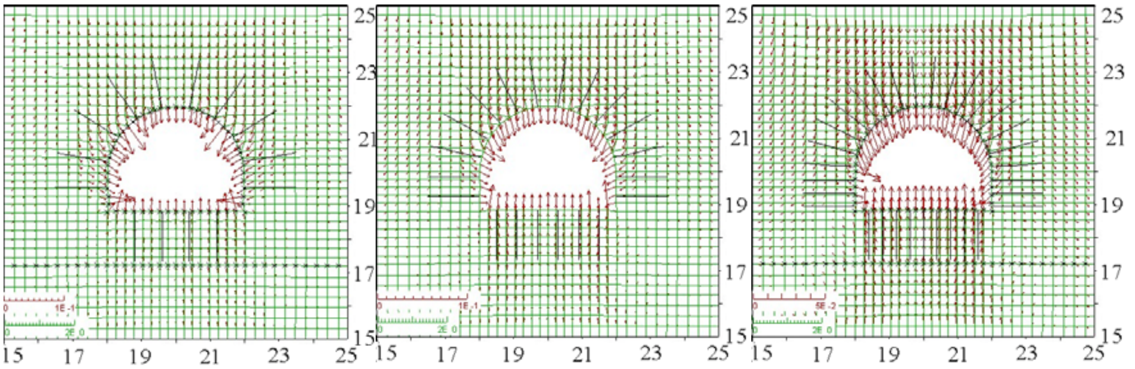

Max vector = 5.191e-2 Max vector = 3.456e-2 Max vector = 2.166e-2

Figure 4.91 Displacement vectors (m) for the models mdf8 (d = 0.8 m), mdf6 (d = 0.6 m), mdf4 (d = 0.4 m) with the same length of bolts l = 1.5 m in all models; Dimension (m).

Displacements are strongly reduced when the distance between bolts are reduced from 0.8 to 0.6 and up to 0.4 m (Fig. 4.91 and 4.92), although the magnitude of about 2 ÷ 5 cm is low.

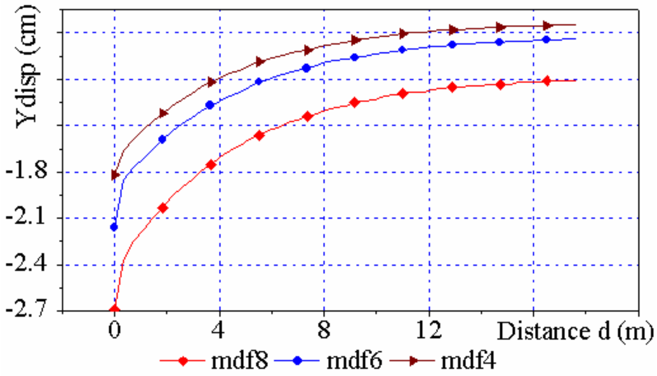

Figure 4.92 Vertical displacement Ydisp (cm) along the top line for the models caf8 (d = 0.8 m), mdf6 (d = 0.6 m) and caf4 (d = 0.4 m) with the same length of bolt l = 1.5 m in all models.

The safety factors increase when rockbolting is applied (Fig. 4.93). Up to a distance of about 3 m the safety factor is about 5 to 30 % higher if bolting is used.

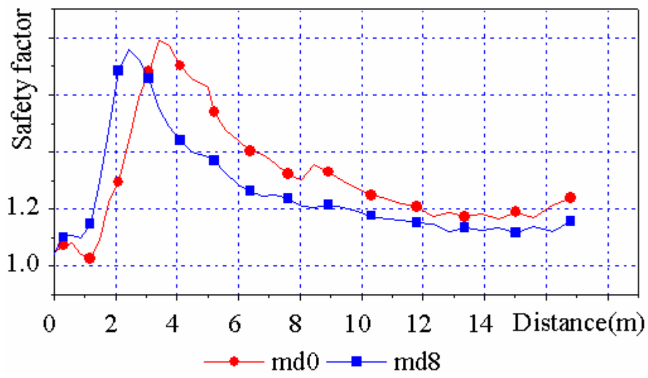

Figure 4.93 Safety factors along the top line for the models without rockbolt md0 and with rockbolts md8 (d = 0.8 m) with the length of bolt l = 1.5 m.

Next figures show the influence of the rockbolt pattern on the roof displacements in comparison between different model groups. Group 1 includes models md8, md28, md38 and md48 with distance between bolts d = 0.8 m and lengths of the bolts are 1.5, 2.0, 3.0 and 4.0 m. Group 2 consists of models md6, md26, md36 and md46 with distance between bolts d = 0.6 m and lengths of the bolts are 1.5, 2.0, 3.0 and 4.0 m. Group 1 and Group 2 belong to model type B1.

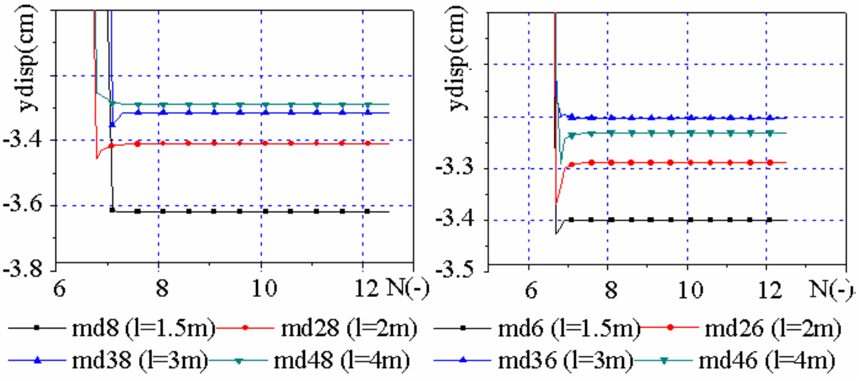

Figure 4.94 Vertical displacements ydisp (cm) versus calculation steps (N x10^4) at the top of the roof in models which belong to group 1 and group 2.

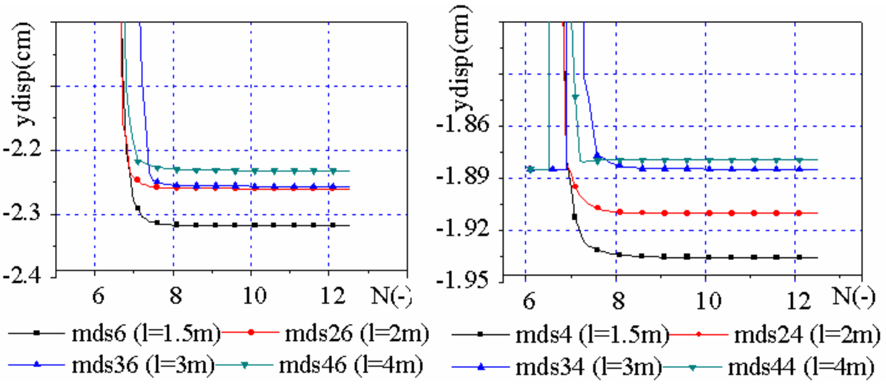

Figure 4.95 Vertical displacements ydisp (cm) versus calculation steps (Nx10^4) at the top of the roof in models which belong to group 3 and group 4.

Group 3 comprises models mds6, mds26, mds36 and mds46 with distance between bolts d = 0.6 m and lengths of the bolts are 1.5, 2.0, 3.0 are 4.0 m. Group 4 includes models mds4, mds24, mds34 and mds44 with distance between bolts d = 0.4 m and lengths of the bolts are 1.5, 2.0, 3.0 and 4.0 m. Group 3 and Group 4 belong to model type B2.

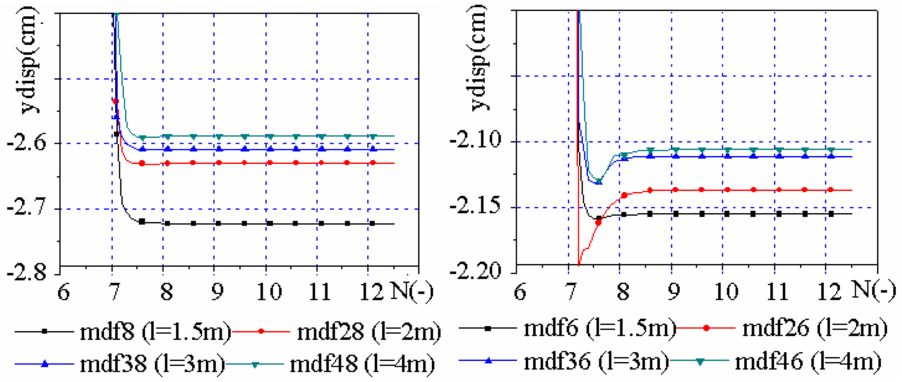

Figure 4.96 Vertical displacements ydisp (cm) versus calculation steps (N x10^4) at the top of the roof in models which belong to group 5 and group 6.

Group 5 consists of models mdf8, mdf28, mdf38 and mdf48 with distance between bolts d = 0.8 m and lengths of the bolts are 1.5, 2.0, 3.0 and 4.0 m. Group 6 includes models mdf6, mdf26, mdf36 and mdf46 with distance between bolts d = 0.6 m and lengths of the bolts are 1.5, 2.0, 3.0 and 4.0 m. Group 5 and Group 6 belong to model mode B3.

General trends are as expected. From a practical point of view the displacement magnitudes are low.

4.4.5 Khe Cham mine

A comparison between the model without rockbolt kh0 and model with rockbolt kh8, which belongs to type B1 where the length of the bolts is 1.5 m and the distance between rockbolts is 0.8 m, reveals that anchorage reduces roof displacements by about 50 %. Whereas the maximum vertical displacements reach about 10 cm in the unbolted case, they are reduced to about 5 cm if bolting is applied (Fig. 4.98 and 4.99).

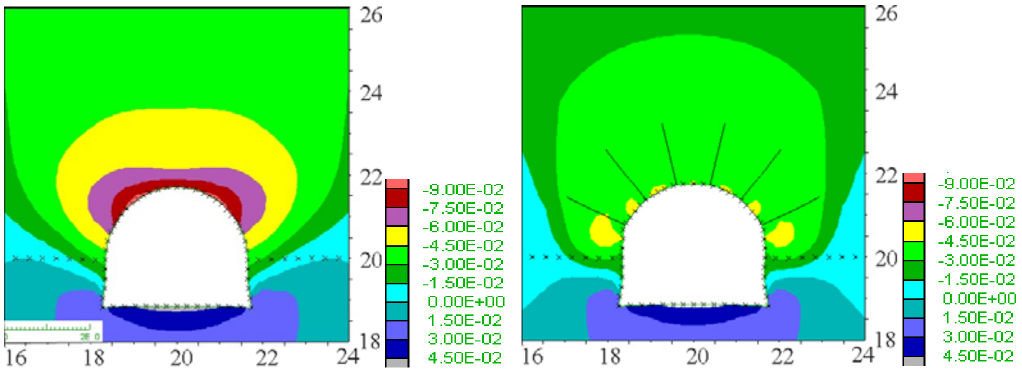

Figure 4.97 Contours of vertical displacement (m) for the models without rockbolts kh0 (left) and with rockbolts kh8 (d = 0.8 m, right), length of bolts l = 1.5 m; Dimension (m).

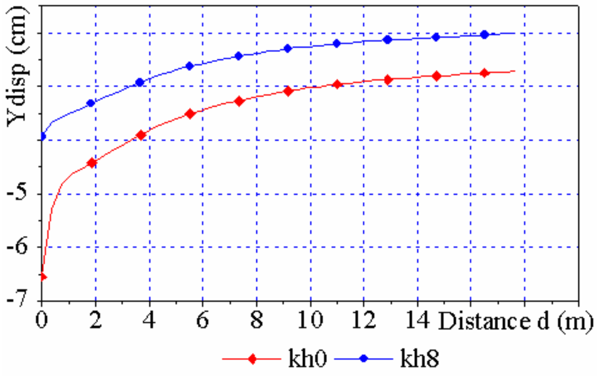

Figure 4.98 Vertical displacements Ydisp (cm) along the top line d (m) for the models without rockbolts kh0 (left) and with rockbolts kh8 (d = 0.8 m, right), length of bolts l = 1.5 m.

The displacement considerably decreases in the roof when rockbolts are installed, but only minor change is observed in the unsupported sidewalls as indicated by Figure 4.99.

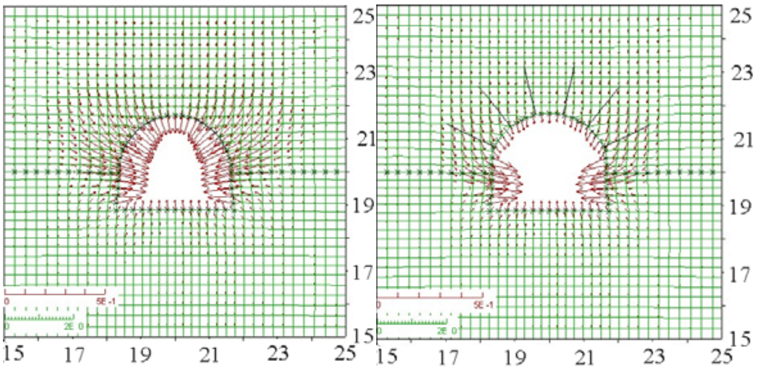

Max vector = 1.545e-1 Max vector = 1.478e-1

Figure 4.99 Displacement vectors (m) for the models without rockbolts kh0 (left) and with rockbolts kh8 (d = 0.8 m, right), length of bolt l = 1.5 m; Dimension (m).

Anchorage in the roof reduces active plasticity in the roof as well as in the sidewalls. Also, the general by plasticity effected area is reduced when roof bolting is applied (Fig. 4.100).

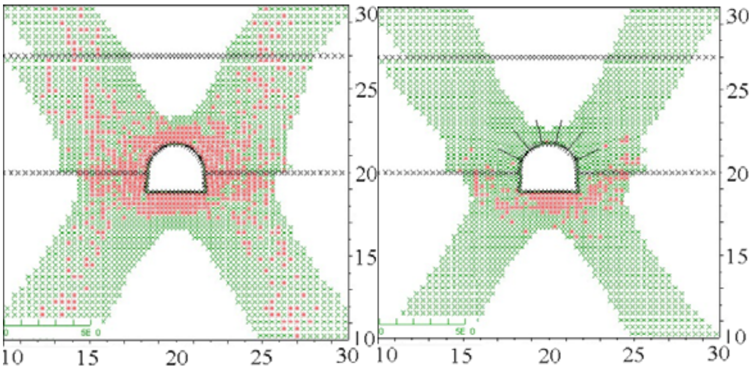

Figure 4.100 Plasticity for the models without rockbolts kh0 (left) and with rockbolts kh8 (d = 0.8 m, right), length of bolt l = 1.5 m. The red elements show the yield in shear, the green ones represent the elastic state but plastic one in the past; Dimension (m).

When the opening is unsupported, the safety factor is close to 1.0. Roof bolting improves the safety factor significantly both in the roof and the sidewalls to values up to 1.3 as documented by Figure 1.101.

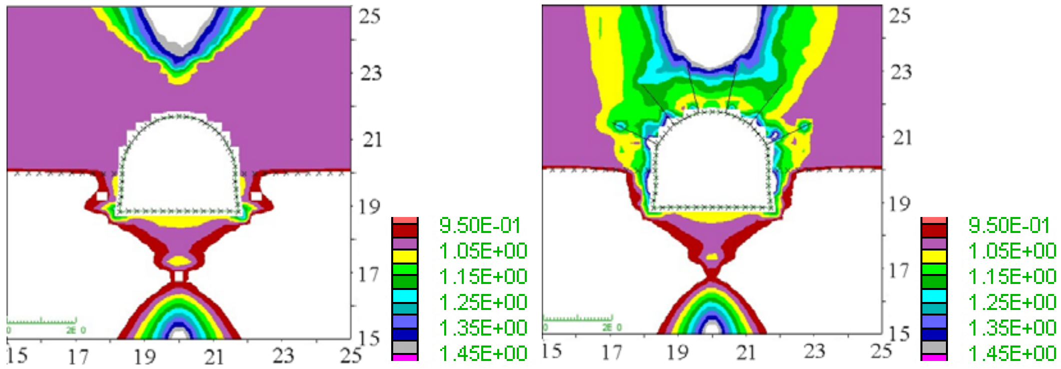

Figure 4.101 Safety factors for the models without rockbolts kh0 (left) and with rockbolts kh8 (d = 0.8 m, right), length of bolt l = 1.5 m; Dimension (m).

The axial forces in the rockbolts is reduced by app. 30% if distance between bolts is reduced from 0.8 m to 0.6 m (Fig. 4.102).

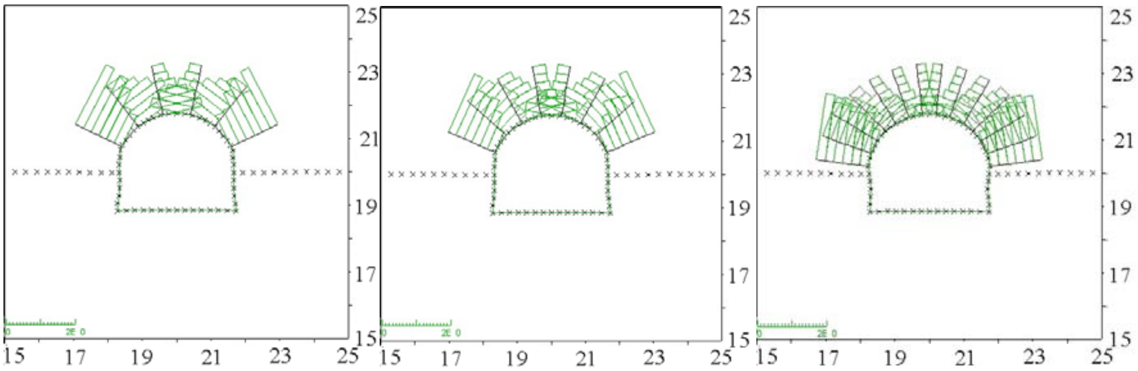

Max value: 0.801	Max value: 0.74	Max value: 0.558
Min value: 0.471	Min value: 0.397	Min value: 0.305

Figure 4.102 Axial force (MN) of the rockbolts for the models kh8 (d = 0.8 m), kh6 (d = 0.6 m) and kh4 (d = 0.4 m) with the same length of bolt l = 1.5 m; Dimension (m).

If bolting is applied in the roof and the sidewalls (type B2 where length of bolts is 1.5 m and distances between bolts change from 0.6 to 0.4 m at same distance between bolts of 0.8 m) the displacements can be lowered significantly as documented by Figure 4.103 and 4.104. Whereas in case only the roof is supported the maximum roof displacements reach about 4 to 7 cm, they are reduced to about 2 cm or less in case bolting is applied in the roof and the sidewalls (Fig. 4.103 and 4.104).

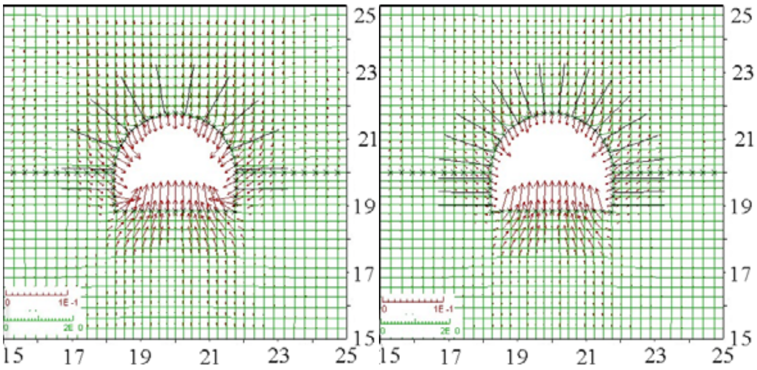

Max vector = 5.127e-2 Max vector = 5.05e-2

Figure 4.103 Displacement vector (m) for the models khs6 (d = 0.6 m) and khs4 (d = 0.4 m) with the same length of bolt l = 1.5 m in the two models; Dimension (m).

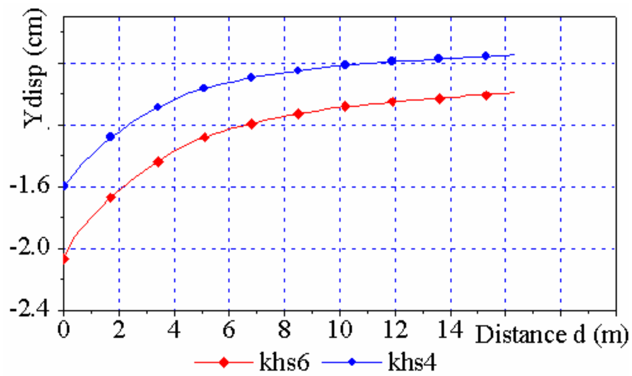

Figure 4.104 Displacement along the top line for the models khs6 (d = 0.6 m), khs4 (d = 0.4 m) with the same length of the bolt l = 1.5 m in all models.

When the distance between rockbolts is reduced from 0.8 m to 0.6 m, axial anchor forces are reduced by app. 20 % (Fig. 4.105).

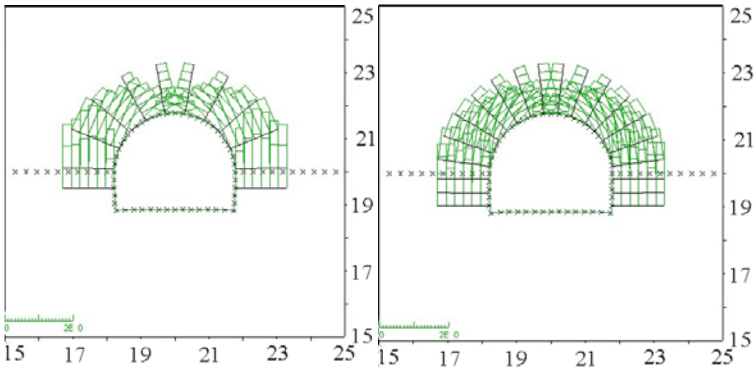

Maximum value: 0.781 Maximum value: 0.638

Minimum value: 0.351 Minimum value: 0.231

Figure 4.105 Axial force (MN) of the rockbolt for the models khs6 (d = 0.6 m), khs4 (d = 0.4 m) with the same length of the bolt l = 1.5 m in all models; Dimension (m).

These models belong to mode B3 with the length of the bolt is 1.5 m, the distance between bolt changes from 0.8 to 0.6, 0.4 m.

If the bolting is extended to the whole boundary (type B3) the situation in respect to displacements to not improve further, but the tendency, that denser rockbolting reduces displacements is also visuable (Fig. 4.106, 4.107 and 4.108).

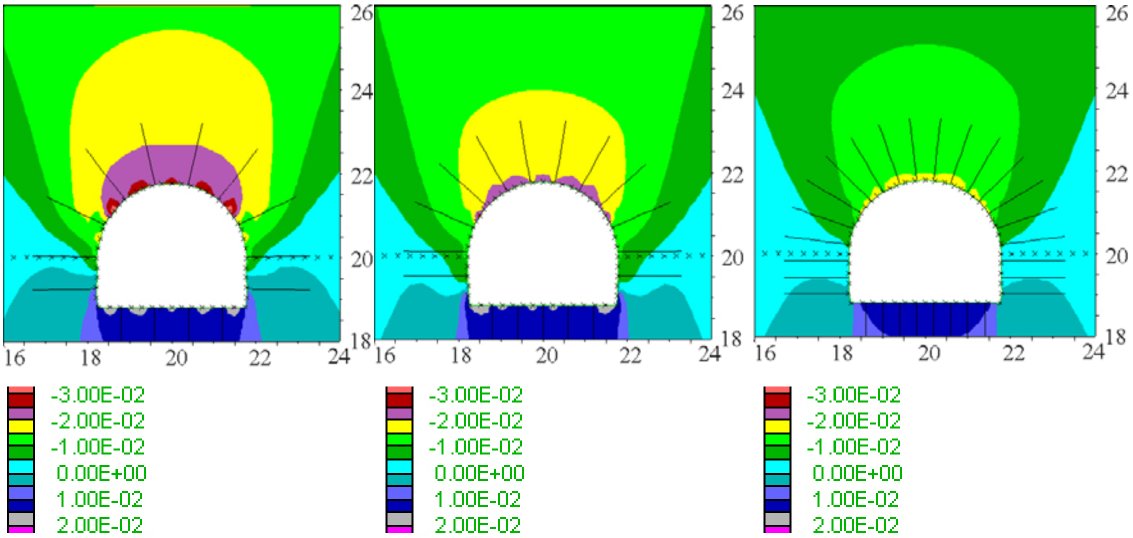

Figure 4.106 Contours of vertical displacements (MPa) for the models khf8 (d = 0.8 m), khf6 (d = 0.6 m) and khf4 (d = 0.4 m) with same length of the bolt l = 1.5 m in all models; Dimension (m).

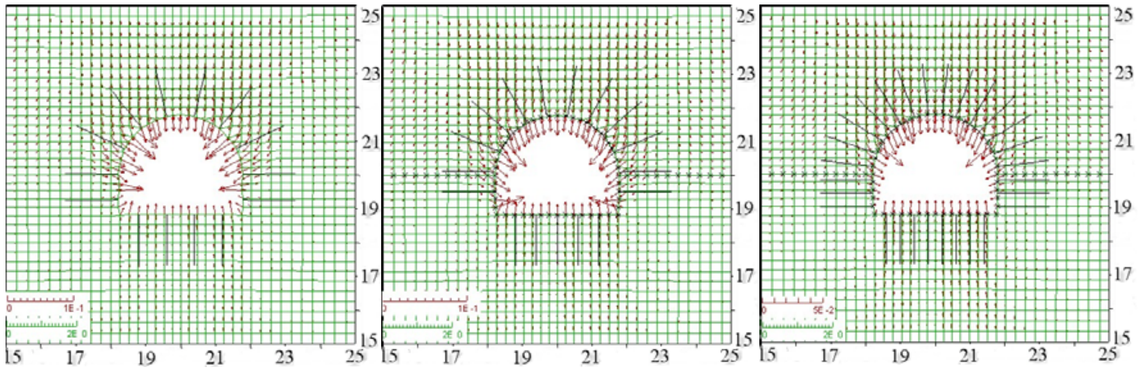

Max vector = 4.81e-2 Max vector = 3.72e-2 Max vector = 2.60e-2

Figure 4.107 Displacement vectors (m) for the models khf8 (d = 0.8 m), khf6 (d = 0.6 m) and khf4 (d = 0.4 m) with same length of the bolt l = 1.5 m in all models; Dimension (m).

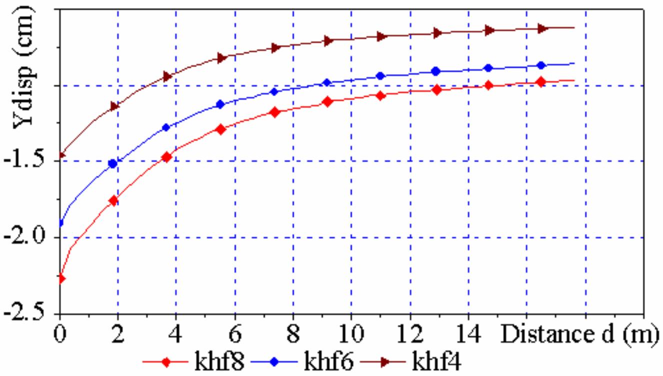

Figure 4.108 Vertical displacements Ydisp (cm) along the top line in model khf8 (d = 0.8 m), khf6 (d = 0.6 m) and khf4 (d = 0.4 m) with the same length of bolt l = 1.5 m in all models.

As Figure 4.109 shows, the safety factor is significantly increased up to a distance of about 3 m from the roof into the rockmass if bolting is applied. The increase is in the order of about 10 to 25 %.

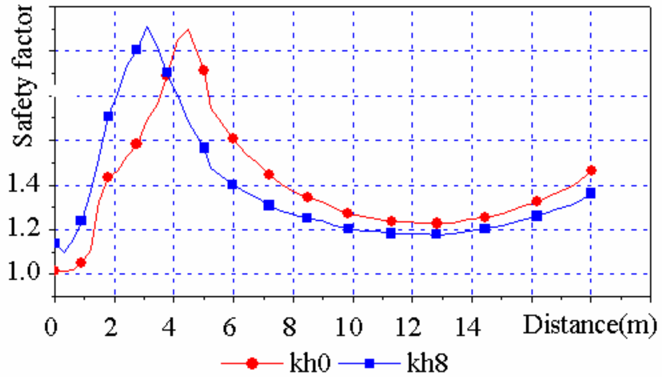

Figure 4.109 Safety factors along the top line for the models without rockbolts kh0 and with rockbolts kh8 (d = 0.8 m) with length of the bolt l = 1.5 m.

The influence of different rockbolt pattern on the displacement field is documented by the following graphs. For comparison several groups were formed. Group 1 includes models kh8, kh28, kh38 and kh48 with distance between bolts d = 0.8 m and lengths of the bolts are 1.5 m, 2.0 m, 3.0 m and 4.0 m. Group 2 comprises models kh6, kh26, kh36 and kh46 with distance between bolts d = 0.6 m and lengths of the bolts are 1.5 m, 2.0 m, 3.0 m and 4.0 m. Group 1 and group 2 belong to model type B1.

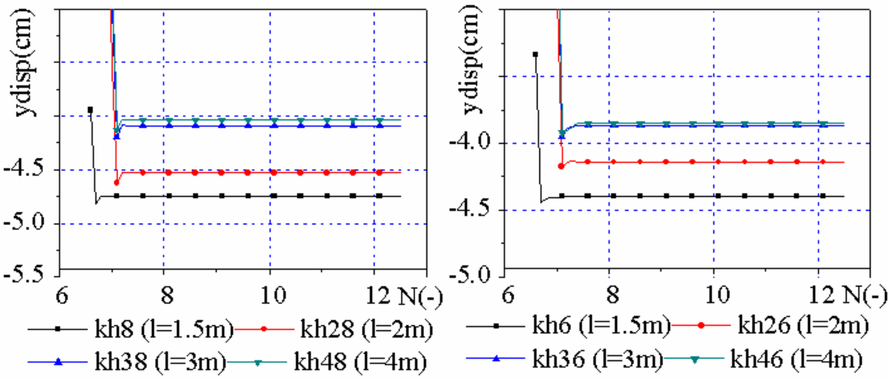

Figure4.110 Vertical displacements ydisp (cm) versus calculation steps ($Nx10^4$) at the top of the roof in the models which belong to group 1 and group 2.

Group 3 consists of models khs6, khs26, khs36 and khs46 with distance between bolts d = 0.8 m and lengths of the bolts are 1.5 m, 2.0 m, 3.0 m and 4.0 m (model type B2). Group 4 includes models khs4, khs24, khs34 and khs44 with distance between bolts d = 0.6 m and lengths of the bolts are 1.5 m, 2.0 m, 3.0 m, 4.0 m. Group 3 and group 4 belong to model type B2.

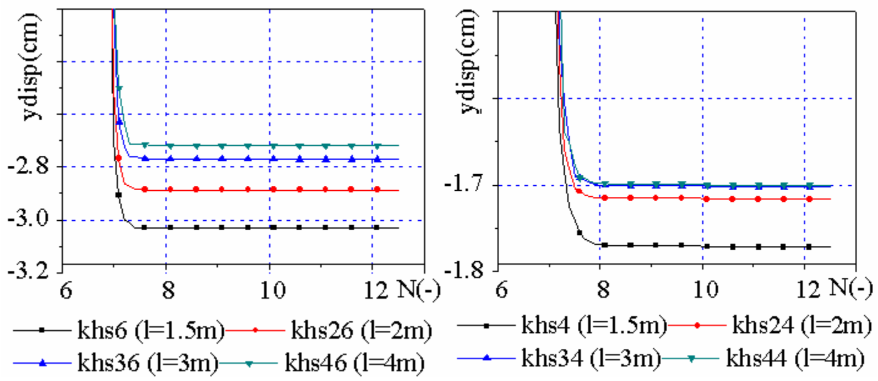

Figure 4.111 Vertical displacements ydisp (cm) versus calculation steps (Nx10^4) at the top of the roof in the models which belong to group 3 and group 4.

Group 5 includes models khf8, khf28, khf38 and khf48 with distance between bolts d = 0.8 m and lengths of the bolts are 1.5 m, 2.0 m, 3.0 m and 4.0 m. Group 6 consists of models khf6, khf26, khf36 and khf46 with distance between bolts d = 0.6 m and the lengths of the bolts are 1.5 m, 2.0 m, 3.0 m and 4.0 m. Group 5 and group 6 belong to model type B3.

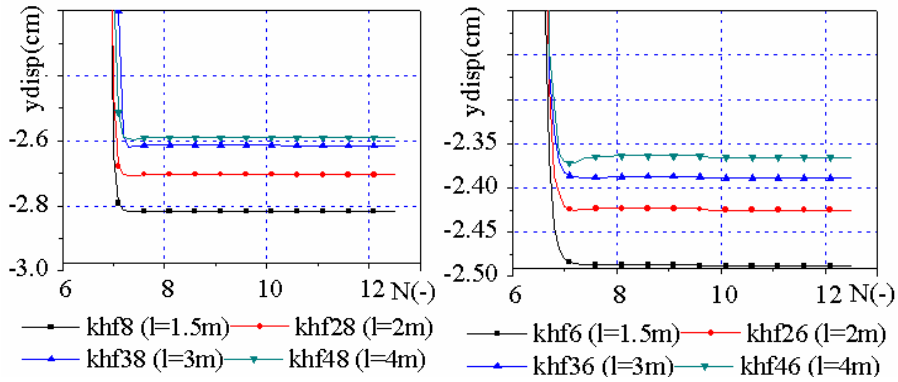

Figure 4.112 Vertical displacements ydisp versus calculation steps (Nx10^4) at the top of the roof in the models which belong to group 5 and group 6.

Remarks:

- The bolting in the roof is very effective, improves the factor of safety and the displacements significantly.
- Extension of the bolting towards the sidewalls leads to significant reductions in the displacements (even in the roof) and to a strong increase in safety.
- A futher extension of the bolting towards the floor do not produce further significant improvements and shall therefore are not necessary.

4.5 Determination of safety factors using the c-Φ reduction method

4.5.1 Theoretical basis of the method

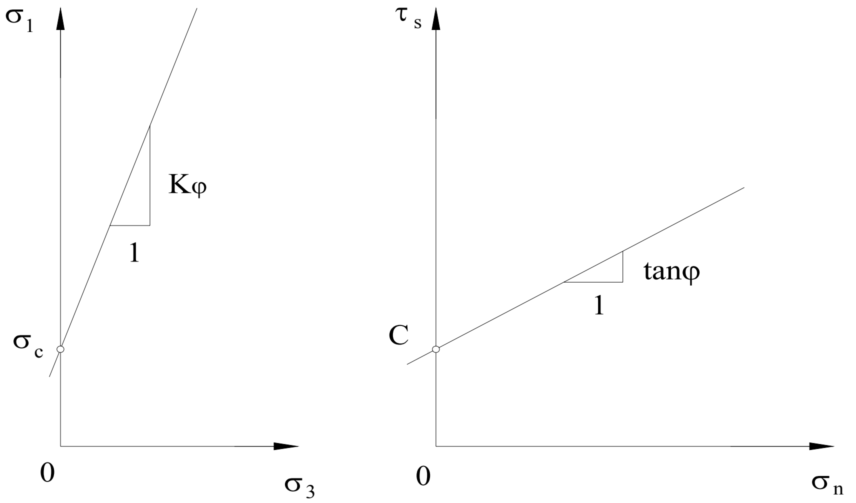

Figure 4.113 Mohr-Coulomb failure criterion in the principal stress space σ_1 versus σ_3 (left) and the shear-normal stress space τ_s vs σ_n (right).

The C- Φ reduction method is based on the Mohr-Coulomb failure criterion. The Mohr-Coulomb yield condition is given by [Parry, 1992]:

$$\sigma_1 = K_\varphi \sigma_3 + \sigma_c \qquad (4.15)$$

In the equation above the coefficient K_φ is related to the friction angle φ according to:

$$K_\varphi = (1 + \sin \varphi)/(1 - \sin \varphi) \qquad (4.16)$$

The unconfined compressive strength σ_c and the uniaxial tensile strength σ_t are related to the cohesion c and the coefficient K_φ as follows:

$$\sigma_c = 2c \cos \varphi /(1-\sin \varphi) \qquad (4.17)$$

$$\sigma_t = 2c \cos \varphi /(1+\sin \varphi)$$

The cohesion can be calculated:

$$c = (1 - \sin \varphi)\, \sigma_c /(2 \cos \varphi) = \sigma_c /(2\sqrt{K_\varphi}) \qquad (4.18)$$

The Mohr envelope can be expressed in the σ_1 - σ_3 space or the τ - σ space (Figure 4.113).

4.5.2 General procedure

The "strength reduction technique" is typically applied in factor-of-safety (FOS) calculations by progressively reducing the shear strength of the material to bring the model to a limit equilibrium state.

The safety factor F is defined according to the equations:

$$F_{\mathrm{trial}} = c/\, F_{\mathrm{trial}} \qquad (4.20)$$

$$\varphi_{\mathrm{trial}} = \arctan(\frac{1}{F_{trial}} \tan \varphi\,)$$

Nowadays the c-Φ-reduction technique is widely used in soil mechanics to characterize slope stabilities [Dawson, Roth & Drescher 1999], but just very recently in rock mechanics and underground mining [Walter & Konietzky 2008] and [Konietzky & Le 2008].

If the material has some tensile strength, as it is the case in the present work, also this parameter has to be reduced. The following equation is proposed:

$$\sigma_{\mathrm{t,\,trial}} = \sigma_{\mathrm{t}}/\, F_{\mathrm{trial}} \qquad (4.21)$$

Iteration is carried out by inserting values of the factor F_{trial} to reduce cohesion c, friction angle φ and tensile strength σ_t until the failure of the model occurs. The maximum value of F_{trial} is called "safety factor" of the rock mass. Whereas the classical c-Φ reduction method does consider only failure in shear, the new proposed method also includes potential tensile failure. The strength reduction technique was applied to the model types A and B.

4.5.3 Safety factors for considered mines

The strength reduction technique was applied to models with different rockbolt patterns such as B1, B2 and B3, but also to the model without rockbolts (Type A). Fish functions were written to perform the c-Φ-reduction, but also for displaying the Mohr envelope and principal stress distributions in order to determine and illustrate the stability of the models. The obtained safety factors for the different mines and different rockbolt pattern are given in Tables 4.28 to 4.42.

Table 4.28 Factors of safety for the Cao Thang mine with distance between rockbolts of 0.8 m (without rockbolts: FOS = 1.14).

Rockbolt Pattern	Factor of safety			
	Distance 0.8 m			
	Length 1.5 m	Length 2.0 m	Length 3.0 m	Length 4.0 m
Type B1	1.18(ca8)	1.21(ca28)	1.26(ca38)	1.29(ca48)
Type B2	1.26(cas8)	1.27(cas28)	1.33(cas38)	1.36(cas48)
Type B3	1.41(caf8)	1.49(caf28)	1.56(caf38)	1.61(caf48)

The factor of safety for the Cao Thang mine without rockbolts (mode A) is 1.14. The investigated distances between rockbolts are 0.8 m, 0.6 and 0.4 m and the length of the bolts change from 1.5 m to 2, 3 and 4.0 m (Tab. 4.28, 4.29 and 4.30). The maximum factors of safety in case of bolting reach 1.61, 1.73 and 2.60 (mode B3), respectively.

Table 4.29 Factors of safety for the Cao Thang mine with distance between rockbolts of 0.6 m(without rockbolts: FOS = 1.14).

Rockbolt Pattern	Factor of safety			
	Distance 0.6 m			
	Length 1.5 m	Length 2.0 m	Length 3.0 m	Length 4.0 m
Type B1	1.20(ca6)	1.23(ca26)	1.26(ca36)	1.28(ca46)
Type B2	1.33(cas6)	1.37(cas26)	1.40(cas36)	1.41(cas46)
Type B3	1.60(caf6)	1.63(caf26)	1.67(caf46)	1.73(caf46)

Table 4.30 Factors of safety for the Cao Thang mine with the distance between rockbolts of 0.4 m(without rockbolts: FOS = 1.14).

Rockbolt Pattern	Factor of safety			
	Distance 0.4 m			
	Length 1.5 m	Length 2.0 m	Length 3.0 m	Length 4.0 m
Type B1	1.20(ca4)	1.23(ca24)	1.30(ca34)	1.30(ca44)
Type B2	1.33(cas4)	1.39(cas24)	1.44(cas34)	1.45(cas44)
Type B3	1.90(caf4)	2.00(caf24)	2.30(caf34)	2.60(caf44)

Table 4.31 Factors of safety for the Mao Khe mine with distance between rockbolts of 0.8 m(without rockbolts: FOS = 1.75).

Rockbolt Pattern	Factor of safety			
	Distance 0.8 m			
	Length 1.5 m	Length 2.0 m	Length 3.0 m	Length 4.0 m
Type B1	1.80(mk8)	1.90(mk28)	1.95(mk38)	1.95(mk48)
Type B2	1.85(mks8)	1.91(mks28)	1.95(mks38)	1.97(mks48)
Type B3	2.0(mkf8)	2.1(mkf28)	2.25(mkf38)	2.3(mkf48)

The factor of safety for the Mao Khe mine without rockbolts (mode A) is 1.75. The investigated distances between rockbolts are 0.8 m, 0.6 and 0.4 m and the length of the bolts change from 1.5 m to 2, 3 and 4 m (Tab. 4.31, 4.32 and 4.33). If bolting is applied the maximum factors of safety are 2.30, 2.50 and 3.10 (mode B3), respectively.

Table 4.32 Factors of safety for the Mao Khe mine with distance between rockbolts of 0.6 m(without rockbolts: FOS = 1.75) .

Rockbolt Pattern	Factor of safety			
	Distance 0.6 m			
	Length 1.5 m	Length 2.0 m	Length 3.0 m	Length 4.0 m
Type B1	1.85(mk6)	1.90(mk26)	1.95(mk36)	2.00(mk46)
Type B2	1.90(mks6)	1.95(mks26)	2.0(mks36)	2.00(mks46)
Type B3	2.25(mkf6)	2.35(mkf26)	2.45(mkf46)	2.50(mkf46)

Table 4.33 Factors of safety for the Mao Khe mine with distance between rockbolts of 0.4 m(without rockbolts: FOS = 1.75) .

Rockbolt Pattern	Factor of safety			
	Distance 0.4 m			
	Length 1.5 m	Length 2.0 m	Length 3.0 m	Length 4.0 m
Type B1	1.80(mk4)	1.85(mk24)	1.90(mk34)	1.90(mk44)
Type B2	1.90(mks4)	1.95(mks24)	2.0(mks34)	2.0(mks44)
Type B3	2.85(mkf4)	2.89(mkf24)	3.0(mkf34)	3.10(mkf44)

Table 4.34 Factors of safety for the Duong Huy mine with the distance between rockbolts of 0.8 m (without rockbolts: FOS = 1.25).

Rockbolt Pattern	Factor of safety			
	Distance 0.8 m			
	Length 1.5 m	Length 2.0 m	Length 3.0 m	Length 4.0 m
Type B1	1.35(dh8)	1.40(dh28)	1.43(dh38)	1.45(dh48)
Type B2	1.40(dhs8)	1.43(dhs28)	1.45(dhs38)	1.47(dhs48)
Type B3	1.55(dhf8)	1.60(dhf28)	1.70(dhf38)	1.75(dhf48)

The factor of safety for the Duong Huy mine without rockbolts (mode A) is 1.25. The investigated distances between rockbolts are equal to 0.8 m, 0.6 and 0.4 m and the length of the bolts change from 1.5 m to 2.0, 3.0 and 4.0 m (Tab. 4.34, 4.35, 4.36). If bolting is applied the maximum factors of safety are 1.75, 1.95 and 2.55 (mode B3), re spectively.

Table 4.35 Factors of safety for the Duong Huy mine with distance between rockbolts of 0.6 m (without rockbolts: FOS = 1.25).

Rockbolt Pattern	Factor of safety			
	Distance 0.6 m			
	Length 1.5 m	Length 2.0 m	Length 3.0 m	Length 4.0 m
Type B1	1.35(dh6)	1.40(dh26)	1.42(dh36)	1.42(dh46)
Type B2	1.40(dhs6)	1.43(dhs26)	1.45(dhs36)	1.47(dhs46)
Type B3	1.75(dhf6)	1.80(dhf26)	1.90(dhf46)	1.950(dhf46)

Table 4.36 Factors of safety for the Duong Huy mine with distance between rockbolts of 0.4 m (without rockbolts: FOS = 1.25).

Rockbolt Pattern	Factor of safety			
	Distance 0.4 m			
	Length 1.5 m	Length 2.0 m	Length 3.0 m	Length 4.0 m
Type B1	1.35(dh4)	1.35(dh24)	1.38(dh34)	1.39(dh44)
Type B2	1.40(dhs4)	1.43(dhs24)	1.45(dhs34)	1.45(dhs44)
Type B3	2.05(dhf4)	2.15(dhf24)	2.40(dhf34)	2.55(dhf44)

Table 4.37 Factors of safety for the Mong Duong mine with the distance between rockbolts of 0.8 m (without rockbolts: FOS = 1.40).

Rockbolt Pattern	Factor of safety			
	Distance 0.8 m			
	Length 1.5 m	Length 2.0 m	Length 3.0 m	Length 4.0 m
Type B1	1.45(md8)	1.50(md28)	1.53(md38)	1.54(md48)
Type B2	1.50(mds8)	1.53(mds28)	1.55(mds38)	1.55(mds48)
Type B3	1.70(mdf8)	1.80(mdf28)	1.90(mdf38)	1.93(mdf48)

The factor of safety for the Mong Duong mine without rockbolts (mode A) is 1.4. The investigated distances between rockbolts are 0.8 m, 0.6 and 0.4 m and the length of the bolts change from 1.5 m to 2, 3 and 4 m (Table 4.37, 4.38 and 4.39). In case of bolting the maximum factors of safety are 1.93, 2.10 and 2.65 (mode B3), respectively.

Table 4.38 Factors of safety for the Mong Duong mine with distance between rockbolts of 0.6 m (without rockbolts: FOS = 1.40).

Rockbolt Pattern	Factor of safety			
	Distance 0.6 m			
	Length 1.5 m	Length 2.0 m	Length 3.0 m	Length 4.0 m
Type B1	1.45(md6)	1.50(md26)	1.53(md36)	1.54(md46)
Type B2	1.50(mds6)	1.55(mds26)	1.57(mds36)	1.59(mds46)
Type B3	1.90(mdf6)	1.95(mdf26)	2.05(mdf46)	2.10(mdf46)

Table 4.39 Factors of safety for the Mong Duong mine with the distance between rockbolts of 0.4 m (without rockbolts: FOS = 1.40).

Rockbolt Pattern	Factor of safety			
	Distance 0.4 m			
	Length 1.5 m	Length 2.0 m	Length 3.0 m	Length 4.0 m
Type B1	1.45(md4)	1.50(md24)	1.53(md34)	1.53(md44)
Type B2	1.50(mds4)	1.55(mds24)	1.62(mds34)	1.62(mds44)
Type B3	2.40(mdf4)	2.5(mdf24)	2.60(mdf34)	2.65(mdf44)

Table 4.40 Factors of safety for the Khe Cham mine with distance between rockbolts of 0.8 m (without rockbolts: FOS = 1.35).

Rockbolt Pattern	Factor of safety			
	Distance 0.8 m			
	Length 1.5 m	Length 2.0 m	Length 3.0 m	Length 4.0 m
Type B1	1.40(kh8)	1.45(kh28)	1.50(kh38)	1.50(kh48)
Type B2	1.45(khs8)	1.50(khs28)	1.55(khs38)	1.55(khs48)
Type B3	1.55(khf8)	1.60(khf28)	1.65(khf38)	1.70(khf48)

The factor of safety for the Khe Cham mine without rockbolts (mode A) is 1.35. The investigated distances between rockbolts are 0.8 m, 0.6 and 0.4 m and the length of the bolts change from 1.5 m to 2.0, 3.0 and 4.0 m (Tab. 4.40, 4.41 and 4.42). In case of bolting the maximum factors of safety are 1.70, 1.95 and 2.80 (mode B3), respectively.

Table 4.41 Factors of safety for the Khe Cham mine with distance between rockbolts of 0.6 m (without rockbolts: FOS = 1.35).

Rockbolt Pattern	Factor of safety			
	Distance 0.6 m			
	Length 1.5 m	Length 2.0 m	Length 3.0 m	Length 4.0 m
Type B1	1.40(kh6)	1.45(kh26)	1.50(kh36)	1.50(kh46)
Type B2	1.55(khs6)	1.58(khs26)	1.60(khs36)	1.65(khs46)
Type B3	1.75(khf6)	1.80(khf26)	1.85(khf46)	1.95(khf46)

Table 4.42 Factors of safety for the Khe Cham mine with distance between rockbolts of 0.4 m(without rockbolts: FOS = 1.35) .

Rockbolt Pattern	Factor of safety			
	Distance 0.4 m			
	Length 1.5 m	Length 2.0 m	Length 3.0 m	Length 4.0 m
Type B1	1.40(kh4)	1.45(kh24)	1.50(kh34)	1.53(kh44)
Type B2	1.55(khs4)	1.57(khs24)	1.60(khs34)	1.60(khs44)
Type B3	2.45(khf4)	2.60(khf24)	2.75(khf34)	2.80(khf44)

Summarizing the results from the above mentioned calculations, the following conclusions can be drawn:

- The stress in the bolted area is redistributed. The stress redistribution depends on the density of the rockbolts and the mode of rockbolt pattern.
- A high rockbolt density can create a helpful stress area near the opening (additional confinement) and will decrease plasticity.
- The higher the density of the rockbolts, the smaller the displacements and the deformations around the opening.
- The relation between the parameters of the rockbolts (length and distance) and the displacements can be obtained by numerical computations.
- The safety factors are directly proportional to the length and inverse proportional to the distance between rockbolts.
- Rockbolts at the floor also influence the displacements of rock mass around the drift. Especially bolting in the sidewalls can lead to a significant reduction of overall displacements and also significant reduction in roof displacements.
- The magnitude of axial force in the rockbolts depends on the anchor density and anchor length.

5 Interaction between rock mass and rockbolt - reinforcement factors

5.1 Analytical model to describe the bolting effect

After the opening is excavated, a change of the stress field in the surrounding rock mass can be observed. Classical solutions exist for the stress redistribution and the corresponding displacement and deformation field in case of unsupported circular openings in homogeneous elastic material. The solution developed below will describe the stress field and induced displacements in case of additional rockbolt installation. The developed analytical model is based on the sketch given in Figure 5.1.

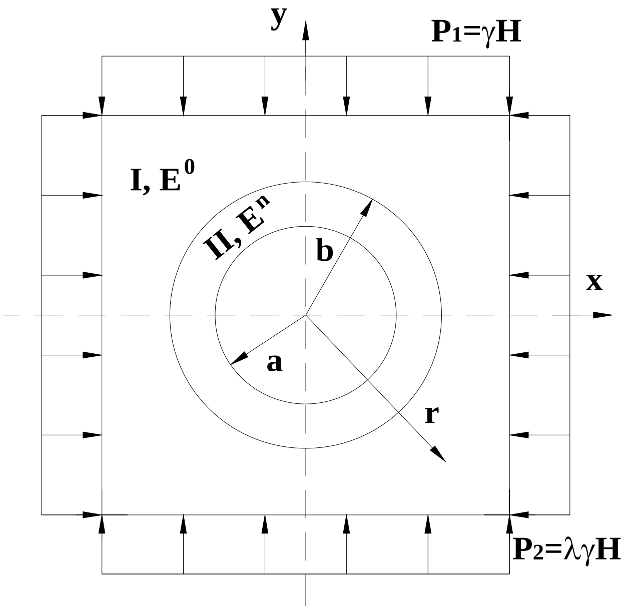

Figure 5.1 Sketch for a circular tunnel model with bolting all around the circumference.

The following assumptions are made:

- Isotropic elastic and homogeneous rock mass with Young's modulus E^0, density γ and Poisson' ratio of 0.5,
- Circular tunnel with radius a, located at depth H,
- Bolted area around tunnel with radius b = a + l, where l is anchor length,
- Diameter of the steel bar and the borehole for bolt d_b and d_s, respectively, distance between the bolts d,

- E^0, E^n, E^g are Young's moduli of rock mass, steel bar and adhesive substance, respectively,
- E^n (r) is the Young's modulus of the bolted area (area II in Fig. 5.1), which is determined by the following formula [Nguyen, 2006]:

$$E^n(r) = E^0(1+\mathrm{A}/r^2) \qquad (5.1)$$

where: E^0 Young's modulus of the rock mass before installing rockbolts

r radius of investigated area,

A empirical coefficient which can be determined by the following formula:

$$\mathrm{A} = \frac{\pi}{4}\frac{d_b^2(E^g - E^0) + d_s^2(E^b - E^g)}{d^2E^0}a^2 \qquad (5.2)$$

where: d_b diameter of the borehole,

d_s diameter of the steel bar,

E^g modulus of cement grout,

E^0 modulus of rock mass,

E^b modulus of the steel bar,

d distance between the bolts,

a radius of the opening,

A coefficient [Nguyen, 1996],

Using the value D[Le, 2002]:

$$\mathrm{D} = \frac{3A}{2b^4} - \frac{3A}{2a^4} - \frac{1}{a^2} \qquad (5.3)$$

the radial and tangential stresses are given by the following formula for both areas I and II:

- For area II:

$$\sigma_\varphi^{(II)} = -\frac{P}{D}\left(\frac{1}{r^2} + \frac{A}{2r^4} - \frac{A}{2a^4} - \frac{1}{a^2}\right) \qquad (5.4)$$

$$\sigma_r^{(II)} = \frac{P}{D}\left(\frac{1}{r^2} + \frac{3A}{2r^4} + \frac{A}{2a^4} + \frac{1}{a^2}\right) \qquad (5.5)$$

- For area I:

$$\sigma_\varphi^{(II)} = \mathrm{P} - \frac{P}{D}\left(1 + \frac{A}{b^2}\right)\frac{1}{r^2} \qquad (5.6)$$

$$\sigma_r^{(I)} = \mathrm{P} + \frac{P}{D}\left(1 + \frac{A}{b^2}\right)\frac{1}{r^2} \qquad (5.7)$$

- Radial displacement in area I ($u^{(I)}$) and II ($u^{(II)}$) are:

$$u^{(II)} = \frac{3P}{2E^{n}D}\left(\frac{1}{r} + \frac{A}{r^{3}}\right) \quad \text{with } a \le r \le b \qquad (5.8)$$

$$u^{(I)} = \frac{3Pr}{2E^{n}D}\left(1 + \frac{A}{b^{2}}\right) \quad \text{with } r \ge b \qquad (5.9)$$

where r is the radius of the investigated area.

The analytical approach outlined above was exemplary applied to the Cao Thang mine using the following parameters:

- Radius of the opening: 2.0 m,
- Density of the rock mass: 2600 kg/$m^{3,}$
- Depth of the opening: 160 m,
- Young's modulus of the rock mass E^0: 6.6e2 Mpa,
- d_b Diameter of the borehole: 36 mm,
- d_s Diameter of the steel bar: 20 mm,
- E^g Modulus of cement grout: 1e4 Mpa,
- E^b Modulus of the steel bar: 2e5 Mpa,
- d Distance of the bolt: 0.8 m,
- l Length of the bolt: 1.5 m.

This leads to values for A = 0.655 m^2 and D = 0.0155 m^{-2}. Exemplary, final results from the calculation are shown in Table 5.1. For comparison values of vertical displacements for the Cao Thang mine are displayed for both analytical and numerical calculations. Both methods show a remarkable good agreement, especially if one considers, that the analytical approach incorporates several significant simplifications, like circular shape and isotropic elastic and homogeneous material behaviour as well as closed ring of bolting. This comparison shows, that the numerical approach gives reasonable results and that the analytical approach may be applied as a fist guess to study the effect of bolting. Nevertheless, the numerical approach gives much deeper and more detailed insight into the effect of bolting and allows to distinguish between different rockbolt pattern.

Table 5.1 Vertical displacements (cm) obtained by analytical and numerical calculations at roof centre.

Distance between bolts	Method of	Length of the bolt (m)			
		1.5	2.0	3.0	4.0

(m)	Calculation				
0.8	Analytical	3.05	3.04	3.04	3.03
	Numerical	4.31	3.96	3.65	3.54
0.6	Analytical	2.66	2.64	2.63	2.63
	Numerical	3.07	3.01	2.72	2.72
0.4	Analytical	1.94	1.93	1.91	1.91
	Numerical	2.08	2.01	1.92	1.88

5.2 Reinforcement factors

Reinforcement factor Kr is defined by dividing the safety factor of a model with rockbolts and that of a model without rockbolts:

$$Kr = sf/sf0 \qquad (5.10)$$

where sf0 safety factor of the opening which is unsupported

sf safety factor of the opening which is supported by rockbolts

Kr reinforcement factor

The safety factors themselves are obtained by applying the c-Φ-reduction method as described above. Using this definition, the reinforcement factors were obtained for five Vietnamese coal mines considering different rockbolt patterns (type B3). The results are listed in the following tables.

Table 5.2 Reinforcement factors (Kr) when distance between the bolts is 1.0 m.

Distance between bolts of 1.0 m	Length of the bolts (m)				sfo without bolts
	1.5	2.0	3.0	4.0	
Cao Thang	1.140	1.184	1.272	1.316	1.14
Mao Khe	1.086	1.143	1.177	1.200	1.75
Duong Huy	1.080	1.120	1.160	1.200	1.25
Mong Duong	1.036	1.071	1.143	1.179	1.40
Khe Cham	1.074	1.111	1.148	1.185	1.35

Table 5.3 Reinforcement factors (Kr) when distance between the bolts is 0.8 m.

Distance between bolt of 0.8 m	Length of the bolts (m)				sfo without bolts
	1.5	2.0	3.0	4.0	

Cao Thang	1.237	1.307	1.368	1.412	1.14
Mao Khe	1.143	1.200	1.286	1.314	1.75
Duong Huy	1.240	1.280	1.360	1.400	1.25
Mong Duong	1.214	1.286	1.357	1.379	1.40
Khe Cham	1.148	1.185	1.222	1.259	1.35

Table 5.4 Reinforcement factors (Kr) when distance between the bolts is 0.6 m.

Distance between bolts of 0.6 m	Length of the bolts (m)				sfo without bolts
	1.5	2.0	3.0	4.0	
Cao Thang	1.404	1.44	1.465	1.518	1.14
Mao Khe	1.286	1.75	1.400	1.429	1.75
Duong Huy	1.400	1.44	1.520	1.560	1.25
Mong Duong	1.357	1.40	1.464	1.500	1.40
Khe Cham	1.296	1.35	1.370	1.444	1.35

Table 5.5 Reinforcement factors (Kr) when distance between the bolts is 0.4 m.

Distance between bolts of 0.4 m	Length of the bolts (m)				sfo without bolts
	1.5	2.0	3.0	4.0	
Cao Thang	1.667	1.754	2.018	2.281	1.14
Mao Khe	1.629	1.651	1.714	1.771	1.75
Duong Huy	1.640	1.720	1.920	2.040	1.25
Mong Duong	1.714	1.786	1.857	1.893	1.40
Khe Cham	1.815	1.926	2.037	2.074	1.35

5.3 Relation between reinforcement factors (K_r) and parameters of bolting pattern

As documented by the calculations of reinforcement factors Kr for five specific mine locations with different rockbolt pattern it is obvious that K_r is a function of rockbolt length l and distance between rockbolts d:

$$K_r = f(l,d) \tag{5.11}$$

In all cases of investigation the cross sections is approximately 10 m^2. A curve fitting procedure is used to find out this relation, where the reinforcement factor is a function of the two parameters l and d. The input data for curve fitting are taken from Tables 5.1, 5.3, 5.4 and 5.5. By using a nonlinear regression analysis the following relation was obtained:

$$K_r = 0.994 \cdot l^{0.139} \cdot d^{-0.524} \tag{5.12}$$

The investigated length of the bolts ranges from 1.5 to 4.0 m. The investigated distance between the bolts varies from 0.4 to 1.0 m. These values are typical for field conditions in Vietnam. The value of reinforcement factors determined by equation (5.12) are given in Table 5.6.

Table 5.6 Reinforcement factors (K_r) determined by equation (5.12).

Distance between bolts (m)	Length of the bolts (m)			
	1.5	2.0	3.0	4.0
1.0	1.052	1.095	1.158	1.205
0.8	1.182	1.230	1.302	1.355
0.6	1.374	1.430	1.513	1.575
0.4	1.700	1.769	1.872	1.948

The diagrams 5.2 to 5.5 illustrate the reinforcement factors which are computed by the formula (5.12) and those determined by the formula (5.10) for the individual mines.

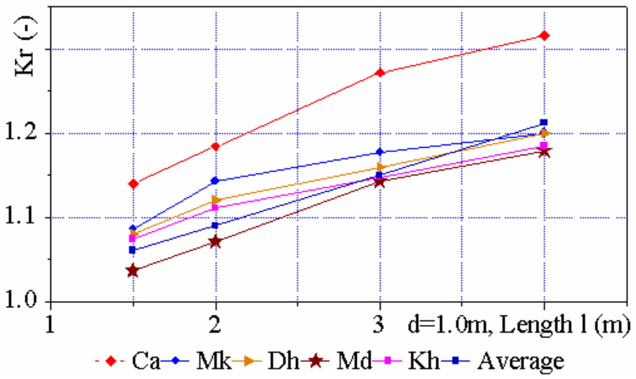

Figure 5.2 Individual reinforcement factors (Kr) for 5 different mines and generalised trend (Average), when distance between bolts is 1.0 m.

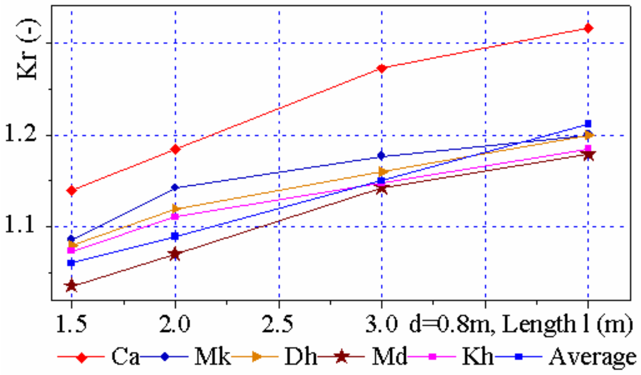

Figure 5.3 Individual reinforcement factors (Kr) for 5 different mines and generalised trend (Average), when distance between bolts is 0.8 m.

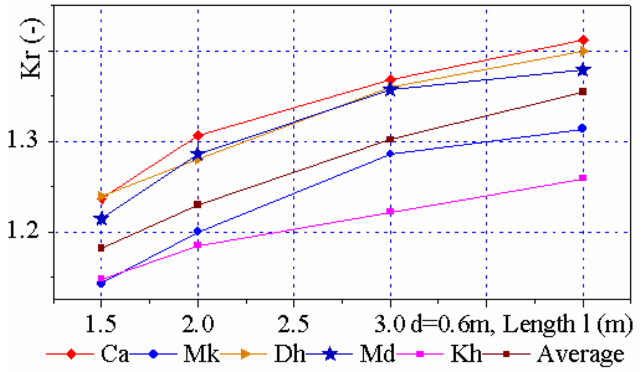

Figure 5.4 Individual reinforcement factors (Kr) for 5 different mines and generalised trend (Average), when distance between bolts is 0.6 m.

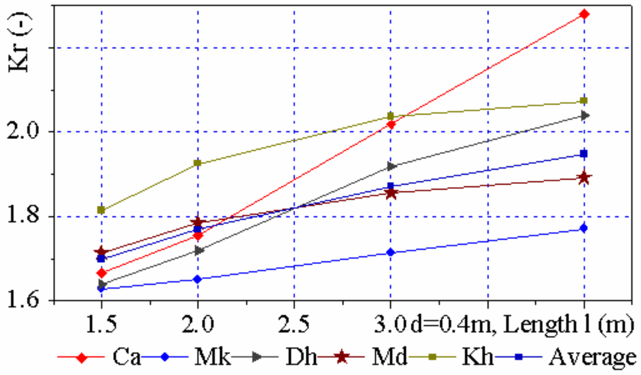

Figure 5.5 Individual reinforcement factors (Kr) for 5 different mines and generalised trend (Average), when distance between bolts is 0.4 m.

The reinforcement factors are direct proportional to the length and inverse proportional to the distance between the bolts. The standard deviation for the generalized reinforcement factor (fitted regression line) is 0.0836.

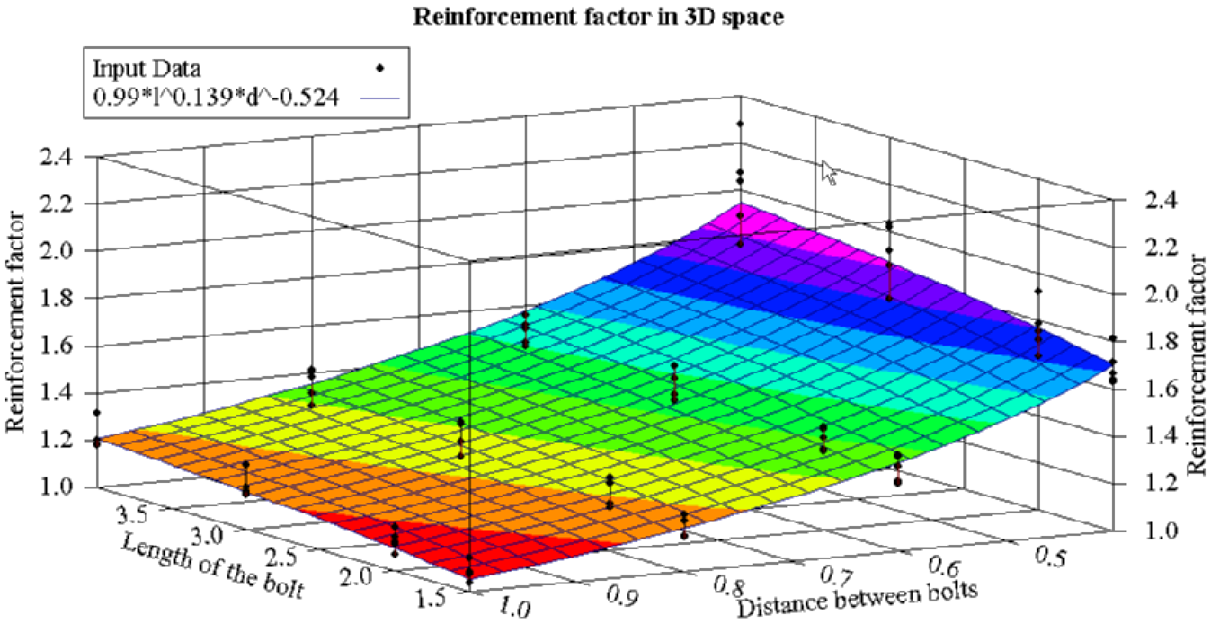

Figure 5.6 Reinforcement factors (Kr) in 3D space, Distance [m], Length [m].

The coefficient of multiple determination R^2 is 0.915, that means that 91.5 % of the variations in the response variable is explained by the regression model. Figure 5.6 illustrates the reinforcement coefficients Kr in a 3D space incorporating the distance between rockbolts, the length of rockbolts and the reinforcement factors K_r which has a minimum value at P_1(d, l, Kr) = 1.0 m, 1.5 m, 1.052 (the distance between bolts reaches the maximum value and the length of the bolts the minimum value) and a maximum value at P_2 (d, l, Kr)= 0.4 m, 4.0 m, 1.95 (the distance between bolts reaches the minimum value and the length of the bolts the maximum value).

6 Conclusions and recommendations

6.1 Conclusions

Based on the results of the presented research on the interaction between rockbolts and rock mass under special consideration of the geomechanical situation in Vietnamese coal mines the following conclusions can be drawn:

- A complete methodology is proposed to design anchor schemes for Vietnamese underground coal mines, which consists of the following steps:
    - Determination of rockmechanical parameters
    - Transformation of rockmechanical parameters into rock mass parameters by using rockmass classification schemes
    - Set-up of numerical model including the real geological situation
    - Simulation of excavation without anchorage and investigation of model response (determination of stability/unstability, deformations, safety factors etc.)
    - Incorporation of anchors into the modelling and investigation of model response, especially in respect to safety factors and the reinforcement effects
    - Parameter studies and optimization by choosing different bolting schemes
    - Development of an proposal for optimized drift anchorage
- The numerical modelling results obtained for the drifts without anchorage show that the openings are close to instability (safety factors close to 1). This is confirmed by observations in situ: unsupported drifts often show local rockfall, collapse or extreme deformations. This indicates that the applied numerical modelling approach and the chosen parameters are realistic.
- Compared to other methods, like empirical relations or simple analytical calculations, numerical modelling offers a much more detailed and physical based insight into the interaction between rockbolts and rock mass. In contrast to the simple analytical approaches, the numerical modelling allows to consider the problem in much more detail, e.g. inhomogeneities, like layering with different parameters and constitutive laws can be considered. Due to the fact, that each

anchor is modelled explicitly the interaction between each bolt and the rock mass can be investigated and any desired anchor scheme can be considered in detail. Consequently, numerical modelling can be used for detailed anchor dimensioning, design and optimization.

- The c-Φ-reduction method, so far widely used in soil mechanics, was successfully further developed by incorproation of tensile strength and applied to determine safety factors for underground drifts with and without bolting.
- To characterize the effect of bolting in a quantitative manner a 'reinforcement factor' is introduced, which is the quotient between the factors of safety obtainned be using the c-Φ-reduction method for unbolted and bolted opening, respectively. The reinforcement factor is proportional to the length of the bolt and inverse proportional to the distance between the bolts. For the investigated mines a reinforcement factor between app. 1.1 and 2.0 was obtained in dependence on the chosen anchor scheme.
- Besides the reinforcement factor the numerical modelling approach offer several other criteria and characteristics to assess the effect of bolting and the interaction between rockbolts and rock mass. These criteria include the displacements, the individual anchor forces, the plastifications, the safety factors or stress redistributions.
- The effect of rockbolting is also documented by reduced displacements. The greater the length of the bolts, the smaller the displacements at the drift boundary. The smaller the distance between the bolts, the smaller the displacements and vice versa.
- When a certain length and/or distance between the rockbolts is reached the physical indicators like displacements, safety factors, reinforcement factors, plastifications etc. do not change any more significantly. This indicates that further improvement or extension of the support is useless. Therefore, the quantitative indicators obtained by the numerical modelling can be used to optimize the bolting system.
- The developed constitutive law for nonlinear and cyclic behaviour of the cable and rockbolt elements both in 2D and 3D allows to investigate the system also under dynamic or cyclic loading. Also the reserves of the anchors activated during a hardening phase can be incorporated into an economic and safe design.

The developed extension to multi-segment cable and rockbolt elements allows to set a better resolution in numerical simulations.

- The visualization of the results obtained by the numerical modelling allow excellent communication between consultants, mining engineers, mining management, authorities, miners and other persons involved in the process.
- Based on the summarized evaluation of different anchor schemes for five different mine situations, generalized trends were deduced in respect of the effectiveness of different anchor schemes expressed by the ‘reinforcement factor’.

6.2 Recommendations

- Further numerical simulations should include the more realistic anchor models developed by the author and described in chapter 3. This will allow to include cyclic loading and strain-hardening effects.
- Numerical simulation of the interaction between rock mass and anchors should be extended towards mathematical based sensitivity analysis and optimisation, like proposed by Schlegel, Will & Konietzky (2007). This will allow effective and comprehensive investigations in highly multidimensional parameter spaces on the basis of intelligent sampling methods like Latin Hypercube Sampling.
- The proposed procedure can be applied also to drifts with larger cross sections (e.g. 20 to 30 m^2) and other shapes of the cross sections such as rectangular, trapezoidal etc.
- Instead of using the soft-core-method to consider 3D effects, further modelling can be performed by full 3D approach, e.g. with FLAC^{3D}. This would also allow to optimize the time of setting the anchors in relation to the drift advance.
- In weak rocks, rockbolting can be combined with other support measures like shotcrete, steel support or concrete. A similar numerical procedure might be applied to characterize the reinforcement effect in a quantitative manner.

References:

Agioutantis, Z.; Stiakakis, C.; Stiakakis, N. (2001):
An interactive roof bolting selection and performance system. In: Proceedings of the Aachen International Symposium on Roofbolting in Mining, july 2001. Publisher: Wissenschaftsverlag Mainz in Aachen; pp 95-110.

Bagheri, M.; Jalalifar, H.; R. Rahmannejad, R. (2008):
The Evaluation and Applicability of Rock Bolts in Coal Mines with regard to the Kerman Province Mines. In: Proceedings of the Aachen international symposium on Roofbolting in Mining, March 2008. Publisher: Wissenschaftsverlag Mainz in Aachen; pp 257-274.

Barton, N.; Lien, R.; Lunde, J. (1974):
Engineering classification of rock masses for the design of tunnel support. In: Rock Mechanics, 6(1974), Issue 4. Publisher: Springer-Verlag, Wien; pp 189 -236.

Barton, N.; Loset, F.; Lunde, J. (1980):
Application of Q system in design decision concerning dimensions and appropriate support for underground installations. In: International Conference on Sub-surface Space, Rockstone, 2(1980). Publisher: Pergamon Press; Stockholm; pp 553-561.

Bieniawski, Z. T. (1976):
Rock mass classification in rock engineering. In: Proceedings of the symposium in Exploration for rock engineering, 1(1976); Publisher: A.A Balkema, Cape Town; pp 97-106.

Bieniawski, Z. T. (1979):
The geomechanics classification in rock engineering applications. In: ISRM Proceedings of the Fourth International Congress for Rock Mechanics, Montreux, Switzerland, 2(1979). Publisher: A.A. Balkema, Rotterdam; pp 41–48.

Bieniawski, Z. T. (1984):
Rock mechanics design in mining and tunnelling, (1984); Publisher: A.A. Balkema, Rotterdam.

Bieniawski, Z. T. (1989):
Engineering rock mass classifications, (1989); Publisher: Wiley, New York; pp 251.

Bieniawski, Z. T. (1989):
Engineering rock mass classification: a Complete Manual for Engineers and Geologists in Mining, Civil, and Petroleum Engineering, (1989). Publisher: John Wiley & Sons, New York; pp 251.

Bobet, A. (2005):
A simple method for analysis of point anchored rockbolts in circular tunnels in elastic ground. In: Rock Mechanics and Rock Engineering; 39(2005); Publisher: Springer-Verlag, Wien; pp 315-338.

Brady, B. H. G.; Brown, E. T. (2006):
Rock mechanics for underground mining, (2006); Publisher: Springer-Verlag, The Nietherlands; pp 312-338.

Dawson, E. M.; Roth, W. H.; Drescher, A. (1999):
Slope Stability Analysis by Strength Reduction. In: Geotechnique Journal; 49(1999), Issue 6; Publisher: Royaume-Uni. London; pp 835-840.

Fahimifar, A.; Sorough, H. (2004):
A theoretical approach for analysis of the interaction between grouted rockbolts and rock masses. In: Tunnelling and Underground Space Technology, 20(2004), Issue 4; Publisher: Elsevier Press; pp 333-343.

Hausdorf, A. (2006):
Numerical studies on the stability of the roofs of the rooms in salt mining taking specially into account a systematic anchoring with an elasto-plastic characteristic curve with hardening and different values of the anchor prestress. Publication of the Geotechnical Institute of the Technical University Bergakademie Freiberg, PhD thesis, Issue 2006-2, 2006.

Hausdorf, A.; Le, V. C.; Konietzky, H. (2006):
The elasto-plastic behaviour of anchor steels in salt mining and its numerical modelling. In: Proceeding of the 35 Geomechanics Colloquium. Publications of the Geotechnical Institute of the Technical University Bergakademie Freiberg, Issue 2006-5, pp 101-114

Hobst, L.; Zajic, J. (1983):
Anchoring in rock and soil. Publisher Elsevier: Amsterdam and others, 2003; pp 311-320.

Hoek, E. (2004):
Numerical modelling for shallow tunnel in weak rock. In: website rocscience.com; discussion paper 3, 6.9.2008.

Hoek, E.; Brown, E. T. (1997):
Practical estimates of rock mass strength. In: International Journal of Rock Mechanics and Mining Science. 34(1997), Issue 8. Publisher Elsevier: Great Britain; pp 1165-1186.

Hoek, E.; Brown, E. T. (1998):
Underground excavation in hard rock. Publisher: Taylor & Francis/Balkema, AK Leiden, the Netherland;

Hoek, E.; Brown, E. T. (2007):
Practical Rock engineering: chapter 3, chapter 11, chapter 14. In: website rocscience.com; 29.11.2007

Hoek, E.; Carranza-Torres.C.; Corkum, T. B. (2002):
Hoek-Brown failure criterion – 2002. In: Proceedings on NARMS-TAC 2002 Conference, (2002); Publisher: University of Toronto, Toronto; pp 267-273.

Hoek, E.; Diederichs, M. (2005):
Empirical estimation of rock mass modulus. In: International Journal of Rock Mechanics and Mining Sciences, 43(2006). Publisher: Elsevier; pp 203–215.

Hudson, J. A. (1997):
Engineering Rock Mechanics Part 1+2, (1997); Publisher: Pergamon, Armsterdam and others.

Hudson, J. A. (2000):
Comprehensive rock engineering Part 4, (2000); Publisher: Pergamon, Armsterdam and others, pp 317.

IMSAT, (1990):
Report of application of fully grouted rockbolt at Mong Duong mine 1990. Publications of The Institute of Mining Science and Technology (IMSAT).

IMSAT, (1998):
Report of application of fully grouted rockbolt at Duong Huy mine 1998. Publications of The Institute of Mining Science and Technology (IMSAT).

IMSAT, (2000):
Report of application of fully grouted rockbolt at Mao Khe mine 2000. Publications of The Institute of Mining Science and Technology (IMSAT).

IMSAT, (2002a):
Report of application of fully grouted rockbolt at Cao Thang mine 2002. Publications of The Institute of Mining Science and Technology (IMSAT).

IMSAT, (2002b):
Report of application of fully grouted rockbolt at Khe Cham mine 2002. Publications of The Institute of Mining Science and Technology (IMSAT).

ITASCA, (2006):
FLAC^{3D} user's manual, Version 3.1; ITASCA Consulting Group Inc, Mineapolis, 2006.

Jeremic, M. L. (1987):
Ground mechanics in hard rock mining (1987). Publisher: Taylor & Francis, pp 495-502.

Jian, Z. ; Weishen, Z. (2003):
Stability analysis and modelling of underground excavations in fractured rocks (2003). Publisher: Elsevier Science, Netherland; pp 247-262.

Jing, L.; Hudson, J. A. (2002):
Numerical methods in rock mechanics. In: International Journal of Rock Mechanics and Mining Science; 39(2002), Issue 4. Publisher: Elsevier; pp 409-427.

Junker, M. et al (2006):
Ground Control for roadways (2006). Publisher: Verlag Glueckauf GmbH, Essen; pp 247-249.

Junlu, L. (1999):
A new rockbolt design criterion and knowledge expert system for stratified roof (1999). The Faculty of the Virginia Polytechnic Institute and State University; Dissertation. In: website: *www.eng.unsw.edu.au/faculty/publicat/2007/Eng%20Research%20Guide.pdf.*

Konietzky, H. (2005):
Lecture notes: support and lining of underground opening.
The Geotechnical Institute of the Technical University Bergakademie Freiberg. Internal educational material. (Not published)

Konietzky, H. (2006):
Lecture notes: Rock Mechanics.
The Geotechnical Institute of the Technical University Bergakademie Freiberg. Internal educational material. (Not published)

Konietzky, H.; Le, V. C. (2008):
Analysis of rockbolt reinforcement by numerical simulations. In: Proceedings of the international conference on advanced in mining and tunnelling (8-2008), Ha Noi, Viet-Nam; Publisher: Publishing house for science and technology; pp 315-323.

Kovari, K. (2004):
History of rockbolt and the sprayed concrete lining method. In: Proceedings of the Aachen International symposium on Roofbolting in Mining (2004); Publisher: Wissenschaftsverlag Mainz in Aachen; pp 39 – 85.

Lautsch, T. (2001):
Roofbolting in three continents, a comparison. In: Proceedings of the Aachen International symposium on Roofbolting in Mining (2004); Publisher: Wissenschaftsverlag Mainz in Aachen; pp 59-76.

Le, V.C. (2002):
The research applied the resin anchor on underground mine opening support (2002); Master thesis, 2002. Publications of the Hanoi Mining and Geology University.

Nguyen, Q. P. (2006):
Rock mechanics (2006). Publisher: Hanoi Construction.

Nguyen, X. M. (1998):
Lecturenote: Structural mechanics and support design (1998). Publications of Ha Noi Geology and Mining University;

Oreste, P. P. (2003):
Analysis of structural interaction in tunnels using the convergence–confinement approach. Tunnelling and Underground Space Technology; 18(2003); Publisher: Pergamon; pp 47-363.

Palmstrom, A. (1996):
Characterizing rock masses by the RMi for Use in Practical Rock Engineering Tunnelling and Underground Space Technology; ll (1996), Issue 2; Publisher: Pergamon; pp 175-188.

Palmstrom, A.; Singh, R. (2001):
The deformation modulus of rock masses: comparisons between in situ tests and indirect estimates. In: Tunnelling and Underground Space Technology Journal; 16(2001); Publisher: Elsevier Science Ltd; pp 115-131.

Parry, R. H. G. (1992):
Mohr circle, Stress paths and Geotechnics (1992). Publisher: E & FN Spon, London.

Pellet, F.; Egger, P. (1996):
Analytical model for the mechanical behaviour of bolted rock joints subjected to shearing. In: The Rock Mechanics and Rock Engineering Journal; 29(1996), Issue 2; Publisher: Springer-Verlag; pp 73-97.

Rockscience (2008):
www.Rockscience.com

RWTH Aachen; 2001, 2002, 2004, 2006:
Roofbolting in mining; In: Proceeding of the Aachen International Mining symposium. Publisher: Wissenschaftsverlag Mainz in Aachen.

Sakurai, S.; Kawashima, I. (1992):
Modelling of jointed rock masses reinforced by rockbolts. In: Proceedings of the International Symposium on Rock Support in mining and underground construction; Publisher: Balkema: Rotterdam, pp 547–550.

Samit, R.; Anand, B. R. (1997):
Analysis of rockbolt reinforcement using beam-column theory. In: International Journal for Numerical and Analytical Methods in Geomechanics; 21(1997), Issue 4; Publisher: John Wiely & Son Ltd, pp 241-253.

Sasaoka, T.; Shimada, H.; Ichinose, M.; Matsui, K. (2008):
Improvement of roof support system under weak roof conditions by way of numerical analysis. In: Proceeding of the Aachen International Mining symposium. Publisher: Wissenschaftsverlag Mainz in Aachen; pp 69-84

Schlegel, R.; Will, J.; Konietzky, H. (2005):
Optimization and sensitivity analysis in mining and geotechnical engineering using numerical approaches - Environment friendly policy in mining activities. In: Proceedings of the first international seminar ecomining;Romania (2005); Publisher: Estfalia, pp 47-54.

Stillborg, B. (1986):
Professional users handbook for rockbolting (1986). Publisher: Trans Tech Publication, pp 69.

Stillborg, B.; Li, C. (1999):
Analytical models for rockbolts. In: International Journal of Rock Mechanics and Mining Sciences; 36 (1999); Publisher: Pergamon, pp 1013–1029.

The Minova, (2006):
Resin grouted rockbolts. Publisher: Piggott Black Bear, Cambridge. UK. Business Publication.

Vo, T. H. (1998):
Lecture notes: Stability of the underground opening. Publications of Ha Noi geology and mining university.

Walter, K.; Konietzky, H. (2008):
Room and pillar dimensioning for gypsum and anhydrites mining in Germany. In: Proceedings of the international conference on advanced in mining and tunnelling (8-2008), Ha Noi, VietNam; Publisher: Publishing house for science and technology; pp 349-362.

Windsor, C. R. (1997):
Rock reinforcement systems. In: International journal of rock mechanics and mining sciences; 34(1997), Numer 6. Publisher: Elsevier Science, Oxford, ROYAUME-UNI (1997); pp 919-951.

Yue, C.; Tetsuro, E.; Yujing, J. (2004):
A rockbolt and rock mass interaction model. In: International Rock Mechanics and Mining Science. Publisher: Elsevier ; pp 1165-1186.

Ziping, H. (2001):
Stabilizing of rock cavern roofs by rockbolts. Department of geology and mineral resources engineering; Faculty of applied earth science; Norwegian University of Science and Technology; PhD thesis (2001);

List of Figures

Figure 2.1 Element of ground control management (Lautsch, 2001)....................... 9
Figure 2.2 Rockbolt types (adopted from Hoek & Brown, 1980).......................... 14
Figure 2.3 Suspension effect of rockbolts. 18
Figure 2.4 Beam building effect of rockbolts.. 18
Figure 2.5 Keying effect of roof bolts. 19
Figure 2.6 Strength increase of the rock mass by increasing confining stress. 20
Figure 2.7 Traditional artificial arch forming [Lang, 1959]................................. 21
Figure 2.8 Nomogram for rockbolt reinforcement of horizontallybedded rock. 24
Figure 2.9 Nomogram for rockbolt design based on Q designation....................... 26
Figure 2.10 Sketch for calculating the length of the bolts...................................... 30
Figure 2.11 Sketch for creating the beam in a laminated flat roof. 32
Figure 2.12 Sketch for creating a beam in a homogeneous flat roof........................ 33
Figure 2.13 Sketch for creating a beam in the arched roof...................................... 34
Figure 2.14 Sketch for beam creation in bolted arch shaped roof. 36
Figure 2.15 Concept of ground reaction curve. 38
Figure 2.16 Experimental stress-strain relation obtained from models with and without bolts.. 39
Figure 3.1 Components of a numerical cable element (t_1, t_2 direction cosines of the element referred to tangential direction)[ITASCA 2005]. 42
Figure 3.2 Outline of numerical cable element [ITASCA 2005]. 42
Figure 3.3 Numerical model for testing cable and rockbolt structural elements.... 47
Figure 3.4 Development of axial force F (MN) versus axial strain (%) of the cable element in the pure loading process [.. 48
Figure 3.5 Development of the axial force F (MN) versus calculation steps of the non-linear one segment cable element in the unloading and reloading process... 49
Figure 3.6 Development of the axial strain (%) versus calculation steps of the nonlinear one segment cable element in the unloading and reloading process... 49
Figure 3.7 Development of axial force F (MN) versus axial strain (%) of the nonlinear one segment cable element (CB) in the unloading and reloading pro-cess. 50

Figure 3.8 Development of axial force F (MN) versus calculation steps of the nonlinear five segment cable element (Seg) in the unloading and reloading process. 51

Figure 3.9 Development of the strain (%) versus calculation steps of the nonlinear cable element for five segments (Seg) in the unloading and reloading process. 51

Figure 3.10 Development of the axial force F (MN) versus axial strain (%) of the nonlinear five segment cable element (Seg) in the unloading and reloading process. 52

Figure 3.11 Development of the axial force F (MN) versus calculation steps of the nonlinear one segment rockbolt element during unloading and reloading. 52

Figure 3.12 Development of the axial force F (MN) versus axial strain (%) of the nonlinear one-segment rockbolt element (1segRB) during unloading and reloading. 53

Figure 3.13 Development of the axial force F (MN) versus calculation steps of nonlinear five segment rockbolt element (Seg) during unloading and reloading. 53

Figure 3.14 Development of the axial force F (MN) versus axial strain (%) of nonlinear five segment rockbolt element (Seg) during unloading and reloading. 53

Figure 3.15 Axial strain (%) versus step number of nonlinear five segment rock bolt element (Seg) during unloading and reloading. 54

Figure 3.16 Distribution of axial force [N] in nonlinear five-segment rockbolt element. 54

Figure 3.17 Cable SELs coordinate system and 2 active degrees-of-freedom of the cable element (SELs-structural elements). 55

Figure 3.18 Development of axial force F (MN) versus axial strain (%) of the nonlinear one segment cable element (CB) in the unloading and reloading process. 56

Figure 3.19 Development of axial force F (MN) versus axial strain (%) of the nonlinear five segment cable element (CBSeg) in the unloading and reloading process. 57

Figure 3.20 Pile-SEL coordinate system and 12 active degrees-of-freedom of the beam finite element used by each pile-SEL in FLAC^{3D} 58
Figure 3.21 Model with one segment structural element in FLAC^{3D}...................... 59
Figure 3.22 Development of axial force F (MN) versus axial strain (%) of the nonlinear one segment rockbolt element during loading, unloading and reloading.. 59
Figure 3.23 Development of axial force F (MN) versus axial strain (%) of the nonlinear five segment rockbolt element (Seg) during loading, unloading and reloading.. 59
Figure 4.1 Mohr - Coulomb failure criterion expressed in the σ_1-σ_3 space........... 61
Figure 4.2 Locations of selected Vietnamese underground coal mines. 62
Figure 4.3 Cao Thang mine stratified log.. 63
Figure 4.4 Cao Thang model with dimensions in meter. 63
Figure 4.5 Mao Khe mine stratified log. 64
Figure 4.6 Mao Khe model with dimensions in meter. 64
Figure 4.7 Duong Huy mine stratified log.. 65
Figure 4.8 Duong Huy model with dimensions in meter 65
Figure 4.9 Mong Duong stratified log.. 66
Figure 4.10 Mong Duong model with dimension in meter. 66
Figure 4.11 Khe Cham mine stratified log. 67
Figure 4.12 Khe Cham model with dimension in meter 67
Figure 4.13 Cross section of Mong Duong roadway with area of 11.08 m^2........... 70
Figure 4.14 Hoek-Brown envelope and equivalent Mohr – Coulomb envelope...... 71
Figure 4.15 Equivalent Mohr envelope in principal stress space for conglomerate (left), sandstone (right); (Cao Thang mine). 76
Figure 4.16 Equivalent Mohr envelope in principal stress space for sandstone (left), siltstone (right); (Mao Khe mine). 76
Figure 4.17 Equivalent Mohr envelope in principal stress space for conglomerate (left), sandstone (right); (Duong Huy mine). 78
Figure 4.18 Equivalent Mohr envelope in principal stress space for conglomerate (left), sandstone (right); (Mong Duong mine). 78
Figure 4.19 Equivalent Mohr envelope in principal stress space for conglomerate (left), sandstone (right); (Khe Cham mine)... 78
Figure 4.20 General solution procedure. 79

Figure 4.21 Types of models used for investigation 81
Figure 4.22 Contours of major principal stresses (MPa) without rockbolt ca0 (left) and with rockbolt ca8 (d = 0.8 m, right) with the length of the bolt l = 1.5 m; Dimension (m). 86
Figure 4.23 Contours of vertical displacement (m) without rockbolt ca0 (left) and with rockbolt ca8 (d = 0.8 m, right) with the length of the bolt l = 1.5 m; Dimension (m). 87
Figure 4.24 Vertical displacements ydisp (cm) along the top line d (m) without rockbolt ca0 and with rockbolt ca8 (d = 0.8 m, right) with the length of the bolt l = 1.5 m. 87
Figure 4.25 Displacement vectors (m) without rockbolts ca0 (left) and with rockbolts ca8 (d = 0.8 m, right) with the length of the bolts l = 1.5 m; Dimension (m). 88
Figure 4.26 Plasticity area without rockbolt ca0 (left) and with rockbolt ca8 (d = 0.8 m, right) with the length of the bolt l = 1.5 m. The red elements show the yield in shear, the green ones represent the elastic state but plastic in past; Dimension (m). 88
Figure 4.27 Safety factors without rockbolts ca0 (left) and with rockbolts ca8 (d = 0.8 m, right) with the length of the bolts l = 1.5 m; Dimension (m).....89
Figure 4.28 Determination of the safety factor by using Mohr-Coulomb criterion. 89
Figure 4.29 Axial anchor forces (MPa) of the rockbolts for the models ca8 (d = 0.8 m), ca6 (d = 0.6 m); ca4 (d = 0.4 m) with the same length of bolts (l = 1.5 m) in all models; Dimension (m). 90
Figure 4.30 Displacement vectors (m) for models cas8 (l = 1.5 m), cas28 (l = 2.0 m), cas38 (l = 3.0 m), cas48 (l = 4.0 m) with the same distance between bolts d = 0.8 m in all models. Dimension (m)......................................91
Figure 4.31 Contours of vertical displacements (m) for the models cas8 (l = 1.5 m), cas28 (l = 2.0 m), cas38 (l = 3.0 m) and cas48 (l = 4.0 m) with the same distance between bolts d = 0.8 m in all models; Dimension (m). 92
Figure 4.32 Vertical displacement Ydisp (cm) along the top line for the models cas8 (l = 1.5 m), cas28 (l = 2.0 m), cas38 (l = 3.0 m) and cas48 (l = 4.0 m) with the same distance between bolts d = 0.8 m in all models. 92

Figure 4.33 Contours of major principal stress (MPa) for the models cas8 (l = 1.5 m), cas28 (l = 2.0 m), cas38 (l = 3.0 m), cas48 (l = 4.0 m) with the same distance between bolts d = 0.8 m in all models; Dimension (m). 93

Figure 4.34 Displacement vectors (m) for the models cas6 (d = 0.6 m, left) and cas4 (d = 0.4 m, right) with the same length of bolt l = 1.5 m; Dimension (m). 94

Figure 4.35 Vertical displacement Ydisp (cm) along the top line for the model cas6 (d = 0.6 m) and cas4 (d = 0.4 m) with the same length of bolt l = 1.5 m. 94

Figure 4.36 Plasticity that occurs in models cas6 (d = 0.6 m, left) and cas4 (d = 0.6 m, right) with the same length of bolt l = 1.5 m. The red elements show the yield in shear, the green ones represent the elastic state but plastic state in past; Dimension (m). 95

Figure 4.37 Contours of major principal stress (MPa) in models cas6 (d = 0.6 m, left), cas4 (d = 0.4 m, right) with the same length of bolt l = 1.5 m; Dimension (m). 95

Figure 4.38 Axial forces (MPa) of the rockbolts in models cas6 (d = 0.6 m, left), cas4 (d = 0.4 m, right) with the same length of bolt l = 1.5 m; Dimension (m). 96

Figure 4.39 Contours of vertical displacements (m) for the models caf8 (d = 0.8 m), caf6 (d = 0.6 m), caf4 (d = 0.4 m) with the same length of bolt l = 1.5 m in all models; Dimension (m). 97

Figure 4.40 Displacement vector (m) for the models caf8 (d = 0.8 m), caf6 (d = 0.6 m), caf4 (d = 0.4 m), with the same length of bolt l = 1.5 m in all models; Dimension (m). 97

Figure 4.41 Vertical displacement Ydisp (cm) along the top line (m) for the models caf8 (d = 0.8 m), caf6 (d = 0.6 m) and caf4 (d = 0.4 m) with the same length of bolt (l = 1.5 m) in all models. 98

Figure 4.42 Plasticity for the models caf8 (d = 0.8 m), caf6 (d = 0.6 m), caf4 (d = 0.4 m) with the same length of bolt (l = 1.5 m) in all models. The red elements show the yield in shear, the green ones represent the elastic state but plastic state in past; Dimension (m). 98

Figure 4.43 Contour of major principal stress (MPa) for the models caf8 (d = 0.8 m), caf6 (d = 0.6 m), caf4 (d = 0.4 m) with the same length of bolts (l = 1.5 m) in all models; Dimension (m). 99
Figure 4.44 Safety factors along the top line for the models without rockbolt ca0 and with rockbolt ca8 (d = 0.8 m) with the length of bolts l = 1.5 m. .. 99
Figure 4.45 Vertical displacements ydisp versus calculation steps ($Nx10^4$) at the top of the roof for the models which belong to group 1 and group 2........ 100
Figure 4.46 Vertical displacements ydisp versus calculation steps ($Nx10^4$) at the top of the roof in the models which belong to group 3 and group 4. 101
Figure 4.47 Vertical displacements ydisp (cm) versus calculation steps $Nx10^4$ at the top of the roof in the models which belong to group 5 and group 6... 101
Figure 4.48 Contours of vertical displacement (m) without rockbolt mk0 and with rockbolts mk8 (d = 0.8 m) with the length of the bolt l = 1.5 m; Dimension (m). 102
Figure 4.49 Vertical displacements Ydisp (cm) along the top line d (m) for the models without rockbolt mk0 and with rockbolt mk8 (d = 0.8 m) with the length of the bolt l = 1.5 m. 103
Figure 4.50 Displacement vector (m) for the models without rockbolt mk0 and with rockbolt mk8 (d = 0.8 m) with the length of the bolt l = 1.5 m; Dimension (m). 103
Figure 4.51 Safety factors for the models without rockbolt mk0 and with rockbolt mk8 (d = 0.8 m) with the length of the bolt l = 1.5 m; Dimensions (m)... 103
Figure 4.52 Axial force (MPa) of the rockbolt for the models mk8 (d = 0.8 m), mk6 (d = 0.8 m), mk4 (d = 0.8 m) with the length of the bolt l = 1.5 m in all models; Dimension (m)... 104
Figure 4.53 Axial force (MPa) of the rockbolts for the models mks6 (d = 0.6 m), mks4 (d = 0.4 m) with the length of the bolts l = 1.5 m in all models; Dimension (m). 105
Figure 4.54 Contours of vertical displacement (MPa) for the models mkf8 (d = 0.8 m), mkf6 (d = 0.6 m), mkf4 (d = 0.4 m) with the length of the bolts l = 1.5 m in all models; Dimension (m). 105

Figure 4.55 Displacement vector (m) for the models mkf8 (d = 0.8 m), mkf6 (d = 0.6 m), mkf4 (d = 0.4 m) with the length of the bolts l = 1.5 m in all models, Dimension (m). 106

Figure 4.56 Vertical displacement Ydisp (cm) along the top line in model mkf8 (d = 0.8 m), mkf6 (d = 0.6 m) and mkf4 (d = 0.4 m) with the same length of bolts l = 1.5 m in all models. 106

Figure 4.57 Safety factors along the top line for the models without rockbolts mk0 and with rockbolt mk8 (d = 0.8 m) with the length of bolts l = 1.5 107

Figure 4.58 Vertical displacements ydisp versus calculation steps (Nx10^4) at the top of the roof in the models which belong to group 1 and group 2. 107

Figure 4.59 Vertical displacements ydisp versus calculation steps (Nx10^4) at the top of the roof in the models which belongs to group 3 and group 4. 108

Figure 4.60 Vertical displacements ydisp versus calculation steps (Nx10^4) at the top of the roof in the models which belongs to group 5 and group 6. 108

Figure 4.61 Contours of vertical displacement (m) for the models without rockbolts dh0 (left) and with rockbolts dh8 (d = 0.8 m, right) with the length of bolt l = 1.5 m; Dimension (m). 109

Figure 4.62 Vertical displacements Ydisp (cm) along the top line (m) for the models without rockbolts dh0 and with rockbolts dh8 (d = 0.8 m) with the length of bolt l = 1.5 m. 110

Figure 4.63 Displacement vector (m) for the models without rockbolt dh0 (left) and with rockbolts dh8 (d = 0.8 m, right) with the length of bolts l = 1.5 m; Dimension (m). 110

Figure 4.64 Plasticity for the models without rockbolts dh0 (left) and with rockbolts dh8 (d = 0.8 m, right) with the length of the bolt l = 1.5 m. The red elements show the yield in shear, the green ones represent the elastic state but plastic in past; Dimension (m). 111

Figure 4.65 Contours of major principal stresses (MPa) for the model without rockbolts dh0 (left) and with rockbolts dh8 (d = 0.8 m, right) with the length of the bolt l = 1.5 m; Dimension (m). 111

Figure 4.66 Safety factors for the models without rockbolt dh0 and with rockbolt dh8 (d = 0.8 m, right) with the length of the bolts l = 1.5 m; Dimension (m). 112

Figure 4.67 Axial force (MPa) of the rockbolts for the models dh8 (d = 0.8 m), dh6 (d = 0.6 m), dh4 (d = 0.4 m) with the same length of the bolt l = 1.5 m in all models; Dimension (m)....................112
Figure 4.68 Displacement vector (m) for the models dhs8 (l = 1.5 m), dhs28 (l = 2.0 m), dhs38 (l = 3.0 m) and dhs48 (l = 4.0 m) with the same distance between bolts d = 0.8 m in all models; Dimension (m). 113
Figure 4.69 Vertical displacement Ydisp (cm) along the top line for the models dhs8 (l = 1.5m), dhs28 (l = 2.0 m), dhs38 (l = 3.0 m) and dhs48 (l = 4.0 m) with the same distance between bolts d = 0.8 m in all models. 113
Figure 4.70 Displacement vector (m) for the models dhs6 (d = 0.6 m) and dhs4 (d = 0.4 m) with the same length of bolt l = 1.5 m;....................114
Figure 4.71 Vertical displacement Ydisp (cm) along the top line for the models dhs6 (d = 0.6 m) and dhs4 (d = 0.4 m) with the same length of bolt l = 1.5 m....................114
Figure 4.72 Axial force (MPa) of the rockbolt for the models dhs6 (d = 0.6 m), dhs4 (d = 0.4 m) with the same length of bolt l = 1.5 m in all models; Dimension (m). 115
Figure 4.73 Contours of vertical displacement (m) for the models dhf8 (d = 0.8 m), dhf6 (d = 0.6 m), dhf4 (d = 0.4 m) with the same length of bolt l = 1.5 m in all models; Dimension (m). 115
Figure 4.74 Displacement vector (m) for the models dhf8 (d = 0.8 m), dhf6 (d = 0.6 m), dhf4 (d = 0.4 m) with the same length of bolt l = 1.5 m in all models; Dimension (m)....................116
Figure 4.75 Vertical displacement Ydisp(cm) along the top line for the models dhf8 (d = 0.8 m), dhf6 (d = 0.6 m) and dhf4 (d = 0.4 m) with the same length of bolt l = 1.5 m in all models....................116
Figure 4.76 Safety factors along the top line for the models without rockbolt dh0 and with rockbolts dh8 (d = 0.8 m) with the length of the bolt l = 1.5 m. 116
Figure 4.77 Vertical displacements Ydisp versus calculation steps ($Nx10^4$) at the top of the roof in the models which belong to group 1 and group 2. 117
Figure 4.78 Vertical displacements Ydisp versus calculation steps ($N x10^4$) at the top of the roof in the models which belong to group 3 and group 4...117

Figure 4.79 Vertical displacements Ydisp versus calculation steps (N x10^4) at the top of the roof in the models which belong to group 5 and group 6...118
Figure 4.80 Contours of vertical displacement (m) for the models without rockbolt md0 (left) with rockbolts md8 (d = 0.8 m, right) with the length of the bolt l = 1.5 m; Dimension (m)...119
Figure 4.81 Vertical displacements Ydisp (cm) along the top line d (m) for the models without rockbolt md0 and with rockbolt md8 (d = 0.8 m) with the length of the bolt l = 1.5 m...119
Figure 4.82 Displacement vectors (m) for the models without rockbolts md0 (left) and with rockbolts md8 (d = 0.8 m, right) with length of bolt l = 1.5 m; Dimension (m). 120
Figure 4.83 Plasticity for the models without rockbolts md0 (left) and with rockbolts md8 (d = 0.8 m, right) with length of bolt l = 1.5 m. The red elements show the yield in shear, the green ones represent the elastic state but plastic one in the past; Dimension (m). 120
Figure 4.84 Safety factors for the models without rockbolt md0 and with rockbolt md8 (d = 0.8 m, right) with the length of the bolt l = 1.5 m; Dimension (m)...121
Figure 4.85 Axial force (MPa) along the rockbolt for the models md8 (d = 0.8 m), md6 (d = 0.6 m), md4 (d = 0.4 m) with the same length of the bolt l = 1.5 m in all models; Dimension (m). 121
Figure 4.86 Vertical displacement Ydisp (cm) along the top line for the model mds8 (l = 1.5 m), mds28 (l = 2.0 m), mds38 (l = 3.0 m) and mds48 (l = 4.0 m) with the same bolt distance d = 0.8 m in all models...............122
Figure 4.87 Displacement vector for the models mds6 (d = 0.6 m) and model mds4 (d = 0.4 m) with the same length of bolt l = 1.5 m in all models; Dimension (m). 122
Figure 4.88 Vertical displacement Ydisp (cm) along the top line for the models mks6 (d = 0.6 m) and mks4 (d = 0.4 m) with the same length of bolt l = 1.5 m in all models...123
Figure 4.89 Axial force (MPa) of the rockbolt for the models mds6 (d = 0.6 m), mds4 (d = 0.4 m) with the same length of bolt l = 1.5 m in all models; Dimension (m). 123

Figure 4.90 Contours of vertical displacement (m) for the models mdf8 (d = 0.8 m), mdf6 (d = 0.6 m), mdf4 (d = 0.4 m) with the same length of bolt l = 1.5 m in all models; Dimension (m). 124

Figure 4.91 Displacement vectors (m) for the models mdf8 (d = 0.8 m), mdf6 (d = 0.6 m), mdf4 (d = 0.4 m) with the same length of bolts l = 1.5 m in all models; Dimension (m). 124

Figure 4.92 Vertical displacement Ydisp (cm) along the top line for the models caf8 (d = 0.8 m), mdf6 (d = 0.6 m) and caf4 (d = 0.4 m) with the same length of bolt l = 1.5 m in all models. 125

Figure 4.93 Safety factors along the top line for the models without rockbolt md0 and with rockbolts md8 (d = 0.8 m) with the length of bolt l = 1.5 m. 125

Figure 4.94 Vertical displacements ydisp (cm) versus calculation steps (N x10^4) at the top of the roof in models which belong to group 1 and group 2. 126

Figure 4.95 Vertical displacements ydisp (cm) versus calculation steps (Nx10^4) at the top of the roof in models which belong to group 3 and group 4. 126

Figure 4.96 Vertical displacements ydisp (cm) versus calculation steps (N x10^4) at the top of the roof in models which belong to group 5 and group 6. 127

Figure 4.97 Contours of vertical displacement (m) for the models without rockbolts kh0 (left) and with rockbolts kh8 (d = 0.8 m, right), length of bolts l = 1.5 m; Dimension (m). 128

Figure 4.98 Vertical displacements Ydisp (cm) along the top line d (m) for the models without rockbolts kh0 (left) and with rockbolts kh8 (d = 0.8 m, right), length of bolts l = 1.5 m. 128

Figure 4.99 Displacement vectors (m) for the models without rockbolts kh0 (left) and with rockbolts kh8 (d = 0.8 m, right), length of bolt l = 1.5 m; Dimension (m). 129

Figure 4.100 Plasticity for the models without rockbolts kh0 (left) and with rockbolts kh8 (d = 0.8 m, right), length of bolt l = 1.5 m. The red elements show the yield in shear, the green ones represent the elastic state but plastic one in the past; Dimension (m). 129

Figure 4.101 Safety factors for the models without rockbolts kh0 (left) and with rockbolts kh8 (d = 0.8 m, right), length of bolt l = 1.5 m; Dimension (m). 130

Figure 4.102 Axial force (MPa) of the rockbolts for the models kh8 (d = 0.8 m), kh6 (d = 0.6 m) and kh4 (d = 0.4 m) with the same length of bolt l = 1.5 m; Dimension (m). 130
Figure 4.103 Displacement vector (m) for the models khs6 (d = 0.6 m) and khs4 (d = 0.4 m) with the same length of bolt l = 1.5 m in the two models; Dimension (m). 131
Figure 4.104 Displacement along the top line for the models khs6 (d = 0.6 m), khs4 (d = 0.4 m) with the same length of the bolt l = 1.5 m in all models.. 131
Figure 4.105 Axial force (MPa) of the rockbolt for the models khs6 (d = 0.6 m), khs4 (d = 0.4 m) with the same length of the bolt l = 1.5 m in all models; Dimension (m). 132
Figure 4.106 Contours of vertical displacements (MPa) for the models khf8 (d = 0.8 m), khf6 (d = 0.6 m) and khf4 (d = 0.4 m) with same length of the bolt l = 1.5 m in all models; Dimension (m). 132
Figure 4.107 Displacement vectors (m) for the models khf8 (d = 0.8 m), khf6 (d = 0.6 m) and khf4 (d = 0.4 m) with same length of the bolt l = 1.5 m in all models; Dimension (m). 133
Figure 4.108 Vertical displacements Ydisp (cm) along the top line in model khf8 (d = 0.8 m), khf6 (d = 0.6 m) and khf4 (d = 0.4 m) with the same length of bolt l = 1.5 m in all models. 133
Figure 4.109 Safety factors along the top line for the models without rockbolts kh0 and with rockbolts kh8 (d = 0.8 m) with length of the bolt l = 1.5 m. 134
Figure4.110 Vertical displacements ydisp (cm) versus calculation steps (Nx10^4) at the top of the roof in the models which belong to group 1 and group 2.. 134
Figure 4.111 Vertical displacements ydisp (cm) versus calculation steps (Nx10^4) at the top of the roof in the models which belong to group 3 and group 4.. 135
Figure 4.112 Vertical displacements ydisp versus calculation steps (Nx10^4) at the top of the roof in the models which belong to group 5 and group 6. 135
Figure 4.113 Mohr-Coulomb failure criterion in the principal stress space σ_1 versus σ_3 (left) and the shear-normal stress space τ_s vs σ_n (right). 136

List of Tables

Table 2.1 Typical design recommendations for rockbolts according to the US Corps of Engineers [Stillborg, 1986]. 22

Table 2.2 Types of bolting according to Peng and Tang Hudson [2000]. 23

Table 2.3 Guidelines for excavation and support systems in rock tunnels [Bieniawsky, 1979] 27

Table 2.4 Value of the structural coefficient (K_s). 28

Table 2.5 Value of the coefficients n_s, n_r. 30

Table 2.6 Value of the rock strength after and before application of rockbolts....38

Table 3.1 Properties of the non-linear elasto-plastic cable element [Hausdorf 2006]. 45

Table 3.2 Input data for rockbolt element used for numerical model. 46

Table 3.3 Input data for simulation of cable element...46

Table 3.4 Properties of the numerical nonlinear 3D cable element. 56

Table 3.5 Properties of the nonlinear 3D rockbolt model. 58

Table 4.1 Physical properties of the intact rock surrounding Cao Thang mine roadway. 68

Table 4.2 Physical properties of intact rock surrounding Mao Khe mine roadway.. 68

Table 4.3 Physical properties of the intact rock surrounding Duong Huy mine roadway. 68

Table 4.4 Physical properties of intact rock surrounding Mong Duong mine roadway. 68

Table 4.5 Physical properties of the intact rock surrounding Khe Cham mine roadway. 69

Table 4.6 Technical properties of used standard rockbolt pattern. 69

Table 4.7 Technical conditions of roadways..69

Table 4.8 Values of constant m_i for intact rock [Rockscience 2008]....................73

Table 4.9 Guidelines for estimating the disturbance factor D (sedimentary rocks) [Rockscience 2008]. 73

Table 4.10 Guidelines for the selection of the modulus ratio MR [Rockscience 2008]. 74

Table 4.11 Values of the geological strength index GSI based on geological descriptions [Rockscience 2008]. 75

Table 4.12 Rock mass parameters for Cao Thang mine. 75
Table 4.13 Rock mass parameters for Mao Khe mine. 76
Table 4.14 Physical properties of the rock mass surrounding Cao Thang roadway. 76
Table 4.15 Physical properties of the rock mass surrounding Mao Khe roadway .. 77
Table 4.16 Rock mass parameters for Duong Huy mine. 77
Table 4.17 Physical properties of the rock mass surrounding Duong Huy roadway. 77
Table 4.18 Rock mass parameters for Mong Duong mine. 77
Table 4.19 Rock mass parameters for Khe Cham mine. 77
Table 4.20 Physical properties of the rock mass surrounding Mong Duong roadway. 78
Table 4.21 Physical properties of the rock mass surrounding Khe Cham roadway.... 79
Table 4.22 Rockbolt parameters used for model simulation. 82
Table 4.23 Types of rockbolt patterns for Cao Thang mine. 83
Table 4.24 Types of rockbolt patterns for Mao Khe mine. 83
Table 4.25 Types of rockbolt patterns for Duong Huy mine. 84
Table 4.26 Types of rockbolt patterns for Mong Duong mine. 84
Table 4.27 Types of rockbolt patterns for Khe Cham mine. 85
Table 4.28 Factors of safety for the Cao Thang mine with distance between rockbolts of 0.8 m (without rockbolts: FOS = 1.14). 137
Table 4.29 Factors of safety for the Cao Thang mine with distance between rockbolts of 0.6 m(without rockbolts: FOS = 1.14). 138
Table 4.30 Factors of safety for the Cao Thang mine with the distance between rockbolts of 0.4 m(without rockbolts: FOS = 1.14). 138
Table 4.31 Factors of safety for the Mao Khe mine with distance between rockbolts of 0.8 m(without rockbolts: FOS = 1.75). 138
Table 4.32 Factors of safety for the Mao Khe mine with distance between rockbolts of 0.6 m(without rockbolts: FOS = 1.75) 139
Table 4.33 Factors of safety for the Mao Khe mine with distance between rockbolts of 0.4 m(without rockbolts: FOS = 1.75) 139
Table 4.34 Factors of safety for the Duong Huy mine with the distance between rockbolts of 0.8 m (without rockbolts: FOS = 1.25). 139

Table 4.35 Factors of safety for the Duong Huy mine with distance between rockbolts of 0.6 m (without rockbolts: FOS = 1.25). 140

Table 4.36 Factors of safety for the Duong Huy mine with distance between rockbolts of 0.4 m (without rockbolts: FOS = 1.25). 140

Table 4.37 Factors of safety for the Mong Duong mine with the distance between rockbolts of 0.8 m (without rockbolts: FOS = 1.40). 140

Table 4.38 Factors of safety for the Mong Duong mine with distance between rockbolts of 0.6 m (without rockbolts: FOS = 1.40). 141

Table 4.39 Factors of safety for the Mong Duong mine with the distance between rockbolts of 0.4 m (without rockbolts: FOS = 1.40). 141

Table 4.40 Factors of safety for the Khe Cham mine with distance between rockbolts of 0.8 m (without rockbolts: FOS = 1.35). 141

Table 4.41 Factors of safety for the Khe Cham mine with distance between rockbolts of 0.6 m (without rockbolts: FOS = 1.35). 141

Table 4.42 Factors of safety for the Khe Cham mine with distance between rockbolts of 0.4 m(without rockbolts: FOS = 1.35) 142

Table 5.1 Vertical displacements (cm) obtained by analytical and numerical calculations at roof centre. 145

Table 5.2 Reinforcement factors (Kr) when distance between the bolts is 1.0 m..... 146

Table 5.3 Reinforcement factors (Kr) when distance between the bolts is 0.8 m..... 146

Table 5.4 Reinforcement factors (Kr) when distance between the bolts is 0.6 m..... 147

Table 5.5 Reinforcement factors (Kr) when distance between the bolts is 0.4 m..... 147

Table 5.6 Reinforcement factors (K_r) determined by equation (5.12). 148

List of Abbreviations

a	Distance between bolts [p33]
a	Hoek-Brown constants for rock mass [p71]
a	Radius of the opening [p144]
A	Cross section area of the cable [p41]
A_b	Cross section area of steel bolt [p19]
A_t	Cross area of the representative volume [p20]
b	Beam width [p35]
b	Radius of bolted area [p144]
Bu	Bulk modulus [p58]
C	Cohesion of rock mass [p39]
C*	Increased cohesion [p39]
CB	Cable [p50]
c_1	Cohesion between steel bar and cement grout [p29]
c_2	Cohesion between borehole wall and cement grout [p29]
D	Diameter of the cable [p43]
D	Disturbance factor [p71]
d	Beam height [p35]
d	Distance of the bolt [p144]
d	Effective thickness of the beam [p33]
d_b	Diameter of the borehole [p29]
Dens	Density [p46]
ds	Diameter of steel bolt [p29]
E	Young's Modulus [p41]
E^0	Young's initial Modulus of rock [p144]
Eb	Young's Modulus of the rockbolt [p19]
Eg	Young' s Modulus of grout [p144]
Ei	Young's Modulus of intact rock [p72]
Em	Young's Modulus of the rock mass [p19]
Emod	Young' s modulus [p56]

E^n	Young's Modulus of bolted area [p144]
ESR	Excavation support ratio [p25]
F	Factor of safety [p89]
F_T	Anchor force [p33]
f	Protodiakonov coefficient [p35]
f_π	Coefficient accounts for joints level of the rock mass [p37]
FS(i)	Force of the i-th prop [p34]
f''	Frictional coefficient between layers [p31]
f^0	Rise of the arch [p35]
f_l	Rise of the arch [p35]
$F_{A,B}$	Reaction force [p34]
Faxial	Axial force [p50]
Fc	Cross section of the steel bar [p29]
f_{dyn}	Coefficient of dynamic load part [p34]
fg	Rock mass structural factor [p35]
F_Q	Resultant shear force [p31]
F_s	Shear force [p31]
f^s	Shear yielding function [p61]
f^t	Tensile yielding function [p61]
F_T	Pressure applied to the beam [p35]
G	Shear modulus [p43]
G_b	Shear modulus of steel bolt [p19]
G	Grout shear modulus grout [p43]
G_m	Shear modulus of rock mass [p19]
GSI	Geological strength index [p71]
H	Depth of the opening [p28]
h	Height of the beam [p31]
I	Moment of inertia [p46]
j	Polar moment of inertia, [p58]
J_a	Joint alteration number [p25]

J_n	Joint set number [p25]
J_r	Joint roughness number [p25]
J_w	Joint water reduction factor [p25]
K	Bulk Modulus of rock mass [p46]
k	Empirical coefficient [p37]
k	Poisson's ratio [p31]
K_1	Concentration coefficient at sidewall [p28]
K_2	Concentration coefficient at roof [p28]
K_{bond}	Grout bond stiffness [p42]
K_F	Force due to gravity of the fissure body [p34]
Kr	Reinforcement factor [p8]
K_s	Structural weakness coefficient [p28]
L	Length of rockbolt / segment / element [p31]
L	Span of the opening [p35]
L	Contributing cable length [p41]
l_0	Span of the beam [P35]
l_a	Length of the bolt [p36]
L_A	Anchor length [p34]
l_z	Length of the steel bar in the grout [p29]
m	Constant of rock type [p70]
m	Size of the rock block [p37]
m_b	Hoek-Brown constant for rock mass [p71]
m_i	Hoek-Brown constant for intact rock [p71]
M_{max}	Maximum bending moment [p35]
MN	Mega Newton [p48]
MR	Modulus ratio [p72]
n	Number of rockbolts / cables [p30]
N	Capacity of the anchor [p30]
N	Axial force of the bolt [p33]
n_r	Safety factor of rock at roof [p28]
n_s	Safety factor of rock at sidewall [p28]

P	Vertical pressure [p31]
P^0	Vertically directed prestress [p30]
P_{rb}	Capacity of the bolt [p29]
P_{rb1}	Yield of the steel bar [p29]
P_{rb2}	Bonding of steel bar and concrete [p29]
P_{rb3}	Bonding of concrete and the borehole wall [p29]
P_v	Vertical pressure [p80]
Q	Quality of rock mass [p25]
q_0	Peak value of the triangle load [p35]
Q_b	Quality of the bond between grout and rock [p43]
q_r	Roof pressure [p29]
r	Radius of investigated [p144]
ra	Radius of the Mohr circle [p89]
rb	Radius of circle of strength of the rock mass [p89]
R_k	Yield in tensile [p29]
RMR	Rock mass rating [p26]
RQD	Rock quality designation [p25]
s	Safety factor [p34]
S	Density of the bolt; Constant of rock type [p29]
s	Hoek-Brown constants [p70]
S_{bond}	cohesive strength of the grout [p43]
sf	Safety factor [p146]
Sh	Shear modulus [p56]
S_l	Longitudinal rockbolt spacing [p39]
SRF	Stress reduction factor [p25]
S_t	Circumferential rockbolt spacing [p39]
t	Thickness of grout annulus [p43]
t	Width of the beam [p35]
t_1, t_2	Direction cosine of the elements [p42]
ti	Distance of the discontinuities [p37]
T_{med}	Mean force along the bolt [p39]

U	Displacement [p145]
U_c	Axial displacement of the cable [p43]
U_m	Axial displacement of the rock mass [p43]
x	Chosen axis of coordinate [p35]
$x(FS(i))$	Distance of i-th prop [p34]
$2b$	Span or width of the openings [p30]
	Greek letters
α	Angle between discontinuities [p37]
α	Angle of the arch [p35]
γ	Density of the rock mass [p28]
δ	Angle of the rock at the abutment [p37]
ΔEx	Increment of the Young’s modulus and shear modulus [p19]
$\Delta e1, 2, 3$	Increment of the principal strains [p60]
Δft	Increment of the axial force [p41]
$\Delta Gy, z$	Increment of the shear modulus [p19]
ΔU^t	Increment of the axial displacement [p41]
$\Delta\sigma_{1,3}$	Increment of the tangential, radial stress [p20]
$\Delta\sigma_{1, 2, 3}$	Increment of the principal stresses [p60]
ε_b	Bolt strain [p20]
η	Rheologic coefficient [p37]
λ	Lateral pressure coefficient [p80]
ν	Poisson coefficient [p80]
ξ	Long term coefficient [p28]
γ	Density of the rock mass [p28]
σ_1, σ_3	Major principal stresses [p70]
$\sigma_{c, ci}$	Compressive strength of the rock mass [p28]
σ_{ci}	Intact rock strength [p72]

σ_{cm}	Uniaxial compression strength of the rock mass [p72]
σ_{max}	Maximum tensile stress [p35]
σ_{3max}	Upper limit of the confining stress [p72]
σ_r	Radial stress [p33]
σ_t	Uniaxial tensile strength of the rock mass [p28]
σ_φ	Tangential stress [p33]
τ	Shear stress [p136]
τ_p	Shear strength of the rock mass [p37]
τ_{peak}	Maximum shear strength. [p43]
τ_{xy}	Shear stress [p31]
φ, Φ	Friction angle [p136]